State interactions, excitation dynamics, hidden states and photofragmentation pathways in hydrogen halides

Helgi Rafn Hróðmarsson

Faculty of Physical Sciences
University of Iceland
2016

State interactions, excitation dynamics, hidden states and photofragmentation pathways in hydrogen halides

Helgi Rafn Hróðmarsson

Dissertation submitted in partial fulfillment of a
Philosophiae Doctor degree in chemistry

Advisor
Ágúst Kvaran

PhD Committee
Gísli Hólmar Jóhannesson
Huasheng Wang
Kristján S. Kristjánsson
Ragnar Jóhannsson

Opponents
Michael N. R. Ashfold
Theofanis Kitsopoulos

Faculty of Physical Sciences
School of Engineering and Natural Sciences
University of Iceland
Reykjavik, March 18th 2016

State interactions, excitation dynamics, hidden states and photofragmentation pathways in hydrogen halides

Photofragmentations of HBr and HI

Dissertation submitted in partial fulfillment of a *Philosophiae Doctor* degree in chemistry

Faculty of Natural Sciences
School of Engineering and Natural Sciences
University of Iceland
Dunhagi 3
107, Reykjavik
Iceland

Telephone: 525 4000

Bibliographic information:
Helgi Rafn Hróðmarsson,
State interaction, excitation dynamics, hidden states and photofragmentation pathways in hydrogen halides, PhD dissertation, Faculty of Natural Sciences, University of Iceland. 2016

ISBN 978-9935-9263-8-8

Printing: Háskólaprent ehf., Fálkagötu 2, 107 Reykjavík.
Reykjavik, Iceland, March 2016

Abstract

The focus of my Ph.D. work is on two separate, but closely related experimental subjects. The first involves the recording of mass resolved two-photon resonance enhanced multiphoton ionization (REMPI) spectra of the hydrogen halides HBr and HI. The REMPI spectra of both molecules reveal extensive perturbation effects; line-shifts, intensity alterations, and line broadenings. These are colloquially referred to as LS-, LI-, and LW-effects, respectively. Measuring these effects quantitatively and qualitatively allows data extraction regarding state interactions (perturbations) between Rydberg and ion-pair states. These interactions include fragmentation via repulsive valence states and subsequent ionization of the fragments. The presence of hidden states is also deduced and they are assigned based on observed perturbation effects.

Velocity map imaging (VMI) experiments are performed on HBr. Such experiments measure the angular distributions of photofragmentations and the total kinetic energy release of the imaged fragments. These experiments allow the roles of photofragment channels in the photodissociation and photoionization to be deduced, where Rydberg and ion-pair states act as intermediary states prior to ionization/fragmentation.

Útdráttur

Þungamiðja doktorsverkefnis míns snerist um tvö aðskilin en náskyld viðfangsefni. Hið fyrra snýst um mælingar á samhrifsstyrktum fjölljóseindajónunar (REMPI) rófum vetnihalíðanna HBr og HI. Skráð róf beggja sameinda leiddu í ljós umtalsverð truflunaráhrif; línuhliðranir, breytingar á línustyrkjum og línuvíkkanir. Þessi áhrif eru til styttingar kölluð LS-, LI- og LW-áhrif. Að mæla þessi áhrif hlutbundið og eigindlega gerir gagnasöfnun varðandi víxlverkanir á milli Rydberg og jónparaástanda mögulega. Þessar víxlverkanir fela m.a. í sér ljóssundrun í gegnum fráhrindandi ástönd og jónun atómbrotanna sem úr þeim myndast. Dulin ástönd eru sömuleiðis fundin í gegnum truflanaáhrif.

Hraðavigurskortlagningar (VMI) eru framkvæmdar á HBr. Slíkar tilraunir mæla stefnu og hreyfiorku jónaðra atómbrota. Með niðurstöðum þessara tilrauna má finna hvaða ljósbrotsferlar koma við sögu í ljósrofnunar- og jónunarferlum sameindarinnar þar sem Rydberg og jónparaástönd taka þátt sem miðbiksástönd.

For my wife Ingibjörg

and our four little bunny children who can't wait to eat this thesis and shit on the floor

Preface

This work is the accumulated work which I have done for the previous 4 years as a PhD student at the University of Iceland. After starting in a M.Sc. program in January 2012, I opted for an upgrade to a full doctorate during the summer of 2013. This upgrade was accepted by the department of natural sciences in accordance with Article 2 of the University of Iceland's set of rules #642-2011. The law states that such an upgrade is allowed only if the student has not has not defended his or her M. Sc. Thesis and not more than two years have passed since the student's inital registration. Since I met both of these criteria, I was eligible for an upgrade to a full doctorate.

It should be noted that the work started out as a continuation of work which I did as a B.Sc. student, as a part of my B.Sc. research project under the supervision of Prof. Ágúst Kvaran, entitled "2D-REMPI of HBr: Study of singlet and triplet states and the ion-pair state". In the first months of my postgraduate research, I finished and polished some of the work which I did as part of my B.Sc. project and is therefore justifiably a part of this thesis.

Table of Contents

List of Figures

List of Tables

Abbreviations

2D – Two dimensional

3D – Three dimensional

BBO – Beta Barium Borate (β-BaB_2O_4)

Br_2 – Molecular Bromine

C_2H_5I – Iodoethane

CCD – Charge Coupled Device

CCl_4 – Tetrachloromethane

CF_3I - Trifluoroiodomethane

CH – Methylidyne

CH_2Br_2 – Dibromomethane

CH_2I_2 – Diiodomethane

CH3Br – Bromoform / Bromomethane

CH_3I – Iodoform / Iodomethane

CH_4 – Methane

CH_xBr_{4-x} – Bromomethane family

Cl_2 – Molecular Chlorine

CO – Carbon Monoxide

DBr – Deuterium Bromide

DCl – Deuterium Chloride

DF – Deuterium Fluoride

DI – Deuterium Iodide

FCF – Franck-Condon Factor

HBr – Hydrogen Bromide

HCHO - Formaldehyde

HCl – Hydrogen Chloride

HF – Hydrogen Fluoride

HI – Hydrogen Iodide

I_2 – Molecular Iodine

IBr – Iodobromide / Bromoiodine

ICl – Iodochloride / Chloroiodine

IO - Iodooxide

LCAO – Linear Combination of Atomic Orbitals

LI – Line intensity

LS – Line Shift

LW – Line-width

MCP – Micro-channel Plate

MO – Molecular Orbital

O_2 – Molecular Oxygen

O_3 - Ozone

PES – Potential Energy Surface

RDA – Retro-Diels-Alder

REMPI – Resonance Enhanced Multiphoton Ionization

SF_6 – Sulfur Hexafluoride

SHG – Second Harmonic Generator

TOF – Time of Flight

VMI - Velocity Map Imaging

VUV – Vacuum Ultraviolet

Glossary

Ab initio – Rigorous computational methods to calculate energies, configurations, potential curves, etc. of molecules.

Anisotropy – Alignment dependent photofragmentations are often anisotropic, which means they are direction dependent. This dependency originates from the symmetry of the orbitals involved in the relevant photofragmentations.

Auger electron – Electrons emitted by the Auger effect, the effect where the filling of an inner shell valency of an atom or molecule (inner relaxation event/s) is accompanied by the emission of an electron.

Branching ratio – The ratio of the amounts of different products formed by molecular dissociation. In this work, branching ratio usually refers to the ratio between the amounts of spin-orbit excited halogen atoms vs ground state halogen atoms from repulsive states.

Dynamics – Classically, dynamics refer to the effects of force and/or torque upon the motion of a system. In this thesis, dynamics refer to effects of the absorption of photons in the process of excitation, ionization, and fragmentation.

Heavy Rydberg states – Heavy Rydberg states consist of a weakly bound positive and negative ion orbiting a common center of mass. The bond strength is very low and the resulting bond length is approximately 10^5 times larger than in a typical diatomic molecule.

Hund's cases – Hund's cases are idealized combinations of quantum numbers that are considered *good* for a specific molecule. The designation of good quantum numbers implies that they can be measured simultaneously. Hund's cases, therefore, provide basis sets that can be applied to the total Hamiltonian of that molecule to extract energies for each set of good quantum numbers.

Ionic states – The ground state and excited states of the molecular ion are commonly referred to as ionic states.

Ionization potential – The minimum energy required for a molecule to lose one of its electrons and form the ground state of the molecular ion.

Ion-pair state – An excited state of a covalently bound molecule described best as a pair of ions. They are usually described in terms of an electron being excited from a bound orbital to an antibonding orbital.

Perturbations – Interactions between excited states are commonly resolved with perturbation theory which describes the interactions in terms of state mixing. Perturbations are manifestations of the resultant state mixing and appear as line shifts, intensity alterations and line broadenings in spectra.

Potential energy curves – Potential energy curves give descriptions of how the atomic nuclei in an electronic state of a molecule, move in tandem with one another. If the curve exhibits a minimum the electronic state is a bound state. If the only minimum is found when the internuclear distance approaches infinity, the state is a repulsive state.

Quantum theory – To accurately describe very small particles like electrons, protons, and molecules, a theory beyond classical mechanics must be employed, namely quantum theory. Quantum theory utilizes wave mechanics to describe electrons orbiting atoms and molecules and gives results in the form of probabilities of finding electrons within orbitals that are designated by quantum numbers.

Rovibrational coupling – Within every bound state of a molecule, both vibrational and rotational sub-levels exist. The vibrational levels correspond to vibrations of the molecular bond and within each vibrational level, there are rotational levels that are derived from the rigid rotor model. Rovibrational coupling refers to when vibrations change the bond length and hence the moment of inertia, which affects the rotational levels.

Rydberg state – A Rydberg state is an excited state of a molecule where an electron has been excited from a non-bonding orbital to a higher Rydberg orbital associated with one of the atoms in the molecule.

Selection rules – Selection rules govern which transition or perturbations are allowed. For transitions they originate from the law of conservation of total momentum when a molecule absorbs a photon. For perturbations they stem from the non-zero off-diagonal matrix elements that arise from the total Hamiltonian of specific system.

Spin-orbit coupling – Spin-orbit refers to interactions between a particle's spin and its motions. The best known spin-orbit effect is when an electron's spin interacts with the magnetic field that is generated by the electron's motion around an atom. E.g. the halogens have five electrons in their valence *p* shell, where one electron is unpaired. The ground state (X) corresponds to that electron having spin 'up'. The spin-orbit excited state (X*) corresponds to that electron having spin 'down'.

Acknowledgements

First of all, I am deeply indebted and grateful to Prof. Ágúst Kvaran for his leadership and encouragement during my stint as a PhD student. His sheer joy when I found previously unrecorded spectral lines and new states always spurred me on to continually scour the spectra for any attenuated lines and rack my brain over accurate spectral assignments in conjunction with resolving perturbation effects. His unsurpassed mentoring abilities have guided me to becoming a more adept researcher. He is a role model that challenges and drives me onwards to do better and expand my horizons to new research areas.

From my group I am eternally thankful to Huasheng Wang for keeping the wheels (almost) perpetually turning on our experimental setup. His knowledge of every single nook and cranny of the experimental apparatus is exemplary of the perfect technician and experimentation supervisor.

I am also very thankful to the previous PhDs of Prof. Kvaran's group, Dr. Kristján Matthíasson and Dr. Jingming Long who helped get me started with experiments and spectral analysis. If Newton stood on the shoulders of giants, I stood on the shoulders of Kristján and Jingming.

To the other current PhD in Prof. Kvaran's group, Arnar, I am extremely thankful for the good companionship, help with simulations, and reviewing the experimental apparatus.

To our co-authors based in Heraklion, Andreas, Dimitris, Pavle, and Petros, I am thankful for the successful cooperation. I have no doubts this cooperation will continue to prosper into the future. I am especially thankful to Pavle Glodic and Dr. Petros Samartzis for their generous help with the experimental section of this thesis. Their contribution and input is gratefully acknowledged.

To my doctoral committee, Gísli Hólmar Jóhannesson, Huasheng Wang, Kristján S. Kristjánsson, Ragnar Jóhannesson, I am very thankful for their questions, comments and discussions during our PhD meetings.

To all my band members from *Carpe Noctem*, *Misþyrming*, and *Naðra*, I am synchronously thankful and honored to have shared a stage with you guys. Alexander, Andri, Árni, Dagur, Gússi, Lölli, Tommi, playing along your side has helped me enormously to keep focus and invigorated my aspirations when they were down. An extra special thanks to Alexander for helping me review this thesis, and to Andri for helping me with illustrations.

To my mother, Kolbrún, and stepfather, Elías, I am forever thankful for all their support over the years, both emotional and fiscal.

The financial support from The Icelandic Science Foundation (Rannís) and the Assistantship fund of the University of Iceland is acknowledged.

Finally, to my wife Ingibjörg. Words cannot describe how lucky I feel for your loving support and companionship. You are my rock, my everything.

“Whence come the highest mountains? So did I once ask. Then did I learn that they came out of the sea.

That testimony is inscribed on their stones and on the walls of their peaks. Out of the deepest must the highest come to its height.”

Thus Spake Zarathustra.

Frederick Nietzsche

1 Introduction – A brief history of hydrogen halides

The hydrogen halides are among the most meticulously studied diatomics in the field of spectroscopy and *ab initio* calculations. As an example their UV photodissociations have been studied for over a century.[1, 2] In recent decades, with the development of the resonance enhanced multiphoton ionization (REMPI) and the velocity map imaging (VMI) techniques, the hydrogen halides have proved to exhibit very interesting characteristics relevant to photofragmentation pathways. These techniques, among other experimental approaches have been used to record a vast body of knowledge of the inner electronic workings of these molecules, including and not limited to electron configurations, perturbations of excited states, rovibrational progressions of their molecular and ionic ground states, branching ratios of photodissociations, etc.

The work of this thesis seeks to characterize and clarify some of the mysteries surrounding the state interaction mechanisms of excited Rydberg and valence states in the heavier hydrogen halides, HBr and HI, by implementing the REMPI and VMI techniques. What follows in chapters 1.1 – 1.6 is a historical review of the spectroscopy of the hydrogen halides and an overview of the work of this thesis is presented in chapter 1.7.

1.1 Pioneering experiments

The very first rotational band spectra belonging to the hydrogen halides were infrared spectra of HCl and HBr published by W. Burmeister in 1913.[3] The initial impetus for the study of the rotational spectra of such molecules was twofold. Firstly, these spectra provided researchers with information relevant to the electronic structure of the molecule and hence, its dynamics. Secondly, during this period, quantum theory was being fully realized and these studies gave stimuli to find viable utilizations of some of quantum theory´s predictions. One of these utilizations was the extension of quantum theory towards the study of rotational energies of molecules.

Continued experimental results included the HCl infrared absorption curve, which was a little later recorded with greater resolutions by E. Von Bahr[4] and J. B. Brinsmade & E. C. Kemble,[5] respectively. The work was then extended to include HBr and HF by E. S. Imes,[6] which included the first published rotational spectrum of HF. Subsequently, between the years 1920 and 1935,[A] several papers were published on the rotational spectroscopy of the hydrogen halides, many of which included an in-depth spectral analyses, yielding the first measured molecular constants of the hydrogen halides.[7-18] This includes the very first

[A] It is noteworthy that during the quantum boom of the 1920's and 1930's, the German publications *Verhandlungen der Deutschen Physikalischen Gesellschaft* and *Zeitschrift für Physik*, were benchmarks for young quantum physicists (and spectroscopists) to make their mark and included historical publications by Heisenberg, Jordan, Pauli, Wigner and others. Hence, many of the referenced papers from this time period are entirely in German.

publication of the rotational spectrum of HI by M. Czerny.[12] The first band spectrum of hydrogen halide cations was recorded in the ultra-violet for HCl^+ by B. A. Brice & F. A Jenkins[19] and was further developed in terms of detailed rovibrational assignments by M. Kulp.[20, 21]

1.2 Antecedents of modern spectroscopy

During the 1930's two monumental figures presented their work on the hydrogen halides. First, the Nobel laureate R. S. Mullikan published several papers,[22-26] where he described electron configurations of excited states, predicted ionization potentials, described the properties of ion-pair states (initially theorized by another historic figure, L. Pauling[27]), calculated potential energy curves of excited states, explicitly applied perturbation theory to molecular spectra, etc. Second, following the measured UV photodissociation of HBr and HI,[28-32] the first discrete absorption measurements of the neutral hydrogen halides were performed by W. C. Price in 1938.[33] He presented the very first absorption spectra of HCl, HBr, and HI, in the ultra-violet part of the spectrum. These spectra showed clear correlations with similar spectra of the alkyl halides, also recorded by W. C. Price.[34, 35] In 1943, L. H. Woods observed a many line emission spectrum from a hollow-cathode discharge with hydrogen fluoride.[36] Although the spectrum was not analyzed, she theorized that the spectrum belonged to a $^2\Sigma$ - $^2\Pi$ transition in HF^+, analogous to systems of HCl^+ and HBr^+ that were previously described by F. Norling.[37-39] The first rotational lines of HI were observed J. P. Cooley & J. H. Rohrbaugh in 1945[40] and in the late 1940´s, the work of J. Romand & B. Vodar extended the previous spectroscopic studies of HCl, HBr, and HI to include the Schumann region (120 – 185 nm) of the molecular ion where most of the absorption stems from unresolved discrete transitions of highly excited states.[41-44]

Over the next few decades absorption and emission spectroscopy of the hydrogen halides, their deuterated counterparts as well as the cations, and anions were continually explored with different levels of resolution.[44-64] Most of that work was co-authored by R. F. Barrow who went on to become a chief editor of a complete six volume overview of molecular spectroscopy.[65] Notable publications by R. F. Barrow during this period include i) a detailed survey of the ultraviolet spectra of HF, DF, and their cationic species with J. W. C. Johns,[48, 49, 52] the first description of the ion-pair states of HCl with J. K. Jacques[53] and HBr with J. G. Stamper,[56] and a detailed spectroscopic survey along with detailed spectral analyses of excited states in the Schumann region of HBr with J. G. Stamper.[54, 55]

The *ab initio* calculation method, pioneered by Kolos & Wolniewicz, was first applied to the calculation of energy levels of the Hydrogen molecule.[66] Thusly, experimentalists received a new weapon in their arsenal for spectral assignments, i.e. computational calculations based on quantum mechanics. Indeed *ab initio* calculations have turned out to be of immeasurable significance to the field of spectroscopy where the hydrogen halides are no exceptions with varied computational techniques and approaches applied to HF,[67-98] HCl,[68, 89, 92, 99-119] HBr,[89, 92, 120-126] and HI.[89, 121, 126-136]

1.3 Encompassing absorption measurements

The first in a series of papers coherently documenting and assigning the Rydberg and ion-pair states of the hydrogen halides HCl,[137] HBr,[138] and HI[139] as well as their deuterated counterparts were published in 1970 and 1971. Initially, studies were performed on the

lowest lying bound Rydberg states $b^3\Pi_i$ (i = 0, 1, 2) and $C^1\Pi_1$. Studying all three hydrogen halides simultaneously allowed attested comparisons of their electronic behaviors i.e. the differences between Λ, S couplings and Ω, ω couplings. These comparisons revealed that the heavier hydrogen halides HBr and especially HI, showed increasing tendencies towards Hunds case c behavior, rather than Hunds cases a and b.

These same authors continued their documentation of excited states of the hydrogen halides for HCl,[140] HBr[141] and HI[142] and the deuterated counterparts. They did so with emphasis on analyses of Rydberg states of $(\sigma^2\pi^3)n\pi$ Rydberg character, where n = 4 for HCl and DCl, n = 5 for HBr and DBr, and n = 6 for HI and DI. The exploration of Rydberg states at higher energies, found that the appearance of state mixings and perturbation effects started to become prevalent in the spectra. Thus, for example, the appearance of the $f^3\Delta_3$ state in HI, made observable via rotational mixing of a Ω = 2 state, which in turn is rotationally mixed with a Ω = 1 state.[142]

These absorption studies culminated in the extensive assignments of Rydberg and ion-pair states for HCl between 82 800 cm^{-1} and 93 500 cm^{-1},[143] for HBr and DBr between 79 500 cm^{-1} and 83 900 cm^{-1},[144] and for HI and DI between 67 800 cm^{-1} and 74 400 cm^{-1}.[145, 146] Going from HCl to HI one can intrinsically come to the conclusion that the frequency of spectral perturbations will increase since, as the ionization potential decreases, the density of excited states will increase. Indeed, just under 20% of the reported bands for HCl were reported as perturbed to a certain extent in comparison with over 40% of those for HI. No perturbation analyses or deperturbation procedures were performed in these studies, but at the time, perturbations in molecular spectra were viewed more begrudgingly than they are today and hence, their utility went unrealized.

Whereas the excited states of the heavier hydrogen halides were being catalogued during this era, spectroscopic interest in HF was by no means dwindling. During the 70's and continuing onwards to the 80's, the configuration of the electronic structure of HF and its ionic states were being probed with a multitude of techniques including photoelectron spectroscopy,[80, 147-149] Auger electron spectroscopy,[150] transmission electron spectroscopy,[151, 152] electron coincidence spectroscopy,[87, 153, 154] overtone emission spectroscopy,[84] magic-angle dipole spectroscopy,[155] K-shell fluorine atom spectroscopy,[156] and ultraviolet spectroscopy.[157, 158] In recent years, however, the emphasis on HF seems to have faded to a certain extent, with only a handful of studies performed. These will be discussed briefly below.

The heavier hydrogen halides were also subject to various other experimental techniques. Thus, HCl was analyzed in terms of e.g. VUV cross sections of HCl,[159] emission spectra of the $H^{35}Cl^+$, $D^{35}Cl^+$, $H^{37}Cl^+$, and $D^{37}Cl^+$ isotopologues,[160] absorption in the 1400 – 2200 Å excitation region,[161] electron scattering for 5 – 19 eV,[162] photoelectron spectroscopy,[163] and VUV fluorescence.[164] HBr was studied via further absorption measurements,[165] high resolution IR spectroscopy,[166] photoabsorption VUV fluorescence,[167] and threshold photoionization over the 11.5 – 31.5 eV range.[168] Dipole spectroscopy was used as well to measure the absolute photoabsorption cross-sections of HCl, HBr and HI.[169] HI was studied even more extensively than HCl and HBr by absorption measurements in the 32 000 cm^{-1} – 50 000 cm^{-1} range,[170] photofragment spectroscopy,[171] photoionization mass spectrometry,[172] angle resolved photoelectron spectroscopy,[173] Doppler spectroscopy,[174-176] and by two photon induced fluorescence of iodine atoms.[177] In particular, the ionic states of HI have been studied with a multitude of techniques.[178-192] Furthermore, the hydrogen halides HCl,

HBr, and HI were utilized as sources of fast H atoms in collision measurements with CO through excimer laser excitation.[193]

1.4 Multiphoton excitation – Bending the rules

Standard absorption measurements, though extremely useful, are limited by the principles of quantum theory. The absorption of a single photon by diatomic molecules is governed by selection rules, derived from approximate solutions of the time-dependent Schrödinger equation for simplified molecular models. These selection rules (whose rigidity depends on the importance of deviations from the simplified models) are maintained for all additionally absorbed photons. Thereby, by further exciting the molecule with additional photons, the one-photon selection rules can be transcended and excited states characterized by a greater variety of quantum numbers than observed in standard one-photon absorption measurements, may be explored.

The REMPI-TOF technique for molecular systems was first described by P. M. Johnson *et al*. in 1975[194, 195] and has subsequently become one of the most utilized spectroscopic technique available (e.g. see [196], [197] and references therein). The first REMPI measurements of the hydrogen halides were performed by Arepalli *et al*.[198, 199] and involved the detection of excited Cl and Br atoms along with a few molecular bands of HCl[198] and HBr.[199] However, these measurements were rather loosely focused on the hydrogen halides and were more focused on a slew of chlorine and bromine containing molecules. Spiglanin *et al*., however, were the first to coherently analyze the REMPI spectrum of HCl with respects to the $E^1\Sigma^+$ state in 1987.[200] During the next few years, several papers were published which emphasized the utility of REMPI spectroscopy for the hydrogen halides. These include momentous, encompassing work such as the first multiphoton and two color study of HF,[201] a detailed two photon REMPI survey of HCl by Green *et al*.,[202-205] and the first and extensive REMPI study of HBr by R. Callaghan & R. J. Gordon.[206] These papers in turn pioneered further REMPI related studies of HCl including a REMPI PES study of several Rydberg states,[207] extensive analyses of the $F^1\Delta_2$ state,[208, 209] REMPI coupled with pulsed field ionization of the $F^1\Delta_2$ and $f^3\Delta_2$ states,[210] delayed pulsed field threshold photoionization of Rydberg states of $4p\pi$ ancestry,[211] and REMPI coupled with *ab initio* calculations to investigate the branching ratios through the photodissociation continuum (often referred to as the *A* band).[212] REMPI has also been used to inspect photo-catalyzed reaction dynamics of the hydrogen halides (e.g. see J. Xie & R. N. Zare and references therein[213]). More recently, however, REMPI experiments on HF have revealed hyperfine splitting in the $B^1\Sigma^+$ state.[214]

The first REMPI study of HI was reported in 1994 by S. A. Wright & J. D. McDonald.[215] Therein, REMPI spectra of several Rydberg states were reported in the energy range of 64 600 – 71 000 cm^{-1}. Unfortunately, the resolution of the spectra were poor, resulting in few visible rotational lines in the spectra. Thus, for example, the respective *Q* branches of several of the states were completely unresolved. In 1995, however, a more detailed and thorough investigation of the same spectra, encompassing an even greater energy range, of about 69 600 – 73 600 cm^{-1}, was reported by S. T. Pratt & M. L. Ginter.[216] Therein, a multitude of Rydberg and ion-pair states were observed, several of which were previously unobserved.

In 2001, Ascenzi *et al*.[217] performed an in-depth three photon excitation study of HBr. Therein, REMPI spectra for the three photon excitation region of 81 900 – 94 900 cm^{-1}, were recorded and assigned to (Λ, S) and (Ω, ω) coupling schemes. Both linearly and circularly

polarized radiation schemes were employed for spectral assignments. A total of 34 bands were analyzed and assigned to transitions from the ground electronic state of HBr to Rydberg states belonging to the sσ, pσ, dσ, pπ, dπ and dδ manifolds, correlating with the ground electronic state of HBr^+.

1.4.1 Mass resolved REMPI of hydrogen halides – Kvaran group´s expertise

After a comprehensive overview of $\Omega = 0^+$ Rydberg states in HCl, HBr, and HI,[218, 219] Á. Kvaran's research group has specialized in REMPI spectroscopy of the hydrogen halides, resulting in numerous publications involving HF,[220] HCl,[221-230] HBr,[218, 221, 222, 230-233] and HI,[234-237] respectively. The growing catalog of REMPI studies of the hydrogen halides by Á. Kvaran *et al*. includes a study of Hönl-London factors for transition strengths in three photon excitations in HBr,[231] two and three photon REMPI of several Rydberg states and ion-pair states of HCl and HBr,[221-223] two- and three-photon REMPI study of the $L^1\Phi_3$ and $m^3\Pi_1$ Rydberg states in HCl and DCl,[224, 225] REMPI of the HF dimer,[220] REMPI study of the state interactions between Rydberg states and ion-pair states in HCl[226, 227, 229] and HBr,[230] and new states observed in two-photon REMPI of HCl[228] and HBr.[232]

Beyond the hydrogen halides the Kvaran group has also specialized in other molecules related to the photochemistry of the atmosphere and interstellar medium such as the molecular halogens,[219, 238-246] interhalogens,[219, 247-249] bromomethane family,[250-252] bromofluorocarbons,[253, 254] and acetylene.[255]

1.5 Imaging photofragments – Changing the game

Since the original work by R. S. Mulliken,[22, 26] the repulsive valence states of the hydrogen halides have greatly intrigued the investigations of branching ratios of their photodissociations. An abundance of studies have delved into relevant branching ratios of HF,[256] HCl,[114, 117, 212, 257-260] HBr,[175, 261, 262] and HI,[175, 263-267] respectively, to elucidate the intricacies of their photodissociation mechanisms.

The first two-dimensional imaging experiments, performed on CH_3I by D. W. Chandler and P. L. Houston,[268] catalyzed a surge in technical improvements and opened up a new world of analyzing photofragmentation processes and photo-catalyzed reaction pathways. Since the experiments suffered from low resolution, then in order for the technique to achieve its concurrent monumental status within the field of reaction dynamics, improvements were needed. These resolution problems were amended by A. T. J. B. Eppink and D. H. Parker who utilized an improved imaging technique for the photodissociation of the O_2 molecule.[269, 270] Since then, the velocity map imaging technique has been extensively applied to a myriad of molecules and has been further developed and expanded upon, to include the possibility of three-dimensional images of photofragments (see Refs.[271, 272] and references therein).

The beauty of the velocity map imaging technique is that it allows the determination of energy thresholds as well as alignments or symmetries relevant to molecular photodissociation pathways. Since the 1990's this technique has become the benchmark for photodissociation analyses resulting in numerous publications involving the hydrogen halides.

In a 1995 review of imaging techniques, A. J. R. Heck and D. W. Chandler[273] reviewed a previous outline of the ultimate study of molecular reaction dynamics,[274] by stating: "In the ultimate experiment one would like to determine the total cross section at specified collision energies; measure the internal-state, angular and velocity distributions, and alignment of the products, and prepare selectively the internal state, alignment, and orientation of the reactants." One can argue that no other experimental technique has come closer to this objective than REMPI coupled with VMI.

In the same publication, A. J. R. Heck and D. W. Chandler also reviewed the progress of imaging studies of HI and DI citing papers already mentioned above.[24, 131, 171, 176, 263]

1.5.1 HCl & HBr

Arriving into the new millennium, a torrent of VMI applications for the hydrogen halides were reported. Baumfalk *et al*. reported on the UV photolysis of HBr molecules and clusters[275] and between 2002 and 2004, Rakitzis *et al*. reported i) on the slice imaging of HCl and HBr in order to assess the relative contributions of the $A^1\Pi_1$ and $a^3\Pi_1$ states in the 193 nm photodissociation region,[262] ii) on the spin polarization of atoms in molecular photodissociations of HCl,[276] and iii) on the orientation and alignments of Br photofragments, and branching ratios HBr.[277] In 2004, two more important papers were published on the VMI applications for HCl and HBr. The first, by Manzhos *et al*.[278] reported angular distributions of H atom photofragments of HCl and HBr via two-photon REMPI state selection. Therein a formalism for the description of angular momentum polarization produced by two-photon absorption was presented and applied to a theoretical analysis of angular resolved data from single photon photodissociation of the $E^1\Sigma^+$ and $H^1\Sigma^+$ Rydberg states in HCl and HBr. The second paper from 2004, by Romanescu *et al*.[279] presented REMPI and VMI experimental results of the $E^1\Sigma^+$ state and ion-pair states of HCl, in order to inspect the superexcited states involved in the photofragmentations processes of HCl above the ionization potential. Therein, branching ratios between autoionization and dissociation channels for different intermediate states were explained in terms of their electron configurations. This was the first time that competition between autoionization and dissociation into H*(n = 2) + Cl and H + Cl*(4s, 4p, 3d) was observed.

The year 2006 was another momentous year for VMI studies of HCl and HBr. Besides a paper on computed potential energy curves, transition dipole moments, and spin-orbit coupling matrix elements for HBr, by A. G. Smolin *et al*.,[125] several other noteworthy publications appeared in the literature. Firstly, C. Romanescu and H.-P. Loock reported on the photodissociation and photoionization dynamics via photoelectron imaging following 2 + 1 REMPI.[280] Therein it was found that the (relatively) unperturbed $F^1\Delta_2$ and $i^3\Delta_2$ Rydberg states autoionize directly into the ionic state whilst excitation via the $E^1\Sigma^+$, $g^3\Sigma^-$, $H^1\Sigma^+$ and $V^1\Sigma^+$ intermediate states results in the formation of vibrational progressions of HBr^+ as well as electronically excited photofragments. A. I. Chichinin *et al*.[281] probed both wells of the adiabatic $B^1\Sigma^+$ state, i.e. the E state and the ion-pair states, by two-photon REMPI and VMI to uncover various information about the photoionization processes, including symmetries of the superexcited states involved, and velocity distributions of formed H^+ fragments. Furthermore, A. I. Chichinin *et al*.[282] published a detailed theoretical description of the intermediate state polarization and angular distributions of photofragments in REMPI experiments, by correlating their findings with their previous experimental work on the $B^1\Sigma^+$ state. Building on this, C. Romanescu & H.-P. Loock[283] reported an in depth examination of

the proton formation pathways in both HCl and HBr comprising superexcited states and their photodynamics.

In 2010, Kauczok *et al*.[284] examined selected *Q* lines of the $F^1\Delta_2(1)$ and $f^3\Delta_2(0)$ Rydberg states and the $V^1\Sigma^+(14)$ ion-pair vibrational states spectra for HCl with REMPI coupled with 3D-VMI. These rotational lines were selected because they had been studied by mass resolved REMPI by the Kvaran group,[227] who found evidences of perturbations between the Rydberg states and the ion-pair states. Those observations as well as interpretations, regarding the involvement of gateway states in the photodynamical process, were corroborated with these results.

After a comprehensive and concise overview article on the electron structure and photodynamics of the HCl molecule by Maul *et al*.,[285] the majority of the published papers on the photoexcitations of HCl as well as HBr have been published by Kvaran's group[229, 230, 232, 233] though a couple of additional articles are noteworthy. Firstly, Poretskyi *et al*.,[286] by using HCl as a benchmark molecule, managed to image both positive and negative product ions to study the photoion-pair formation process via REMPI and thus to identify the gateway states leading to photoion-pairs. Since the 3D-VMI technique provides complete information about fragment quantum states, momentum vector distributions as well as spatial fragment anisotropies, the simultaneous detection of positive and negative ions greatly facilitates the data analyses of ion-pair formation and relevant fragmentation processes. Secondly, Broderick *et al*.[287] demonstrated that two-color Rydberg state excitation of hydrogen atoms using a circularly polarized tagging laser can be combined with pulsed-field ionization to allow for direct VMI of the hydrogen atom spin polarization. This technique was used to measure the coherent spin polarization in HBr photodissociation.[287]

1.5.2 HI

The HI molecule has been the subject of study by a number of experimental techniques as previously mentioned. Whereas a majority of these techniques (including VMI and *ab initio* calculations) have been utilized to study the direct photodissociation band,[132, 135, 136, 288-293] a few more have been focused on the high energy excitation dynamics. As a matter of fact, HI was one of the first molecules to be inspected with the coherent control technique in which the molecule was simultaneously excited above its ionization potential *via* two competing pathways.[294-296] These paths were absorption of three ultraviolet photons of frequency ω_1 and one ultraviolet photon of frequency $\omega_3 = 3\omega_1$. Through several implementations of this technique, mechanisms involving autoionization and predissociation were proposed.[294-299]

In 2000 Regan *et al*.[300] were among the first to incorporate the VMI technique into the REMPI experimental scheme. They employed three-photon REMPI excitation, achieving higher excitation energies than previous absorption[139, 142, 145] and REMPI experiments.[215, 216, 218] They reported mass resolved REMPI spectra, and H^+ ion images for several new $\Omega = 0$ and $\Omega = 3$ Rydberg states and obtained their corresponding rotational constants. This study revealed two different mechanisms for H^+ formation. One through autoionization to high vibrational levels of the ionic states and one through repulsive superexcited states to form H*(n = 2) atoms. These routes are analogous to those revealed later for HCl and HBr.[279, 280]

A year later, Loock *et al*.[301] employed the VMI technique to image the iodine fragments that were formed via two-photon resonances to the $F^1\Delta_2(0)$ and $I^1\Delta_2(0)$ Rydberg states, followed by immediate excitation of a third photon above the dissociation continuum of the ionic

states. These images allowed Loock *et al*. to clarify some of the fragment formation channels involved in high energy excitations of the molecule. Furthermore, it was found that nonadiabatic interactions between the $A^2\Sigma^+$ excited ionic state and repulsive ionic states take place in this excitation region and thus, mechanisms based on these interactions were proposed.

Although not VMI based, but involving 2D imaging, Y. Hikosaka & K. Mitsuke contributed as well to the knowledge of electronic structure and the photodynamics above the ionization potential of HI by using two-dimensional photoelectron spectroscopy.[302] They managed to identify a $[A^2\Sigma^+]5d\pi$ superexcited state which acts as an intermediate state prior to autoionization.

1.6 Exploring the utilities

1.6.1 Hydrogen halides and astrophysics

In the cosmic context, the lighter hydrogen halides HF and HCl have proven to be omnipresent in interstellar clouds.[303, 304] Although their presence was initially merely theoretically predicted,[305-307] their presence has now been firmly established. Furthermore, the chemical properties of HF and HCl in the interstellar medium have been studied extensively (e.g. see Refs.[308, 309] and references therein for HF and Ref. [304] and references therein for HCl). The intrigue of these molecules to the astrophysical community stems from the uniqueness of their thermochemical properties. These properties involve two distinct thermochemical considerations. Firstly, the dissociation energy of the neutral hydrogen halide (HX) determines whether the neutral halogen (X) can react exothermically with H_2 to form HX. Secondly, the dissociation energy of the hydrogen halide molecular ion (HX^+) similarly determines whether halogen cations (X^+) can react exothermically with H_2 to form HX^+. In the interstellar medium F is the only atom that fulfills the first consideration whilst Cl^+ is the only ion that fulfills the second.[310]

The heavier hydrogen halides HBr and HI, on the other hand, have not been found in interstellar molecular clouds, but have been tentatively suggested as sources of bromine and iodine atomic lines in spectra of white dwarfs.[311]

There is, however, another interesting utility of these species in the astrophysical context, which is that of spectra calibrations in the search for extrasolar planets. Early designs of absorption-cell spectrographs used HF as the absorbing medium, but due to its lethality and corrosive nature, it was abandoned for a more practical, less toxic molecule, namely I_2.[312] The absorption spectrum of I_2 can only be described as a forest of absorption lines originating from molecular and atomic transitions, but using these lines in specifically designed iodine cells to calibrate stellar spectra,[313, 314] has resulted in the discovery of a wealth of extrasolar planets.[315]

1.6.2 Hydrogen halides in the atmosphere

Though not by any means abundant in the atmosphere, the photochemistry of the hydrogen halides is of enormous importance to our species. The importance stems from the photochemically induced catalytic cycles involving chlorine and bromine atoms which result in ozone destruction in the stratosphere.[316] In the troposphere, however, chlorine and bromine atom reactions are of minor importance due the efficient formation of the relatively

stable HCl and HBr molecules which are formed by reactions of the halogen atoms with CH_4 or HCHO, respectively, and subsequent rainout.[317] This is not the case for iodine due to the low H-I bond energy. The major reaction pathway of iodine atoms in the atmosphere is likely to be with ozone (O_3) to form IO and molecular oxygen (O_2)[318] but a plethora of other reactions are involved in the photochemistry of iodine containing molecules which have to be considered during modelling of halogen involved ozone depletion.[317-319]

Whereas the Cl and Br atoms in the atmosphere usually originate from sea salt,[320] the iodine atoms are largely derived photochemically from several biogenic alkyl iodides such as CH_2I_2, C_2H_5I, CH_3I, which are released from the sea. (see Refs.[321, 322] and references therein).

1.6.3 Enhancements in physical constants

Another intriguing potential for this work may also be found in the search for strong effects of the variation of fundamental constants. It has been suggested that the molecular ions of the heavy hydrogen halides, namely HBr^+ and HI^+ and their deuterated counterparts, are suitable candidates for future studies of variations of the fine structure constant, $\alpha = e^2/\hbar c$, and the proton to electron mass ratio, $\mu = m_p/m_e$.[323] Molecular spectra are namely quite sensitive to both of these fundamental constants and it is possible to search for variations in the values in cases of near-degenerate energy levels (see discussion below concerning perturbation theory).

1.6.4 Heavy Rydberg states

A novel approach to the utility of studies on ion-pair states, are heavy Rydberg states. Heavy Rydberg states are positive-negative ion-pairs at large internuclear separation which are weakly bound by the Coulombic electric force. While traditional ion-pair states have been known since the original work of L. Pauling,[27] the existence of heavy Rydberg states have only recently been theorized[324] and their existence experimentally verified.[325-329]

The most recent works on heavy Rydberg states are twofold. Firstly, dynamics and lifetimes of intermediate states formed in the reactions of excited Rydberg K atoms with several halogen containing molecules such as SF_6 and CCl_4[325], as well as CH_2Br_2 and CF_3I.[326] Second, quantum defect analysis of ion-pair states (obtained from various spectral techniques) have been used to locate the effects of heavy Rydberg states in the diatomic halogens and interhalogens I_2, ICl, Cl_2, IBr,[327] and Br_2.[328]

On the horizon, REMPI experiments on HCl and DCl are being prepared in cooperation with R. J. Donovan and K. P. Lawley who have expressed a keen interest in further collaboration on investigating heavy Rydberg states in the hydrogen halides with the REMPI technique.

1.6.5 Chemical Synthesis

The final but perhaps the most tentative utility of this work involves molecular photosynthesis *via* state selection with multiphoton absorption. By reaching an electronically excited state, the molecule's electron configuration (and hence, the electron distribution) significantly changes. Thereby, the reactivity of the molecule can change dramatically and the reaction spectrum of a family of compounds can be considerably broadened.[330] In some instances, using photochemical steps significantly shortens the timescale of syntheses but overall, by photochemically activating a substrate is usually performed without additional

reagents which diminishes the formation of dangerous byproducts. Axiomatically, light activated syntheses are a subject of great interest to the field of green chemistry.[331]

The utility of the VMI technique has is also being explored in terms of photo-catalyzed organic reactions. E.g. Diels-Alder (RDA) reactions of cyclohexene, 1-methylcyclohexene, and 4-methylcyclohexene following photoexcitations at 193 nm, have been inspected in terms of product angular distributions and translational energy distributions to elucidate the dynamics of the RDA process.[332]

1.7 Summary of this work

1.7.1 REMPI of HBr

In Article 1[233] entitled: "Photofragmentations, state interactions, and energetics of Rydberg and ion-pair states: Two-dimensional resonance enhanced multiphoton ionization of HBr via singlet-, triplet-, $\Omega = 0$ and 2 states", the two-photon resonance excitation region 79 040 – 80 300 cm^{-1} was analyzed. It yielded characterizations of state interactions between the $F^1\Delta_2(v' = 1)$ Rydberg state and $V^1\Sigma^+(v' = m + 7)$ ion-pair state, on the one hand, and on the other, interactions between the $E^1\Sigma^+(v' = 1)$ and $H^1\Sigma^+(v' = 0)$ Rydberg states, and the ion-pair vibrational states.

Large varieties of J' dependent line widths, line intensities, and line positions in mass resolved REMPI spectra, were found to be indicative of a number of different predissociation channels connected *via* quantum inference effects. Observed bromine atomic lines were found to support the significance of Rydberg state predissociation channels. Finally, a new Rydberg state was observed and assigned to the $k^3\Pi_0(0)$ progression.

1.7.2 REMPI of HI

Four articles on HI are included in this thesis whose main purpose is to elucidate and catalog energetics, state interactions, and photofragmentation processes relevant to the high energy region of the molecule.

In Article 2[234] entitled: "New REMPI observations and analyses for Rydberg and ion-pair states of HI", the two-photon excitation region 69 600 cm^{-1} – 71 500 cm^{-1} was explored and cataloged in terms of Rydberg and ion-pair states. Therein, the $E^1\Sigma^+$ and $H^1\Sigma^+$ Rydberg states were re-assigned. Furthermore, new states were discovered or observed in REMPI for the first time, and more. Unfortunately, the paper suffers from minor errors which are corrected in chapter 6 and will be published as an erratum.

In Article 3[235] entitled: "Photofragmentation, state interaction, and energetics of Rydberg and ion-pair states: Resonance enhanced multiphoton ionization of HI", spectral perturbations, previously observed in article 2 are addressed and interpreted in terms of state interactions. The spectral perturbations are classified according to line-shifts, line-intensity and line-width alterations, and an overall dynamical scheme, describing the interacting systems, is presented.

In Article 5[236] entitled: "State interactions and illumination of hidden states through perturbations and observations of new states: High energy resonance enhanced multiphoton ionization of HI", Rydberg and ion-pair states in the excitation region of 72 300 cm^{-1} – 74

600 cm^{-1} are analyzed and catalogued in terms of interacting systems. Furthermore, observed perturbations are utilized to assign hidden (non-observable) states.

In Article 6[237] entitled: "Revealing photofragmentation dynamics through interactions between Rydberg states: REMPI of HI as a case study", interactions between the $j^3\Sigma^-(0)$ and $k^3\Pi_1(2)$ Rydberg states are thoroughly analyzed. The relative yield of ionized fragments is utilized to illuminate the photodissociation and photoionization pathways present in multiphoton ionization of HI following the resonance excitations.

1.7.3 REMPI coupled with VMI of HBr

In Article 4[333] entitled: "Rydberg and valence state excitation dynamics: a velocity map imaging study involving the *E*-*V* state interaction in HBr" the photoexcitation dynamics of the $E(0)$ Rydberg state and the $V(m + i)$, i =4, 5, 6, 7, 8, 9 ion-pair states are investigated by the velocity map imaging technique. Images relevant to resonance excitations to several rotational levels of these states were recorded and the kinetic energy releases (KER) and angular distributions determined. Analysis of the data and comparison with mass resolved REMPI spectra allowed detailed descriptions of the excitation dynamics involved.

Article 7 is presented as a "manuscript in progress". The final draft of the article requires a little more work but the essential results and analyses have been performed and are presented here. The article is entitled: "Rydberg and valence state excitation dynamics: One and two color VMI study of singlet states in HBr" and presents one and two color VMI experiments on HBr where the $H(0)$ and $E(1)$ Rydberg state and $V(m + 7)$ and $V(m + 8)$ ion-pair states are explored. One color H^+ images reveal the effects of state interactions on photofragmentations and two color Br^+ images give insights into the dynamics of one-photon dissociations as well as predissociation in the two-photon energy region 79 100 – 80 700 cm^{-1}.

2 Theory

The advent of quantum mechanics signified a momentous paradigm shift for the field of chemistry. Armed with a calculated description of electronic configurations within atoms, scientist were able to predict various physical properties of atoms and molecules.

Soon after the original publication by E. Schrödinger,[334] and its complementary matrix representation by W. Heisenberg,[335] the theoretical aspects of electronic behavior were soon manipulated to include atoms as well as molecules.

The Schrödinger equation is uniquely formulated to extract the energies and properties of a given system. Or

$$\mathcal{H}\Psi = E\Psi \qquad (1)$$

where E denotes the energy of the corresponding wavefunction, Ψ, and $\mathcal{H}$ denotes the Hamiltonian operator, which in three dimensions takes the form

$$\mathcal{H} = -\frac{\hbar^2}{2m}\nabla^2 + U_0 \qquad (2)$$

where ħ is Dirac's constant ($h/2\pi$), m is the mass of the particle, ∇ is the gradient operator, and U_0 is the potential energy of the particle.

Later inducted by P. A. M. Dirac, the Dirac notation amalgamated the quantum notations by Schrödinger and Heisenberg, respectively, with so-called brackets (i.e. brahs and kets). In Dirac notation, the Schrödinger equation is written as

$$\mathcal{H}|\Psi_n\rangle = E_n|\Psi_n\rangle \qquad (3)$$

The Dirac notation will be utilized throughout most of the following text.

Whereas the Schrödinger equation can be solved exactly only for a few systems, solutions to most molecular systems require approximate methods. One of the most common methods used is perturbation theory.

2.1 Perturbation theory

"Most quantum problems cannot be solved exactly with the present resources of mathematics, as they lead to equations whose solutions cannot be expressed in finite terms with the help of ordinary functions of analysis." This is how P. A. M. Dirac opened his discussion about perturbation theory in the very first textbook written on quantum mechanics.[336] There is a subtle elegance embedded in the concision of Dirac's phrasing of the problem. i) It explicitly realizes the enormity of the problem of applications of quantum mechanics to larger systems (such as molecules) and ii) it expresses a somewhat optimistic opinion that mathematical rigor may eventually find solutions to some of those problems.

In short, perturbation theory consists in splitting up the Hamiltonian into two parts, one of which is considered as the Hamiltonian of a simplified or unperturbed system and another; an additive factor that requires small corrections depending on the nature of the perturbation. Explicitly, perturbation theory is a systematic procedure for obtaining approximate solutions to perturbed systems by building on the exact solutions to the corresponding unperturbed system.

In the context of this thesis, it turns out that more sophisticated mathematics are not required since the perturbation theory adequately allows us to approximate the interaction strengths between excited states of the hydrogen halides.

2.1.1 Non-degenerate perturbation theory

For perturbed systems, we write the Hamiltonian as the sum of two terms

$$H = H^0 + \lambda H' \quad (4)$$

where H' is the perturbation term, H^0 represents the unperturbed system and λ is a small numerical factor. We then write the wave function, ψ_n, and the energy, E_n, as power series in λ

$$\psi_n = \psi_n^0 + \lambda\psi_n^1 + \lambda^2\psi_n^2 + \cdots \quad (5)$$

$$E_n = E_n^0 + \lambda E_n^1 + \lambda^2 E_n^2 + \cdots \quad (6)$$

where ψ_n^1 and E_n^1 are the first order corrections to the *n*th eigenfunction and eigenvalue, respectively; ψ_n^2 and E_n^2 are second order corrections, etc. Furthermore,

$$E_n^1 = \langle\psi_n^0|H'|\psi_n^0\rangle \quad (7)$$

i.e. the first order correction to the energy of a perturbed state equals the expectation value of the perturbation, in the unperturbed state. The first-order correction of the eigenfunction, ψ_n^1, becomes

$$\psi_n^1 = \sum_{m\neq n} \frac{\langle\psi_m^0|H'|\psi_n^0\rangle}{(E_n^0 - E_m^0)}\psi_m^0 \quad (8)$$

For a full derivation of these results see e.g. Ref.[337].

Further corrections to the wavefunction and the energies are possible but are not necessarily useful in praxis (at least for this thesis). For higher order corrections see Refs.[338] and [339].

This approximation is only valid when $m \neq n$, i.e. when the unperturbed energies are non-degenerate. This approximation is, therefore, often referred to as "non-degenerate perturbation theory". If $m = n$, this approximation becomes invalid (as we divide by zero) so in those cases a different method is used, namely "degenerate perturbation theory".

2.1.2 Degenerate perturbation theory

If the unperturbed states are degenerate, for example if two distinct wavefunctions (ψ_a^0 and ψ_b^0) share the same energy (or eigenvalues), then our previous expressions fail. Hence,

$$H^0\psi_a^0 = E^0\psi_a^0, \qquad H^0\psi_b^0 = E^0\psi_b^0, \qquad \langle\psi_a^0|\psi_b^0\rangle = 0 \tag{9}$$

We can choose any linear combination of these wavefunctions

$$\psi^0 = \alpha\psi_a^0 + \beta\psi_b^0 \tag{10}$$

that is still an eigenfunction of H^0, with an eigenvalue E^0. If we substitute ψ^0 and E^0 into equations (5) and (6) and insert into equation (4), we obtain

$$H^0\psi^0 + \lambda(H'\psi^0 + H^0\psi^1) + \cdots = E^0\psi^0 + \lambda(E^1\psi^0 + E^0\psi^1) + \cdots \tag{11}$$

which simplifies to

$$H'\psi^0 + H^0\psi^1 = E^1\psi^0 + E^0\psi^1 \tag{12}$$

By taking the inner product with ψ_a^0

$$\langle\psi_a^0|H'\psi^0\rangle + \langle\psi_a^0|H^0\psi^1\rangle = E^1\langle\psi_a^0|\psi^0\rangle + E^0\langle\psi_a^0|\psi^1\rangle \tag{13}$$

which, since $\langle\psi_a^0|H^0\psi^1\rangle = E^0\langle\psi_a^0|\psi^1\rangle$, simplifies to

$$\alpha\langle\psi_a^0|H'|\psi_a^0\rangle + \beta\langle\psi_a^0|H'|\psi_b^0\rangle = \alpha E^1 \tag{14}$$

Similarly by taking the inner product with ψ_b^0.

$$\alpha\langle\psi_b^0|H'|\psi_a^0\rangle + \beta\langle\psi_b^0|H'|\psi_b^0\rangle = \beta E^1 \tag{15}$$

Now, since $\langle\psi_a^0|H'|\psi_a^0\rangle$ and $\langle\psi_b^0|H'|\psi_b^0\rangle$ give the zero-order level energies, E_a^0 & E_b^0, for the unperturbed states ψ_a^0 & ψ_b^0, and $\langle\psi_a^0|H'|\psi_b^0\rangle$ & $\langle\psi_b^0|H'|\psi_a^0\rangle$ give the interaction strengths (or matrix elements) between the states of concern we can compress equations (14) & (15) into the generalized matrix form:

$$\begin{pmatrix} E_a^0 & W_{ab} \\ W_{ba} & E_b^0 \end{pmatrix}\begin{pmatrix}\alpha\\ \beta\end{pmatrix} = E^1\begin{pmatrix}\alpha\\ \beta\end{pmatrix} \tag{16}$$

Where $W_{ba}{}^* = W_{ab}$ represent the interaction strength parameter or the off-diagonal matrix elements. Now the eigenvalues of the Hamiltonian matrix equal the energies of the perturbed states with eigenkets $\begin{pmatrix}\alpha\\ \beta\end{pmatrix}$, expressed as

$$E_{ab}^1 = \frac{1}{2}\left[E_a^0 + E_b^0 \pm \sqrt{(E_a^0 - E_b^0)^2 + 4|W_{12}|^2}\right] \tag{17}$$

Finally, in cases of three interacting states the matrix equation takes the form

$$\begin{pmatrix} E_a^0 & W_{ab} & W_{ac} \\ W_{ba} & E_b^0 & W_{bc} \\ W_{ca} & W_{cb} & E_c^0 \end{pmatrix} \begin{pmatrix} \alpha \\ \beta \\ \gamma \end{pmatrix} = E^1 \begin{pmatrix} \alpha \\ \beta \\ \gamma \end{pmatrix} \quad (18)$$

and for *N* interacting states,

$$\begin{pmatrix} E_a^0 & \cdots & W_{aN} \\ \vdots & \ddots & \vdots \\ W_{Na} & \cdots & E_N^0 \end{pmatrix} \begin{pmatrix} \alpha \\ \vdots \\ \omega \end{pmatrix} = E^1 \begin{pmatrix} \alpha \\ \vdots \\ \omega \end{pmatrix} \quad (19)$$

2.2 Quantum numbers

2.2.1 Commutation – quantum communication

Some of the deepest mysteries of quantum mechanics can be traced to a single factoid: "Position and momentum do not commute!" Commutation is a way for us to assess how well certain quantum properties "communicate". Simply written, the commutation of two operators, A & B, is expressed as

$$[\mathbf{A}, \mathbf{B}] = \mathbf{AB} - \mathbf{BA} \quad (20)$$

If [**A**, **B**] = 0, then the operators commute and their relevant properties *can be simultaneously measured*. However, if [**A**, **B**] ≠ 0, then the operators do not commute, in which case the corresponding properties cannot be simultaneously measured. Thus, as made famous by the Heisenberg uncertainty principle, you cannot simultaneously measure the position and momentum of a particle, since the relevant operators do not commute. In other words, they have dissimilar eigenstates and there is no communication between the two on a quantum scale basis.

2.2.2 Principle characters and operators in the monatomic & diatomic show

Solving the Schrödinger equation for the hydrogen atom yields solutions which depend on quantum numbers that determine the electron distribution (orbitals) around the nuclei and the corresponding energy. The quantum numbers (n, l, m_l) that determine the states of the hydrogen atom are defined in Table 1.

Table 1 Quantum numbers obtained from the Schrödinger equation for the hydrogen atom and their values.

Quantum number	*Value*	*Name*
n	1, 2, 3, …	The principle quantum number
l	0, 1, 2, … (n – 1)	The azimuthal quantum number
***m*$_l$**	0, ±1, ±2, …(±l)	The magnetic quantum number

A combination of quantum numbers provides a probability function for finding an electron, hence an overall shape and symmetry of a given electron orbital in an atom. The principle quantum number, *n*, describes the size of an orbital, i.e. the size of the orbital increases with *n*. The azimuthal quantum number, *l*, describes the number of orbital nodes and hence, the shape of the orbital. It also gives the orbital angular momentum, *L*,

$$L = \hbar\sqrt{l(l+1)} \qquad (21)$$

The magnetic quantum number, m_l, specifies the orientation in space of an orbital and refers to the projection of the angular momentum onto the z axis (L_z) for any given direction.

$$L_z = m_l\hbar \qquad (22)$$

For quantum systems, angular momentum is of major importance. For atoms in general, the essential quantum numbers are the principal quantum number (*n*), the total spin quantum numbers (*S*), the orbital angular momentum quantum number (*L*), the total angular momentum quantum number (*J*), and the magnetic quantum number (M_J). These quantum numbers are considered *good quantum numbers* since the corresponding Hamiltonian operators commute and thus, their relevant properties can be measured simultaneously (see above). The commutation is based on the symmetry properties of the wavefunctions and orbitals involved. Therefore, the spherical symmetry of atoms makes these quantum numbers good (see Figure 1).

For diatomic molecules, however, we lose symmetric properties by replacing the spherical symmetry with cylindrical symmetry. During this process good quantum numbers are lost and therefore, new quantum numbers need to be specified. Specifically for diatomic molecules the following quantum numbers are considered to be “good”.

L : for electronic orbital angular momentum

S : for electronic spin angular momentum

J : for total angular momentum ($J = L + S$)

N : for total angular momentum excluding electron spin ($N = J - S$)

R : for nuclear rotational angular momentum ($R = N - L$)

Furthermore, we can express the corresponding angular momenta as vectors and relevant operators,

$$\mathbf{A}^2 = \mathbf{A}_x^2 + \mathbf{A}_y^2 + \mathbf{A}_z^2 \qquad (23)$$

where **A** = **L**, **S**, **J**, **N**, **R** are expressed in terms of their three spatial components.

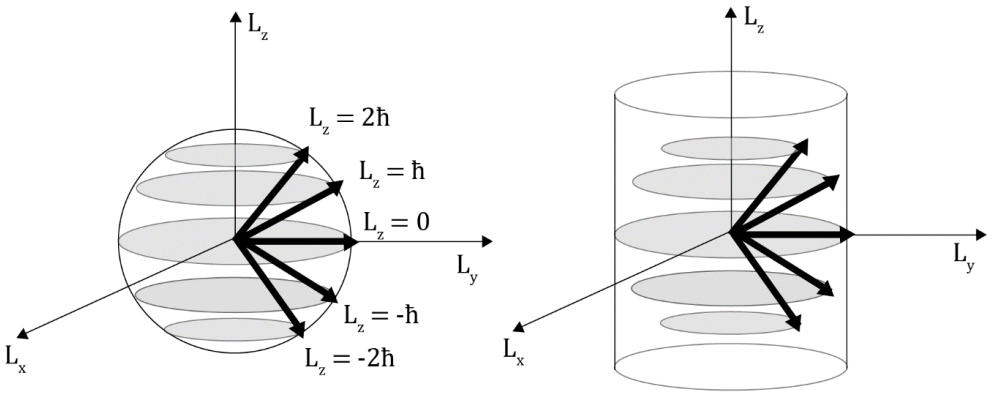

Figure 1 The spherical symmetry of atoms makes the magnetic quantum number, m_l, good. For diatomic molecules which exhibit cylindrical symmetry, the spherical symmetric properties are lost and thence, new good quantum numbers need to be defined.

It is also important to introduce the heightening and lowering operators who, when applied to a specific quantum system, either increases of decreases that quantum number of the system by one. Thus, if we apply the operators $\mathbf{A}^+$ or $\mathbf{A}^-$ (who correspond to heightening and lowering operators of the quantum number A) to a quantum system, we get

$$\mathbf{A}^+|A\rangle = |A+1\rangle \quad (24)$$

$$\mathbf{A}^-|A\rangle = |A-1\rangle \quad (25)$$

These operators are expressed as

$$\mathbf{A}^\pm = \mathbf{A}_x \pm i\mathbf{A}_y \quad (26)$$

Furthermore, we need to define the following important quantum numbers and corresponding angular momenta, which are tied to the molecule-fixed frame of reference. (The quantum numbers we have hitherto dealt with have all been defined in the space fixed reference.)

Λ : for electronic orbital angular momentum

Σ : for electronic spin angular momentum

Ω : for total electronic angular momentum ($\Omega = \Lambda + \Sigma$)

Their vectorial forms are $\mathbf{\Lambda}$, $\mathbf{\Sigma}$, and $\mathbf{\Omega}$, respectively, which include the same three spatial components as well as heightening and lowering operators mentioned above.

2.2.3 Term symbols & symmetry

An abbreviated description of the angular momentum quantum numbers in a multi-electron system is commonly used. Term symbols are used to describe states with respect to good quantum numbers. Thus, the symbols

$$^{2S+1}\mathrm{L}_J$$

$$^{2\Sigma+1}\Lambda_\Omega$$

are used for atoms and molecules, respectively. However, instead of the numerical values for L and Λ, classical orbital designations are used (see Table 2).

Table 2 Orbital designations according to electronic angular momentum quantum numbers.

L	*Atomic orbital*	*Λ*	*Molecular orbital*
0	S	0	Σ
1	P	1	Π
2	D	2	Δ
3	F	3	Φ

The term symbols provide us with all of the information necessary to deduce the symmetry of the electron orbital in question. Therefore, for future reference, term symbols will be widely used regarding discussions involving symmetry or symmetry properties. I.e. symmetry and term symbols will be used interchangeably.

2.2.4 Lambda doubling - Parity

Molecular states in diatomic molecules with $\Lambda \neq 0$ (Π states, Δ states, Φ states, etc.) are doubly degenerate in the absence of rotation. I.e. these are doubly degenerate states, that differ in the direction of the projection of the orbital angular momentum onto the internuclear axis. This phenomenon is commonly referred to as lambda doubling.

Diatomic molecules with $\Lambda = 0$ (Σ states), however, are not changed upon reflection through the internuclear axis. Σ states are, therefore, nondegenerate. If the wavefunction of the Σ state is not altered by the reflection operation, then the state is classified as a Σ^+ state. If the wavefunction changes sign, however, then the state is classified as a Σ^- states.

2.3 Diatomic energy distribution

In this theoretical overview we now, logically, present expressions for the unperturbed energies, E^0. In 1932 J. L. Dunham showed how a generalized description of the energy levels of molecules could be extracted from solutions to the Schrödinger equation by applying the W.K.B method on a vibrating rotor,[340, 341] which since has been coined the Dunham expansion.

$$E_{\mathrm{v},J} = \sum_{l,m_l=0}^{l_{max}m_{l,max}} Y_{lm}\left(\mathrm{v}+\frac{1}{2}\right)^l [J(J+1)]^{m_l} \qquad (27)$$

Here, v denotes the vibrational quantum number of a molecule, J denotes the rotational quantum number, $E_{v,J}$ denotes the v and J dependent energies (i.e. the rovibrational energies of the molecular system in question), l is the azimuthal quantum number, m_l is the magnetic quantum number, and Y_{lm} are the Dunham parameters (see Table 3). The Dunham parameters are usually derived with spectroscopic techniques, employing a least squares analysis to fit analytical functions to experimental data.

Table 3 Dunham parameters appropriated towards the sign conventions used in the book by K. P. Huber and G. Herzberg.[342]

	***m* = 0**	***m* = 1**	***m* = 2**	***m* = 3**	***m* = 4**
***l* = 0**	$Y_{0,0} = E_{el}$	$Y_{0,1} = B_e$	$Y_{0,2} = -D_e$	$Y_{0,3} = H_e$	$Y_{0,4} = L_e$
***l* = 1**	$Y_{1,0} = \omega_e$	$Y_{1,1} = -\alpha_e$	$Y_{1,2} = -\beta_e$		
***l* = 2**	$Y_{2,0} = -\omega_e x_e$	$Y_{2,1} = \gamma_e$			
***l* = 3**	$Y_{3,0} = \omega_e y_e$				
***l* = 4**	$Y_{4,0} = \omega_e z_e$				

Energies in diatomic molecules can be separated according to the three types of internal excitations, which correspond to the electronic, vibrational, rotational energies.

2.3.1 Electronic energies – Rydberg and valence states

The electronic energy of a molecule depends on the internuclear distance. For the average internuclear distance (r_e), the electronic energy is commonly referred to as T_e. For molecular Rydberg states, a simplified formalism is utilized. Rydberg states are typically the result of an excitation of an electron in a molecular orbital (MO) to a high energy atom-like orbital. The energies of Rydberg states that converge to the ground state of the molecular ion can be formulated with the modified Rydberg formula

$$T_e = IE - \frac{\Re}{(n-\delta)^2} \qquad (28)$$

where IE is the ionization potential of the molecule, $\Re$ is the Rydberg constant, n is the principal quantum number and δ is the quantum defect of the excited molecular orbital. The quantum defect value arises from the shielding effects of the core electrons. Thus, Rydberg electrons, with a low value of the orbital angular momentum, penetrate relatively easily through the core electron density close to the atomic nuclei which results in significant lowering of the energy levels. In order to account for this deviancy in the electron's behavior, the quantum defect is introduced. Its values typically range from almost zero for *f* orbitals to about $n - 2$ for *s* orbitals.

When using LCAO in its simplest form, two atomic orbitals are combined to form molecular orbitals. The molecular orbitals vary in energy in accordance with the nature of the atomic

orbitals involved. E.g. two s orbitals combine to make a σ orbital but two p orbitals can combine in two different ways to form either a σ or a π orbital. To keep track over the different combinations, it is handy to specify the type of atomic and molecular orbitals involved as λ (see Table 4).

Table 4 **Possible LCAO molecular orbitals formed by combining specific atomic orbitals.**

Atomic orbitals, l	*Bonding molecular orbitals, λ*
s	*sσ*
p	*pσ*, *pπ*
d	*dσ*, *dπ*, *dδ*
f	*fσ*, *fπ*, *fδ*, *fϕ*

Whereas Rydberg states are typically accessed by exciting electrons to high energy atomic-like MOs, valence states are the result of excitations of electrons within MOs formed by linear combinations of valence atomic orbitals. Logically, this weakens the bond between the two atoms of concern, resulting in i) the complete dissociation of the molecule (repulsive or continuum state) or ii) the average internuclear distance between the atoms being largely increased. An example of the latter distinction is referred to as an ion-pair state which in the case of the hydrogen halides, corresponds to an electron density transfer from the hydrogen atom (H) to the halogen atom (X), represented as H^+X^-.

2.3.2 Vibrational energies

The vibrational energy is described empirically by a truncated series, in v + 1/2.

$$G(\mathrm{v}) = \omega_e\left(\mathrm{v}+\frac{1}{2}\right) - \omega_e x_e\left(\mathrm{v}+\frac{1}{2}\right)^2 + \omega_e y_e\left(\mathrm{v}+\frac{1}{2}\right)^3 + \omega_e z_e\left(\mathrm{v}+\frac{1}{2}\right)^4 + \cdots \quad (29)$$

G is traditionally used to denote the vibrational energy, v is the vibrational quantum number (v = 0, 1, 2, …), ω_e is, to the first approximation, the harmonic vibrational wavenumber,

$$\omega_e = \frac{1}{2\pi c}\sqrt{\frac{k}{\mu}} \quad (30)$$

where *k* is the force constant of the molecule, formulated as the second derivative of the internuclear potential energy function *U*(*R*), as dictated by Hooke's law for springs.

$$k = \left(\frac{d^2U(R)}{dR^2}\right)_{R=r_e} \quad (31)$$

2.3.3 Rotational energies

Classically, rotational energies, denoted by F, are described empirically by a truncated power series in $J(J+1)$, where J symbolizes the rotational quantum number.

$$F(J) = B_{\mathrm{v}}J(J+1) - D_{\mathrm{v}}[J(J+1)]^2 + H_e[J(J+1)]^3 + L_e[J(J+1)]^4 \ldots \quad (32)$$

B_{v} is the rotational constant and D_{v} is the centrifugal distortion constant for the vth vibrational level, both represented empirically by a truncated power series in v + ½.

$$B_{\mathrm{v}} = B_e - \alpha\left(\mathrm{v}+\frac{1}{2}\right) + \gamma\left(\mathrm{v}+\frac{1}{2}\right)^2 + \cdots \quad (33)$$

$$D_{\mathrm{v}} = D_e - \beta\left(\mathrm{v}+\frac{1}{2}\right) + \cdots \quad (34)$$

The constants B_e and D_e are the rotational and centrifugal distortion constants of the individual electronic states, respectively. B_e is dependent on the reduced mass,

$$\mu = \frac{m_1 m_2}{m_1 + m_2} \quad (35)$$

and equilibrium internuclear distance, r_e.

$$B_e = \frac{\hbar}{4\pi c \mu {r_e}^2} \quad (36)$$

2.3.4 Summary

Having found the total energy ($E^0{}_T$) of a diatomic molecule to consist of electronic (E^{el}), vibrational (G(v)), and rotational ($F(J)$) energies, we can write

$$E_T^0 = E^{el} + G(\mathrm{v}) + F(J) \quad (37)$$

to represent the unperturbed / zero order energy of a molecule. Therefore, the total Hamiltonian of a diatomic molecule can also be separated into three separate components, as will be dealt with in the next subsection.

2.4 The Born–Oppenheimer approximation

A year after the publication of the Schrödinger equation, M. Born and J. R. Oppenheimer published a paper on molecular quantum mechanics in 1927.[343] In this historical paper, approximations to the Schrödinger equation were proposed which went on to become the theoretical foundations upon which essentially everything that is known about the structure of bound states in molecules is based.

In essence, the Born-Oppenheimer (BO-) approximation exploits the disparity between the masses of atomic nuclei and electrons. The estimation is made that the electrons move very rapidly in comparison with the nuclei such that the energies of the electrons can be

determined for stationary nuclei. For a comprehensive historical perspective of the BO-approximation and its derivations see Ref.[344].

Without going into specific details, the BO-approximation reduces the total (or exact) Hamiltonian of a diatomic molecule into the following form

$$\mathbf{H} = \mathbf{H}^{el} + \mathbf{T}^{N}(R) + \mathbf{H}^{ROT} + \mathbf{H}^{SO} \quad (38)$$

Here, $\mathbf{H}^{el}$ essentially gives rise to the potential energy, as a function of the internuclear distance (i.e. the potential curve), of the molecule. It describes how the nuclei move in tandem with one another but is not representative of a physical observable. It is, therefore, more conceptual as a pedagogical tool to understand the bounds of molecular motions. $\mathbf{T}^{N}(R)$ is the radial variable of the Hamiltonian which gives rise to vibrational motions as function of *R*, the internuclear distance. $\mathbf{H}^{ROT}$ is the angular variable which gives rise to rotational motions, and $\mathbf{H}^{SO}$ originates from the relativistic treatment of the Hamiltonian to give spin-orbit interactions.

This form of the Hamiltonian can be applied to an approximation of the total wavefunction of the molecule (via the Schrödinger equation) in order to obtain satisfactory expressions of the energy levels. The wavefunction ($\psi_{i,v}^{BO}$) is a product of two functions

$$\psi_{i,v}^{BO} = \mathbf{\Phi}_{i,\Lambda,S,\Sigma}(r;R)\chi_{v}(R,\theta,\phi) \quad (39)$$

Here, $\mathbf{\Phi}_{i,\Lambda,S,\Sigma}(r;R)$ represents the electronic wavefunction and $\chi_{v}(R,\theta,\phi)$ is the vibration-rotation wavefunction. θ and ϕ specify the orientation of the internuclear axis (molecule-fixed coordinate system) relative to the laboratory coordinate system and *r* represents all the electron coordinates in the molecule-fixed system.

2.4.1 A closer look at perturbations

Having found a simplified expression of the molecular Hamiltonian for a diatomic system, we can now take a closer look at perturbations. As already mentioned in chapter 2.1, the off-diagonal matrix elements of the Hamiltonian represent the strength of a given perturbation between two interacting states (also called state mixing). Using the Dirac notation the Hamiltonian matrix can be represented as

$$\left\langle \mathbf{\Phi}_{i,\Lambda,S,\Sigma}\chi_{v_i}\middle|\mathbf{H}\middle|\mathbf{\Phi}_{j,\Lambda',S',\Sigma'}\chi_{v_j}\right\rangle \quad (40)$$

Since the Hamiltonian can be split up, as mentioned above, we can evaluate the off-diagonal matrix elements of each individual part where the off-diagonal matrix elements of $\mathbf{H}^{el}$ give the electrostatic perturbations, those of $\mathbf{T}^{N}(R)$ give the nonadiabatic perturbations, those of $\mathbf{H}^{ROT}$ give the rotational perturbations, and those of $\mathbf{H}^{SO}$ give the spin-orbit perturbations.

2.4.2 Diabatic vs adiabatic

The terms *diabatic* and *adiabatic* refer to the use of different potential curves to represent excited states corresponding to certain electron configurations. Considering their Greek origins, these terms are appropriately utilized. In Greek the word *diabatos* means “able to be crossed” whereas *adiabatos* means “incapable of being crossed”. In relation to potential

curves, the term *diabatic* means that a certain potential curve is calculated with a single electron configuration in mind so it can "cross curves" of states with different electron configurations. The term *adiabatic*, therefore means that a certain potential curve cannot cross to follow a path of an unchanged electron configuration, whereas the electron configuration changes. Depending on which representation (diabatic or adiabatic) is used, perturbations arise from different operators in the total Hamiltonian. For the hydrogen halides the $E^1\Sigma^+$ Rydberg state and the $V^1\Sigma^+$ ion-pair state are commonly represented either as separate diabatic curves or adiabatic $B^1\Sigma^+$ state (see Figure 2).

If a diabatic potential is used, then perturbations arise from the off-diagonal matrix elements of the $\mathbf{H}^{el}$ operator. This is to be expected as the diabatic potential is expressed in terms of a single electron configuration and, therefore, perturbations are expressed in terms of mixing with another electron configuration. These types of matrix elements can only appear between states with different symmetry and give rise to so-called heterogeneous perturbations.

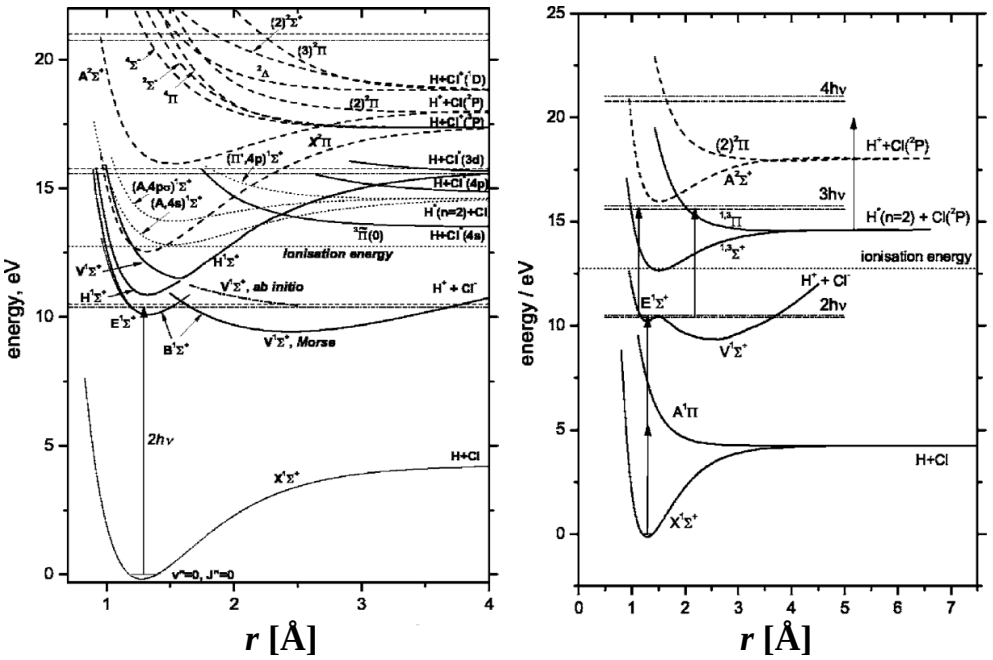

Figure 2 For the hydrogen halides, the potential curves of the respective $E^1\Sigma^+$ Rydberg state and the $V^1\Sigma^+$ ion-pair state are either represented as two distinctive diabatic curves (left) or the amalgamated $B^1\Sigma^+$ state (right). The figures represent the potential curves of excited and superexcited states of HCl and are reproduced from Refs.[281] and [282], respectively. Internuclear distances are presented in Å.

If an adiabatic potential is used, then perturbations arise from the off-diagonal matrix elements of the $\mathbf{T}^N(R)$ operator as it does not act on the electronic wavefunction. These type of matrix elements can only appear between states with identical symmetry and give rise to so-called homogeneous perturbations.

2.4.3 The spin-orbit factor

Taking account of relativistic effects into the Hamiltonian allows the inclusion of electron spin-effects. These include both spin-orbit effects from $\mathbf{H}^{SO}$, but also spin-spin effects,

which arise from $\mathbf{H}^{SS}$ which is neglected in this discussion because for the hydrogen halides in particular, it gives rise to much smaller matrix elements than those of $\mathbf{H}^{SO}$.

The electronic angular momentum quantum numbers that are well defined for the system are Λ, Σ, S, and Ω (= Λ + Σ) (see chapter 2.5). Non-zero off-diagonal matrix elements of

$$\left\langle \mathbf{\Phi}_{i,\Lambda,\Sigma,\Omega} \middle| \mathbf{H}^{SO} \middle| \mathbf{\Phi}_{j,\Lambda',\Sigma',\Omega'} \right\rangle \quad (41)$$

arise between states of different Λ and S, but identical Ω.

When taking relativistic effects into the Hamiltonian, the electronic part is defined by adding $\mathbf{H}^{SO}$ to $\mathbf{H}^{El}$. Curiously, the quantum numbers S, Σ, and Λ cease to be classified as *good*, and thusly the only good quantum number left, is Ω.

2.4.4 Gyroscopic perturbations

Gyroscopic or rotational perturbations arise from off-diagonal matrix elements of the $\mathbf{H}^{ROT}$ operator or rotational part of the Hamiltonian. The operator can be expressed in terms of the nuclear rotational angular momentum operator, **R**.

$$\mathbf{H}^{ROT} = \frac{1}{2\mu R^2}(\mathbf{R}^2) \quad (42)$$

Furthermore, the nuclear motion is bound to the plane that includes the internuclear axis ($\mathbf{R}_z^2$ = 0). Now, using the expressions from chapter 2.2.2 and

$$\mathbf{R^2} = \mathbf{J^2} - \mathbf{L^2} - \mathbf{S^2} \quad (43)$$

$$\mathbf{A_x^2} + \mathbf{A_y^2} = \mathbf{A^2} - \mathbf{A_z^2} \quad (44)$$

for **A** = **J**, **L**, **S**, the expression for the Hamiltonian becomes

$$\begin{aligned} \mathbf{H}^{ROT} &= \frac{1}{2\mu R^2}\left(\mathbf{R}_x^2 + \mathbf{R}_y^2\right) \\ &= \frac{1}{2\mu R^2}[(\mathbf{J^2} - \mathbf{J}_z^2) + (\mathbf{L^2} - \mathbf{L}_z^2) + (\mathbf{S^2} - \mathbf{S}_z^2) + (\mathbf{L^+S^-} + \mathbf{L^-S^+}) \\ &\quad - (\mathbf{J^+L^-} + \mathbf{J^-L^+}) - (\mathbf{J^+S^-} + \mathbf{J^-S^+}) \end{aligned} \quad (45)$$

The first three terms of this equation have only diagonal values. Therefore, when they are applied to a specific basis set (see chapter 2.5) for a molecule, they yield its unperturbed rotational energies. The last three terms, however, correspond to the coupling of spin, orbital momentum, and the total angular momentum operators, respectively. These terms make up the off-diagonal matrix elements of the Hamiltonian and are responsible for the rotational (or gyroscopic) perturbations between excited states. Each coupling of operators corresponds to different perturbations as:

1. $+\frac{1}{2\mu R^2}(\mathbf{L^+S^-} + \mathbf{L^-S^+})$ causes *homogeneous* (Ω = 0) spin-electronic perturbations between states that have the same value of Ω and S, but different values of Λ and Σ.

2. $-\frac{1}{2\mu R^2}(\mathbf{J}^+\mathbf{L}^- + \mathbf{J}^-\mathbf{L}^+)$ causes *heterogeneous* ($\Omega = \pm 1$) electronic rotational perturbations between states of the same Ω and Λ, but different values of S and Σ.
3. $-\frac{1}{2\mu R^2}(\mathbf{J}^+\mathbf{S}^- + \mathbf{J}^-\mathbf{S}^+)$ causes *heterogeneous* ($\Omega = \pm 1$) electronic rotational perturbations between states of the same Ω and Σ, but different values of S and Λ.

2.5 Hunds cases

There are two different ways of looking at Hunds cases. The first is by inspecting vector precession diagrams which offer a valuable insight into the reliability of quantum numbers in coupling schemes. The second is by comparing the hierarchical contributions of the operators $\mathbf{H}^{el}$, $\mathbf{H}^{SO}$, and $\mathbf{H}^{ROT}$ in terms of the total Hamiltonian.[345] But first it is important to define basis functions.

2.5.1 Basis functions

Working with a Hamiltonian operator requires a specification of the relevant wavefunction. For a diatomic molecule, such as a hydrogen halide, the wavefunction is usually expressed in terms of a set of quantum numbers, each representing electronic and orbital properties of the molecule that commute with the Hamiltonian operator, hence a measureable quantity. Depending on the size and shape of the molecule, the reliability of these quantum numbers (or commutation with the Hamiltonian) may vary. It is, therefore, desirable to construct different basis sets of quantum numbers to represent which electronic properties of the molecule are measurable and which are not. The Hunds cases correspond to different basis sets of quantum numbers which are good (or reliable) for molecules. Thus, molecules are classified according to which set of quantum numbers are measureable. The basis sets of Hunds cases a – e are presented in Table 5.

Table 5 Basis sets of good quantum numbers and the relative importance of the operators corresponding to the electronic, spin-orbit, and rotational contributions, to the total Hamiltonian for Hunds cases a – e. The table is reproduced from the book by H. Lefebvre-Brion and R. W. Field.[345]

Hunds case	*Basis set*	*Relative importance of operators*		
		$\mathbf{H}^{el}$	$\mathbf{H}^{SO}$	$\mathbf{H}^{ROT}$
a	$\lvert nJS\Omega\Lambda\Sigma\rangle$	Strong	intermediate	Weak
b	$\lvert nJSN\Lambda(S_R)\rangle$	Strong	Weak	Intermediate
c	$\lvert nJ[J_a]\Omega\rangle$	Intermediate	Strong	Weak
d	$\lvert nJSN(S_R)J^+N^+S^+\Lambda^+l(l_Rs_R)\rangle$	Intermediate	Weak	Strong
e	$\lvert nJJ^+[J_a^+ or S^+ and\ \Lambda^+]\Omega^+lj(j_R)\rangle$	Weak	Intermediate	Strong

2.5.2 Vector precession

Vector precession diagrams are figures that provide the reader with useful insights into the conserved quantities and dynamics that describe a particular scheme of coupled nuclear, rotation, electron spin, and electron orbital angular momenta.[345] For the purpose of this thesis, we will only focus on vector precession diagrams for Hunds cases a and c. Classically, the ground state and excited states of HF and HCl are always represented as Hunds cases a.[52, 62, 63, 77, 200, 201, 203-205, 207, 209] The electronic states of HBr and HI, on the other hand, correlate better with Hunds case c classification, but are traditionally represented with Hunds case a assignments.[139, 142, 145, 215, 216, 234-237] Furthermore, it has been shown that superexcited states of HI correlate with Hunds case e classification.[182] Vector precession diagrams of Hunds cases a and c are presented in Figure 3.

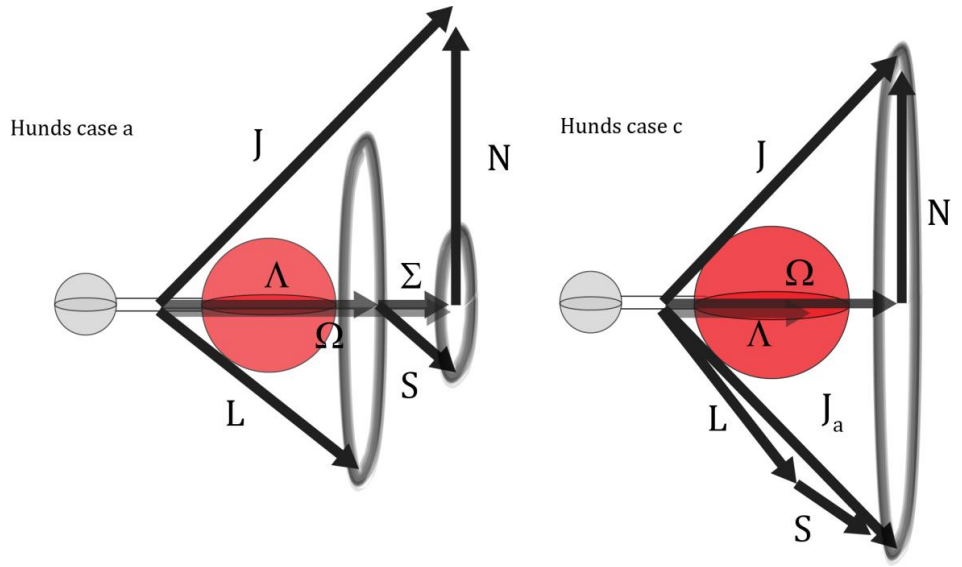

Figure 3 Vector precession diagrams for Hunds cases a (left) and c (right)

2.6 Molecular alignments

A molecule is said to be polarized with respect to a particular coordinate system, e.g. the laboratory or the molecule fixed system, if any of its internal angular momenta are either aligned or oriented. Alignment corresponds to an inequality in the populations of the M_J levels for a given J, whereas orientation corresponds to an inequality in the M_J populations for any one of the $|M_J|$ values.[345]

These identies are firmly anchored in various vector couplings. It is therefore useful to introduce so-called Clebsch-Gordan (CG) coefficients which will now be defined.

2.6.1 Clebsch-Gordan coefficients

CG coefficients can be interpreted as giving the probability amplitude (C) that two vectors,[B] $\mathbf{j}_1$ and $\mathbf{j}_2$ (each with projections m_1 and m_2 onto the z-axis), at any instant couple together to form the resultant vector $\mathbf{j} = \mathbf{j}_1 + \mathbf{j}_2$ with the projection $m = m_1 + m_2$.

$$\langle j_1 m_1, j_2 m_2 | j m \rangle = \langle j m | j_1 m_1, j_2 m_2 \rangle = C(j_1 j_2 j, m_1 m_2 m) \qquad (46)$$

These CG coefficients are, however, most commonly rewritten as Wigner 3-j symbols

$$\begin{pmatrix} j_1 & j_2 & j \\ m_1 & m_2 & m \end{pmatrix} = (-1)^{j_1 - j_2 - m} (2j+1)^{-\frac{1}{2}} \langle j_1 m_1, j_2 m_2 | j \quad -m \rangle \qquad (47)$$

and

$$\langle j_1 m_1, j_2 m_2 | j \ \ m \rangle = (-1)^{j_1 - j_2 + m} (2j+1)^{\frac{1}{2}} \begin{pmatrix} j_1 & j_2 & j \\ m_1 & m_2 & -m \end{pmatrix} \qquad (48)$$

The squares of the CG coefficients represent probabilities whose values range from 0 to 1.

2.6.2 Tensorial form, rotation matrix, Euler angles

The polarization of the molecule can be expressed in tensorial form. According to R. N. Zare[346] a spherical irreducible operator of rank k can be assumed to be a set of $(2k + 1)$ functions $T(k, q)$ with components $q = -k, -k + 1, \ldots, k$ that transform under rotation of the coordinate frame as

$$\mathbf{R} T(k, q) \mathbf{R}^{-1} = \sum_{q'} D^k_{q' q}(R) T(k, q') \qquad (49)$$

Here, $\mathbf{R}$ denotes the active rotation of any physical system of our choosing. It is also commonly noted as $\mathbf{R}(\phi, \theta, \chi)$, representative of i) rotation about an angle θ about the z axis, ii) rotation about an angle ϕ about the N axis, and iii) rotation about an angle χ about the Z axis (see Figure 4).

Under rotation of the Euler angles, $T(k, q')$ is transformed into a closed set of $(2k + 1)$ operators $T(k, q')$, and the coefficients of this expansion are the Wigner rotation matrix elements $D^k_{q' q}(R)$. I.e.

$$D^k_{q' q}(\phi, \theta, \chi) = \langle k q' | \mathbf{R}(\phi, \theta, \chi) | k q \rangle \qquad (50)$$

are the elements of a $(2k + 1)*(2k + 1)$ unitary matrix for $\mathbf{R}$; the rotation matrix. In fact, the tensor operators $T(k, q)$ are proportional to the spherical harmonics, Y_{lm}, of the classical atomic orbitals.

[B] The corresponding ‚Dirac-ian' ket notation for the $\mathbf{j}_1$ and $\mathbf{j}_2$ vectors are $|j_1\rangle$ and $|j_2\rangle$, respectively.

$$\mathbf{R}Y_{lm}(\phi,\theta)\mathbf{R}^{-1} = \sum_{m'} D^{l}_{m'm}(\phi,\theta,\chi)\, Y_{lm'}(\phi,\theta) \qquad (51)$$

where the expansion coefficients can be reduced to the form

$$D^{l}_{m'm}(\phi,\theta,\chi) = e^{-i\phi m'} d^{l}_{m'm}(\theta) e^{-i\chi m} \qquad (52)$$

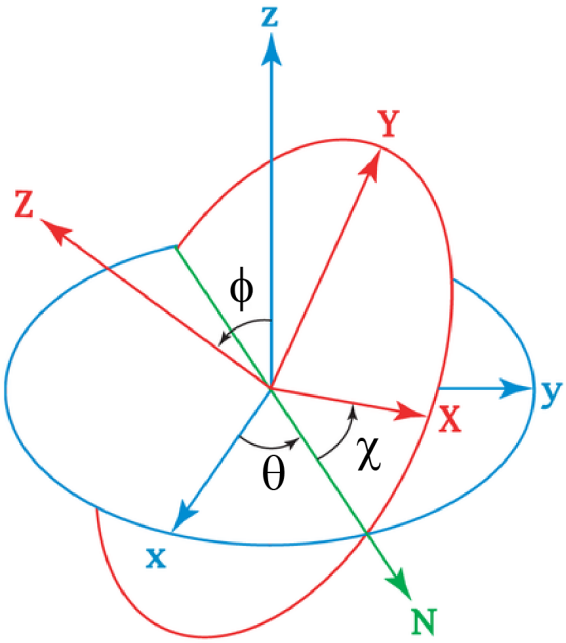

Figure 4 Euler angles ϕ, θ, and χ, relating the space fixed (xyz) and molecule fixed (XYZ) frames. Figure credit: L. Brits.[347]

Suppose that **R** transforms the state $|JM\rangle$ in a diatomic molecule from the xyz space fixed frame to the XYZ molecule frame with a common origin. The probability of finding J making the projection M' onto the Z axis in the molecular frame is

$$\left|D^{J}_{M'M}(\phi,\theta,\chi)\right|^2 = \left|d^{J}_{M'M}(\theta)\right|^2 \qquad (53)$$

Hence, $D^{J}_{M'M}(\phi,\theta,\chi)$ denotes the probability amplitude of the vector **J** making a projection M on the space fixed z axis will be found making a projection M' on the molecule fixed Z axis.

The connections between uncoupled $|J_1M_1\rangle|J_2M_2\rangle$ and coupled $|JM\rangle$ representations under rotational transformations are given by Clebsch-Gordan series

$$D^{J_1}_{M_1'M_1}(\phi,\theta,\chi)D^{J_2}_{M_2'M_2}(\phi,\theta,\chi) = \sum_J \langle J_1M_1, J_2M_2|JM\rangle \langle J_1M_1', J_2M_2'|JM'\rangle D^J_{M'M}(\phi,\theta,\chi) \quad (54)$$

or the inverse Clebsch-Gordan series

$$D^J_{M'M}(\phi,\theta,\chi) = \sum_{M_1M_1'} \langle J_1M_1, J_2M_2|JM\rangle \langle J_1M_1', J_2M_2'|JM'\rangle D^{J_1}_{M_1'M_1}(\phi,\theta,\chi)D^{J_2}_{M_2'M_2}(\phi,\theta,\chi) \quad (55)$$

2.6.3 Alignment of a rigid rotor

The wavefunction of the rigid rotor can be represented with the spherical harmonic $|JM\rangle = Y_{JM}(\phi,\theta)$. The probability of finding the rotor axis pointing into the angle element $\sin(\theta)\,d\theta d\phi$, is given by

$$P_{JM}(\theta) = \left|Y_{JM}(\alpha,\beta)\right|^2 \sin(\theta)\,d\theta d\phi \quad (56)$$

Now, by utilizing the spherical harmonic addition theorem[346]

$$P_J\big(\cos(\theta_{ij})\big) = \frac{4\pi}{2J+1}\sum_M Y^*_{JM}(\theta_i,\phi_i)Y_{JM}(\theta_j,\phi_j) \quad (57)$$

In the case of an absorption of plane a polarized photon ($J_2 = 1, M_2 = 0$), the probability amplitude is proportional to the CG coefficients

$$\langle J''M'', 10|JM\rangle = (-1)^{J''-1+M}(2J+1)^{\frac{1}{2}}\begin{pmatrix} J'' & 1 & J \\ M'' & 0 & -M \end{pmatrix} \quad (58)$$

where $|J''M''\rangle$ is the initial state of the rigid rotor. It can be shown[346] that

$$P_J(\theta) = \frac{1 + \mathrm{A}_0(J)P_2(\cos(\theta))}{4\pi} \quad (59)$$

where

$$P_2(\cos(\theta)) = \frac{3cos^2(\theta) - 1}{2} \quad (60)$$

Here, A_0 is the alignment parameter which ranges from +2 for a pure cosine distribution to –1 for a pure sine distribution. These are more commonly referred to as parallel (+2) and perpendicular (–1) distributions, respectively. The numerical restrictions of the alignment parameter are derived by rewriting the previous expression for $P_J(\theta)$ as

$$P_J(\theta) = a\,sin^2(\theta) + b\,cos^{\,2}(\theta) \quad (61)$$

in which case

$$A_0 = \frac{2(b-a)}{2a+b} \quad (62)$$

where A_0 = +2 for a = 0 (pure cosine distribution) and A_0 = –1 for b = 0 (pure sine distribution).

2.6.4 Angular distribution of photofragments

If we denote the dipole moment of a molecule by $\boldsymbol{\mu}$ and the electric vector of a linearly polarized light beam by **E**, the probability of a successful one photon excitation to a repulsive (dissociative) state is proportional to $|\boldsymbol{\mu} \cdot \boldsymbol{E}|^2$. Furthermore, we can denote the final recoil distribution of the fragment in the molecular frame as an expansion in the complete set of spherical harmonics

$$f(\theta_m, \phi_m) = \sum_{k,q} b_{kq} Y_{kq}(\theta_m, \phi_m) \quad (63)$$

where (θ_m, ϕ_m) are the polar and azimuthal angles about the direction of $\boldsymbol{\mu}$ and the expansion coefficients are given by

$$b_{kq} = \int_0^{2\pi} d\phi_m \int_0^{\pi} \sin(\theta_m) d\theta_m Y_{kq}^*(\theta_m, \phi_m) f(\theta_m, \phi_m) \quad (64)$$

If we now let $I(\theta_m, \phi_m)$ denote the angular distribution of the fragment in the lab frame where θ_s, ϕ_s are the polar and azimuthal angles about the direction of **E**, we can show that it takes the form[346]

$$I(\theta_m, \phi_m) = \frac{\sigma}{4\pi}[1 + \beta P_2(\cos(\theta_s))] \quad (65)$$

where σ is the total cross section and β is the anisotropy parameter, which ranges from +2 to – 1.

3 Excitation dynamics

Before reviewing the experimental apparatus, it is useful to account for the actual dynamics involved in the excitation processes of the hydrogen halides. Here we will review some important points concerning photoexcitation processes which are involved in the experiments.

3.1 Ground state & excited states

3.1.1 Electron configuration

The electron configurations of the electronic states of hydrogen halides can be easily derived from LCAO. According to molecular orbital diagrams (see Figure 5) the valence electrons of a ground state hydrogen halide molecule are in one bonding σ orbital and two non-bonding π orbitals, i.e. $\sigma^2\pi^4$. This electron configuration gives rise to the $^1\Sigma^+$ symmetry because, i) -the total spin of the system equals: $\Sigma = 0$, ii) -$\Lambda = 0$, and iii) -the total wavefunction is unaffected by the reflection operation, giving rise to a + parity.

An excitation to a Rydberg state is elicited in Figure 5a. An electron is excited from a non-bonding orbital to a higher Rydberg orbital associated with the halogen atom. Since the bonding orbital is unaffected by this process, the binding energy of Rydberg states is similar to that of the ground state. In Figure 5b, the excitation process to an ion-pair state is presented where an electron is excited from the bonding orbital to the antibonding orbital. This weakens the binding potential of the molecule because the antibonding orbital is located away from the center of the molecular bond. Since the antibonding electron is more attracted to the halogen atom than the hydrogen atom, the atoms exhibit ion-like properties (H^+ and X^-) and the molecule remains bound through electrostatic effects.

Excitations of the non-bonding electrons to the antibonding orbitals can, on the other hand, give repulsive states, which result in dissociation of the molecule. Such states are also referred to as continuum states and are classified along with ion-pair states as valence states.

3.1.2 Morse Potentials

The Morse function is useful to describe the potential energies of the bound states of the hydrogen halides.

$$V_{Morse}(r) = T_e + D_e(1 - e^{-\beta(r-r_e)})^2 \quad (66)$$

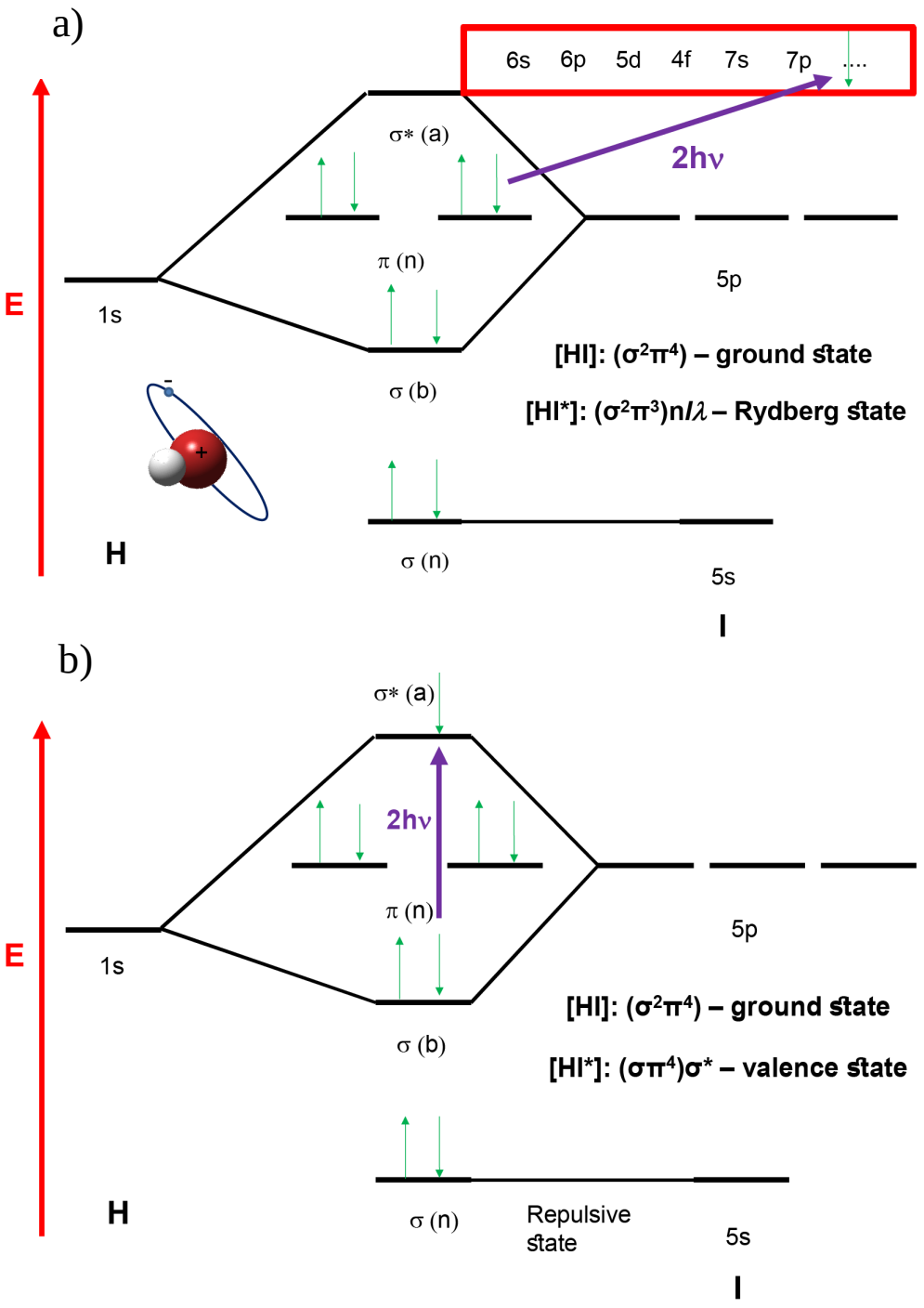

Figure 5 **Molecular orbital diagrams and two-photon excitation processes for HI. a) Excitation to a Rydberg state. b) Excitaion to an ion-pair state.**

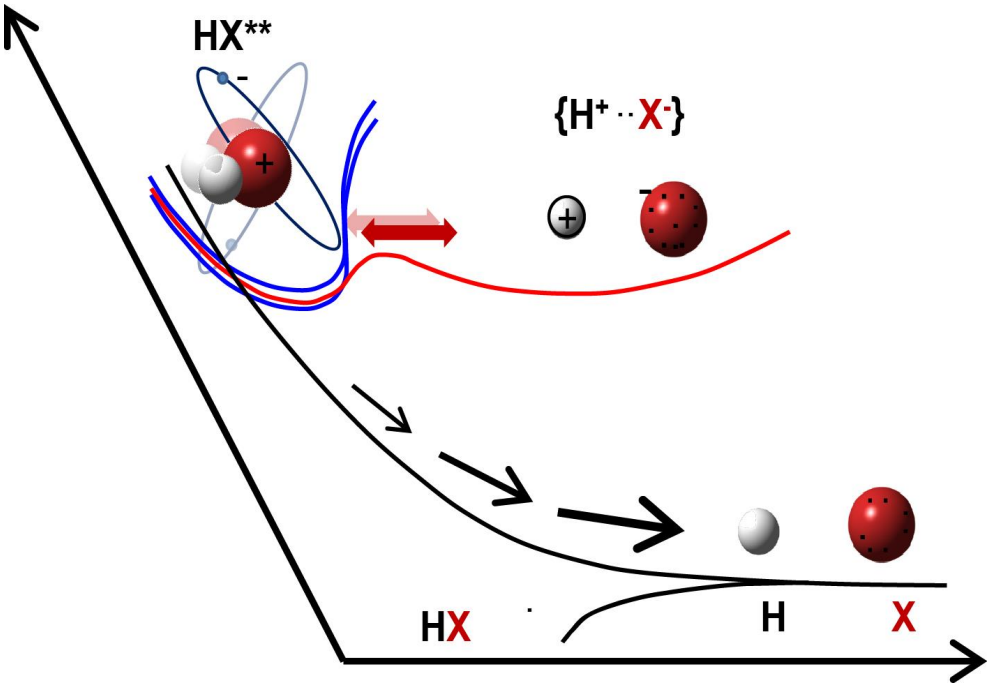

Figure 6 Pictorial diagram of potential curves of the hydrogen halides. Highlighted are couplings between diabatic Rydberg states with i) the adiabatic $B^1\Sigma^+$ state and ii) repulsive states which yield the neutral atomic fragments.

Here, T_e is the zero point energy of the excited state (for the ground state $T_e = 0$), and D_e is the binding energy of the molecule (or the well depth), defined as

$$D_e = \frac{\omega_e^2}{4\omega_e x_e} \quad (67)$$

β depends on the well depth, and the reduced mass, μ.

$$\beta = \omega_e \sqrt{\frac{2\pi^2 c\mu}{D_e h}} \quad (68)$$

and r_e is the equilibrium bond distance determined from

$$r_e = \sqrt{\frac{h}{8\pi^2 \mu c B_e}} \quad (69)$$

where B_e is the corresponding rotational constant at the equilibrium distance, defined in chapter 2.3.3.

3.2 Selection rules

3.2.1 Transition moment integral

For a transition to take place between two electronic states, the following condition must be fulfilled, namely

$$\langle 1|\boldsymbol{\mu}|0\rangle \neq 0 \qquad (70)$$

Here, $\boldsymbol{\mu}$ is the transition moment operator and $|0\rangle$ and $|1\rangle$ are the wave functions of the two states involved in the transition. If the value of this bracket is zero, the transition is forbidden. In practice, it suffices to determine the symmetry of the transition moment function to decipher whether a transition is allowed or forbidden.

3.2.2 Transitions in terms of electron configurations

In terms of electron configurations, the excitations from the ground state to a Rydberg state are

$$(\sigma^2\pi^4) + h\nu \rightarrow (\sigma^2\pi^3)nl\lambda$$

where $nl\lambda$ are the quantum numbers that describe the Rydberg orbital. The corresponding excitation to the ion-pair state is

$$(\sigma^2\pi^4) + h\nu \rightarrow (\sigma\pi^4)\sigma^*$$

3.2.3 Basic selection rule

The origin of selection rules for electronic transitions can be traced back to the conservation of orbital angular momentum during the excitation process of atoms. I.e. during the absorption of a photon. The rigorous selection rule which arises from this process is

$$\Delta l = \pm 1 \qquad (71)$$

This rule satisfies the transition moment integral, eq. (70), since a transition between states of different orbital angular momentum inherently involves a change in the dipole moment.

3.2.4 One-photon selection rules for molecules

When a molecule absorbs a photon, in classical terms, the total angular momentum must be conserved. This requirement, gives rise to the following selection rules

$$\begin{gathered} \Delta J = +1, for\ \Lambda = 0 \\ \Delta J = 0, \pm 1, for\ \Lambda \neq 0 \end{gathered} \qquad (72)$$

The $\Delta J = 0$ selection rule does not hold for Σ states ($\Lambda = 0$) because such a transition does not involve a change in the dipole moment due to the symmetry properties of the orbitals involved. Therefore, the transition moment integral yields zero transitional probability amplitude, hence a forbidden transition.

States of $\Lambda > 0$ (i.e. Π states, Δ states, etc.), on the other hand, exhibit degeneracies which allow rotational transitions between states with the same value of Λ, i.e. $\Pi \leftrightarrow \Pi$, $\Delta \leftrightarrow \Delta$, etc. These transitions fulfill the $\Delta J = 0$ condition when $\Delta S = 0$ (keeping in mind that $J = L + S$ and Λ is the projection of L onto the molecular axis) and they fulfill the $\Delta J = \pm 1$ condition when $\Delta S = \pm 1$. Therefore, triplet states are readily observable in one-photon excitation schemes.

3.2.5 Two-photon selection rules for molecules

When two photons are absorbed by a molecule, both excitations are scrutinized by the one-photon selection rules to yield

$$\Delta J = 0, \pm 2 \; for \; \Delta\Omega = 0$$
$$\Delta J = 0, \pm 1, \pm 2 \; for \; \Delta\Omega \neq 0 \qquad (73)$$

Numerous excited states accessible by two-photon excitations of HI, expressed in both term symbols and electron configurations are presented in Table 1 in Article #2. Similar presentations of a myriad of excited states of HBr can be found in Refs.[206] and [217].

3.3 Step 1: Virtual states

Two-photon excitations of the hydrogen halides to Rydberg and ion-pair states, can be considered to occur in two steps, first of which involves a transition to a so-called virtual state. The virtual state can involve the repulsive valence states to give

$$(\sigma^2\pi^4) + h\nu \rightarrow (\sigma^2\pi^3)\sigma^*$$

and/or

$$(\sigma^2\pi^4) + h\nu \rightarrow (\sigma\pi^4)\sigma^*$$

The first electron configuration gives rise to the excited states $A^1\Pi_1$, $a^3\Pi_{2,1,0}$. Since this process involves the excitation of an electron from a π orbital to a σ orbital, in terms of alignment, this is classified as a perpendicular transition. The latter gives rise to the excited states $t^3\Sigma^+_{1,0}$ (see Figure 7), where an electron is excited from a σ orbital to a σ* orbital (parallel transition). The perpendicular transitions are generally found to be dominant (see Article #4 and Ref.[282]).

The transition via a virtual state can also be viewed, roughly, in terms of a transition of an electron from a sp^3 orbital, in which case the excitation can be construed as a transition of a mixed (approx. 1:3) σ/π orbital to a σ* orbital. This would imply that the virtual state is also mixed (see Figure 8). This is, however, an overly simplified picture and should be taken as such.

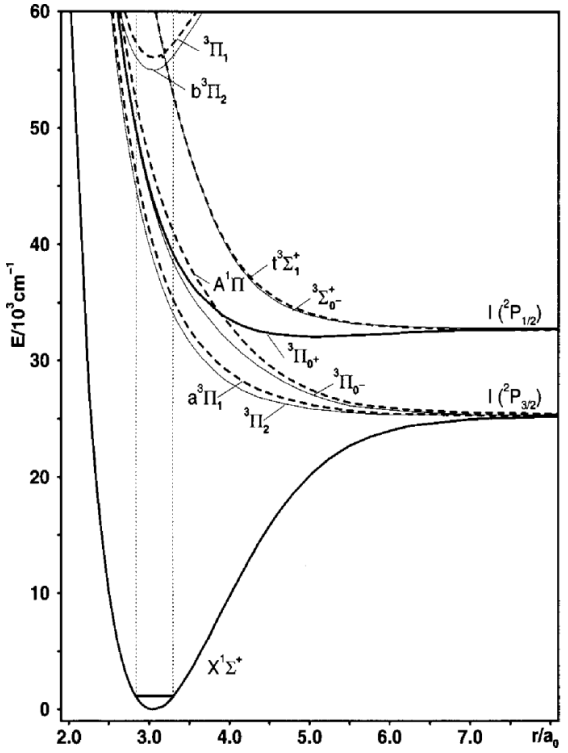

Figure 7 Potential energy diagram of the ground state and the first excited (virtual) states of HI. The figure is reproduced from Ref.[132]

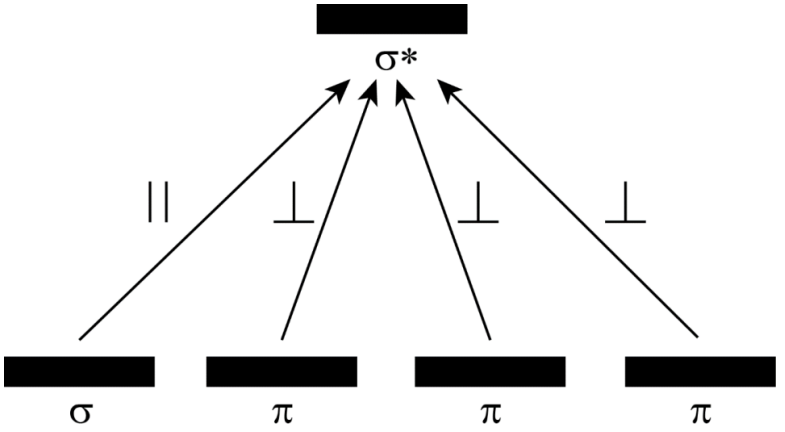

Figure 8 Alignment of transitions from the ground state to a virtual state, assuming the ground state is sp^3 hybridized.

3.4 Step 2: Bound states - characteristics

For the hydrogen halides, absorption of two photons via virtual states can yield two types of bound states. i) Rydberg states with electron configurations $(\sigma^2\pi^3)nl\lambda$ or ii) ion-pair states with the electron configuration $(\sigma\pi^4)\sigma^*$. Several factors govern the characteristics of the spectra, such as transition probabilities, state interactions etc. Here, these characteristics will be explored with regards to their underlying theoretical background and how they can be discerned from molecular spectra.

3.4.1 Spectral appearance

A transition to an excited state exhibits several different branches in its multiphoton spectrum. These branches stem from transitions between states with the same or different J quantum numbers. They arise from transitions from certain rotational levels in the ground state (each denoted with J'') to rotational levels in the excited state (denoted with J'). (See Figure 9). The rotational branches arising in two-photon excitations are presented in Table 6.

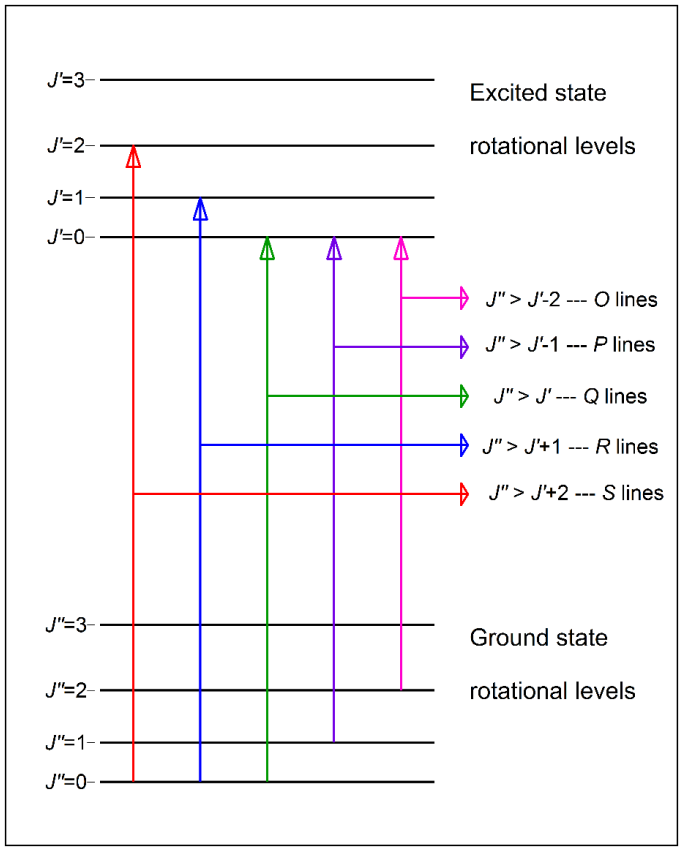

Figure 9 **The origin of the *O*, *P*, *Q*, *R*, and *S* line series in two-photon REMPI spectra of the hydrogen halides.**

Table 6 Rotational transitions and matrix elements for the *O*, *P*, *Q*, *R*, and *S* branches in the two-photon REMPI spectra of the hydrogen halides.

Branch	*Transition*	*Bracket notation*
O	$J'' \rightarrow J' - 2$	$\langle J''\|\boldsymbol{\mu}\|J' - 2\rangle \neq 0$
P	$J'' \rightarrow J' - 1$	$\langle J''\|\boldsymbol{\mu}\|J' - 1\rangle \neq 0$
Q	$J'' \rightarrow J'$	$\langle J''\|\boldsymbol{\mu}\|J'\rangle \neq 0$
R	$J'' \rightarrow J' + 1$	$\langle J''\|\boldsymbol{\mu}\|J' + 1\rangle \neq 0$
S	$J'' \rightarrow J' + 2$	$\langle J''\|\boldsymbol{\mu}\|J' + 2\rangle \neq 0$

Not all branches are visible for all excited states. Rydberg states and ion-pair states which exhibit the $^1\Sigma^+$ symmetry only produce *O*, *Q*, and *S* lines as mentioned in chapter 3.2.5 above. Furthermore, the lowest observable rotational J' level of an excited state (i.e. the eigenstate with the lowest value of J') equals its value of the Ω quantum number. Thus, for example, the lowest observable J' level of $k^3\Pi_0$ is $J' = 0$, of $k^3\Pi_1$ is $J' = 1$, and of $k^3\Pi_2$ is $J' = 2$.

3.4.2 Line strengths, i) The Franck Condon principle

As mentioned above, the transition moment integral yields the probability amplitude for a transition between the states involved.

$$a^2 = \langle 1|\boldsymbol{\mu}|0\rangle^2 \qquad (74)$$

A common approximation method to estimate relative transition probabilities is to evaluate Franck-Condon (FC) factors. These are defined as the square of the vibrational overlap integral of the two vibronic wavefunctions involved,

$$q = \left\langle \chi_{v_1} \middle| \chi_{v_0} \right\rangle^2 \qquad (75)$$

According to this the transition probability increases with an increasing overlap of the two vibrational wavefunctions (Figure 10). To a first approximation, the FC factor is not affected by the rotational excitations within the same vibrational state.

In the case of two-photon transitions, a representation of the transition probability is given by the resonance excitation cross section (σ_{res}) which is directly proportional to the transition rate (K) which is calculated with first order perturbation theory.[219, 348, 349]

$$\sigma_{res} \sim K = \left| \sum_i \frac{\langle 1|\boldsymbol{\varepsilon}\cdot\boldsymbol{\mu}|i\rangle\langle i|\boldsymbol{\varepsilon}\cdot\boldsymbol{\mu}|0\rangle}{E_{0i} - h\nu + C(\Gamma_i)} \right|^2 \qquad (76)$$

Here, hv is the photon energy and E_{0i} is the energy difference between the intermediate state, $|i\rangle$ and the ground state, $|0\rangle$, and $|1\rangle$ is the resonance state. $C(\Gamma_i)$ is a factor dependent on the lifetime of the intermediate state.

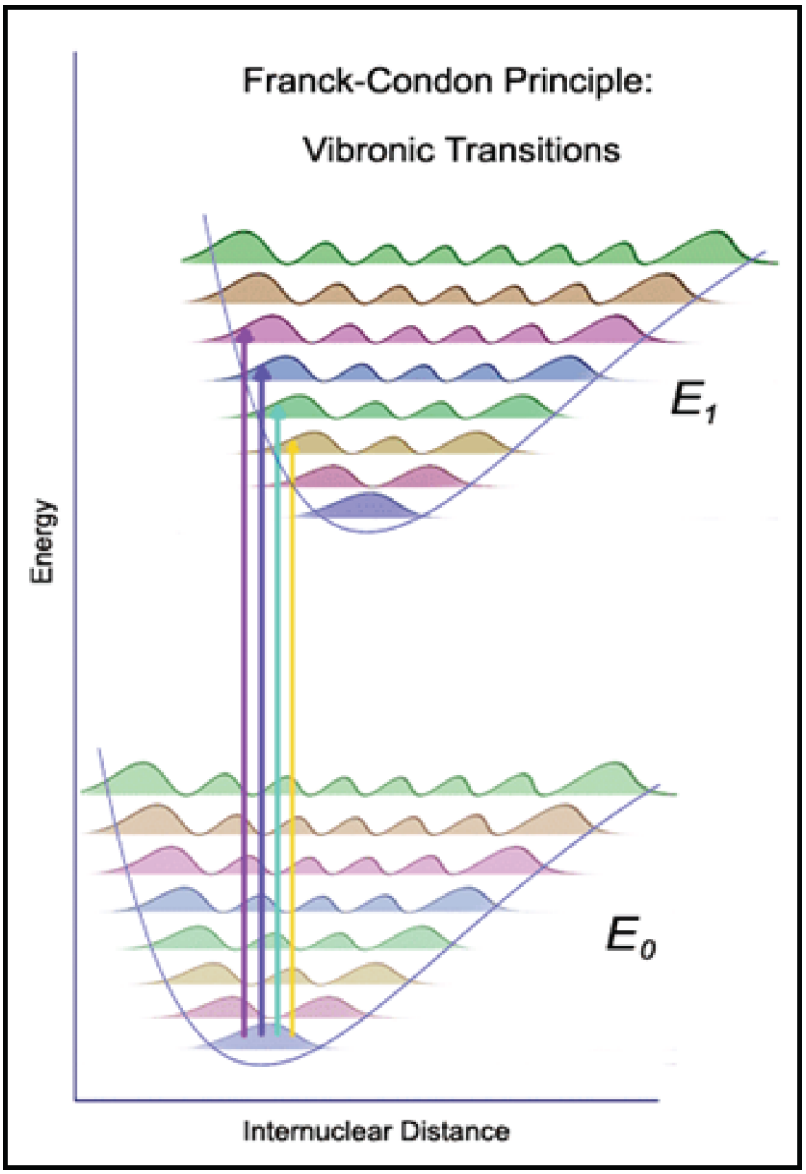

Figure 10 Vibrational overlaps between different vibrational levels of two fictional states, E_0 and E_1. Assuming transitions from the ground vibrational state (E_0: v´´ = 0), the greatest overlap, hence the largest FC factors are found for v´ = 2 – 5.

3.4.3 Line strengths, ii) Rotational effects

A general expression for two-photon transition strengths (S) as a function of J', J'', Ω', and Ω'' for linearly polarized radiation has been derived by R. G. Bray and R. M. Hochstrasser.[348]

$$S(\Delta\Omega, J', J'') = s_0\mu_0^2 + s_2\mu_2^2 \qquad (77)$$

Here, s_0 and s_2 can be written in terms of zeroth order and second order Clebsch-Gordon (CG) coefficients as shown by J. B. Halpern *et al.*[349] For the hydrogen halides, with $\Omega'' = 0$, these factors can be expressed in terms of J' for different Ω' states and the various rotational branches (O – S; see Table 7). Furthermore, the factors μ_0^2 and μ_2^2, are sum and product functions of the one-photon transition dipole moments that correspond to the transition via the virtual intermediary states

$$\mu_{||} = \langle \Omega | \boldsymbol{\varepsilon} \cdot \boldsymbol{\mu} | \Omega \rangle \qquad (78)$$

$$\mu_{\perp} = \langle \Omega \pm 1 | \boldsymbol{\varepsilon} \cdot \boldsymbol{\mu} | \Omega \rangle \qquad (79)$$

Table 7 **Two-photon transition strengths for transitions from a Σ ground state ($\Omega'' = 0$).**

	$\Omega' = 0$ (Σ)		$\Omega' = 1$ (Π)	$\Omega' = 2$ (Δ)
	s_0	s_2	s_2	s_2
O	0	$\frac{1}{30}\frac{J(J-1)}{(2J-1)}$	$\frac{1}{15}\frac{J(J-2)}{(2J-1)}$	$\frac{1}{30}\frac{(J-2)(J-3)}{(2J-1)}$
		$J'' \geq 2; J' \geq 0$	$J'' \geq 3; J' \geq 1$	$J'' \geq 4; J' \geq 2$
P	0	0	$\frac{1}{30}(J+1)$	$\frac{1}{15}(J-2)$
			$J'' \geq 2; J' \geq 1$	$J'' \geq 3; J' \geq 2$
Q	$\frac{1}{9}(2J+1)$	$\frac{1}{45}\frac{J(2J+1)(J+1)}{(2J+3)(2J-1)}$	$\frac{1}{10}\frac{(2J+1)}{(2J+3)(2J-1)}$	$\frac{1}{5}\frac{(2J+1)(J+2)(J-1)}{(2J+3)(2J-1)}$
	$J'' \geq 0; J' \geq 0$	$J'' \geq 1; J' \geq 1$	$J'' \geq 1; J' \geq 1$	$J'' \geq 2; J' \geq 2$
R	0	0	$\frac{1}{3}J$	$\frac{1}{15}(J+3)$
			$J'' \geq 1; J' \geq 2$	$J'' \geq 1; J' \geq 2$
S	0	$\frac{1}{30}\frac{(J+1)(J+2)}{(2J+3)}$	$\frac{1}{15}\frac{(J+1)(J+3)}{(2J+3)}$	$\frac{1}{30}\frac{(J+3)(J+4)}{(2J+3)}$
		$J'' \geq 0; J' \geq 2$	$J'' \geq 0; J' \geq 2$	$J'' \geq 0; J' \geq 2$

For further discussions on factors governing line intensities in two-photon REMPI of the hydrogen halides see Refs.[218, 219] and Article #6.

3.4.4 Line strengths, iii) Laser power

Intensities of spectral lines (I) in REMPI are also affected by the laser power (P_{laser}). The laser power, being the photon energy per time unit, is associated with the density of photons as well as the photon energies used in the ionization process. This relationship can therefore be described as

$$I \sim P_{laser}^{n} \quad \textbf{(80)}$$

where n is the number of photons required for the ionization.

3.4.5 Line strengths, iv) Populations

The final factor that affects the line strengths in REMPI spectra are the rotational level populations in the ground state ($N_{J'',v''}$). Rotational populations of excited state are generally formulated with Boltzmann distributions,

$$N_{J'',v''} = N_0 e^{\left(\frac{-E_{J'',v''}}{k_B T}\right)}(2J'' + 1) \quad \textbf{(81)}$$

N_0 is the total number of molecules in the ground state, $(2J'' + 1)$ is the degeneracy, $E_{J'',v''}$ is the rotational energy, k_B is the Boltzmann constant, and T is the temperature.

By cooling the gas sample, a greater number of molecules will populate the lower rovibrational levels which decreases the chances of excitations from higher energy levels. This simplifies the spectra and their analyses.

3.4.6 State interactions - perturbation selection rules

State interactions in HBr and HI are omnipresent. They affect the spectra in several ways, namely in terms of line positions (energies), line intensities, and line widths. These effects will all be dealt with in chapter 5. Here we present a brief overview of the types of state interactions involved and their origins.

As already mentioned in chapter 2.4, perturbations arise from off-diagonal matrix elements of the Hamiltonian for an excited state. Each spectral line corresponds to a particular eigenvalue of an eigenstate, to which the total Hamiltonian is applied. It is described in terms of the electron configuration as well as the vibrational and rotational motions. The eigenstate can be described in terms of more than one excited state, i.e. a mixed state.

Interactions between states arise from rotational operators according to the BO-approximation. Interactions between states with different symmetries arise from different operators. The nature of the different state interactions are presented in Table 8, derived from Ref.[113]

As seen from Table 8, not all excited states couple together / mix. There are limitations to state interactions which are commonly presented as perturbation selection rules. The perturbation selection rules are presented for all the different parts of the Hamiltonian in Table 9.

Table 8 Couplings between excited states. Abbreviations are used for spin-orbit (SO), spin-spin (SS), L-uncoupling (JL), S-uncoupling (JS) and electrostatic (E) interactions.

	$^1\Pi_1$	$^3\Pi_0$	$^3\Pi_1$	$^3\Pi_2$	$^1\Sigma^-_0$	$^3\Sigma^-_0$	$^3\Sigma^-_1$	$^1\Sigma^+_0$	$^3\Sigma^+_0$	$^3\Sigma^+_1$
$^1\Pi_1$	E		SO		JL		SO	JL		SO
$^3\Pi_0$		E	JS		SO	SO		SO	SO	
$^3\Pi_1$	SO	JS	E	JS			SO		JL	SO
$^3\Pi_2$			JS	E			JL			JL
$^1\Sigma^-_0$	JL	SO			E				SO	
$^3\Sigma^-_0$		SO	JL			E	JS	SO		JS
$^3\Sigma^-_1$	SO		SO	JL		JS	E		JS	SO
$^1\Sigma^+_0$	JL	SO				SO		E		
$^3\Sigma^+_0$		SO	JL		SO		JS		E	JS
$^3\Sigma^+_1$	SO		SO	JL		JS	SO		JS	E
$^1\Delta_2$	JL			SO						
$^3\Delta_1$	SO	JL	SO							
$^3\Delta_2$			JL	SO			SS			SS

State interactions are further divided into bound-bound interactions, for two bound states, and bound-continuum interactions, for interactions between bound and repulsive states. The former case involves quantum level-to-level interactions, whereas the latter case involves predissociation via a repulsive state. Predissociation will affect the lifetime of the bound states, which can appear as bandwidth alterations (see chapter 5).

3.4.7 Hidden states

Excited states may not appear in REMPI spectra for to a number of reasons. Firstly, the resonance transition probability may be so small that no lines are visible. Second, an excited state may couple strongly with a repulsive state, leading to dissociation prior to ionization. This latter process is particularly common amongst states of same symmetry. (In that case the couplings are via electrostatic interactions.)

Excited states that are not observed in spectra for one of these reasons are termed hidden or dark states. In this work the term hidden state is used because it has the subtle indication that it may be found.

Table 9 Off-diagonal elements of the different parts of the total Hamiltonian, leading to selection rules for state interactions. It is customary to further classify the interactions as homogeneous (ΔΩ = 0) and heterogeneous (ΔΩ ≠0).

Operator	*Interactions*	*Selection rules including ΔJ = 0*			
		ΔΛ	ΔΣ	Δ*S*	ΔΩ
$\mathbf{H}^{el}$	Electronic (homogeneous)	0	0	0	0
$\mathbf{T}^{N}$	Vibrational (homogeneous)	0	0	0	0
$\mathbf{H}^{SO}$	Spin-orbit (homogeneous)	0, ±1	0, ±1	0, +1	0
$-\frac{\mathbf{1}}{\mathbf{2}\mu\mathbf{R}^{2}}\mathbf{JL}$	L-uncoupling (heterogeneous)	±1	0	0	±1
$-\frac{\mathbf{1}}{\mathbf{2}\mu\mathbf{R}^{2}}\mathbf{JS}$	S-uncoupling (heterogeneous)	0	±1	0	±1

One of the peculiarities that have been observed in the REMPI spectra of the hydrogen halides is that in some cases, observed state interactions seem to violate the perturbation selection rules. Such interactions are usually indicative of a hidden state that acts as an intermediary state; a remote perturber. It couples/interacts/mixes, via allowed interactions, with two or more states to allow the observed interactions.

A clear example can be found for HI in Article #3, where the $m^3\Pi_2$ Rydberg state interacts with the $H^1\Sigma^+$ Rydberg state and the $V^1\Sigma^+$ ion-pair state. In accordance with Table 8, these interactions are forbidden. Thus, Table 8 can also be used to theorize what type of hidden states are present that mix with states to allow the observed interactions. E.g. $^3\Pi_2$ states interacts with $^3\Pi_1$ states (via JS coupling), and $^3\Pi_1$ states interact with $^1\Pi_1$ states (via SO coupling). $^1\Pi_1$ states interact with $^1\Sigma^+$ states (via JL coupling) and thus, $^3\Pi_2$ states can interact with $^1\Sigma^+$ states through interactions with hidden states that have $^3\Pi_1$ and $^1\Pi_1$ symmetry.

Further information about hidden states can be derived from known vibrational progressions. (See Articles #3, #4, and #6, for details and more examples).

3.5 Step 3: Fragmentations and ionization

Once a bound Rydberg or ion-pair state is accessed, there are a number of additional excitation pathways in REMPI. These excitation pathways can yield i) atomic lines, ii) superexcited states, or iii) molecular ions.

3.5.1 Predissociation – atomic line formation

First, predissociation of a Rydberg state yields the neutral atomic fragments. The halogen atoms are formed in the ground state or their spin-orbit excited states. These can be further excited to atomic Rydberg states by two photons; a subsequent third photon ionizes the atom. This process yields (2 + 1) atomic REMPI lines which are useful for spectral calibrations since the energies of these lines are well documented for HBr and HI.[350] The step-by-step process of predissociation via Rydberg states is typically:

$$HX(\sigma^2\pi^4) + 2h\nu \rightarrow HX^{**}(\sigma^2\pi^3)nl\lambda - resonance\ excitation$$

$$HX^{**}(\sigma^2\pi^3)nl\lambda \rightarrow H(n=1) + X(\,^3P_{3/2}) \,/\, X^*(\,^3P_{1/2}) - \ predissociation$$

$$X(\,^3P_{3/2}) \,/\, X^*(\,^3P_{1/2}) + 2h\nu \rightarrow X^{**}(^{2S+1}\mathrm{L}_J) \ - resonance\ excitation$$

$$X^{**}(^{2S+1}\mathrm{L}_J) + h\nu \rightarrow X^+ - ionization$$

For ion-pair states the process is similar with the exception of the first step which yields $HX^{**}(\sigma\pi^4)\sigma^*$. Predissociation of ion-pair states has, furthermore, been shown to include various interaction with gateway states allowing the ion-pair states to interact with repulsive states indirectly (see Articles #1 and #3).

3.5.2 Autoionization – Superexcited and ionic states

Superexcited states are defined as neutral excited states with energies higher than that of the ground state molecular ion. For the hydrogen halides, the molecular ion ground states are $X^2\Pi_{3/2}$ and $X^2\Pi_{1/2}$ with the electron configuration ($\sigma^2\pi^3$). Since the removed electron originates from a non-bonding π orbital, the bonding character of the molecular ion, is comparable to that of the molecular ground state. Superexcited states are either bound or repulsive states with a Rydberg electron ($nl\lambda$) orbiting an excited ion core. The electron configuration of the excited ion core is the same as that of an excited state of the molecular ion. Thus, series of superexcited states correlate with a particular ionic state. An example is the bound $[A^2\Sigma^+]5d\pi$ superexcited state in HI that correlates with the $A^2\Sigma^+$ ionic state (see Article #6).

Repulsive superexcited states dissociate to form electronically excited fragments, e.g. (from Article #4)

$$HBr^{\#}[B^2\Sigma^+]nl\lambda \rightarrow H^*(n=2) + Br(^2P_{3/2})$$

Here, a superexcited state ($HBr^{\#}[B^2\Sigma^+]nl\lambda$) correlates with the $B^2\Sigma^+$ repulsive ionic state and converges to H*(n = 2) and Br($^2P_{3/2}$). If the molecule dissociates via this photofragmentation pathway, H*(n = 2) requires only one additional photon to ionize.

Superexcited states can also autoionize to form either of the ionic ground states. The dynamics of autoionization can be described in terms of the Auger effect, where an antibonding electron is ejected while a Rydberg electron relaxes to yield the configuration that correlates with the ionic ground state. E.g. (from Article #4)

$$HBr^{\#}[^{1,3}\Sigma([^{2}\Pi, \sigma^{1}\pi^{3}\sigma^{*1}]5p\pi^{1})] \rightarrow HBr^{+}/HBr^{**}[^{2}\Pi_{\frac{3}{2},\frac{1}{2}}(\sigma^{2}\pi^{3})] + e^{-}$$

Here, an electron is ejected from the σ* orbital and the electron in the 5pπ orbital relaxes back into the ground state configuration.

3.5.3 Summary of photofragmentation pathways

The major photofragmentation processes, following two-photon resonance excitations, of the hydrogen halides to Rydberg and/or ion-pair states are summarized in Table 10.

Table 10 Summary of photofragmentation mechanisms following two-photon excitations to Rydberg (Ry) and ion-pair (V) states.

	$HX(^{1}\Sigma^{+}) \overset{h\nu}{\rightarrow} \overset{h\nu}{\rightarrow}$
(i)	$HX^{**}(Ry,V) \overset{h\nu}{\rightarrow} HX^{+} + e^{-};\ HX^{+} \overset{h\nu}{\rightarrow} H^{+} + X/X^{*}$
(ii)	$HX^{**}(Ry,V) \overset{pre^{C}}{\longrightarrow} H + X/X^{*};\ X/X^{*} \overset{3h\nu}{\longrightarrow} X^{+} + e^{-}$
(iii)	$HX^{**}(Ry,V) \overset{h\nu}{\rightarrow} H + X^{*};\ X^{*} \overset{h\nu}{\rightarrow} X^{+} + e^{-}$
(iv)	$HX^{**}(Ry,V) \overset{h\nu}{\rightarrow} H^{*} + X/X^{*};\ H^{*} \overset{h\nu}{\rightarrow} H^{+} + e^{-}$
(v)	$HX^{**}(V) \overset{h\nu}{\rightarrow} H^{+} + X^{-}$

Process (i) describes the formation of H^+ where the molecular ionic ground state acts as an intermediate state. Excitation from the ionic state allows the molecule to access repulsive ionic states that correlate with H^+ and X/X*. Process (ii) describes predissociation which yields the neutral atomic fragments H + X/X*. The halogen atoms, X/X*, then require three photons to ionize. Process (iii) describes excitations to repulsive superexcited states which correlate with H + X**, where X** is a Rydberg state. X** requires one photon to ionize. Process (iv) describes a similar pathway as (iii), whereas these yield the neutral hydrogen in an excited state, $n > 1$. The hydrogen atom is subsequently ionized upon absorption of one additional photon. Process (v) describes the formation of an ion-pair, $H^+ + X^-$. This process has been found in HCl by the observation of negative ions,[286] whereas negative ions have not been detected for HBr[280] or HI.[189]

3.6 Direction dependence – Anisotropy

For linearly polarized laser excitations in REMPI experiments, the photofragment angular distributions are cylindrically symmetric and can be expressed, to a first approximation, as[351]

[C] Here, predissociation is abbreviated as "pre".

$$I(\theta) = A(1 + \beta_2 P_2(\cos(\theta)) + \beta_4 P_4(\cos(\theta)) + \beta_6 P_6(\cos(\theta)) \quad (82)$$

where A is a normalizing constant, β_2, β_4, β_6 are the anisotropy parameters, and P denotes Legendre polynomials.

$$P_n(x) = \frac{1}{2^n n!}\frac{d^n}{dx^n}[(x^2 - 1)^n] \quad (83)$$

For (2_r + $n_{r,i}$) REMPI[D], the observed angular distribution of the photoproducts can be expressed, more precisely, as the product of the anisotropy of the two-photon resonance excitation, and the two-photon fragmentation.

$$I(\theta) = AI_f(\theta)I_{ph}(\theta) \quad (84)$$

Here, $I_f(\theta)$, and $I_{ph}(\theta)$, represent the angular distribution of the resonance step and the fragmentation step, respectively.

$$I_f(\theta) = 1 + \beta_{f,2} P_2(\cos(\theta)) + \beta_{f,4} P_4(\cos(\theta)) + \beta_{f,4} P_6(\cos(\theta)) \quad (85)$$

$$I_{ph}(\theta) = 1 + \beta_{ph,2} P_2(\cos(\theta)) + \beta_{ph,4} P_4(\cos(\theta)) + \beta_{ph,6} P_6(\cos(\theta)) \quad (86)$$

3.6.1 Anisotropy of the two-photon resonance excitation

Chichinin *et al.*[282] introduced a way of estimating the anisotropy parameter for two-photon transitions from the $X^1\Sigma^+$ ground state to the $B^1\Sigma^+$ state in the HCl molecule. This approximation has also been used for HBr (see Article #4). Therein, the two-photon absorption intensity was estimated by

$$I = F_0 \mu_{00} P_0 \quad (87)$$

where F_0 is the excitation matrix, μ_{00} is the ground state multipole,[E] and P_0 is the line strength factors, which for the *O*, *Q*, and *S* lines are

$$P_0^Q = \frac{\sqrt{2J''+1}}{3}\left[|S_{00}|^2 + \frac{2}{5}\frac{J''(J''+1)}{(2J''-1)(2J''+3)}|S_{20}|^2\right] \quad (88)$$

$$P_0^S = \frac{\sqrt{2J''+1}}{5}\frac{(J''+2)(J''+1)}{(2J''+1)(2J''+3)}|S_{20}|^2 \quad (89)$$

[D] REMPI experiments will be dealt with in chapter 4. Here, 2_r refers to the two-photon resonance excitation of the parent molecule and $n_{r,i}$ refers to further n photons required for resonance and/or ionization excitations. The fragment ions can be formed by further resonance or non-resonance excitations of the neutral fragments.[252]

[E] For complete derivations / calculations of the excitation matrix and state multipoles, see the original paper by A. I. Chichinin et al.[282]

$$P_0^O = \frac{\sqrt{2J''+1}}{5}\frac{J''(J''-1)}{(2J''-1)(2J''+1)}|S_{20}|^2 \quad (90)$$

Here, $|S_{00}|^2$ and $|S_{20}|^2$ are the zeroth and second rank tensors which contain the transition matrix elements and the energy denominator of second order time-dependent perturbation theory.

$$S_{00} = \sum_{q_1,q_2}\begin{pmatrix}1 & 1 & 0\\ q_2 & q_1 & 0\end{pmatrix} * \sum_i \frac{\langle 1|\boldsymbol{\varepsilon}\cdot\boldsymbol{\mu}_{q_2}|i\rangle\langle i|\boldsymbol{\varepsilon}\cdot\boldsymbol{\mu}_{q_1}|0\rangle}{E_{0i}-h\nu+C(\Gamma_i)} \quad (91)$$

$$S_{20} = \sum_{q_1,q_2}\sqrt{5}\begin{pmatrix}1 & 1 & 2\\ q_2 & q_1 & 0\end{pmatrix} * \sum_i \frac{\langle 1|\boldsymbol{\varepsilon}\cdot\boldsymbol{\mu}_{q_2}|i\rangle\langle i|\boldsymbol{\varepsilon}\cdot\boldsymbol{\mu}_{q_1}|0\rangle}{E_{0i}-h\nu+C(\Gamma_i)} \quad (92)$$

Thus, the intensity ratios of rotational line series for the same initial state, *J´´*, can be written as

$$\frac{I_Q}{I_S} = \frac{10}{3}\frac{(2J''+1)}{(J''+2)}\left[|b|^2\frac{(2J''+3)}{(J'+1)}+\frac{1}{5}\frac{J''}{(2J''-1)}\right] \quad (93)$$

$$\frac{I_Q}{I_O} = \frac{10}{3}\frac{(2J''+1)}{(J''-1)}\left[|b|^2\frac{(2J''-1)}{J''}+\frac{1}{5}\frac{(J''+1)}{(2J''+3)}\right] \quad (94)$$

for the *b* parameter, which includes the contributions of the parallel ($\Sigma \rightarrow \Sigma \rightarrow \Sigma$; $D_{||}$) and perpendicular ($\Sigma \rightarrow \Pi \rightarrow \Sigma$; $D_{\perp}$) transitions,

$$b = \frac{S_{00}}{\sqrt{2}S_{20}} = \frac{D_{\perp}-D_{||}}{D_{\perp}+2D_{||}} \quad (95)$$

In the case of linearly polarized light, the excited state multipoles can be written as

$$\rho_{00} = \frac{2C'|S_{00}|^2}{3\sqrt{3}}\left(|b|^2+\frac{2}{25}\right) \quad (96)$$

$$\rho_{20} = -\frac{2C'|S_{20}|^2}{75}\sqrt{\frac{2}{3}}(1-10Re[b]) \quad (97)$$

to give

$$\beta_{f,2} = -\frac{\sqrt{2}\rho_{20}}{\rho_{00}} = \frac{2-20\,Re[b]}{2+25|b|^2} \quad (98)$$

Finally, the alignment parameter, A_{20}, of the angular momentum *J´*, can be calculated as

$$A_{20} = \sqrt{\frac{(2J'+3)(2J'-1)}{5J'(J'+1)}}\frac{Re[\rho_{20}]}{\rho_{00}} \quad \textbf{(99)}$$

4 Experimental

4.1 Experimental apparatus I. Resonance enhanced multiphoton ionization (REMPI)

In the case of the mass resolved REMPI experiments performed on HBr[233] and HI[234-236] tunable laser radiation was generated via a Coherent ScanMatePro dye laser, pumped by a Lambda Physik COMPex 205 excimer laser. The excimer laser utilizes the emission from the XeCl exciplex created by an electrical discharge from high voltage electrodes. The laser radiation at 308 nm follows a bound-to-free electronic transition from the *B* ion-pair state to the repulsive ground state of the XeCl molecule (e.g. see Ref.[352] and references therein). The excess energy from this process is exported via a 308 nm wavelength photon.

The radiation from the excimer laser was directed into two dye cells in the dye laser containing various dye solutions depending on the region being scanned (see Table 11). The bandwidth of the generated tunable dye-laser radiation was about 0.095 cm^{-1}. The radiation from the dye laser was then frequency doubled with a second harmonic generator (SHG). For our experiments, an interchangeable BBO-2 crystal was placed in the radiation pathway to achieve the frequency doubling. Thus, the generated radiation provided data resolution of approximately: 4 x 0.095 $cm^{-1} \approx 0.4$ cm^{-1}.

The laser beam was directed into a vacuum chamber containing electric platings designed to direct any ions formed into a TOF (time-of-flight) tube. The platings consist of a single repeller which is a highly charged positive plate and several extractors which, having less positive charges, serve as focal and directional lenses for the ions. The laser beam was focused by a 20 cm focal length lens.

Table 11 Wavelength and wavenumber ranges of photons used for specific dyes and relevant references.

Molecule	*Wavelength range [nm]*	*Wavenumber [cm^{-1}]*	*Dyes*	*Ref.*
HBr	498.13 – 506.07	79 040 – 80 300	C503	233
HI	534.05 – 579.71	69 000 – 74 900	R-590, C540A	234-236

A jet-cooled molecular stream was directed through a nozzle orthogonally with respect to the radiation beam. The vacuum chamber was pumped by a diffusion pump backed by an Edwards mechanical pump whereas the TOF tube was pumped by a Pfeiffer turbo pump also backed by an Edwards mechanical pump.

The HBr gas sample (99.8% purity) was acquired from Merck-Schuchardt whereas the the HI gas sample (99.5%) was obtained from Matheson gas products Inc. Undiluted gases were

pumped through a 500 µm nozzle from a sample backing pressure of about 2.0 – 2.5 bar into the vacuum chamber. The pressure inside the chamber never exceeded 10^{-6} mbar during experiments. The nozzle opening time was kept between 150 and 200 µs and the delay time for laser excitation was between 450 and 550 µs. Typical repetition rates were 50-100 pulses for each frequency point. Figure 11 shows a schematic of the experimental setup.

REMPI-TOF data for jet-cooled gas were sampled by detecting ions formed at the focal point after separation in the TOF tube, and detection by MCPs (micro channel plates). Signals from the MCPs were fed into a LeCroy WaveSurfer 44MXs-A, 400 MHz storage oscilloscope and stored as a function of the ion time-of-flights and the laser radiation wavenumbers.

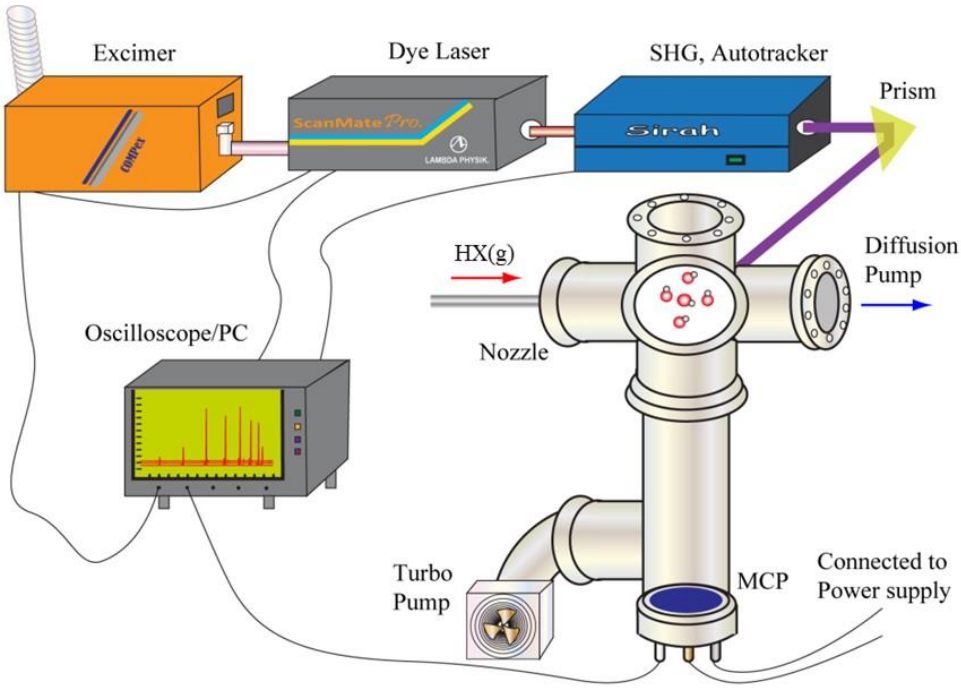

Figure 11 Schematic figure of the REMPI-TOF experimental equipment.

4.1.1 Analysis Methodology

The described equipment allowed simultaneous measurements of all ions within a defined mass range. The data was collected by use of a Labview program which was also used to control the wavenumber scanning and further data acquisition.

Individual ion signals were integrated as a function of the recorded wavenumbers to yield REMPI spectra for H^+, X^+, and HX^+ (X = ^{79}Br, ^{81}Br, ^{127}I). The mass spectrum is an intensity vs *m*/*z* (mass-to-charge ratio) but the time-of-flight principle (see chapter 4.1.3) allows the mass spectrum to be recorded as intensity vs the ions‘ time-of-flight. See Figure 12 for mass spectra and Figure 13 for REMPI spectra of HBr and HI.

Igor Pro version 6.37[353] was used to process and analyze the compiled spectra.

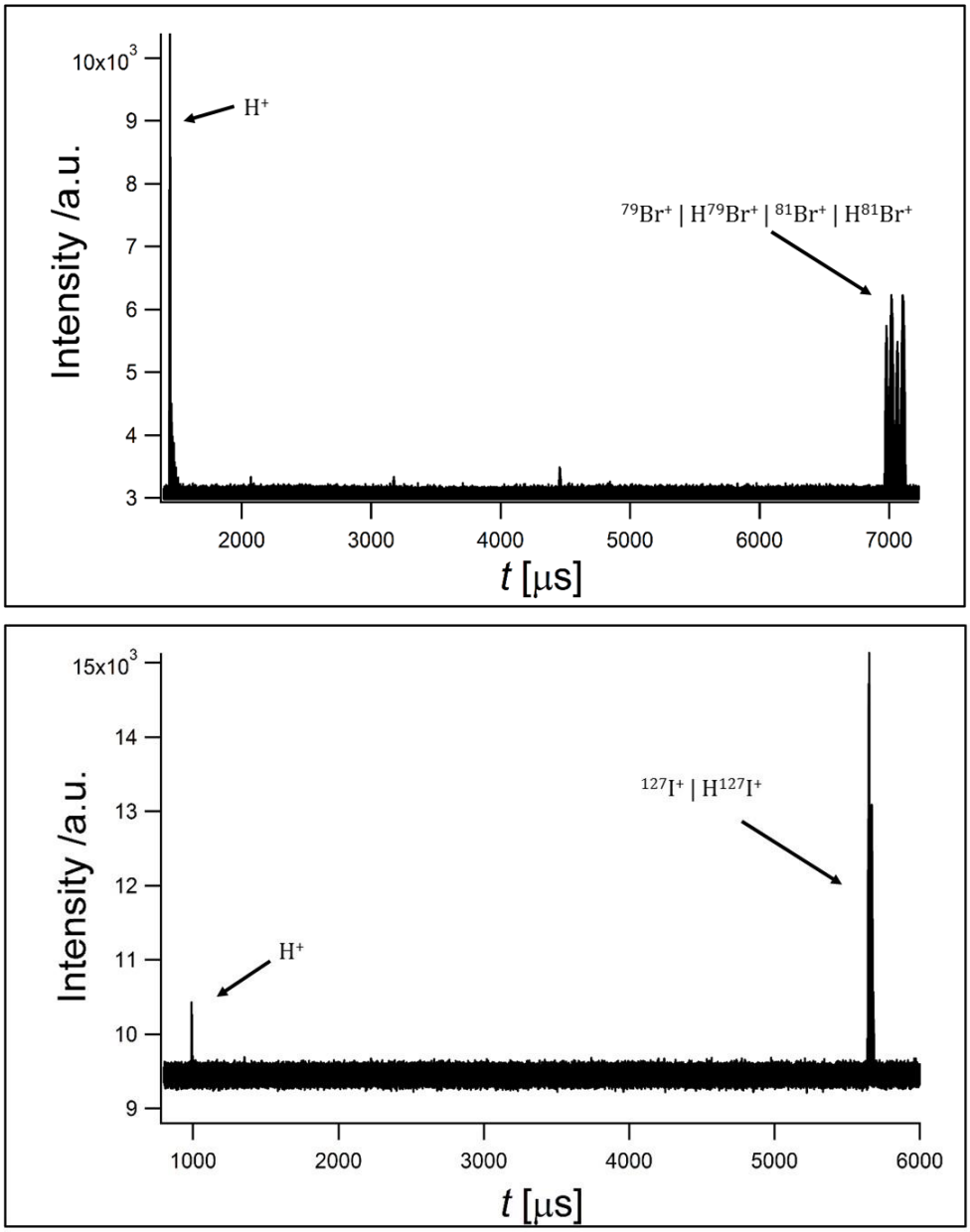

Figure 12 (Above) Compiled mass spectra of HBr from 79330 to 79350 cm^{-1}. The strongest observed peaks correspond to ion counts of H^+, $^{79}Br^+$, $H^{79}Br^+$, $^{81}Br^+$, and $H^{81}Br^+$, as marked. Other peaks correspond to impurities such as C^+ and C_2^+. (Below) Compiled mass spectra of HI from 70756 to 70778 cm^{-1}. The strongest observed peaks correspond to ion counts of H^+, $^{127}I^+$, and $H^{127}Br^+$, respectively.

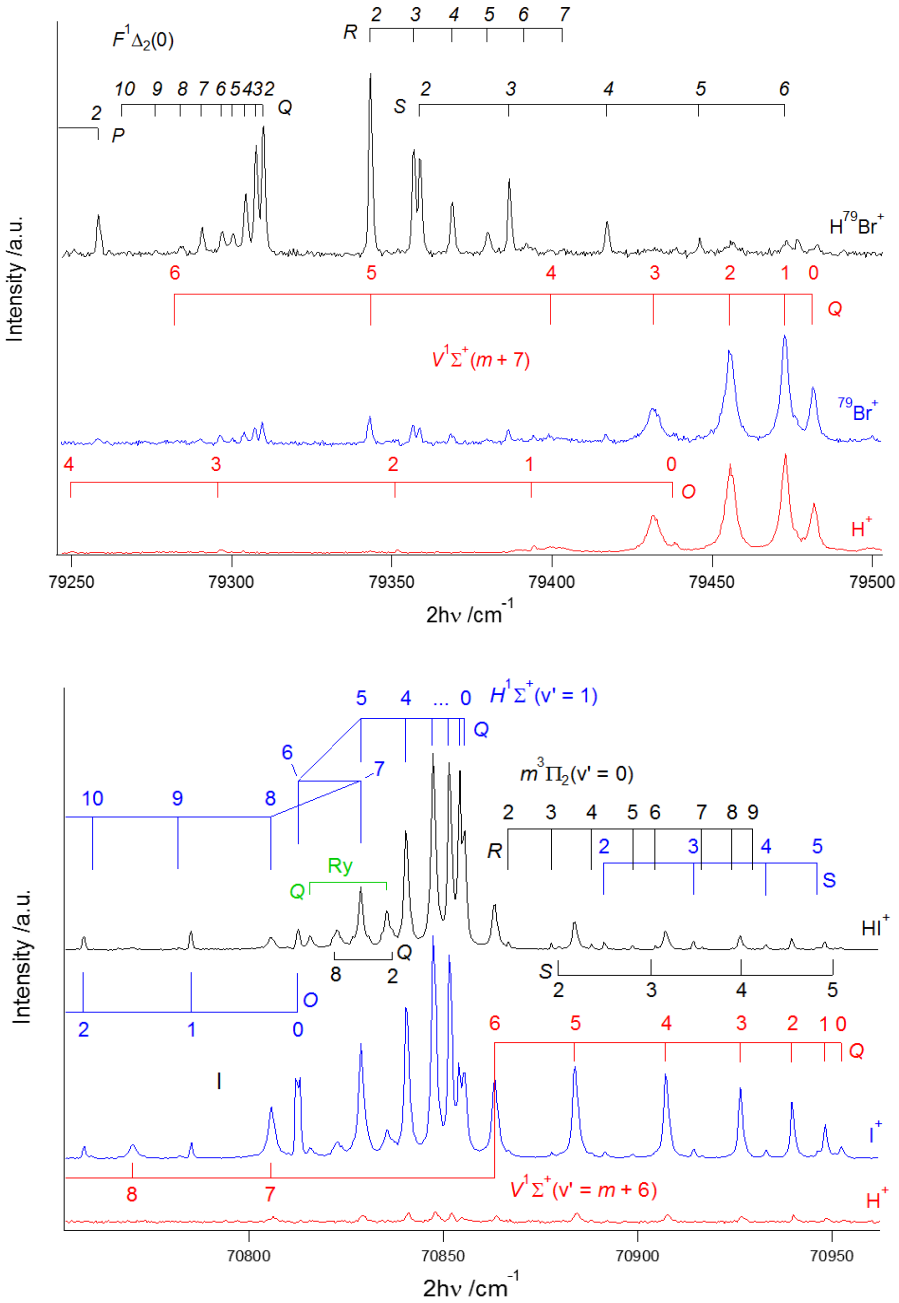

Figure 13 (Above) A mass resolved REMPI spectrum of HBr for the fragments H^+, $^{79}Br^+$, and $H^{79}Br^+$. Displayed are some of the rotational branches of the $F^1\Delta_2(0)$ Rydberg state and the $V^1\Sigma^+(m + 7)$ ion-pair state. Nota bene, the *O* lines of the $V^1\Sigma^+(m + 7)$ state have not been reported. (Below) A mass resolved REMPI spectrum of HI for the fragments H^+, $^{127}I^+$, and $H^{127}I^+$. Displayed are some of the rotational branches of the $H^1\Sigma^+(1)$ and $m^3\Pi_2(0)$ Rydberg states and the $V^1\Sigma^+(m + 6)$ ion-pair state. Also presented is an unassigned (hidden) Rydberg state, responsible for forbidden perturbations between the $m^3\Pi_2(0)$ Rydberg state and the $V^1\Sigma^+(m + 6)$ ion-pair state.

4.1.2 Simulations

In some cases, spectra simulations were performed to assist with peak assignments. In order to simulate the perturbed spectra (though rudimentarily), the program PGOPHER developed by C. M. Western[354] was used. The program allows for a wealth of input parameters. For rotational assignments, as emphasized in this thesis, the key input parameters were the rotational and centrifugal constants, band origins, and off-diagonal matrix elements, as well as the symmetries of the states involved. An example of a simulation of a spectrum showing the effects of near-degenerate perturbations, is presented in Figure 14.

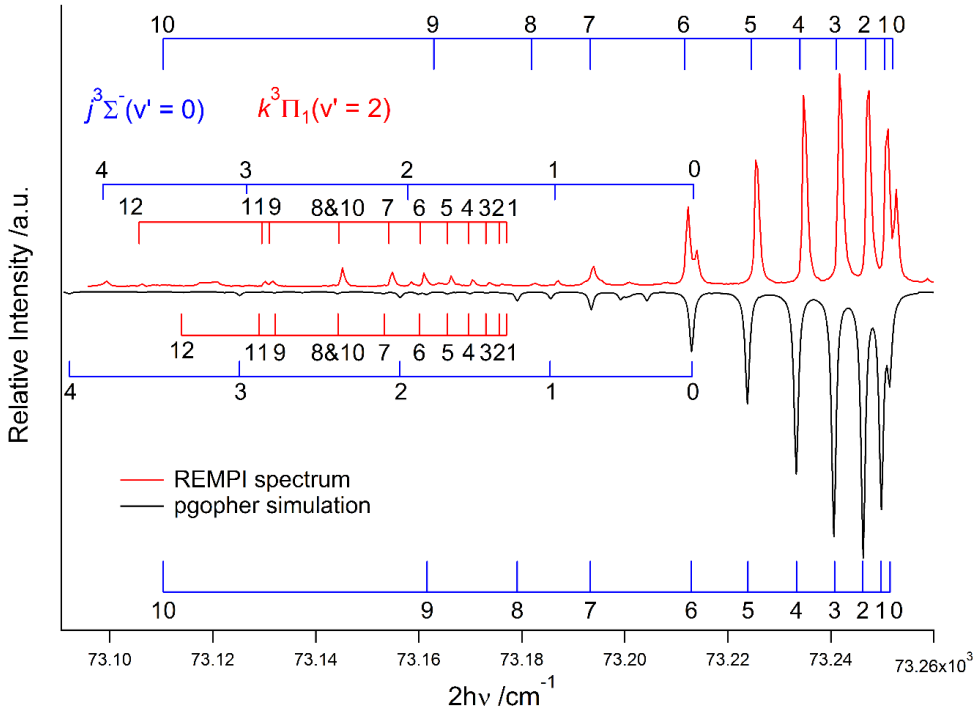

Figure 14 Example of a simulation by PGOPHER of a REMPI spectrum due to two-photon resonance excitations to the $j^3\Sigma^-(0)$ and $k^3\Pi_1(2)$ Rydberg states of HI, which was utilized in Article #6. The simulation includes a perturbing $^3\Sigma^-$ state with origins at about 73 200 cm^{-1} and the ion-pair vibrational states $V^1\Sigma^+(m + 12)$ and $V^1\Sigma^+(m + 13)$.

4.1.3 Time of flight analysis

When a molecule (or atom) is ionized in an electric field, it gains momentum in the direction of the field. The relationship between the ion masses (M_w) and the time-of-flight (t) for our equipment is

$$t = a\sqrt{M_W} + b \qquad (100)$$

The constants a and b vary between experiments and are evaluated for each measurement. Using eq. (100), calibration of the mass spectra (i.e. evaluation of a and b) normally is

relatively easy for two reasons: i) The number of expected ion peaks arising from fragment ions of the hydrogen halides is small and easily distinguishable, and ii) additional peaks, due to impurities such as C^+ and C_2^+, are frequently present, which further validate the calibration.

4.1.4 Equipment control

The experimental control is based on a sequence of triggers directed through the LabVIEW program. REMPI data are thusly sampled by scanning the dye laser over specific spectral ranges with a wavelength appropriate dye.

To initiate an experimental procedure, commands are sent to the dye laser to move its grating to the position of the inital wavelength, λ_1. The dye laser control unit typically generates a chain of 30 to 100 pulses at 10 Hz, each of which triggers the opening of the nozzle. Each pulse is delayed and fed to the excimer pump laser. Subsequently, the dye laser changes the wavelength from λ_1 to λ_2 by previously specified step sizes. This process is repeated until the total wavelength range is covered. During a scan, the laser output energy is kept at a maximum by turning the SHG crystal through auto-tracking.

4.2 Experimental apparatus II. Velocity map imaging (VMI)

When photofragments dissociate, they do so via repulsive states. The repulsive states converge to fragments, whose energy is somewhat lower than the energy obtained from the (three) photons absorbed. The excess energy is translated into kinetic energy of the atoms that fly apart from each other. The direction of the fragmentation is governed by the alignments of the molecules against the laboratory frame, the polarization of the laser radiation, and the symmetry of the orbitals involved in the photodissociation.

The experimental apparatus used for velocity map imaging experiments on HBr is presented in Figure 15 and has been described in detail elsewhere.[355-357] It consists of two differentially pumped chambers. Firstly, a source region which is pumped by a Leybold, DI 3000 diffusion pump. Secondly, a detection region which is pumped by a Leybold, Turbovac 600 turbo-molecular pump. The valve design is based on original work of D. Proch & T. Trickl[358] with a modification similar to the work of F. Dong *et al.*[359] and Q. Ran *et al.*[360]

The detection chamber is equipped with an ion optics assembly. It is described in detail in Ref.[357] A schematic of the ion optics used in these experiments is displayed in Figure 16. Focusing is achieved by translating the laser position along the TOF axis, i.e. when the starting position along the TOF axis is at a specific distance from either the repeller or the extractor.

A supersonic molecular beam, typically of a 15% HBr mixture in He, was formed by expansion through a home-made piezoelectrically actuated nozzle valve before being skimmed prior to entering the detection chamber. A stagnation pressure of $P_0 \leq 1$ bar and a nozzle diameter of 1 mm was used. A skimmer (ø1.5 mm Beam Dynamics) was positioned approximately 5 cm from the nozzle orifice.

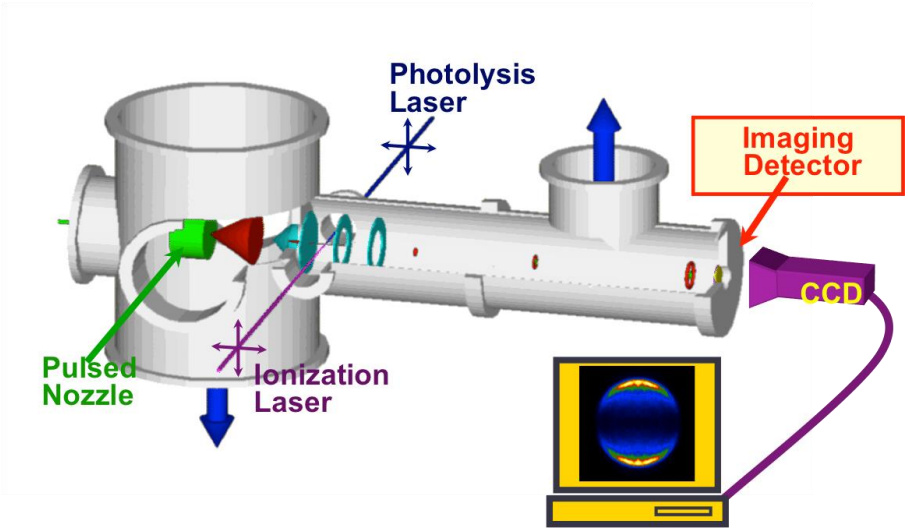

Figure 15 Velocity map imaging experimental apparatus. Laser radiation perpendicularly intersects with the molecular beam from the pulsed nozzle. Ionized photofragments are accelerated onto a phosphorescent screen which is imaged by a charged coupled device (CCD) camera.

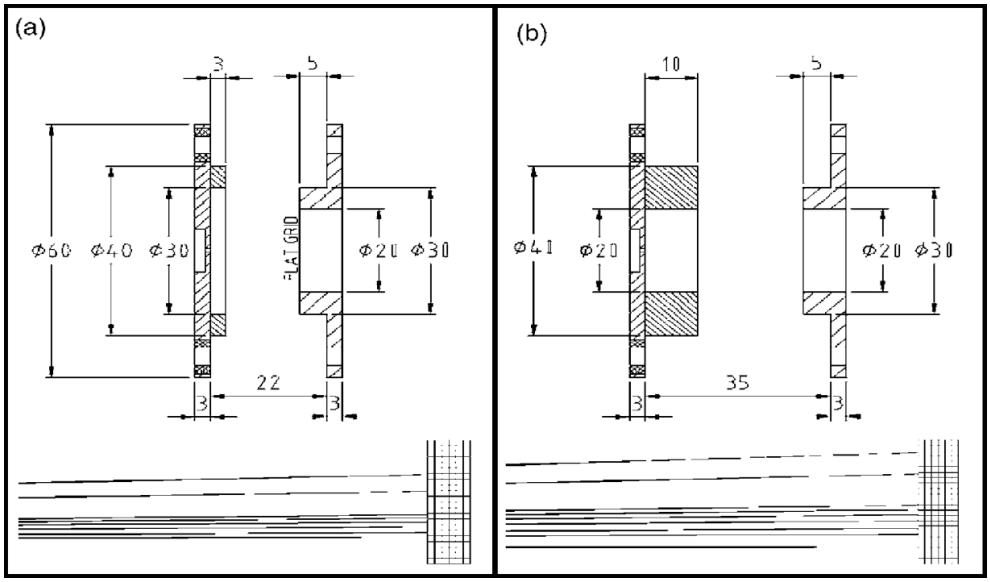

Figure 16 Scaled schematic of the ion optics (numerical values are in mm). Dimensions are optimized for a TOF length of about 45 cm. Panel a) shows the dimensions for when a flat grid is placed on the extractor and panel b) shows when the grid is removed. In both cases velocity mapping is achieved with the presented dimensions as shown on the figures below the ion optics assembly. The figure is reproduced from Ref.[357]

A photolysis/photofragment ionization laser beam is focused (f = 20 cm) on the geometric focal point of the repeller and extractor plates where it intersects the collimated molecular beam at right angles. In one-color experiments, the laser beam is generated by a pulsed Nd^{3+}:YAG (Spectra Physics Quanta Ray Pro 250) pumping a master oscillator - power

oscillator system (Spectra Physics MOPO 730-10) set at the appropriate wavelength. In two-color experiments, a second excimer-pumped (Lambda Physik LPX300, operating with XeCl) pulsed-dye laser (Lambda Physik LDP3000) pulses are also used with an appropriate dye and a BBO crystal to achieve (2 + 1) REMPI of the quantum-state-selected photofragments generated by the MOPO system. In the latter case of two-color experiments, the two lasers are counter-propagating and focused onto the collimated molecular beam by f = 30 cm lenses. The photolysis laser is used to generate neutral fragments and after a suitable time delay, the probe laser is used to ionize one of the quantum-state-selected fragments by REMPI.

The probe laser pulses are delayed with respect to the photolysis pulse, in order to allow a sufficient density of photofragments to build up prior to REMPI detection. Moreover, the time delay between the photolysis and photoionization pulses had to be carefully adjusted in order to avoid photofragment "fly-out". Typically, the delay is set at about 10 ns.

In a one-color experiment, the photolysis laser pulse is also used for the REMPI of the nascent photofragments. The laser power is kept relatively low; below 3 mJ/pulse in order to minimize space-charge effects from excessive ion production in the interaction region.

Ions produced are accelerated into a field free space of the detection chamber, where they fly towards a position-sensitive detector located approximately 45 cm from the molecular beam / laser pulse interaction point. Due to the mass difference of the possible photofragments (H^+ and $^{79/81}Br^+$) only one fragment mass is imaged at a time while the others are separated by the time-of-flight during their field-free trajectory on route to the detector.

The velocity distribution of the photofragments produces a Doppler broadening in the resonant transition used for their REMPI which is larger than the probe-laser bandwidth. Therefore, for VMI experiments the laser wavelength has to be scanned, so that all photofragments are ionized with equal probability.

The imaging detector consists of a dual, imaging-quality MCP array coupled to a P47-phosphor-coated anode (Proxitronix) with an effective diameter of 40 mm. After passing through the TOF region, ions hit the surface of the front MCP, which is pulsed between 0 and –700 V. For each ion detected, the MCPs produce a large amount of electrons (~10^6) at the rear side, which is kept at positive voltage (+1200 V). These electrons are accelerated onto the phosphor screen (kept at +6 kV) to create phosphorescence spots. Ion selection is achieved by "gating" the front MCP from 0 (no detection) to –700 V with a fast (<20 ns) high voltage switch circuit. The timing of the experiment is controlled by using a pulse generator (Berkeley Nucleonics 565 Series) and is optimized by monitoring the ion signal on an oscilloscope (Hameg HM1007; 100 MHz). During the "gated" operation, scope signal monitoring is stopped, as the high voltage pulse will capacitively couple to the monitoring oscilloscope.

Images appearing on the phosphor anode are recorded asynchronously every second (~10 laser shots) using a charge-coupled-device (CCD) video camera (Unibrain Fire-I 702), equipped with a 50 mm f1.4 lens, with on-chip integration capabilities and connected to a PC through Firewire (IEEE1394) interface. Typically, several thousand such frames are averaged to form images. 2D slices of the 3D ion distributions from a final image were extracted by an inverse Abel transformation. Those images (see Figure 17) were integrated from their centers over angle to obtain the velocity distribution and over radius to extract the

angular distribution of the fragments. Background images were obtained either by tuning the photoionizing laser off-resonance or by changing the delay timing of the laser pulses so that the probe pulses arrived at the interaction region long after the molecular beam pulse has crossed this region or by turning the molecular beam off. The background images are subtracted from the signal images.

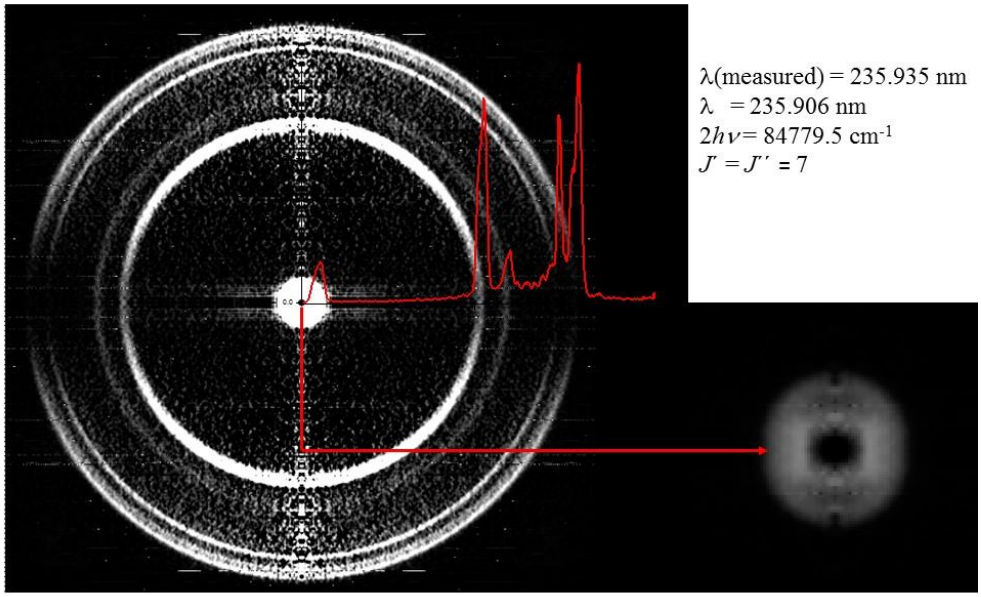

Figure 17 An Abel transformed H^+ velocity map image for resonance excitation to the $J' = 7$ rotational line of the $^3\Sigma^-(6p\pi)(v' = 0)$ Rydberg state. The kinetic energy release (KER) spectrum is superimposed on the image. On the right, a close-up of the innermost ring is presented. The data is unpublished.

4.2.1 Analysis methodology

A typical 2D image is shown in Figure 17, Along with the KER spectrum (red line) obtained by integrating the image over angle. For the simple case of no focusing fields (ion imaging), the kinetic energy (E) of mass (m), if the time-of-flight (t) is known (from the scope or the detector gate setting), is

$$E = \frac{1}{2} m * \left(\frac{R}{t}\right)^2 \qquad (101)$$

where R is the radius (distance from the center) on the image. However, in VMI focusing fields (i.e. einzel lens or the two-electrode slicing scheme of Papadakis *et al.*[357]) are employed, which add a magnification factor, M, to the above formula

$$E = \frac{1}{2} mM \left(\frac{R}{t}\right)^2 \quad \textbf{(102)}$$

If we set

$$M' = \frac{1}{2} m \frac{M}{t^2} \quad \textbf{(103)}$$

the formula becomes

$$E = M' * R^2 \quad \textbf{(104)}$$

M´ is dependent upon the repeller voltage and has to be determined for the pixel-to-energy transformation. Therefore, for a VMI image, energy calibration for each repeller voltage is required; the *R* for a mass of known kinetic energy *E* is measured at the required repeller voltage and the *M´* is determined from the last formula. In HBr we have done so by using the energy difference in the H images of the two spin-orbit states of Br ($^2P_{3/2}$ and $^2P_{1/2}$) which should differ by the spin orbit splitting (2685.24 cm^{-1}).[350]

To assign each individual KER peak, the expected KERs for various channels were calculated and compared with the observed KER peaks. These analyses are described in detail in Article #4.

5 Spectroscopic analysis

As the two experimental setups discussed in chapter 4 yield different data, different analytical approaches are adopted. Here we will briefly discuss i) the analysis of mass resolved REMPI data, and ii) analysis of velocity map images.

5.1 Analyzing mass resolved REMPI spectra

For most of the analyses of mass resolved REMPI data, emphasis was placed on the identification of perturbation effects resulting from state interactions. As previously mentioned, perturbations are categorized as homogeneous ($\Delta\Omega = 0$) and heterogeneous ($\Delta\Omega \neq 0$). In the literature, these interactions were frequently referred to as off-resonance and near-resonance interactions, respectively, based on their appearance in the spectra. At later stages, to avoid confusion with "resonance transitions" these were expressed as non-degenerate and near-degenerate interactions, respectively.

Other naming conventions were also introduced in this work to distinguish the three major types of perturbation effects, notable in the REMPI spectra. These are *LS-effects*, *LI-effect*, and *LW-effects*, which refer to line-shift effects, line intensity-effects, and line-width effects, respectively. Here, these effects will be outlined, as well as quantum defects, which have been useful in spectral assignments.

5.1.1 LS-effects

Perhaps the most common appearance of perturbation effects take the form of LS-effects where spectral lines are shifted because of quantum level shifts due to level-to-level state interactions. In the case of homogeneous perturbations, the interaction strength parameters, W' (i.e. the off-diagonal Hamiltonian matrix elements), are independent of J', whereas in case of heterogeneous perturbations, the W's are J' dependent,

$$W = W'\sqrt{J'(J'+1)} \qquad \textbf{(105)}$$

where W' is a constant.

Two useful methods to identify LS-effects in the spectra were applied, i) -plotting graphs of $\Delta E_{J',\,J'+1}$ vs J's, where $\Delta E_{J',\,J'+1}$ is the energy difference between "neighboring quantum energy levels J' and J' + 1 (i.e. LS-plots), and ii) –making reduced term value plots.

In accordance with theory, LS-plots for unperturbed spectra should yield approximately linear graphs. Observed deviations from such behavior have proved useful in identifying a multitude of level-to-level interactions between excited states of the hydrogen halides.[226, 227, 229, 230, 232-237] Reduced term value plots are useful for the same reason but are even more sensitive to level-to-level interaction effects. Reduced term values are calculated as the energetic difference between measured energies (E) and the fitted or deperturbed energies for a give J'.

$$\Delta E = E - (v^0 + B'J'(J'+1) - D'J'^2(J'+1)^2 \quad (106)$$

Examples of non- and near-degenerate interactions, resulting LS-plots and reduced term value plots, are presented in chapter 6.5.1 (supplementary material for Article #5).

To obtain deperturbed values of the rotational constants, as well as interaction strengths, the observed line positions were fitted to the appropriate equations as presented in chapter 2.1. Igor Pro version 6.37[353] was used for the procedure. Known rotational constants of HBr and HI were used as input parameters.

5.1.2 LI-effects

Formation of molecular ions is the likeliest result of an excitation via a "pure"/unmixed Rydberg state. On the other hand, if Rydberg states are readily mixed with ion-pair states, the increased ion-pair character will result in excitations at longer internuclear distances, to a greater extent. This frequently results in excitations to repulsive superexcited states or repulsive ionic states to produce excited photofragments or atomic ions. Thus, highly mixed Rydberg states yield a greater amount of H^+ and X^+ ions in their respective REMPI spectra.

By using these characteristics of ion formations, the weight factors (c_i^2) for the mixing of Rydberg and ion-pair states can be evaluated. If we denote the eigenfunctions of the perturbed states as $\psi_1$and ψ_2, and of the unperturbed states as ψ_1^0 and ψ_2^0, the perturbed levels can be represented as

$$\begin{aligned} |\psi_1\rangle &= c_1|\psi_1^0\rangle - c_2|\psi_2^0\rangle \\ |\psi_2\rangle &= c_1|\psi_1^0\rangle + c_2|\psi_2^0\rangle \end{aligned} \quad (107)$$

for the weight factors

$$c_i^2 = \frac{1}{2} \pm \frac{\sqrt{|\Delta E|^2 - 4|W_{12}|^2}}{2|\Delta E|} \quad (108)$$

Where $\Delta E = E_1 - E_2$.

Based on the above assumptions, the X^+ intensities are proportional to the fraction of HX** molecules in the Rydberg state (c_1^2) and the ion-pair state (c_2^2).

$$I(X^+) = \alpha_2 c_2^2 + \beta_1 c_1^2 \quad (109)$$

Similarly, the HX^+ intensity are derived as

$$I(HX^+) = \alpha_1 c_1^2 + \beta_2 c_2^2 \quad (110)$$

If we set $\alpha = \alpha_2/\alpha_1$, $\gamma = \beta_1/\alpha_2$, $\delta = 1 - (\beta_2/\alpha_1)$, and $c_1^2 = 1 - c_2^2$, the ratio between the ion intensities is

$$\frac{I(X^+)}{I(HX^+)} = \alpha \frac{(\gamma + c_2^2(1-\gamma))}{(1 - \delta c_2^2)} \quad (111)$$

This expression can be further simplified by assuming that HX^+ produced by excitation from a "pure" (diabatic) ion-pair state is negligible, in which case the factor β_2 is assumed to approach zero and thus, $\delta = 1 - (\beta_2/\alpha_1) \approx 1$. This assumption leaves the parameters α and γ, as suitable variables for fitting observed intensity ratios as a function of energy levels, J'.

The γ factor measures the relative rate of formation of X^+ from the diabatic Rydberg state (β_1) to that of its formation from the diabatic ion-pair state (α_2). As the latter is the major formation channel for X^+, the value of γ is expected to be small, but non-zero and serves as a measure of the relative importance of the two dissociation channels.

The α factor measures the relative rate of the main formation channel of X^+ from the ion-pair state (α_2) to the main formation channel of HX^+ from the Rydberg state (α_1). Therefore, in the case of Rydberg resonance excitations, α factor increases with state mixing.

Combined, the multiplicative factor $\alpha\gamma = \beta_1/\alpha_1$, measures the relative contributions to the X^+ formation and HX^+ formation from the Rydberg state. Further discussion about comparison of these results for HCl, HBr, and HI is presented in chapter 8.

The $I[X^+]/I[HX^+]$ intensity ratios as a function of J' were used throughout as a measure of evidences of state interactions. More explicitly, these gave evidences of hidden states (see Articles #5 and #6).

5.1.3 LW-effects

Line-widths are strongly influenced by bound-to-bound and bound-to-continuum state interactions. This instability results in decreased lifetimes, hence line-width broadenings. These effects are referred to as LW-effects.

Lower limit lifetimes (τ_{min}) can be derived from the line-widths (Γ) by[345]

$$\tau_{min}(ps) = 5.3/\Gamma(cm^{-1}) \quad (112)$$

In the absence of Doppler broadening, the line shape can be assumed to be Lorentzian. The Lorentzian function (χ) is dependent on the frequency (ν)

$$\chi(\nu, \nu_0) = \frac{\Gamma/2\pi}{(\nu - \nu_0)^2 + (\Gamma/2)^2} \quad (113)$$

for any line position ν_0. Otherwise, the line shapes can be described by a Gaussian.

$$\chi(\nu, \nu_0) = \frac{2}{\Gamma}\sqrt{\frac{\ln(2)}{\pi}}e^{-\left(\frac{4\ln(2)(\nu-\nu_0)^2}{\Gamma^2}\right)} \quad (114)$$

Generally, the broadest peaks observed, correspond to highly perturbed rotational levels of ion-pair states. They were better fitted by Gaussian line shapes rather than Lorentzian. Ion-pair states, however, do not predissociate directly[230, 232, 233] but observed line-width alterations due to interactions with one or more predissociating Rydberg states.

If we let τ be the total lifetime of a perturbed state (the perturbation can both be in the form of bound level-to-level interactions or bound-continuum interactions) and $k_1(J')$, $k_2(J')$, ..,

$k_n(J')$, are the J' dependent predissociation rates of relevant Rydberg states, then the number of molecules that dissociate from the perturbed state during a time interval, *dt*, is given by

$$dN = \sum_i^n -k_i(J')Ndt \quad (115)$$

with the solution

$$N(t) = N_0 \prod_i^n e^{-k_i(J')t} = N_0 \prod_i^n e^{-t/\tau} \quad (116)$$

where N_0 is the initial population. The total lifetime can, subsequently, be expressed in terms of the sum of predissociating rates of interacting Rydberg states and a J' dependent coupling rate ($f_i(J')$) for the Rydberg to ion-pair interaction.

$$\frac{1}{\tau} = \sum_i^n f_i(J')k_i(J') = \sum_i^n f_i(J')\frac{1}{\tau_i} \quad (117)$$

5.1.4 Quantum defects

To a first approximation, quantum defect values (δ) are constant for a series of converging Rydberg states. Therefore, determinations of quantum defects has proven useful in assignments of Rydberg state spectra for both HBr and HI. From eq. (28), the quantum defect, δ, can be derived as

$$\delta = n - \sqrt{\frac{\Re}{IE - T_e}} \quad (118)$$

for v′ dependent ionization energies IE.

5.2 Analyzing a VMI image

Analysis of velocity map images are discussed in Article #4. A short summary, in terms of kinetic energy release spectra, alignment parameters, for HBr will be presented here.

5.2.1 Kinetic energy release (KER) spectra

Rings or a set of rings in a velocity map image correspond to different formation routes of the photofragment being imaged. For H^+, typically four or five formation paths were observed. These correspond to i) formation through repulsive superexcited states (i.e. pathway (iv) described in chapter 3.5.3) and ii) formations through the ionic ground states (i.e. pathway (i) in chapter 3.5.3). In the majority of the cases of H^+ formations in (i) the H*(n = 2) fragment was involved. For the resonance Rydberg state ($^3\Sigma^-6p\pi$) a pathway involving H*(n = 3) was also observed.

The assignments of the KER spectra were based on calculations of the expected KERs for the various channels, by using the relevant energetic parameters. These calculations are presented in detail in Article #4.

5.2.2 Anisotropy parameters

Significant alterations in the angular distribution of the H^+ ions were observed for the various fragmentation channels as a function of J' resonance excitations, in tandem with perturbation strengths. Thus, in Article #4, the angular distributions of the so-called Br (via H* + Br) and Br* (via H* + Br*) channels seem to switch character. The Br channel is found to become increasingly more parallel with J', whereas the Br* channel becomes increasingly more perpendicular. For the highest observed value of J' for the Br* channel, the anisotropy parameter is measured as almost zero.

Different fits were used to estimate the anisotropy of the relevant photofragmentation (ph) channels. To a first approximation, a "single step" fitting procedure was used (see eq. (82)), but with the β_6 parameter omitted since it gave no extra improvements to the evaluation of the principle β_2 parameter. The limitation of the single step is that it estimates the anisotropy of the entire ionization process based on a one step procedure. As an improvement, a "two-step" fitting procedure was implemented where the intensity ratios between the *Q*, *O*, and *S* lines, in mass resolved REMPI spectra, were used to obtain the *b* parameter in eqs. (93) and (94). The *b* parameter was subsequently used to extract the $\beta_{f,2}$ parameter for the resonance excitation. Eqs. (84) – (86) were used to fit the $\beta_{ph,2}$ parameter (as well as $\beta_{f,4}$ and $\beta_{ph,4}$ parameters) for the photofragmentation processes.

Angular distributions of all rings were found to exhibit parallel or perpendicular character. The angular distributions data was derived as intensities as a function of scattering angles (0 – 180). Examples of angular distribution data along with fits from the two-step analysis are presented in Figure 18 along with the relative contributions of the alignment of angular distributions in the resonance state ($P_f(\theta)$) and the photofragmentation ($P_{ph}(\theta)$).

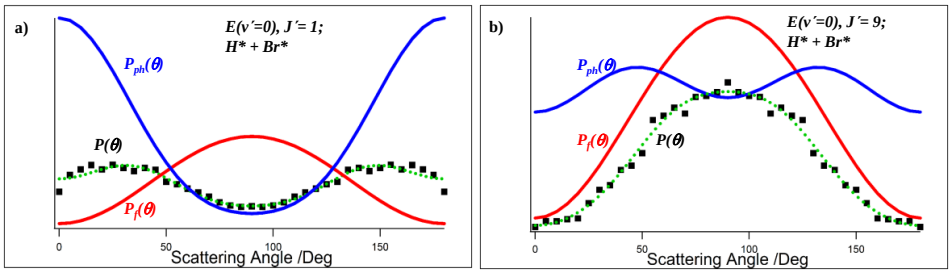

Figure 18 Angular distributions of H^+ for resonance excitations to the $E\ ^1\Sigma^+$ (v´= 0) Rydberg state followed by photoexcitations to form H* (*n* = 2) + Br*(1/2) for $J'' = J' = 1$ (a) and $J'' = J' = 9$ (b): Experimental dots, least square fit curves ($P(\theta)$;dotted curves) for two-step excitation mechanism and calculated "step-contributions", $P_f(\theta)$ (red) and $P_{ph}(\theta)$ (blue). The processed data is from experiments presented in Article #4.

6 Included Papers

The following papers are included in this thesis.

- Jingming Long, Helgi Rafn Hróðmarsson, Huasheng Wang, and Ágúst Kvaran. **Photofragmentations, state interaction, and energetics of Rydberg and ion-pair states: Two-dimensional resonance enhanced multiphoton ionization of HBr via singlet- triplet- Ω = 0 and 2 states.** *Journal of Chemical Physics.* (2012) **136.** 214315.

- Helgi Rafn Hróðmarsson, Huasheng Wang, and Ágúst Kvaran. **New REMPI observations and analyses for Rydberg and ion-pair states of HI.** *Journal of Molecular Spectroscopy.* (2013) **290**. 5-12.

- Helgi Rafn Hróðmarsson, Huasheng Wang, and Ágúst Kvaran. **Photofragmentations, state interactions, and energetics of Rydberg and ion-pair states: Resonance enhanced multiphoton ionization of HI.** *Journal of Chemical Physics.* (2014) **140.** 244304.

- Dimitris Zaouris, Andreas Kartakoullis, Pavle Glodic, Peter C. Samartzis, Helgi Rafn Hróðmarsson, and Ágúst Kvaran. **Rydberg and valence state excitation dynamics: A velocity map imaging study involving the E-V state interactions in HBr.** *Physical Chemistry Chemical Physics*. (2015) **17.** 10468.

- Helgi Rafn Hróðmarsson, Huasheng Wang, and Ágúst Kvaran. **State interactions and illumination of hidden states through perturbations and observations of new states: Highy energy resonance enhanced multiphoton ionization of HI.** *Journal of Chemical Physics.* (2015) **142.** 2443012.

- Helgi Rafn Hróðmarsson and Ágúst Kvaran. **Revealing photofragmentation dynamics through interactions between Rydberg states: REMPI of HI as a case study.** *PCCP*. 2015, 17, 32517.

- Pavle Glodic, Dimitris Zaouris, Peter C. Samartzis, Helgi Rafn Hróðmarsson, Huasheng Wang, and Ágúst Kvaran. **Rydberg and valence state excitation dynamics: One and two color VMI study of singlet states in HBr.** *Manuscript in progress – unpublished.*

Article 1

Photofragmentations, state interactions, and energetics of Rydberg and ion-pair states: Two-dimensional resonance enhanced multiphoton ionization of HBr via singlet-, triplet- Ω = 0 and 2 states.

Jingming Long, Helgi Rafn Hróðmarsson, Huasheng Wang, and Ágúst Kvaran

Journal of Chemical Physics. **136**. 214315 (2012).

DOI: 10.1063/1.4723810

Helgi Rafn Hróðmarsson actively participated in the measurements along with Dr. Huasheng Wang ang Dr. Jingming Long. Helgi conducted majority of data analyses for the $F(1)$, $V(m + 7)$, and the $H(0)$ states and contributed to editing until publication.

Photofragmentations, state interactions, and energetics of Rydberg and ion-pair states: Two-dimensional resonance enhanced multiphoton ionization of HBr via singlet-, triplet-, $\Omega = 0$ and 2 states

Jingming Long, Helgi Rafn Hróðmarsson, Huasheng Wang, and Ágúst Kvaran[a)]
Science Institute, University of Iceland, Dunhagi 3, 107 Reykjavík, Iceland

(Received 15 March 2012; accepted 16 May 2012; published online 7 June 2012)

Mass spectra were recorded for one-colour resonance enhanced multiphoton ionization (REMPI) of H^iBr ($i = 79, 81$) for the two-photon resonance excitation region 79 040–80 300 cm^{-1} to obtain two-dimensional REMPI data. The data were analysed in terms of rotational line positions, intensities, and line-widths. Quantitative analysis of the data relevant to near-resonance interactions between the $F^1\Delta_2(v' = 1)$ and $V^1\Sigma^+(v' = m + 7)$ states gives interaction strengths, fractional state mixing, and parameters relevant to dissociation of the F state. Qualitative analysis further reveals the nature of state interactions between ion-pair states and the $E^1\Sigma^+$ ($v' = 1$) and $H^1\Sigma^+(v' = 0)$ Rydberg states in terms of relative strengths and J' dependences. Large variety in line-widths, depending on electronic states and J' quantum numbers, is indicative of number of different predissociation channels. The relationship between line-widths, line-shifts, and signal intensities reveals dissociation mechanisms involving ion-pair to Rydberg state interactions prior to direct or indirect predissociations of Rydberg states. Quantum interference effects are found to be important. Moreover, observed bromine atom (2 + 1) REMPI signals support the importance of Rydberg state predissociation channels. A band system, not previously observed in REMPI, was observed and assigned to the $k^3\Pi_0(v' = 0) \leftarrow\leftarrow X$ transition with band origin 80 038 cm^{-1} and rotational parameter $B_{v'} = 7.238$ cm^{-1}.
 [http://dx.doi.org/10.1063/1.4723810]

INTRODUCTION

Photofragmentation (photodissociation and photoionization) studies of small volatile molecules is a vast research field associated with a number of intriguing and contemporary fields such as atmospheric chemistry,[1] astrochemistry,[2] and photochemical synthesis.[3] Although the literature in the field of molecular photodissociation is abundant, it is limited in terms of excitation energy ranges studied and energy- and time-resolution used in experiments. Most work deals with processes following excitations to low energy repulsive valence states. Photodissociation processes of neutrals in the less explored high energy regions largely occur via excitations to Rydberg states[4–6] followed by state interactions and curve crossings to repulsive and/or ion-pair states.[5,7]

The hydrogen halides are ideal molecules to study molecular photodissociation processes via Rydberg state excitations on a quantum energy level basis. The UV, VUV, and multiphoton excitation spectroscopy of these compounds show clearly resolved rotational structures due to excitations to Rydberg and ion-pair states.[8–11] The spectral structures are found to be rich in intensity anomalies due to state interactions and predissociation processes.[9,12–14] Since the pioneering work of Green *et al.* on HCl in 1991 (Ref. 9) and Callaghan and Gordon on HBr in 1990 (Ref. 10) a large emphasis has been on spectroscopic studies of these compounds as well as on HI to determine its high energy state properties.[11–13,15,16] More recently an increased emphasis has been on studies of state interactions and photofragmentation (photodissociation and photoionization) processes in HCl. Resonance enhanced multiphoton ionization (REMPI) techniques have proven to be powerful tools in this respect. Photofragment imaging techniques coupled with REMPI (Refs. 17 and 18) have shone light on a number of photodissociation and photoionization processes in HCl and HBr. Detailed studies of spectroscopic anomalies, such as line shifts and signal intensity irregularities, in one-colour REMPI spectra have revealed state interaction strengths as well as importance of photodissociation processes in HCl.[19–22] Theoretical *ab initio* calculations to determine excited state potential energy surfaces for HCl (Ref. 23) have proven to be very helpful for interpreting experimental data.

Most recent work, relevant to state interactions and photofragmentation processes in the hydrogen halides, in our group, has been on a number of Rydberg states and the $V^1\Sigma^+$ ion-pair state for HCl (Refs. 19–22) by the one-colour REMPI technique. Our observations can be grouped into categories depending on the strengths of Rydberg to ion-pair state interactions as follows:

a) Very weak near-resonance state interactions, distinguishable by negligible rotational line shifts but significant alterations in signal line intensities,[20] observed for triplet Rydberg states and $\Delta\Omega > 0$ state interactions.
b) Weak near-resonance state interactions, distinguishable by localized line shifts, (hence energy level shifts), as well as alterations in signal line intensities,[19,22] observed for singlet states and $\Delta\Omega > 0$ state interactions.

a)Author to whom correspondence should be addressed. Electronic mail: agust@hi.is. Telephone: +354-525-4672/+354-525-4800. Fax: +354-552-8911.

c) Medium to strong off-resonance state interactions, distinguishable by large scale line/energy level shifts, as well as alterations in signal intensities,[22,24] observed for triplet and singlet states and $\Delta\Omega = 0$ state interactions.

Whereas quite an extensive study, relevant to photofragmentations via Rydberg states of the hydrogen halides, relating to HCl has been performed, as mentioned above, limited emphasis has been placed on the heavier compounds HBr and HI. State assignments for HBr and HI resemble those for HCl. Energies for analogous states decrease with increasing molecular masses. Vibrational assignments (v') for the ion-pair states, $V^1\Sigma^+$ are uncertain and marked as $v' = m + i$, where i is integer numbers starting from $i = 1$ for the lowest energy level observed and m is an unknown integer. Based on the resemblance in the energetics of the HX's (X = Cl, Br, I) there is a reason to believe that the major photofragmentation processes in one-colour ($2 + n$) REMPI of the hydrogen halides is similar to that summarized, pictorially, for HCl in Ref. 20. Thus the major photofragmentation processes following two-photon excitations to rovibrational (v', J') quantum levels of Rydberg (HX^{**}(Ry)) and ion-pair states (HX^{**}(V)) will typically be

(i) $HX^{**}(Ry) + h\nu \rightarrow HX^+ + e^-$;
(ii) $HX^+ + h\nu \rightarrow H^+ + X$;
(iii) $HX^{**}(V) + h\nu \rightarrow HX^+ + e^-$;
(iv) $HX^+ + h\nu \rightarrow H^+ + X$;
(v) $HX^{**}(V) + h\nu \rightarrow H + X^{**}$; $X^{**} + h\nu \rightarrow X^+ + e^-$;
(vi) $HX^{**}(V) + h\nu \rightarrow H^{**} + X$; $H^{**} + h\nu \rightarrow H^+ + e^-$;
(vii) $HX^{**}(V) + h\nu \rightarrow H^+ + X^-$;
(viii) $HX^{**}(Ry) \rightarrow H{+}X/X^*$; $X/X^* + 3h\nu \rightarrow X^+ + e^-$;
(ix) $HX^{**}(Ry) + h\nu \rightarrow H + X^{**}$; $X^{**} + h\nu \rightarrow X^+ + e^-$.

H^{**} and X^{**} are atomic Rydberg states but X and X* refer to the ground ($^2P_{3/2}$) and the spin-orbit excited ($^2P_{1/2}$) states, respectively. Channels (i) and (v–vi) typically dominate. The number of photons in the excitation processes (i–ix), however, may vary, depending on the photon energies. The initial Rydberg or ion-pair state excitations may either occur by direct two-photon excitations or via J' quantum number dependent state mixing.

In this paper, we present a REMPI work on HBr with main focus on photofragmentation and state interaction processes involving singlet Rydberg and ion-pair states. Quantitative and qualitative multiparameter analysis of line-shifts, signal intensities, and line-widths illuminate state involvements and interactions in photodissociation processes. Furthermore, observations of new spectral features will be presented.

EXPERIMENTAL

Two-dimensional (2D) REMPI data were recorded for a HBr molecular beam, created by jet expansion of a pure sample through a pulse nozzle. Apparatus used is similar to that described in Refs. 16 and 25. Excitation radiation was generated by a pulsed excimer laser-pumped dye laser systems, using a Lambda Physik COMPex205 excimer laser and a Coherent ScanMatePro dye laser. Frequency doubled radiation was focused on the molecular beam inside an ionization chamber between a repeller and an extractor plate. Ions formed by multiphoton excitations were directed into a time-of-flight tube and detected by a micro-channel plate (MCP) detector. Signals were fed into a LeCroy WaveSurfer 44MXs-A, 400 MHz storage oscilloscope and stored as a function of ion time of flights and laser radiation wavenumbers. Average signal levels were evaluated and recorded for a fixed number of laser pulses. The data were corrected for laser power and mass-calibrated to obtain ion yields as a function of mass and excitation wavenumber (2D-REMPI data). REMPI spectra for certain ions as a function of excitation wavenumber (1D-REMPI) were obtained by integrating mass signal intensities for the particular ion. Care was taken to prevent saturation effects as well as power broadening by minimising laser power. Laser calibration was based on observed (2 + 1) bromine atom REMPI peaks. The accuracy of the calibration was typically found to be about ± 2.0 cm^{-1} on a two-photon wavenumber scale. Equipment condition parameters are listed in Table I.

TABLE I. Typical equipment/condition parameters for REMPI experiments.

HBr gas sample	Merck Schuchardt, Germany, Purity: 99.8%
Laser dye	C503
Frequency doubling crystal	BBO-2
Laser repetition rate	10 Hz
Dye laser bandwidth	0.095 cm^{-1}
Laser intensity used	0.1–0.3 mJ/pulse
Nozzle size	500 μm
Sample backing pressure	2.0–2.5 bars
Pressure inside ionization chamber	10^{-6} mbar
Nozzle opening time	150–200 μs
Delay time for laser excitation	450–550 μs
Excitation wavenumber step sizes	0.05–0.1 cm^{-1}
Time of flight step sizes	10 ns

RESULTS AND ANALYSIS

Spectra

2D-REMPI data corresponding to resonance transitions to the $F^1\Delta_2(v' = 1)$, $E^1\Sigma^+(v' = 1)$, $H^1\Sigma^+(v' = 0)$, $V^1\Sigma^+(v' = m + 7)$, and $V^1\Sigma^+(v' = m + 8)$ states of H^{i}Br ($i = 79$, 81) (see Fig. 1) in the two-photon wavenumber region 79 040–80 300 cm^{-1} were recorded, assigned, and analysed in terms of rotational line-shifts, signal intensities, and line-widths. These are hereafter named $F(1)$, $E(1)$, $H(0)$, $V(m + 7)$, and $V(m + 8)$, respectively. Figure 2 shows 1D-REMPI spectra for the H^+, $^{81}Br^+$, and $H^{81}Br^+$ ions. Within experimental error, no significant difference in rotational line positions are observed for the two isotopes, $i = 79$ and 81. Rotational line positions are listed in Table II. Several new rotational lines, not previously reported,[10] are observed. Most other peak positions agree reasonably well with those given by Callaghan and Gordon.[10] In addition to the above-mentioned resonances, weak peaks due to transitions to a Rydberg state, previously unobserved in REMPI, are observed in the region 80 028–80 040 cm^{-1} (see Fig. 2 and Table II). Furthermore, three Br atomic

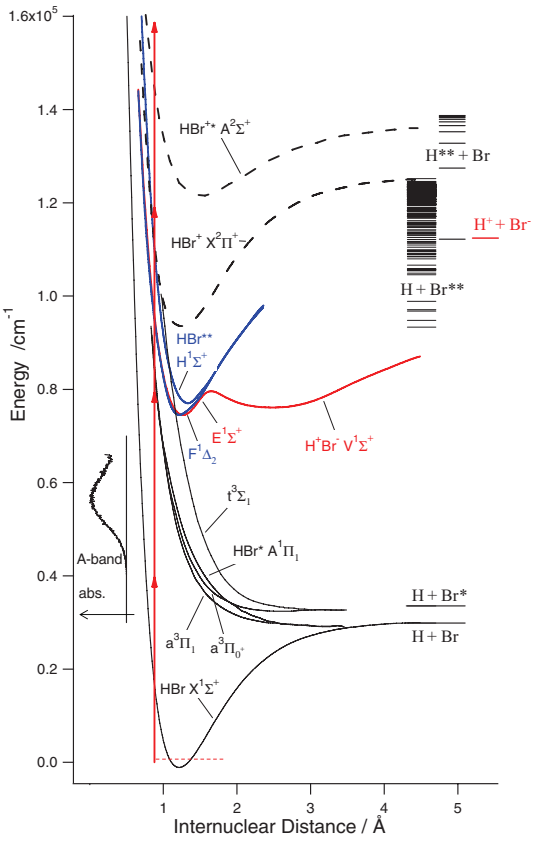

FIG. 1. HBr energetics. Potential energy curves, asymptotic energies (right), photon excitations (red arrows; left) corresponding to two-photon resonance excitation to the $F^1\Delta_2(v' = 1)$ state and relative absorption intensity of the *A*-band (Ref. 33) (tilted to the left). Potential curves other than the repulsive states are derived from Fig. 1 in Ref. 18. Repulsive potentials (*A*, *t* and the *a* states) are derived from Fig. 1 in Ref. 34. Threshold energies are derived from atom energy levels.[35]

(2 + 1) REMPI resonances, due to transitions from ground state $Br(^2P_{3/2})$ to the excited states $^4S_{3/2}$ (79 178 cm^{-1}), $^2P_{3/2}$ (79 696 cm^{-1}), and $^2P_{1/2}$ (79 868 cm^{-1}), were identified in the spectral region.

Analysis of the spectrum near 80 040 cm^{-1}, based on the assumption that the peaks are *Q* lines, gave rotational constants $B_{v'} = 7.238 \pm 0.070\ cm^{-1}$ and $D_{v'} = -0.016 \pm 0.005\ cm^{-1}$ and band origin value of 80 038 $\pm$ 2 cm^{-1} for the Rydberg state. Based on comparison with absorption data given by Ginter *et al.*,[26] the state of concern is assigned $k^3\Pi_0$ $(v' = 0)$.

Energetics and line-shifts vs. state interactions

Rotational level energies for all five states were derived from the line positions (Table II) and the rotational level energies of the $H^{81}Br$ ground state[27] (see Fig. 3). To a first approximation an unperturbed state will show linear behaviour

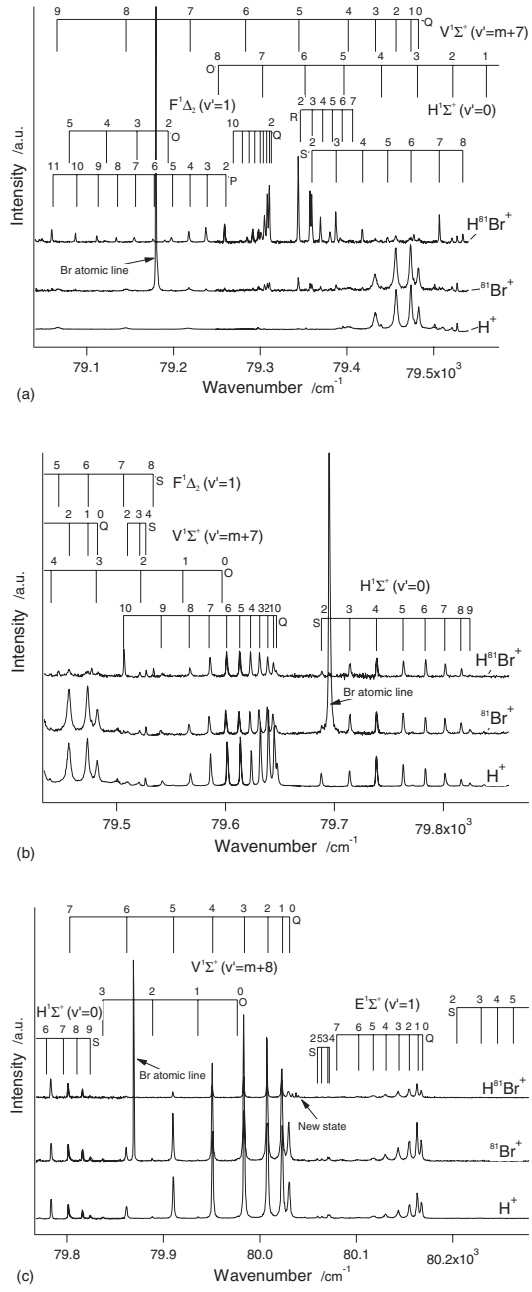

FIG. 2. 1D-REMPI spectra for H^+, $^{81}Br^+$, and $H^{81}Br^+$ and J' assignments for rotational peaks corresponding to two-photon resonance excitations to the $F^1\Delta_2(v' = 1)$, $V^1\Sigma^+(v' = m + 7)$, $H^1\Sigma^+$ $(v' = 0)$, $V^1\Sigma^+(v' = m + 8)$, and $E\,^1\Sigma^+$ $(v' = 1)$ states. New, previously unreported spectrum in REMPI, assigned to two-photon resonance transition to the $k^3\Pi_0(v' = 0)$ state is marked in figure (d). Three atomic lines due to (2 + 1) REMPI of Br are also marked (see Table VI).

TABLE II. Rotational lines for H^iBr ($i = 79, 81$), due to two-photon resonance transitions to the $V^1\Sigma^+(v' = m + 7)$, $V^1\Sigma^+(v' = m + 8)$, $E^1\Sigma^+(v' = 1)$, $F^1\Delta_2(v' = 1)$, $H^1\Sigma^+(v' = 0)$ and "New" ($k^3\Pi_0(v' = 0)$) states (see text).

	$V(m+7)$		$V(m+8)$			E(1)				
J'	Q	S	O	Q	S	Q	S			
0	79 481.3		79 975.5	80 029.0		80 166.3				
1	79 472.5		79 934.8	80 021.8		80 162.0				
2	79 455.4	79 508.8	79 887.3	80 006.6	80 058.5	80 153.8	80 203.1			
3	79 431.7	79 520.0	79 836.0	79 982.4	80 069.3	80 142.2	80 228.3			
4	79 399.6	79 525.6[a]		79 949.7	80 070.9	80 129.1	80 245.2			
5	79 343.4[a]			79 909.0	80 063.3	80 116.4	80 261.6			
6	79 282.1[a]			79 860.5	80 045.5	80 101.2[a]	80 278.0[a]			
7	79 218.1[a]			79 801.8[a]		80 083.5[a]	80 296.3[a]			
8	79 144.2[a]						80 314.6[a]			
9	79 064.5[a]									

	$F(1)$					$H(0)$			New
J'	O	P	Q	R	S	O	Q	S	Q
0						79 595.6	79 645.6		80 039.8[a]
1						79 559.5	79 642.9		80 037.5[a]
2	79 191.2	79 258.2	79 309.6	79 343.0	79 358.6	79 520.9	79 637.7	79 686.8	80 033.8[a]
3	79 155.2	79 236.6	79 307.3	79 356.6	79 386.5	79 480.1	79 630.2	79 712.9	80 028.8[a]
4	79 120.1	79 216.9	79 304.1	79 368.6	79 417.0	79 438.6	79 621.8	79 737.3	
5	79 077.1[a]	79 196.6	79 300.2	79 379.7	79 445.8	79 395.5	79 611.8	79 761.7	
6	79 047.0	79 175.5	79 296.7	79 391.2	79 472.7	79 350.5	79 599.8	79 782.0	
7		79 153.9	79 290.4	79 403.1	79 505.2[a]	79 301.6[a]	79 583.7	79 800.0	
8		79 133.2[a]	79 283.9		79 532.4[a]	79 250.6[a]	79 565.4	79 814.8	
9		79 111.0[a]	79 276.1				79 539.7	79 823.2[a]	
10		79 086.2[a]	79 265.7				79 505.2[a]		
11		79 058.9[a]							

[a]New, previously unobserved peaks in REMPI.

for the energy spacing between neighbour energy levels, $\Delta E_{J',J'-1}$ $(= E(J') - E(J' - 1))$ as a function of J' with a slope value $2B_{v'}$, where $B_{v'}$ is the v'-dependent rotational constant. Irregular, nonlinear, shape of $\Delta E_{J',J'-1}$ vs J' plots is a clear indication of perturbation effects due to state interactions (see Fig. 4) showing as level-to-level repulsions between levels with same J' numbers.[12,28] The shift of an energy level of a perturbed state (1) ($\Delta E_{J'}(1) = E_{J'}(1) - E^0_{J'}(1)$, where $E^0_{J'}(1)$ is the zero order energy for the unperturbed state) depends on the interaction strength (W_{12}) between that state (1) and the perturbing state (2) and the observed energy level difference, between the two states, for same J' (i.e., $\Delta E_{J'}(1, 2) = E_{J'}(1) - E_{J'}(2)$),

$$\Delta E_{J'}(1) = \frac{1}{2}\left(\Delta E_{J'}(1,2) - \sqrt{(\Delta E_{J'}(1,2))^2 - 4\,|W_{12}|^2}\right). \tag{1a}$$

Equation (1a) is derived from the classical expression given by Herzberg[28] for energies in case of level-to-level interactions,

$$E_{J'}(i) = \frac{1}{2}\left(E^0_{J'}(1) + E^0_{J'}(2)\right) \pm \frac{1}{2}\sqrt{4\,|W_{12}|^2 + (\Delta E^0_{J'}(1,2))^2}; \quad i = 1, 2$$
$$\Delta E^0_{J'}(1,2) = E^0_{J'}(1) - E^0_{J'}(2). \tag{1b}$$

Small, but significant, positive deviation of the $\Delta E_{J',J'-1}$ value from linearity for $J' = 6$ (slight negative deviation for $J' = 7$) in $F(1)$ is an indication of near-resonance interactions between $F(1)$ and $V(m + 7)$ (Ref. 13) (see Fig. 3(a)). Strictly, interaction between the $F^1\Delta_2$ and $V^1\Sigma^+(0^+)$ states violates the selection rule $\Delta\Omega = 0, \pm 1$. Most probably, however, the F-state is a mixed state analogous to HCl, where the F-state wave function is believed to be a linear combination of $\Omega = 1$, 2, and 3 components, and F to V perturbations observed therefore due to heterogeneous ($\Delta\Omega = 1$).[19,29] The larger irregularities in energy levels, observed for the $V(m + 7)$ state, however, (Fig. 4(a)) indicates further involvement of larger homogeneous ($\Delta\Omega = 0$) state interactions with $\Omega = 0$ states, of which interaction with the $E(1)$ state, slightly higher in energy, will dominate. Involvement of the closer in energy $H(0)$ state, however, will also be affective. A positive deviation in $\Delta E_{J',J'-1}$ values vs. J' observed for $E(1)$ (see Fig. 4(a)) acts in accordance with a large negative deviation observed for $V(\mathrm{m} + 7)$ near $J' = 4$–6. The $E(1)$ state does, however, "experience" still stronger interactions from the "closer in energy" $V(m + 8)$ and $V(m + 9)$ states which all together will affect the observed irregularities in $\Delta E_{J',J'+1}$ vs. J' for $E(1)$. Whereas almost a linear behaviour of $\Delta E_{J',J'-1}$ vs. J' is observed for $H(0)$ (Fig. 4(b)), in the low J' region, large negative deviation is observed for high J' ($J' > 6$). The major perturbation effects on $H(0)$ will be due to interactions

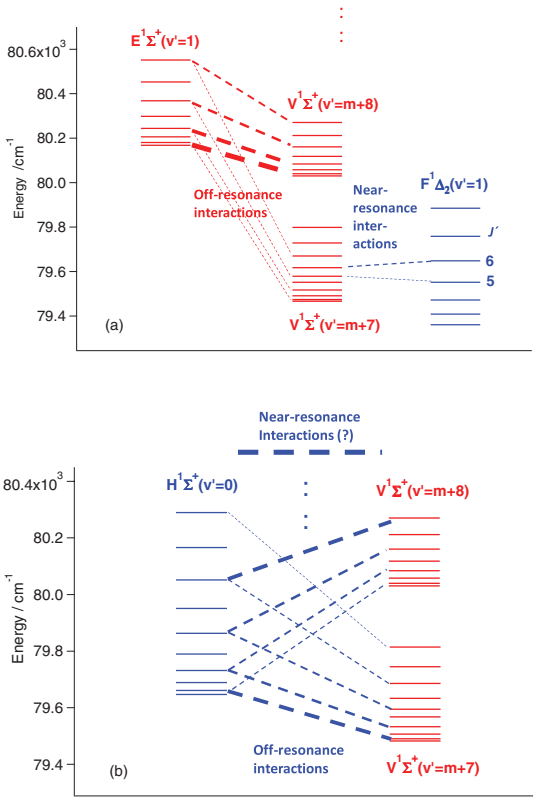

FIG. 3. Rotational energy levels, derived from observed REMPI rotational peaks for the $F^1\Delta_2(v' = 1)$(a), $V^1\Sigma^+(v' = m+7)$((a) and (b)), $H^1\Sigma^+(v' = 0)$(b), $V^1\Sigma^+(v' = m + 8)$((a) and (b)) and $E\,^1\Sigma^+$ $(v' = 1)$(a) states. Observed level-to-level near-resonance interactions between $F(1)$ and $V(m + 7)$ and off-resonance interactions between the $V(m + 7)$ and $V(m + 8)$ ion-pair states and the $E(1)$ and $H(0)$ Rydberg states are indicated by broken lines. Strength and alterations in state mixings are indicated, roughly, by varying thickness of broken lines.

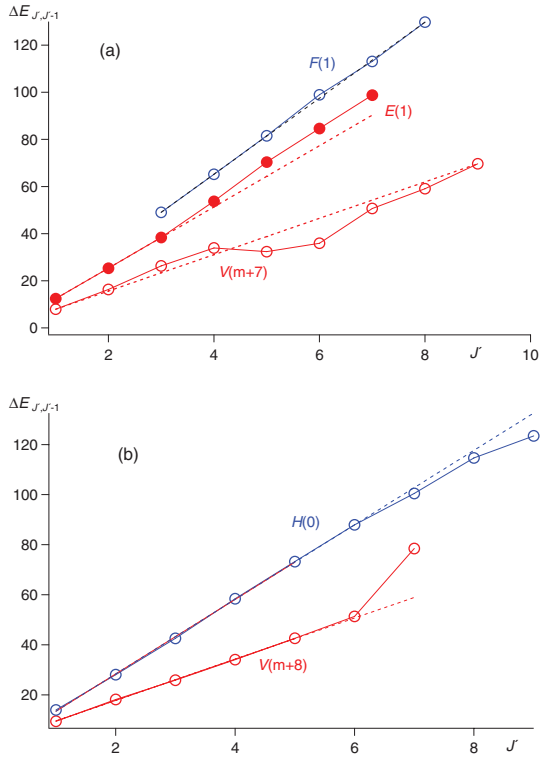

FIG. 4. H^iBr: Spacings between rotational levels ($\Delta E_{J',J'-1}$) as a function of J' for $F^1\Delta_2(v' = 1)$(a), $E^1\Sigma^+(v' = 1)$(a), $V^1\Sigma^+(v' = m + 7)$(a), $H^1\Sigma^+(v' = 0)$(b), and $V^1\Sigma^+(v' = m + 8)$(b). Dots connected by solid lines are derived from Q rotational lines. Broken lines are line fits for, $J' = 3$–5 and 8 values for $F(1)$, $J' = 1$–3 values for $E(1)$, $J' = 1$–6 values for $H(0)$, and $J' = 1$–5 values for $V(m + 8)$. The broken line for $V(m + 7)$ joins the dots for $J' = 1$ and 9 to guide the eye.

with the V state. These observations, therefore, suggest that overall effects due to level-to-level interactions with the $V(m + 7)$ and $V(m + 8)$ states "cancel", such that a decreasing level repulsions with J' by $V(m + 7)$ matches an increasing repulsions with J' by $V(m + 8)$ (Fig. 3(b)), resulting in an effective lowering in the slope, hence the rotational constant. The growing negative deviation for high J', on the other hand, is due to increasing near-resonance-interactions with $V(m + 8)$ also observed as positive deviation in the $\Delta E_{J',J'-1}$ vs. J' plot for $V(m + 8)$.

Assuming only level-to-level interaction with $V(m + 7)$ to be responsible for the energy deviations observed in $F(1)$ (Fig. 4(a)), the interaction strength for $J' = 6$ could be evaluated from Eq. (1) as $W_{12} = 4.4 \pm 0.4$ cm^{-1}. Furthermore, by assuming the heterogeneous interaction to change with J' as

$$W_{12} = W'_{12}(J'(J' + 1))^{1/2}. \tag{2}$$

$W'_{12} = 0.68 \pm 0.07$ cm^{-1} was derived and W_{12} values for J' = 2–7 evaluated (Table III). The fractional contributions to the state mixing, c_1^2 and c_2^2, for the states 1(F(1)) and 2(V(m + 7)) respectively can now easily be derived from

$$c_1^2 = \frac{1}{2} + \frac{\sqrt{(\Delta E_{J'}(1,2))^2 - 4\,|W_{12}|^2}}{2\,|\Delta E_{J'}(1,2)|}; \quad c_2^2 = 1 - c_1^2 \tag{3}$$

(see Table III).

Signal intensities vs. state interactions

Rotational lines were fitted by Lorentzian functions to obtain integrated intensities as well as line-widths. $^iBr^+$ signal intensities relative to H^iBr^+ signal intensities ($I(^iBr^+)/I(H^iBr^+)$) as a function of J', for the Rydberg state spectra (see Fig. 5) show certain resemblance to analogous plots of $I(^iCl^+)/I(H^iCl^+)$ for H^iCl (Refs. 19–22) where an increase in the ratio has been shown to indicate an accession of state mixing and stronger interaction with the $V^1\Sigma^+$ ion-pair state. Thus the plot of the Q line intensity ratios for the $F(1)$ state shows a weak but significant increase for $J' = 6$ (Fig. 5(a)) corresponding to the near-resonance

TABLE III. Parameters derived from line-shift and intensity-ratio ($I(^iBr^+)/I(H^iBr^+)$) analysis of the $F(1) \leftarrow\leftarrow X$ system (see Figs. 4(a), 6(a), and 6(b))

J'	$\Delta E = E(F(1) - E(V(m+7)))$	W_{12}	${c_1}^2$	${c_2}^2$
2	−145.9	1.67	1.00	0.000
3	−124.4	2.36	1.00	0.000
4	−95.5	3.046	1.00	0.000
5	−43.2	3.73	0.993	0.007
6	14.6	4.41	0.898	0.102
7	72.3	5.09	0.995	0.005
W'_{12}	0.68 ± 0.07 cm^{-1}			
γ (β_1/α_2)	0.11			
α (α_2/α_1)	1.3			
$\alpha\gamma$ (β_1/α_1)	0.14			

interaction with $V(m+7)$ (see Fig. 3(a)). This near-resonance effect also displays itself as alterations in absolute ion signals. Thus the P line series for H^iBr^+ displays minimum for $J' \sim 6$ (see Fig. 2(a)) and the $J' = 6$ peak for H^+ in the Q line series exhibits enlargement. The intensity ratios ($I(^iBr^+)/I(H^iBr^+)$) for the $E(1)$ state gradually decrease with J' (Fig. 5(c)), indicating less off-resonance interactions with $V(m+8)$ as the spacing between the levels ($\Delta E_{J'}(E(1),V(m+8))$) increases with equal J' (Fig. 3(a)). There is, however, a slight indication of an enhanced ratio near $J' = 6$ (Fig. 5(c)). The intensity ratios for $H(0)$ show clear effect of "double" state interactions, showing decreasing values with J' for low J' (for $J' > 0$) but increasing values with J' for high J', with minimum at $J' \sim 5$ (Fig. 5(d)). This is due to a decreasing interaction with $V(m+7)$ but increasing interaction with $V(m+8)$ as a function of J' and the $\Delta E_{J'}(H(0),V)$'s increase and decrease for $V(m+7)$ and $V(m+8)$ respectively (Fig. 3(b)).

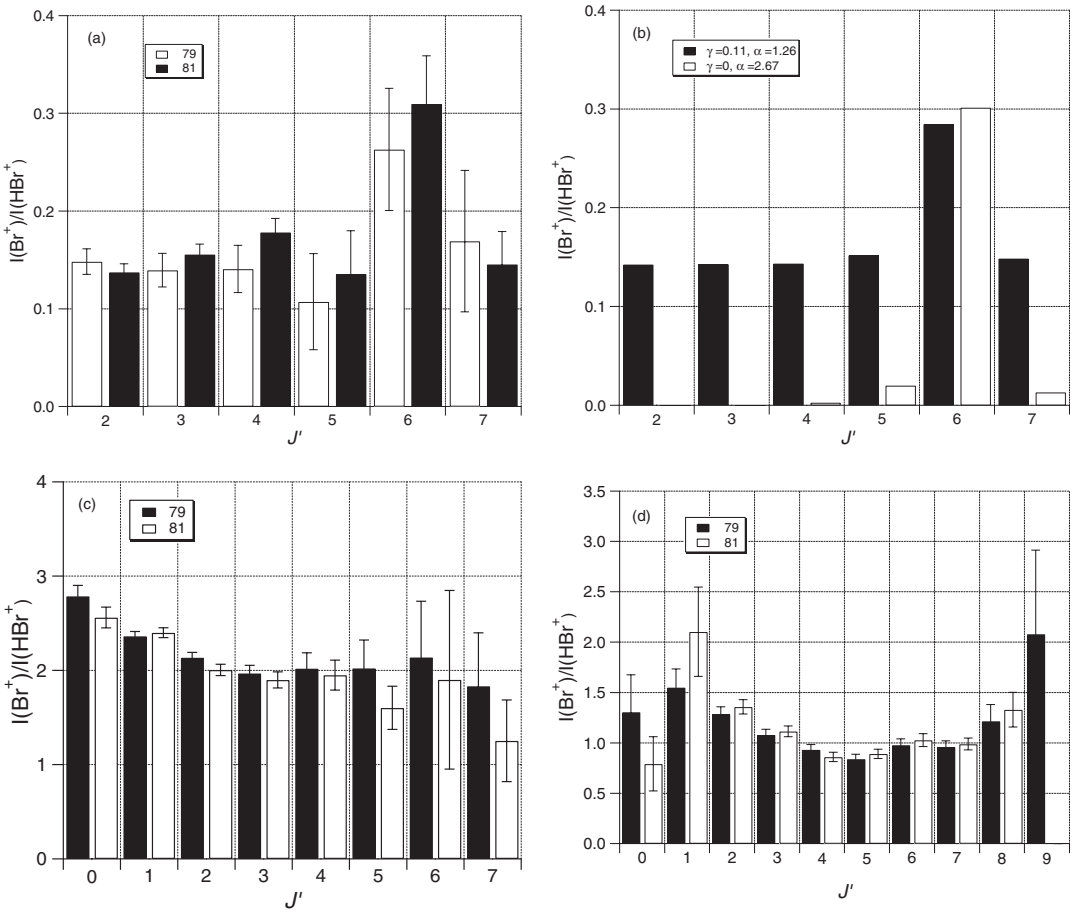

FIG. 5. Relative ion signal intensities, $I(^iBr^+)/I(H^iBr^+)$ ($i = 79, 81$) vs. J' derived from Q rotational lines of REMPI spectra due to two-photon resonance transitions to the Rydberg states $F(1)$ (a), $E(1)$(c), and $H(0)$(d). (b) shows simulation for (a), assuming J' level-to-level interactions between the $F(1)$ and $V(m+7)$ states (black columns) for $W'_{12} = 0.68$ cm^{-1}, $\alpha = 1.26$, and $\gamma = 0.11$ as well as calculated ratios for same W'_{12}, $\alpha = 2.67$, and $\gamma = 0$ (white columns) (see text).

By analogy with the observations for HCl, as mentioned before, in case of level-to-level interactions between two states (1) (Rydberg state) and (2) (ion-pair state), $I(^iBr^+)/I(H^iBr^+)$ can be expressed as

$$\frac{I(^iBr^+)}{I(H^iBr^+)} = \frac{\alpha\left[\gamma + c_2^2(1-\gamma)\right]}{\left(1-c_2^2\right)}, \tag{4}$$

where

$$I(^iBr^+) = \alpha_2 c_2^2 + \beta_1 c_1^2; \quad I(H^iBr^+) = \alpha_1 c_1^2 + \beta_2 c_2^2$$
$$\alpha = \alpha_2/\alpha_1; \quad \gamma = \beta_1/\alpha_2; \quad \alpha\gamma = \beta_1/\alpha_1$$

α_i and β_i (i = 1, 2) are ionization rate coefficients for the excited molecular states (1) and (2). By least square fitting the expression on the right side of Eq. (3) to the experimental intensity ratios, as a function of J', derived from the $F(1)$ state spectra (Fig. 5(a)) using the W_{12} values obtained from the line shift analysis mentioned above and the energy level differences ($\Delta E_{J'}(1, 2)$; Table III), $\alpha = 1.26$, $\gamma = 0.11$, and $\alpha\gamma = 0.14$ values were obtained (see Fig. 5(b)). γ, hence $\alpha\gamma$, are measures of $^iBr^+$ ion formations via dissociation of the Rydberg state, relative to that of the formations of $^iBr^+$ via exciations of the ion-pair state and relative to that of the formations of H^iBr^+ via excitation of the Rydberg state respectively. Whereas no γ and $\alpha\gamma$ values have been reported for HBr before, γ derived for HCl are found to be in the range γ = 0–0.03 (Refs. 20 and 22) depending on Rydberg states. The significance of the nonzero and relatively high γ value of 0.11, derived here, can be deduced from the dramatic effect of replacing it with $\gamma = 0$ in the calculations (see Fig. 5(b)). This suggests that predissociation of the $F(1)$ state to form H + Br/Br* is important.

Line-widths and fragmentations vs. state interactions

Rotational line-widths vary a lot depending on the resonance excited states and rotational levels as seen in Fig. 2, indicating a large variation in lifetimes of states. Figure 6 shows rotational line-widths (Γ) as a function of J'. Lower limit lifetimes (τ) derived from[6,30]

$$\tau(\text{ps}) = 5.3/\,\Gamma(\text{cm}^{-1}) \tag{5}$$

are listed in Table IV. The line-widths for the Q lines of the $H(0)$ spectrum (Fig. 6(f)) show close correspondence to the intensity ratios as a function of J' (Fig. 5(d)) previously explained to reflect interactions with both $V(m + 7)$ and $V(m + 8)$. For $F(1)$, line-widths as a function of J', derived from the line series P, Q, R, and S all show small but significant maxima, hence lifetime minima, near $J' = 5$ (see Figs. 6(a)–6(c)). The $V(m + 7)$ state, showing very broad peaks, also exhibits maximum bandwidth (minimum lifetime) for $J' \sim 5$–6 and much shorter lifetimes than $F(1)$ (Fig. 6(d)). Due to very weak intensity and breadth of the $V(m + 7)$, Q line, $J' = 5$ peak line-width could not be determined. Line-widths for the $E(1)$ state are in range between those for $F(1)$ and $V(m + 7)$, also reaching maximum for $J' = 5$ (Fig. 6(e)). This further indicates close interactions between the states involved in agreement with previous interpretations of line shifts and intensity ratios. There are, however, considerable, important correlation differences between the various observation parameters for $F(1)$ and $E(1)$. The maximum line-shifts and $I(^iBr^+)/I(H^iBr^+)$ intensity ratios, for $F(1)$, are observed for $J' = 6$ whereas the maximum bandwidths (minimum lifetime) are found for $J' = 5$. Furthermore, line-widths of the Q lines for $E(1)$ (Fig. 6(e)) show significantly different behaviour with J' compared to that of the intensity ratios (Fig. 5(c)). The explanation lies in the fundamental differences in the observation parameters. Line-widths, hence lifetimes, are primarily determined by the rates of crossing from the bound excited states to continua (i.e., predissociation), whereas the line-shifts and intensity irregularities are primarily indicative of bound-to-bound state interactions. However, predissociation can occur via interacting gateway states, thus making the lifetimes state interaction dependent. Figures 3(a) and 3(b) summarize the major level-to-level state interactions of concern. The large average internuclear distance of the V state makes crossing to repulsive states, for which the repulsive walls are at much shorter internuclear distances (see Fig. 1), highly improbable. The Rydberg states, on the other hand, are either in close vicinity of or crossed by repulsive states to make predissociation processes more probable. Therefore, we believe that the short lifetimes observed, are mainly due to predissociation of Rydberg states, either directly or via Rydberg gateway states analogous to that assumed to hold for HCl.[20,22,31] Hence, the particularly short lifetimes, observed for the $V(m + 7)$ state are due to predissociation processes following crossings from $V(m + 7)$ to Rydberg states such as the $E(1)$, $F(1)$, and $H(0)$ states. This is demonstrated schematically in Fig. 7 for the $V(m + 7)$, $E(1)$, and $F(1)$ states. Based on a coupling scheme given by Alexander *et al.*[31] a summary of state couplings due to spin-orbit-(SO) and rotational-(JL and JS) interactions between relevant states are shown in Table V. SO couplings, generally, are the strongest interactions with coupling strengths independent of rotational energies, whereas weaker rotational interactions will increase with rotational energies. It should be noted, however, that in both cases the bound-to-bound state mixing (c_i^2) will depend on the spacing between the rotational levels with same rotational quantum numbers ($\Delta E_{J'}$) (Eq. (3)) making the effective interaction in both

TABLE IV. (Lower limit) lifetimes (ps) of rotational states (J') derived from REMPI spectra line-widths (see text). The values were derived from Q lines of H^iBr^+ (i = 79, 81) signals for $E(1)$, $F(1)$, and $H(0)$ but from Q lines of H^+ signals for $V(m + 7)$.

J'	$V(m+7)$	$E(0)$	$F(1)$	$H(0)$
0	1.69 ± 0.34	2.29 ± 0.07		1.96 ± 0.38
1	1.64 ± 0.28	2.50 ± 0.04		3.86 ± 0.38
2	1.41 ± 0.07	1.86 ± 0.04	3.96 ± 0.05	3.65 ± 0.15
3	1.16 ± 0.12	1.39 ± 0.04	4.01 ± 0.07	3.78 ± 0.13
4	0.65 ± 0.06	1.24 ± 0.07	3.10 ± 0.08	4.38 ± 0.15
5		1.08 ± 0.11	2.37 ± 0.16	4.52 ± 0.16
6	0.48 ± 0.13	1.36 ± 0.34	3.23 ± 0.22	4.10 ± 0.17
7	0.59 ± 0.03	1.46 ± 0.63	3.84 ± 0.27	3.63 ± 0.15
8	0.86 ± 0.05		4.05 ± 0.74	2.99 ± 0.31
9	1.03 ± 0.07		3.44 ± 2.23	3.21 ± 1.46

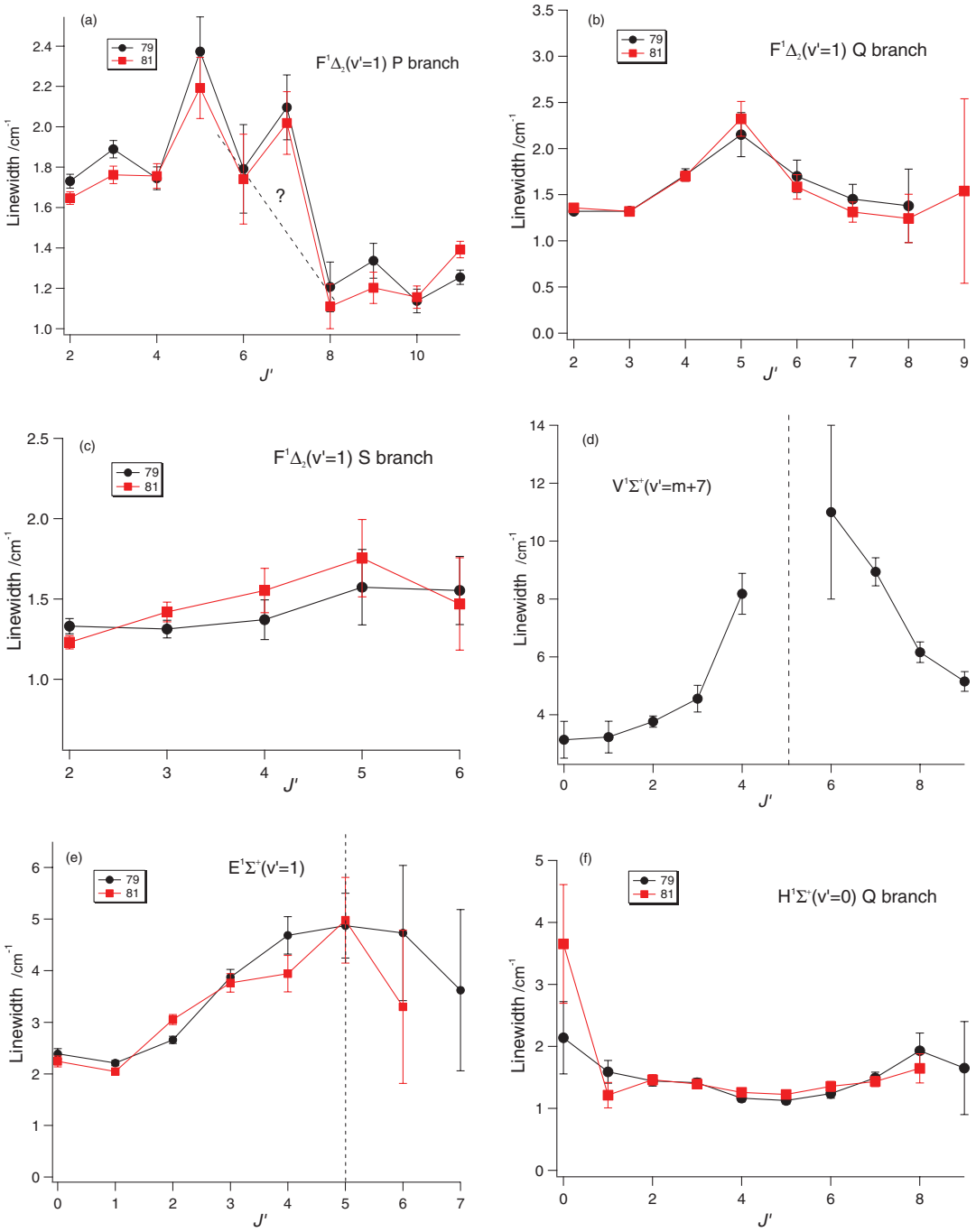

FIG. 6. Rotational line-widths vs. J' derived from REMPI spectra for (a) $F(1)$, P lines, H^iBr^+ (i = 79, 81), (b) $F(1)$, Q lines, H^iBr^+, (c) $F(1)$, S lines, H^iBr^+, (d) $V(m + 7)$, Q lines, H^+, (e) $E(1)$, Q lines, H^iBr^+, (f) $H(0)$, Q lines, H^iBr^+. The line-width derived for $F(1)$, P line, J' = 7 (a) is overestimated due to overlap of peaks $P(J' = 7)$ and $O(J' = 4)$ (see Fig. 2(a)). Due to very weak intensity and breadth of the $V(m + 7)$, Q line, $J' = 5$ peak line-width could not be determined (d).

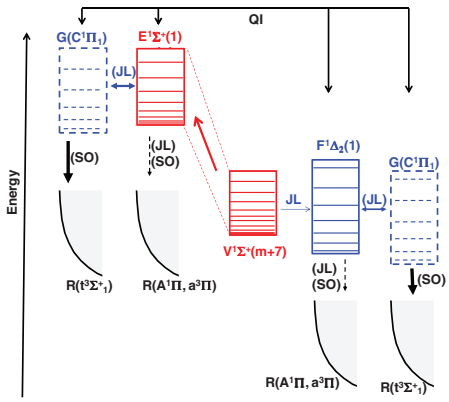

FIG. 7. Semischematic figure, showing the H^{i}Br energetics, state interactions, and transfers of relevance. Rotational and spin-orbit couplings are marked *JL* and *SO*, respectively. States marked *G* and *R* are gateway and repulsive states, respectively. States and couplings inside brackets are example cases believed to be of importance. Relative importance of couplings and transfers are indicated by different boldness of arrows. Quantum interference effects between states are indicated by arrows marked *QI*.

cases rotational energy dependent. Furthermore, interaction strengths will depend on Franck-Condon-overlaps, favouring interactions between Rydberg states and repulsive states close to curve-crossings. Involvements of the repulsive states $t^3\Sigma$ (see Fig. 1) are therefore expected to be important in predissociation processes. Considering all these factors, the $E(1)$ and $F(1)$ states (hence the mixed $V(m+7)$ state) could be largely affected by *SO* couplings of the $C^1\Pi_1$-gateway state with the repulsive $t^3\Sigma^+{}_1$ state following rotational (*JL*) couplings with the *C*-state. Direct predissociation of the $E(1)$ and $F(1)$ states by the *A* and the *a* states will also be involved but to a less extent (see Fig. 7). Furthermore the *C* to *F* state mixing will be important in enhancing the rotational/heterogeneous ($\Delta\Omega = 1$) coupling between the $V(m+7)$ and the $F(1)$ state. The bound-bound rotational couplings (*JL*) will have the greatest effect on the rotational

TABLE V. State couplings based on correlation diagrams from Ref. 31. Spin-orbit couplings are marked *SO*. Rotational couplings, *L* uncoupled and *S*-uncoupled, are marked *JL* and *JS*, respectively.

State interactions		Bound states					
		E, H, V	*F*	*C,D* $^1\Pi_1$	$b^3\Pi_0$	$b^3\Pi_2$	$g^3\Sigma_0^-$
Continuum states	$A^1\Pi_1$	*JL*	*JL*				
	$a^3\Pi_2$		*SO*				
	$a^3\Pi_1$			*SO*	*JS*	*JS*	*JL*
	$a^3\Pi_0^-$(e)	*SO*					*SO*
	$t^3\Sigma_1^+$			*SO*		*JL*	
	$t^3\Sigma_0^+$(f)				*SO*		
Bound states	*C,D* $^1\Pi_1$		*JL*				
	$b^3\Pi_0$	*SO*					
	$b^3\Pi_2$		*SO*				
	$g^3\Sigma_0^-$	*SO*					

energy dependence of the line-width/lifetime. The close correlation observed between the $E(1)$ and $F(1)$ states, in terms of the J'-dependent line-widths, showing as maxima for the same J' ($J' \sim 5$) strongly suggests that quantum interference (*QI*; Fig. 7) effects apply, involving the Rydberg states $E(1)$, $F(1)$, and $C^1\Pi$. The slight increases observed in the intensity ratios ($I(^i\mathrm{Br}^+)/I(\mathrm{H}^i\mathrm{Br}^+)$) both for the $E(1)$ and $F(1)$ states at $J' = 6$ (Figs. 5(a) and 6(c)) further demonstrate this.

Considering interaction schemes such as the one presented in Fig. 7, an approximation expression, relating lifetimes of the $V(m+7)$, $E(1)$, $F(1)$, and $H(1)$ states, can be derived. The basic idea is that the lifetime of $V(m+7)$ is determined by the lifetimes of the Rydberg states, which $V(m+7)$ couples with. Assuming the rate of dissociation of $V(m+7)$, due to a coupling with a Rydberg state, to be proportional to the rate of dissociation of that Rydberg state and the state mixing the following approximation expression, relating rate coefficients ($1/\tau_i$), can be written,

$$\frac{1}{\tau_{V7}} = f_{E1}\frac{1}{\tau_{E1}} + f_{F1}\frac{1}{\tau_{F1}} + f_{H0}\frac{1}{\tau_{H0}} + f_{\mathrm{other}}\frac{1}{\tau_{\mathrm{other}}}, \qquad (6)$$

where τ_i ($i = V7$, $E1$, $F1$, $H0$, other) are the lifetimes of the $V(m+7)$, $E(1)$, $F(1)$, $H(0)$, and other states, respectively. The f_i's are proportionally coefficients, depending on coupling rates. Since the rate of dissociation of $V(m+7)$, via coupling with a particular Rydberg state, cannot exceed the rate of dissociation of that Rydberg state the corresponding f_i-factor cannot be larger than one, hence $0 \le f_i \le 1$. Consistent variations in the bandwidths with J', observed for all measurements in ranges larger than our detection limit of about 0.3 cm^{-1}, make us believe that the lifetime values for the $V(m+7)$, $E(1)$, $F(1)$, and $H(0)$ states (Table IV) are reasonable estimates for the absolute values within uncertainty limits. There is a reason to expect that the states $E(1)$, $F(1)$, and $H(0)$ contribute the most to the observed dissociation rate of $V(m+7)$ and that contributions from other states are less or minor in the case of the shortest lifetimes. For $J' = 4$, 6, and 7 the rate of dissociation for $V(m+7)$ ($1/\tau_{V7}$) derived from the lifetimes in Table IV is in fact found to be close to or only slightly higher than the sum of the dissociation rates of the $E(1)$, $F(1)$, and $H(0)$ ($1/\tau_{E1} + 1/\tau_{F1} + 1/\tau_{H0}$), within uncertainty limits. This suggests that the corresponding f_i factors are close to unity. Analogous comparison could not be made for $J' = 5$, since its bandwidth for $V(m+7)$ could not be determined (see figure caption 6(d)). Assuming $fi = 1$ ($i = E1$, $F1$, $H0$) and $f_{\mathrm{other}} = 0$ the lifetime for $J' = 5$ is estimated to be about 0.64 ps, hence the line-width about 8.3 cm^{-1}.

Bromine atomic lines

Generally it is believed that Br atomic lines observed in REMPI of HBr are primarily due to REMPI of Br atoms following one-photon photodissociation via the repulsive state $A^1\Pi$.[18] Considering the number of evidences for photofragmentations via Rydberg states, mentioned above, these must also be, partly or largely, due to REMPI of Br atoms formed by predissociations of Rydberg states following two-photon excitations. Thus it will resemble

TABLE VI. (2 + 1) REMPI bromine atomic lines and closest H^{i}Br rotational lines.

Bromine atomic lines			H^{i}Br rotational peaks		
Two-photon transitions	ν (cm^{-1}), our values	Relative intensity	Rotational transition	ν (cm^{-1}), our values	$\Delta\nu$ (cm^{-1})
$^4S_{3/2} \leftarrow\leftarrow {}^2P_{3/2}$	79 178.70	573	$F(1; J' = 6) \leftarrow\leftarrow X(0,J'' = 7); P$	79 175.5	3.2
$^2P_{3/2} \leftarrow\leftarrow {}^2P_{3/2}$	79 693.67	1000	$H(0;J' = 2) \leftarrow\leftarrow X(0,J'' = 0); S$	79 686.8	6.8
$^2P_{1/2} \leftarrow\leftarrow {}^2P_{3/2}$	79 867.67	319	$V(m + 8;J' = 6) \leftarrow\leftarrow X(0,J'' = 6);Q$	79 860.5	7.2

analogous findings for other Br-containing compounds.[32] The three strong bromine atomic lines observed in the spectral region discussed here (see above) are all observed in an excitation region corresponding to the low energy tail of the weak *A*-band spectrum where one-photon absorption cross section is very low, of the order 10^{-21} cm^2 molecule^{-1} at room temperature (to be compared with the cross section of about 2.5 $\times$ 10^{-18} cm^2 molecule^{-1} for the maximum of the *A*-band[33]) (see Fig. 1). The two-photon excitation wavenumbers for these lines happen to be very close to HBr molecular resonances (see Fig. 2), the closest of which are listed in Table VI along with details concerning the observed atomic lines. These two-photon absorptions will involve small but nonzero molecular excitations corresponding to the tails of the closest molecular bands. Based on the analysis above all these molecular resonances correspond to excitations to predissociating states which will form bromine atoms. The atom resonance signals will depend on uncertain transition probability parameters, for the molecule and the bromine atom, as well as the density of bromine atoms formed. The relatively largest signal due to the $^2P_{3/2} \leftarrow\leftarrow {}^2P_{3/2}$ atom resonance could be mainly associated with favourable selection rules ($\Delta L = \Delta S = \Delta J = 0$) whereas the significantly larger signal for the $^4S_{3/2} \leftarrow\leftarrow {}^2P_{3/2}$ ($\Delta L = \Delta S = 1$, $\Delta J = 0$) resonance compared to that for the $^2P_{1/2} \leftarrow\leftarrow {}^2P_{3/2}$ ($\Delta L = \Delta S = 0$, $\Delta J = 1$) resonance could be associated with the smaller difference in molecular vs. atom resonances in the former case (Table VI).

CONCLUSIONS

The analyses presented in this paper shine important light on mechanisms of photodissociation processes for H^{i}Br involving Rydberg and ion-pair state interactions. One colour REMPI spectra for atom- and molecular ions of H^{i}Br ($i = 79$, 81) in the two-photon excitation region 79 040–80 300 cm^{-1} have been analysed in terms of rotational line positions, intensities and line-widths. The analyses reveal state interactions of varying strength between Rydberg and ion-pair states. Quantitative analysis of the data relevant to near-resonance interactions between the $F^1\Delta_2(v' = 1)$ and $V^1\Sigma^+(v' = m + 7)$ states give interaction strengths (W_{12}) and fractional state mixing (c_1^2 and c_2^2) as a function of rotational quantum numbers and parameters characteristic for the degree of state mixing (α) and dissociation (γ) of the $F(1)$ state (Table III). Qualitative analysis further reveals the nature of state interactions between the ion-pair states $V(m + k)$ ($k = 7,8$) and the $E^1\Sigma^+(v' = 1)$ and $H^1\Sigma^+(v' = 0)$ Rydberg states in terms of relative strengths and J' dependences. A great variety in line-widths, hence lifetimes (Table IV), depending on electronic states and J' quantum numbers, is indicative of a number of different predissociation channels. Correlations between those observations and line-shifts and signal intensities reveal dissociation mechanisms involving ion-pair to Rydberg state interactions prior to direct or indirect (via Rydberg gateway states) predissociations of Rydberg states. Major channels are summarized in Fig. 7. The interaction between the $V(m + 7)$ and $F(1)$ states is made possible via heterogeneous coupling(s) of the $F(1)$ state, of which mixing with the $C^1\Pi_1$ state is believed to be important. The $C^1\Pi_1$ state is likely to be a gateway state prior to predissociating by the $t^3\Sigma$ repulsive state, both for the $F(1)$ and the $E(1)$ states. Furthermore, quantum interference effects between states clearly play an important role. Thus lifetimes, of the $E(1)$ state, hence the $V(m + 7)$ state, as well as interactions between these states as a function of J' are found to depend on the interaction between the $V(m + 7)$ and $F(1)$ states. Observed bromine atom (2 + 1) REMPI signals support the importance of Rydberg states predissociation channels. A band system, not previously reported in REMPI, is assigned to the Q branch of the $k^3\Pi_0(v' = 0) \leftarrow\leftarrow X^1\Sigma^+$ transition and analysed to give the band origin 80 038 $\pm$ 2 cm^{-1} and the rotational parameters $B_{v'} = 7.238 \pm 0.070$ cm^{-1} and $D_{v'} = -0.016 \pm 0.005$ cm^{-1} for the k state.

ACKNOWLEDGMENTS

The financial support of the University Research Fund, University of Iceland, the Icelandic Science Foundation as well as the Norwegian Research Council is gratefully acknowledged.

[1] J. H. Seinfeld and S. N. Pandis, *Atmospheric Chemistry and Physics: From Air Pollution to Climate Change* (Wiley, 2006); M. J. Simpson, R. P. Tuckett, K. F. Dunn, C. A. Hunniford, and C. J. Latimer, J. Chem. Phys. **130**, 194302 (2009).
[2] J. I. Lunine, *Astrobiology* (Pearson/Addison-Wesley, 2005); A. M. Shaw, *Astrochemistry: From Astronomy to Astrobiology* (Wiley, 2006).
[3] N. Hoffmann, Chem. Rev. **108**, 1052 (2008).
[4] C. Sandorfy, *The Role of Rydberg states in Spectroscopy and Photochemistry: Low and High Rydberg States* (Kluwer Academic, New York, 2002).
[5] H. Lefebvre-Brion, in *The Role of Rydberg states in Spectroscopy and Photochemistry: Low and High Rydberg States*, edited by C. Sándorfy (Kluwer Academic, New York, 2002), Vol. 20, p. 267.
[6] H. Lefebvre-Brion and R. W. Field, *The Spectra and Dynamics of Diatomic Molecules* (Elsevier, 2004).
[7] A. J. Yencha, D. K. Kela, R. J. Donovan, A. Hopkirk, and Á. Kvaran, Chem. Phys. Lett. **165**, 283 (1990); Á. Kvaran, A. J. Yencha, D. K. Kela, R. J. Donovan, and A. Hopkirk, *ibid.* **179**, 263 (1991); D. Kaur, A. J. Yencha, R. J. Donovan, Á. Kvaran, and A. Hopkirk, Org. Mass Spectrom. **28**, 327 (1993); A. J. Yencha, D. Kaur, R. J. Donovan, Á. Kvaran, A. Hopkirk, H. Lefebvre-Brion, and F. Keller, J. Chem. Phys. **99**, 4986 (1993); K. P. Lawley, A. C. Flexen, R. R. J. Maier, A. Manck, T. Ridley, and R. J. Donovan, Phys. Chem. Chem. Phys. **4**, 1412 (2002); T. Ridley, J. T. Hennessy, R. J.

Donovan, K. P. Lawley, S. Wang, P. Brint, and E. Lane, J. Phys. Chem. A **112**, 7170 (2008).
[8]A. E. Douglas and F. R. Greening, Can. J. Phys. **57**, 1650 (1979).
[9]D. S. Green, G. A. Bickel, and S. C. Wallace, J. Mol. Spectrosc. **150**, 303 (1991); **150**, 354 (1991); **150**, 388 (1991).
[10]R. Callaghan and R. J. Gordon, J. Chem. Phys. **93**, 4624 (1990).
[11]D. Ascenzi, S. Langford, M. Ashfold, and A. Orr-Ewing, Phys. Chem. Chem. Phys. **3**, 29 (2001).
[12]Á. Kvaran, Á. Logadóttir, and H. Wang, J. Chem. Phys. **109**, 5856 (1998).
[13]Á. Kvaran, H. Wang, and Á. Logadóttir, J. Chem. Phys. **112**, 10811 (2000).
[14]R. Liyanage, R. J. Gordon, and R. W. Field, J. Chem. Phys. **109**, 8374 (1998).
[15]Á. Kvaran, B. G. Waage, and H. Wang, J. Chem. Phys. **113**, 1755 (2000); Á. Kvaran, H. Wang, and B. G. Waage, Can. J. Phys. **79**, 197 (2001); Á. Kvaran and H. Wang, J. Mol. Spectrosc. **228**, 143 (2004); S. M. Hurley, Q. Zhong, and J. A. W. Castleman, J. Chem. Phys. **112**, 4644 (2000).
[16]Á. Kvaran and H. Wang, Mol. Phys. **100**, 3513 (2002).
[17]A. I. Chichinin, C. Maul, and K. H. Gericke, J. Chem. Phys. **124**, 224324 (2006); A. I. Chichinin, P. S. Shternin, N. Godecke, S. Kauczok, C. Maul, O. S. Vasyutinskii, and K. H. Gericke, *ibid.* **125**, 034310 (2006); S. Kauczok, C. Maul, A. I. Chichinin, and K. H. Gericke, *ibid.* **133**, 24301 (2010); C. Romanescu and H. P. Loock, *ibid.* **127**, 124304 (2007); C. Romanescu, S. Manzhos, D. Boldovsky, J. Clarke, and H. Loock, *ibid.* **120**, 767 (2004).
[18]C. Romanescu and H. P. Loock, Phys. Chem. Chem. Phys. **8**, 2940 (2006).
[19]Á. Kvaran, H. Wang, K. Matthíasson, A. Bodi, and E. Jonsson, J. Chem. Phys. **129**, 164313 (2008).
[20]A. Kvaran, K. Matthiasson, and H. S. Wang, J. Chem. Phys. **131**, 044324 (2009).
[21]K. Matthiasson, H. S. Wang, and A. Kvaran, J. Mol. Spectrosc. **255**, 1 (2009).
[22]K. Matthíasson, J. M. Long, H. Wang, and Á. Kvaran, J. Chem. Phys. **134**, 164302 (2011).
[23]M. Bettendorff, S. D. Peyerimhoff, and R. J. Buenker, Chem. Phys. **66**, 261 (1982); H. Lefebvre-Brion, H. P. Liebermann, and G. J. Vazquez, J. Chem. Phys. **134** (2011); D. M. Hirst and M. F. Guest, Molecular Physics **41**, 1483 (1980).
[24]J. Long, H. Wang, and A. Kvaran (unpublished).
[25]Á. Kvaran, Ó. F. Sigurbjörnsson, and H. Wang, J. Mol. Struct. **790**, 27 (2006).
[26]D. S. Ginter, M. L. Ginter, and S. G. Tilford, J. Mol. Spectrosc. **90**, 152 (1981).
[27]*NIST Chemistry WebBook* (NIST (National Institute of Standards and Technology) Chemistry WebBook); K. P. Huber and G. Herzberg, *Constants of Diatomic Molecules* (Van Nostrand Reinhold, New York, 1979); online at http://webbook.nist.gov/chemistry/form-ser.html.en-us.en.
[28]G. Herzberg, *Molecular Spectra and Molecular Structure; I. Spectra of Diatomic Molecules*, 2nd ed. (Van Nostrand Reinhold, New York, 1950).
[29]Y. Xie, P. T. A. Reilly, S. Chilukuri, and R. J. Gordon, J. Chem. Phys. **95**, 854 (1991).
[30]A. Kvaran, K. Matthiasson, and H. S. Wang, Chem. Phys. Lett. **458**, 58 (2008).
[31]M. H. Alexander, X. N. Li, R. Liyanage, and R. J. Gordon, Chem. Phys.**231**, 331 (1998).
[32]A. Kvaran, H. S. Wang, K. Matthiasson, and A. Bodi, J. Phys. Chem. A **114**, 9991 (2010); A. Kvaran, K. Sveinbjornsson, J. M. Long, and H. S. Wang, Chem. Phys. Lett. **516**, 12 (2011).
[33]C. E. Brion, A. Dyck, and G. Cooper, J. Electron Spectrosc. Relat. Phenom. **144**, 127 (2005).
[34]A. G. Smolin, O. S. Vasyutinskii, G. G. Balint-Kurti, and A. Brown, J. Phys. Chem. A **110**, 5371 (2006).
[35]J. M. W. Chase, *NIST-JANAF Thermochemical Tables*, 4th ed. (1998), p. 1; online at http://www.nist.gov/pml/data/asd.cfm.

Article 2

New REMPI observations and analyses for Rydberg and ion-pair states of HI.

Helgi Rafn Hróðmarsson, Huasheng Wang, and Ágúst Kvaran

Journal of Molecular Spectroscopy. **290**. 5-12 (2013).

DOI: 10.1016/j.jms.2013.06.007

Helgi Rafn Hróðmarsson developed the research concept along with Ágúst Kvaran, and performed all the experiments along with Huasheng Wang. Helgi performed all of the data analysis and independently wrote the first manuscript. He contributed to editing until publication.

Journal of Molecular Spectroscopy 290 (2013) 5–12

Contents lists available at SciVerse ScienceDirect

Journal of Molecular Spectroscopy

journal homepage: www.elsevier.com/locate/jms

New REMPI observations and analyses for Rydberg and ion-pair states of HI

Helgi Rafn Hróðmarsson, Huasheng Wang, Ágúst Kvaran *

Science Institute, University of Iceland, Dunhagi 3, 107 Reykjavík, Iceland

ARTICLE INFO

Article history:
Received 23 May 2013
In revised form 22 June 2013
Available online 4 July 2013

Keywords:
Rydberg states
Ion-pair states
REMPI
State interactions
Photoionization
Photofragmentation

ABSTRACT

Two-dimensional REMPI data, obtained by recording ion mass spectra for HI as a function of two-photon wavenumber were recorded and analyzed. Several previously observed spectra due to resonance transitions to $\Omega = 0$ states were (re)assigned. The spectral data revealed several previously unobserved $(2 + n)$ REMPI spectra. These were assigned and analyzed to derive band origins and rotational parameters of Rydberg and ion-pair states. Perturbation effects, showing as line-shifts and/or signal intensity alterations, were found to be helpful in spectra assignments.

1. Introduction

Rotational and vibrational structures in electronically excited states of the hydrogen halides are of great spectroscopic interest. Since the original work by Price [1] on the hydrogen halides, an abundance of spectroscopic data and identities have been derived and studied. These studies include standard absorption measurements [2–6], fluorescence studies [6] and resonance enhanced multiphoton ionization (REMPI) experiments [7–22]. A majority of previous studies of the hydrogen halides has placed emphasis on HCl [2,4,6–13,15,16,23–29], whereas the other halide counterparts HBr [5,15–17,22,29–36] and HI [15,16,37–41] have been studied to a lesser extent.

An extensive study of HI and DI was reported by Ginter et al. [38,42] in 1982. Therein, a broad band of excited states was reported and a large number of spectral lines assigned from single photon absorption spectra. Numerous perturbations due to state interactions were observed but none were analyzed quantitatively. Observations were restricted by single-photon selection rules. Later, Wright and McDonald [40] and Pratt and Ginter [41] published REMPI data for resonance two-photon excitations of HI and provided additional spectroscopic information about the molecule. Thus, for example, spectra due to previously unobserved $\Omega = 0^+ - X^1\Sigma^+$ and $I^1\Delta_2 - X^1\Sigma^+$ transitions to excited Rydberg states were observed. However, the $\Omega = 0^+$ state was not characterized any further. Previously identified states of HI as well as states dealt with in this work are characterized in Table 1.

Different notations for the excited states of the hydrogen halides are adopted by Ginter et al. [38]and Callaghan and Gordon [32]. In Table 1 we use the notation adopted by Callaghan et al., where the nature of the excited molecular orbital is specified (σ, π, δ) as well as the halogen atom orbitals involved (s, p, d) along with the ion core configurations. A clear exception to this rule is the *V*-state which is an ion-pair state.

Whereas most of the studies of HI have focused on spectral assignments and the energetics of the Rydberg and ion-pair states, no emphasis has been placed on spectral perturbations. All the hydrogen halide spectra are rich in intensity deviations and line shifts due to perturbation effects. This makes them ideal for the study of state mixing and photo-fragmentation processes. Furthermore, perturbation effects have been shown to be valuable in spectra assignments [35]. In recent years, a number of papers have been published, which place emphasis on state interactions, energy transfers and photo dissociation processes, in HCl [24,27–29,43–48] and HBr [29,35,36]. Interactions between ion-pair vibrational states and Rydberg states can be organized into three main categories:

(a) Very weak near-resonance state interactions, distinguishable by negligible rotational line shifts but significant alterations in signal line intensities [27,35], observed for triplet Rydberg states and $\Delta\Omega > 0$ state interactions.
(b) Weak near-resonance state interactions, distinguishable by localized line shifts (hence energy level shifts), as well as alterations in signal line intensities [24,26], observed for singlet states and $\Delta\Omega > 0$ state interactions.

* Corresponding author. Fax: +354 552 8911 (main office).
E-mail address: agust@hi.is (Á. Kvaran).

0022-2852/$ - see front matter © 2013 Elsevier Inc. All rights reserved.
http://dx.doi.org/10.1016/j.jms.2013.06.007

Table 1
Electron configurations and corresponding electronic states for HI.

Configurations Callaghan et al. [32]	Corresponding singlet states	Corresponding triplet states
$(\sigma^2\pi^4)$	$X^1\Sigma^+$ (0^+)	None
$(\sigma^2\pi^3)\sigma^*$	$A^1\Pi$ (2)	$a^3\Pi$ $(2,1,0^\pm)$
$(\sigma\pi^4)\sigma^*$	$V^1\Sigma^+$ (0^+)	$t^3\Sigma^+$ $(1,0^-)$
$(\sigma^2\pi^3)6s\sigma$	$C^1\Pi$ (1)	$b^3\Pi$ $(2,1,0^\pm)$
$(\sigma^2\pi^3)6p\sigma$	$D^1\Pi$ (1)	$d^3\Pi$ $(2,1,0^\pm)$
$(\sigma^2\pi^3)6p\pi$	$E^1\Sigma^+$ (0^+)	$e^3\Sigma^+$ $(1,0^-)$
	$F^1\Delta$ (2)	$f^3\Delta$ (3,2,1)
	$G^1\Sigma^-$ (0^-)	$g^3\Sigma^-$ $(1,0^+)$
$(\sigma^2\pi^3)5d\pi$	$H^1\Sigma^+$ (0^+)	$h^3\Sigma^+$ $(1,0^-)$
	$I^1\Delta$ (2)	$i^3\Delta$ (3,2,1)
	$J^1\Sigma^-$ (0^-)	$j^3\Sigma^-$ $(1,0^+)$
$(\sigma^2\pi^3)5d\sigma$	$N^1\Pi$ (1)	$n^3\Pi$ $(2,1,0^\pm)$
$(\sigma^2\pi^3)5d\delta$	$K^1\Pi$ (1)	$k^3\Pi$ $(2,1,0^\pm)$
	$L^1\Phi$ (3)	$l^3\Phi$ (4,3,2)
$(\sigma^2\pi^3)7s\sigma$	$M^1\Pi$ (1)	$m^3\Pi$ $(2,1,0^\pm)$
$(\sigma^2\pi^3)7p\sigma$	$R^1\Pi$ (1)	$r^3\Pi$ $(2,1,0^\pm)$
$(\sigma^2\pi^3)4f\pi$	$O^1\Sigma^+$ (0^+)	$^3\Sigma^+$ $(1,0^-)$
	$^1\Delta$ (2)	$^3\Delta$ (3,2,1)
	$^1\Sigma^-$ (0^-)	$^3\Sigma^-$ $(1,0^+)$

(c) Medium to strong off-resonance state interactions, distinguishable by large scale line- and energy level shifts, as well as alterations in signal intensities [26], observed for triplet and singlet states and $\Delta\Omega = 0$ state interactions.

We will now present two-dimensional REMPI data within the two-photon excitation region 69 600–71 500 cm^{-1} for HI and interpretations relevant to new spectroscopic identifications. An energy level diagram of all known states, including new states presented in this paper, is given in Fig. 1.

2. Experimental

Mass resolved REMPI data, referred to as "Two dimensional (2D) REMPI data" (see below) were recorded for a HI molecular beam, created by jet expansion of a pure sample through a pulsed nozzle. Apparatus used is similar to that described elsewhere [24–28,49,50]. Excitation radiation was generated by pulsed excimer laser-pumped dye laser systems, using a Lambda Physik COMPex 205 excimer laser and a Coherent ScanMatePro dye laser. Frequency doubled radiation was focused on the molecular beam inside an ionization chamber between a repeller and extractor plates. Ions formed by multiphoton excitations were directed into a time-of-flight tube and detected by a micro-channel plates (MCP's) detector. Signals were fed into a LeCroy WaveSurfer 44MXs-A, 400 MHz storage oscilloscope and stored as a function of ion time-of-flights and laser radiation wavenumbers. Average signal

Table 2
Typical equipment/condition parameters for REMPI experiments.

HI gas sample	Matheson gas products Inc.
Laser dye	C540A
Frequency doubling crystal	Sirah BBO-2
Laser repetition rate	10 Hz
Dye laser bandwidth	0.095 cm^{-1}
Intensity repetition used	0.1–0.3 mJ/pulse
Nozzle size	500 μm
Sample backing pressure	2.0–2.5 bar
Pressure inside ionization chamber	10^{-6} mbar
Nozzle opening time	150–200 μs
Delay time for laser excitation	450–550 μs
Excitation wavenumber step sizes	0.05–0.10 cm^{-1}
Time of flight step sizes	10 ns

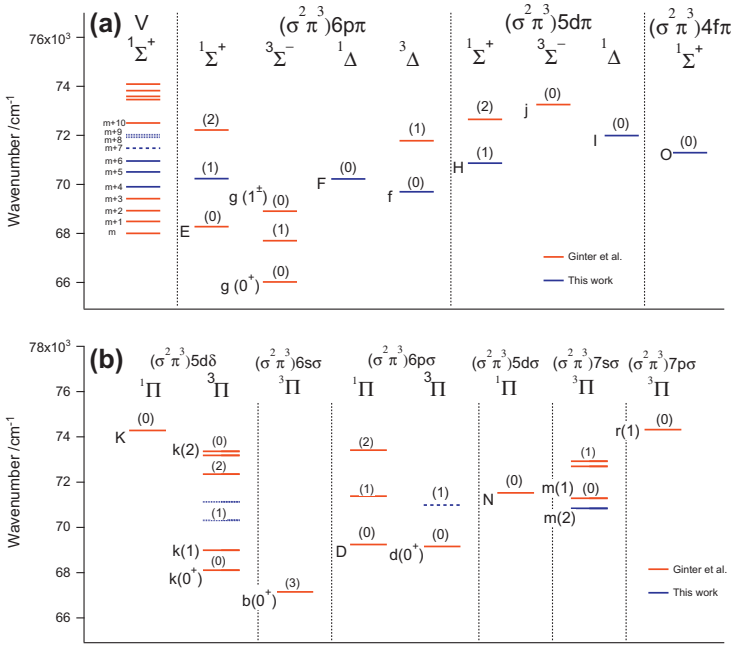

Fig. 1. Energy level diagram of all the known electronic states for HI. The ion-pair states and the $^{1,3}\Sigma$ and $^{1,3}\Delta$ Rydberg states with π Rydberg electrons are presented in (a). The $^{1,3}\Pi$ Rydberg states with σ and δ Rydberg electrons are in (b). Red lines correspond to previously detected bands [38] whereas blue lines correspond to states observed in this work, some of which have been detected before (see text). Dotted lines correspond to states that have been previously detected in single-photon spectroscopy but not in REMPI whereas dashed lines correspond to bands that have neither been detected in single-photon spectroscopy or in REMPI. Vibrational numberings are shown in parenthesis on top of every line for the Rydberg states. Vibrational levels for the V states are labeled as $v' = m + i$; $i = 0, 1, 2, \ldots$. (For interpretation of the references to color in this figure legend, the reader is referred to the web version of this article.)

levels were evaluated and recorded for a fixed number of laser pulses. The data were corrected for laser power and mass calibrated to obtain ion yields as a function of mass and excitation wavenumber (2D-REMPI data). REMPI spectra for certain ions as a function of excitation wavenumber (1D-REMPI) were obtained by integrating mass signal intensities for the particular ions. Care was taken to prevent saturation effects as well as power broadening by minimizing laser power. Laser calibration was based on an optogalvanic spectrum, obtained from a built-in neon cell as well as on observed (2 + 1) iodine atom REMPI peaks [51]. The accuracy of the calibration was typically found to be about ±0.5 cm^{-1} on a laser wavenumber scale, hence about ±2.0 cm^{-1} on a two-photon wavenumber scale. Equipment parameters are listed in Table 2.

3. Results and analysis

Most HI spectra, previously detected in the excitation region 69 600–71 500 cm^{-1}, were identified and assigned. Spectra which have been assigned [38] to resonance transitions to the $E^1\Sigma^+$ and $H^1\Sigma^+$ Rydberg states were reassigned (see below). Partly unassigned spectrum at $v^0 = 71\,295$ cm^{-1} was fully assigned (see below). In addition, several "new spectra" and/or "new lines" were observed and assigned. These can be categorized into four main groups (see Table 3 and Fig. 2):

(i) Spectra due to two-photon resonance transitions to Rydberg states not previously detected in REMPI [41] but identified in single-photon absorption studies [38].
(ii) Spectra due to two-photon resonance transitions to Rydberg states, not previously detected.
(iii) Spectra due to two-photon resonance transitions to ion-pair states, not previously detected in REMPI [41] but identified in single-photon absorption studies [38].
(iv) Spectra due to two-photon resonance transitions to ion-pair states not previously detected.

Spectroscopic parameters of all observed states are summarized in Table 3. Newly observed states are marked specifically according to the categories mentioned above (i–iv). Corresponding rotational lines are listed in Table 4. In Fig. 2, the relevant 1D-REMPI spectra for parent and fragment ions are shown. The $k^3\Pi_0(v' = 1)$ Rydberg state spectrum, which previously has been identified in single-photon absorption spectroscopy [38], but not in two-photon REMPI, is shown in Fig. 2a along with some of the *R* and *S* lines of the nearby $F^1\Delta_2(v' = 0)$ spectra. Another Rydberg state spectrum, also identified previously in single-photon absorption, for the $k^3\Pi_1(v' = 1)$ state, is shown in Fig. 2b as well as the previously undetected $d^3\Pi_0(v' = 1)$ band, which *Q* lines in the I^+ spectrum coincide partly with a strong atomic iodine line at 70988.2 cm^{-1}. In Fig. 2c the previously unreported $V^1\Sigma^+(v' = m + 7)$ ion-pair state spectrum is shown along with the *S* lines of the $O^1\Sigma^+(v' = 0)$ state spectrum [41]. The ion-pair states spectra for $V^1\Sigma^+$ $(v' = m + 8)$ and $V^1\Sigma^+$ $(v' = m + 9)$ were detected in the spectral region shown in Fig. 2d, where the $I^1\Delta_2(v' = 0)$ spectrum also appears [41]. For clarity reason, the H^+ fragment spectrum from Fig. 2d is enlarged in Fig. 2e.

3.1. Spectra due to resonance transitions to the $H^1\Sigma^+$ and $E^1\Sigma^+$ Rydberg states; reassignments

Ginter et al. [38] assign the $v^0 = 70850.5$ cm^{-1} and 72650.8 cm^{-1} bands to the $E^1\Sigma^+((\sigma^2\pi^3)6p\pi)$, $v' = 0$ and 1 Rydberg states respectively and the $v^0 = 68277.3$ cm^{-1}, 70242.1 cm^{-1} and 72217.6 cm^{-1} bands to the $H^1\Sigma^+((\sigma^2\pi^3)5d\pi$, $v' = 0$, 1, and 2 Rydberg states respectively without any clear arguments. This we believe that should be reassigned such that the $v^0 = 68277.3$ cm^{-1}, 70242.1 cm^{-1} and 72217.6 cm^{-1} bands correspond to the $E^1\Sigma^+((\sigma^2\pi^3)6p\pi)$, $v' = 0$, 1, and 2 Rydberg states, respectively and that the $v^0 = 70850.5$ cm^{-1} and 72650.8 cm^{-1} bands belong to the $H^1\Sigma^+((\sigma^2\pi^3)5d\pi)$, $v' = 1$ and 2 states, respectively, for the following reasons (a–c):

(a) Based on comparison with HCl [8–11] and HBr [32] the energies of the E states are lower than those of the corresponding *H* states. Thus the band origin differences (Δv^0) between the $v' = 0$ states ($v^0(H(v' = 0) - v^0(E(v' = 0))$ are found to be 4905 cm^{-1} and 1706 cm^{-1} for HCl and HBr respectively. We therefore believe that the lower energy $\Omega = 0^+$ serie

Table 3
HI: Band origin (v^0) and rotational parameters (B_v and D_v) for all states observed in the 69 600–72 100 cm^{-1} excitation region. The identifications (i)–(iv) are according to a categorization specified in the text.

States[c]	v^0 (cm^{-1})		B_v (cm^{-1})		$D_v \times 10^4$ (cm^{-1})		Identification
	This work[e]	Others	This work	Others	This work	Others	
$f^3\Delta_1$ (0)	69699.9	69687.0[a]	6.31 ± 0.02	6.135	4.6 ± 1.0	1.92	
$V^1\Sigma^+$ $(m + 4)$	69903.3	69909.9[a]	2.94 ± 0.18	3.27	10 ± 40	6,5	
$F^1\Delta_2$ (0)	70223.6	70228.3[a]	6.32 ± 0.01	6.30	2.6 ± 0.6	1.2	
$E^1\Sigma^+$ (1)[d]	70236.1	70242.1[a]	6.34 ± 0.01	5.95	1100 ± 20	125	
$k^3\Pi_0$ (1)	70310.8	70320.4[a]	5.13 ± 0.03	5.058	−4 ± 9	−21.0	(i)
$V^1\Sigma^+$ $(m + 5)$	70511.0	70512[a]	3.66 ± 0.02	3.800	83 ± 4	−70.2	
$m^3\Pi_2$ (0)	70841.5	70837.6[a]	6.21 ± 0.04	6.11	12 ± 5	1.94	
$H^1\Sigma^+$ (0)[d]	70866.3	70850.5[a]	5.94 ± 0.17	6.00	−11 ± 21	128	
$V^1\Sigma^+$ $(m + 6)$	70952.3	70948.6[a]	3.56 ± 0.10	4.09	24 ± 10	44	
$d^3\Pi_0$ (1)	70988.2	–	5.79 ± 0.12	–	−290 ± 40	–	(ii)
$k^3\Pi_1$ (1)	71126.4	71125.0[a]	6.22 ± 0.02	6.30	−2.6 ± 1.6	4.82	(i)
$m^3\Pi_1$ (0)	–	71287.3[a]	–	6.254	–	3.18	
$O^1\Sigma^+$ (0)[d]	71294.7	71301.9[b]	6.25 ± 0.22	5.82	33 ± 26	–	
$D^1\Pi$ (1)	–	71382.4[a]	–	6.052	–	1.92	
$V^1\Sigma^+$ $(m + 7)$	71478.4	–	2.95 ± 0.10	–	−4 ± 5	–	(iv)
$N^1\Pi$ (0)	–	71526.2[a]	–	6.163	–	1.74	
$f^3\Delta$ (1)	–	71780.5[a]	–	5.957	–	9.73	
$V^1\Sigma^+$ $(m + 8)$	71924.4	71920.3[a]	4.17 ± 0.17	3.97	270 ± 70	158	(iii)
$I^1\Delta_2$ (0)	71989.4	71990[b]	6.31 ± 0.01	6.312	2.4 ± 0.1	2.7	
$V^1\Sigma^+$ $(m + 9)$	72023.2	72022.4[a]	2.84 ± 0.03	2.792	1 ± 4	−4.61	(iii)

[a] Ref. [38].
[b] Ref. [41].
[c] Term symbol (vibrational quantum numbers).
[d] (Re)assigned.
[e] v^0 for $\Omega = 0$ states equal observed v for the $J' = 0 \leftarrow\leftarrow J'' = 0$ transitions; v^0 for $\Omega > 0$ were derived from fitting of observed rotational lines ($J' > 0$).

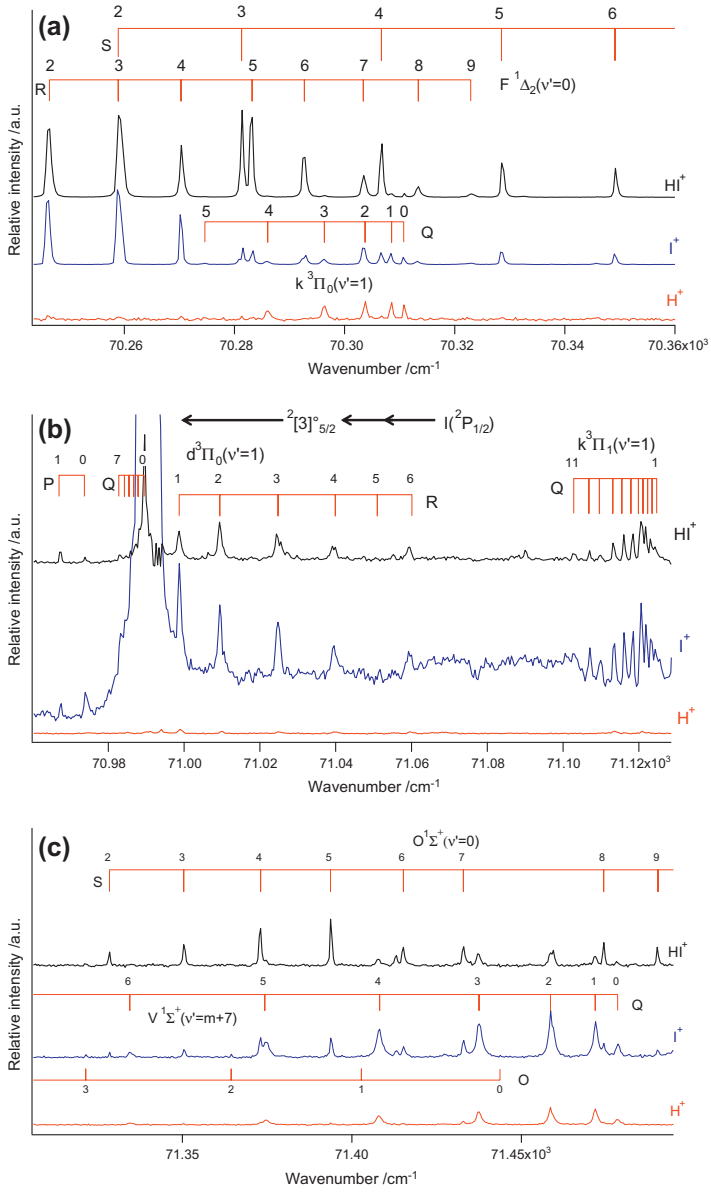

Fig. 2. 1D-REMPI spectra for H^+, I^+, and HI^+ and J' assignments of rotational peaks corresponding to two-photon resonance excitations to $F^1\Delta_2(v' = 0)$ (a), $k^3\Pi_0(v' = 1)$ (a), $d^3\Pi_0(v' = 1)$ (b), $k^3\Pi_1(v' = 1)$ (b), $O^1\Sigma^+$ $(v' = 0)$ (c), $V^1\Sigma^+$ $(v' = m + 7)$ (c), $V^1\Sigma^+$ $(v' = m + 8)$ (d and e), $I^1\Delta_2(v' = 0)$ (d), and $V^1\Sigma^+$ $(v' = m + 9)$ (d and e). In Fig. 2e, the H^+ spectrum from Fig. 2d is intensified to show the presence of the ion-pair states $V^1\Sigma^+$ $(v' = m + 7)$ and $V^1\Sigma^+$ $(v' = m + 8)$ more clearly.

($v^0 = 68277.3$ cm^{-1}, 70242.1 cm^{-1} and 72217.6 cm^{-1} bands) belongs to $E^1\Sigma^+((\sigma^2\pi^3)6p\pi)$ whereas the higher energy serie ($v^0 = 70850.5$ cm^{-1} and 72650.8 cm^{-1}) is for $H^1\Sigma^+((\sigma^2\pi^3)5d\pi)$. If, on the other hand, the $v^0 = 68277.3$ cm^{-1} band belongs to $E(v' = 0)$ and that the $v^0 = 70850.5$ cm^{-1} is for $H(v' = 0)$, $\Delta v^0 = 2573.2$ cm^{-1}, which contradicts a decreasing Δv^0 as the halogen atom increases (see above). We therefore assign the $v^0 = 70850.5$ cm^{-1} band to $H(v' = 1)$ in which case v^0 for $H(v' = 0)$ should be close to 69 000 cm^{-1} and Δv^0 about 720 cm^{-1}. No spectrum for an $\Omega = 0^+$ state in that region has been found yet. Judging from the information concerning the spectral intensities for the $v^0 = 70850.5$ cm^{-1} band [38,41], which are marked vvw (very very weak) there is a reason to believe that the spectrum for $H(v' = 0)$ is still weaker.

(b) For HCl and HBr it has been found that the interaction strength between E and V states is stronger than any other Rydberg to ion-pair interactions, including the H and V interactions, showing in the form of large line, hence energy level shifts as well as intensity irregularities [24,27–29,35,36]. Thus, characteristic large irregularities in energy gaps between ion-pair vibrational states are found closest in energy to E states for HCl and HBr [15]. This shows as enhancements in

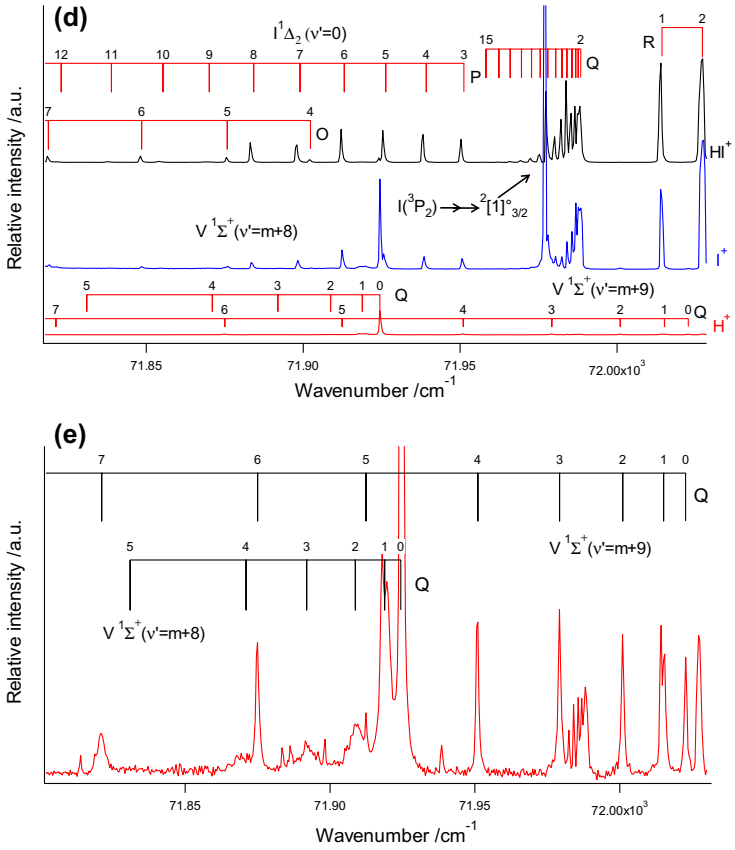

Fig. 2 (*continued*)

energy gaps between ion-pair vibrational states closest in energy to E states and corresponding lowering in the energy gaps above and below in energy (see Figs. 3 and 5 in Ref. [15]). As shown in Fig. 3 the same effect is seen for HI for the reassigned E state. Thus the energy gaps between $V(v' = m)$ and $V(v' = m + 1)$, $V(v' = m + 4)$ and $V(v' = m + 5)$ as well as between $V(v' = m + 9)$ and $V(v' = m + 10)$ which are closest to the $E(v' = 0)$, $E(v' = 1)$, and $E(v' = 3)$ states, respectively, all are enhanced whereas the energy gaps between $V(v' = m + 1)$ and $V(v' = m + 2)$, $V(v' = m + 3)$ and $V(v' = m + 4)$, $V(v' = m + 5)$ and $V(v' = m + 6)$ as well as $V(v' = m + 8)$ and $V(v' = m + 9)$ all are reduced.

(c) Ion intensity ratios, $I(X^+)/I(HX^+)$ (X = Cl, Br), for Rydberg states, are found to be clear indications of interaction strengths between Rydberg and ion-pair states. Largest values have been found for the E state spectra [29,36]. This also holds for the reassigned E state spectra in the case of HI. Thus, these ratios are typically found to be about 4 for the E state spectra but only about 1 for the reassigned H state spectra.

(d) Quantum defect analysis [35] and comparison with iodine atomic Rydberg states [51] with np^1 and nd^1 configurations further support this assignment.

3.2. The 71 295 cm^{-1} spectrum; assignment

The spectrum observed near 71 295 cm^{-1} has been assigned to an $\Omega = 0^+$ state without any further specifications [41]. The spectrum shows dominating HI^+ signals but also significant fragment ion signals (I^+ and H^+) for large range of J' levels (see S lines in Fig. 2b). This is characteristic for an $\Omega = 0(^1\Sigma^+)$ Rydberg state showing strong homogeneous, off resonance, coupling with ion-pair vibrational state [28,35,36]. Spectral analysis give a rotational constant $B' = 6.25 \pm 0.22$ cm^{-1} and band origin $\nu^0 = 73294.7$ cm^{-1} (see Table 3). This state can neither be a vibrationally excited E or H state, since it does not fit into the corresponding vibrational state series. Quantum defect analysis [36] show that this state cannot be a $^1\Sigma^+$ state in the E and H Rydberg state series corresponding to excitations to orbitals with higher principal quantum numbers (i.e. not $(s^2p^3)7p\pi$ and $(\sigma\ ^2\pi\ ^3)6d\pi$ states. Such analysis and comparison with quantum defect values (δ) for iodine atomic Rydberg states [51], on the other hand, suggest that this state could correspond to an excitation to the 4f orbital, $v' = 0$ ($\delta \approx 1.0$). We therefore assign the $\nu^0 = 73\,295$ cm^{-1} state to $O^1\Sigma^+(v' = 0)$ with the electron configuration $(\sigma^2\pi^3)4f\pi$.

3.3. Spectra due to two-photon resonance transitions to Rydberg states not previously detected in REMPI but identified in single-photon absorption studies

The $k^3\Pi$ Rydberg states correspond to an electron excitation to a $6d\delta$ Rydberg orbital (Table 1). Several vibrational bands for these states have been identified (see Fig. 1b) and analyzed (Table 3 and Ref. [38]). However, in the two-photon REMPI experiments, performed by Pratt and Ginter [41], only $k^3\Pi$ Rydberg bands for

Table 4
Rotational lines for HI due to two-photon resonance transitions to the $k^3\Pi_0(v'=1)$, $k^3\Pi_1(v'=1)$, $d^3\Pi_0(v'=1)$, $V^1\Sigma^+(v'=m+7)$, $V^1\Sigma^+(v'=m+8)$, and $V^1\Sigma^+(v'=m+9)$ states.

J'	$k^3\Pi_0$	$k^3\Pi_1$	$d^3\Pi_0$		
	Q	Q	P	Q	R
0	70310.8			70989.5	70998.5
1	70308.6	71125.4	70973.7	70989.3	71009.2
2	70304.0	71124.1	70967.4	70988.0	71024.6
3	70296.4	71123.1		70986.8	71039.4
4	70286.1	71121.6		70985.7	71051.5
5	70274.7	71120.4		70984.6	71059.0
6		71118.4		70983.0	
7		71115.9		70981.5	
8		71113.2			
9		71109.7			
10		71106.9			
11		71107.2			

	$V^1\Sigma^+(m+7)$		$V^1\Sigma^+(m+8)$	$V^1\Sigma^+(m+9)$
	O	Q	Q	Q
0		71478.4	71924.4	72022.7
1		71471.8	71918.8	72015.5
2	71443.7	71458.6	71908.7	72001.0
3	71402.8	71437.5	71890.2	71979.2
4	71364.4	71408.2	71871.4	71950.6
5	71321.5	71374.3	71831[a]	71912.4
6	71265.9	71334.3		71875.0
7	71214.3	71291[a]		71820.8
8		71240.6		71769.9
9		71186.8		71706.8
10				71631.7

[a] Uncertainty of peak positions is ±5 cm^{-1}.

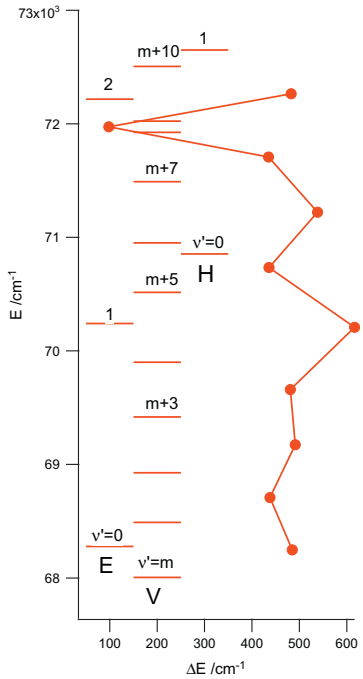

Fig. 3. Vibrational energy levels for the E, H, and V ($^1\Sigma^+$) states and vibrational level spacings between the V states vs. energy.

the $k^3\Pi_0(v'=2)$ and $k^3\Pi_1(v'=2)$ states were observed. Now the $k^3\Pi_0(v'=1)$ and $k^3\Pi_1(v'=1)$ vibrational bands have been observed in REMPI for the first time (see Fig. 2a and b), centered at $v^0 = 70310.8\ cm^{-1}$ and $71126.4\ cm^{-1}$ respectively. Spectral analyses give values of rotational constants, B_v and D_v, in good agreement with previously determined values (see Table 3).

No perturbations are observed for the $k^3\Pi_0(v'=1)$ state in terms of line shifts or intensity alterations, in good agreement with the findings of Ginter et al. [38]. For the $k^3\Pi_1(v'=1)$ Rydberg state, on the other hand, Ginter et al. reported that it "may be perturbed at high J'". We observe line shifts for high J' values as well as $I(I^+)/I(HI^+)$ intensity ratios for $J'=8$–11 (Fig. 4) which is characteristic of near-resonance interactions with an ion-pair state [25–28,35,36] (see Section 3.6).

3.4. Spectra due to two-photon resonance transitions to Rydberg states, not previously detected

A new, previously unobserved spectrum is seen in the two-photon excitation region 70 970–71 070 cm^{-1} (see Fig. 2b). Clear peaks are observed on the high wavenumber side of a strong iodine atomic line (79991.6 cm^{-1}; $^3[3]^\circ_{5/2} \leftarrow\leftarrow {}^2P_{1/2}$ transition) in the I^+ spectrum and in the HI^+ spectrum. These peaks are assigned to R lines, whereas the structure in the HI^+ spectrum in the region of the atomic line is assigned to overlapping Q lines. On the short wavenumber side, two P lines are observed. The I^+ signals are found to be stronger than the parent ion signals whereas the H^+ signals are very weak. Furthermore, no significant line shifts or significant changes in the intensity ratios or bandwidths of the spectral lines, as a function J', are observed. This is characteristic of a predissociating Π state. Analysis of the rotational structure revealed an $\Omega = 0$ state, which excludes $^1\Delta$ or $^3\Delta$ states. Furthermore, appearance of R and P lines, rules out a Σ state. We therefore believe that the "new spectrum" corresponds to transitions to a $^3\Pi_0$ state, which could either belong to the $b^3\Pi_0$ or the $d^3\Pi_0$ Rydberg series (see Fig. 1b). The third vibrational band for $b^3\Pi_0$ state has been observed at energies approximately 4000 cm^{-1} lower than the "new state" [38], whereas the first vibrational band ($v'=0$) of $d^3\Pi_0$ has been observed at 69157.8 cm^{-1}. If the "new band" belongs to the second vibrational level ($v'=1$) of the $d^3\Pi_0$ Rydberg state, the energy spacing between the vibrational levels is 1830.4 cm^{-1}, which one might expect for a Rydberg state of HI (see Fig. 1). We therefore assign the "new band" at $v^0 = 70988.2\ cm^{-1}$ to the $d^3\Pi_0(v'=1)$, $(\sigma^2\pi^3)6p\sigma$ Rydberg state.

3.5. Spectra due to two-photon resonance transitions to ion-pair states, not previously detected in REMPI but identified in single-photon absorption studies

The ion-pair states $V^1\Sigma^+(v'=m+8)$ and $V^1\Sigma^+(v'=m+9)$ have not been detected in two-photon REMPI before. In the REMPI spectra shown in Fig. 2d and e, weak structures are observed which are assigned to the ion-pair states $V^1\Sigma^+(v'=m+8)$ and $V^1\Sigma^+(v'=m+9)$. Strongest signals are found for H^+. Spectral analyses reveal rotational constants, B_v and D_v, as well as spectral origin, v^0, in good agreement with previously determined values [38] (Table 3).

In the work by Ginter et al. [38] the $V^1\Sigma^+(v'=m+8)$ spectrum was found to be perturbed and very diffuse for low J's whereas the $V^1\Sigma^+(v'=m+9)$ spectrum showed sharp lines. This agrees with our findings (see Fig. 2e). The $J'=0$, Q-line for $V^1\Sigma^+(v'=m+8)$ is a sharp peak at 71924.4 cm^{-1}, whereas all other subsequent peaks exhibit clear line broadenings (see Fig. 5). By analogy with HBr and HCl this is most probably associated with interactions with predissociating Rydbergs states [29,35,36]. Several state interactions, involving the V states can be of importance in this energy region (see Fig 6). Thus the $V^1\Sigma^+(v'=m+9)$ will experience

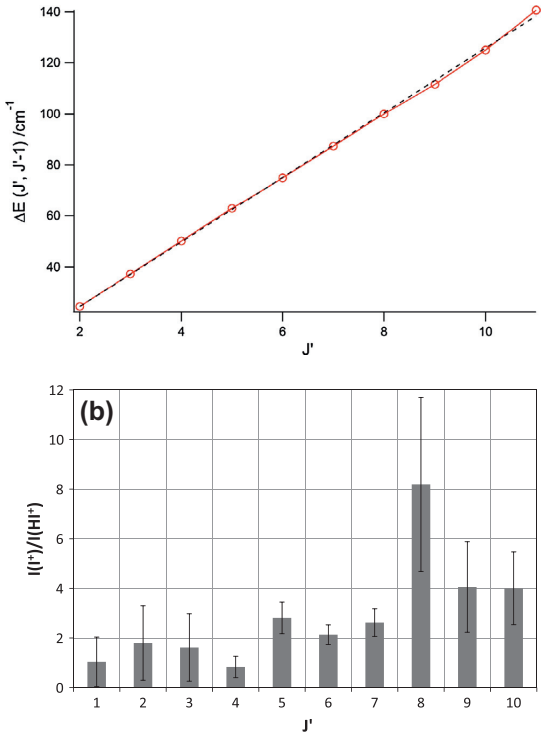

Fig. 4. (a) Energy differences of rotational levels for the $k^3\Pi_1(v' = 1)$ Rydberg state as a function of J'. Perturbations are seen for high J'. (b) Relative ion signal intensities, $I(I^+)/I(HI^+)$ vs. J' derived from Q rotational lines of REMPI spectra due to two-photon resonance transitions to the Rydberg state $k^3\Pi_1(v' = 1)$.

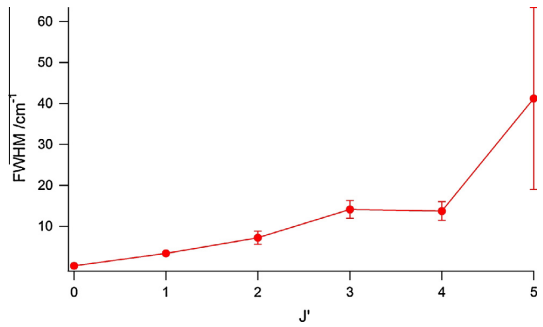

Fig. 5. Rotational line-widths vs. J' derived from the Q lines of the H^+ REMPI spectrum for $V^1\Sigma^+$ ($v' = m + 8$). The large increase in line-widths as J' increases is evidence of a strong off-resonance interaction with another $^1\Sigma^+$state.

off-resonance interactions mainly with the $E^1\Sigma^+(v' = 2)$ state resulting in energy level lowering of the $V^1\Sigma^+(v' = m + 9)$ state whereas the $V^1\Sigma^+(v' = m + 7)$ state (see text below) will mainly experience off-resonance interactions with the $O^1\Sigma^+(v' = 0)$ state resulting in an increase in the energy levels of the $V^1\Sigma^+(v' = m + 7)$ state. The $V^1\Sigma^+(v' = m + 8)$, on the other hand, state may experience significant off-resonance interaction both with the $O^1\Sigma^+(v' = 0)$ and the $E^1\Sigma^+(v' = 2)$ states. As a result, the $V^1\Sigma^+(v' = m + 8)$ state will be "clenched" between the two ion-pair states, $V^1\Sigma^+(v' = m + 7)$ and $V^1\Sigma^+(v' = m + 9)$. This explains the small vibrational energy spacing

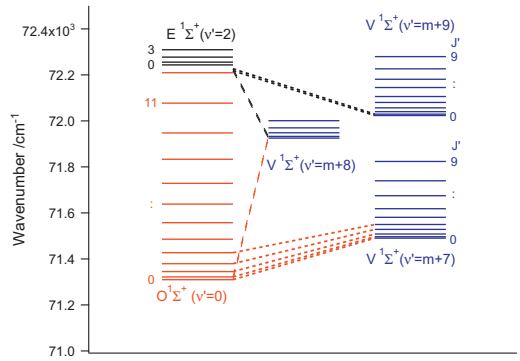

Fig. 6. Rotational energy levels, derived from observed REMPI rotational peaks for the $O^1\Sigma^+$ ($v' = 0$), $V^1\Sigma^+$ ($v' = m + 7$), $V^1\Sigma^+$ ($v' = m + 8$), $V^1\Sigma^+$ ($v' = m + 9$) and $E^1\Sigma^+$ ($v' = 2$) states. The rotational energy levels for the $E^1\Sigma^+$ ($v' = 2$) state were derived from rotational constants reported by Ginter et al. [38]. Proposed off-resonance interaction between the $O^1\Sigma^+$ ($v' = 0$) and the ion-pair states $V^1\Sigma^+$ ($v' = m + 7$) and $V^1\Sigma^+$ ($v' = m + 8$) is indicated by red broken lines by varying thickness as an indication of an alternating state mixing. Likewise, off-resonance interactions between the $E^1\Sigma^+$ ($v' = 2$) and the ion-pair states $V^1\Sigma^+$ ($v' = m + 8$) and $V^1\Sigma^+$ ($v' = m + 9$) is indicated by black broken lines by varying thickness. (For interpretation of the references to color in this figure legend, the reader is referred to the web version of this article.)

between these states (Table 3). Furthermore, the ion-pair state $V^1\Sigma^+(v' = m + 9)$, is found to experience some near-resonance interaction [52].

3.6. Spectra due to two-photon resonance transitions to ion-pair states not previously detected

The ion-pair state $V^1\Sigma^+(v' = m + 7)$ for HI has not been detected or analyzed before. A structure characteristic for an ion-pair state spectrum is observed (Fig 2c) close to the $O^1\Sigma^+$ ($v' = 0$) state spectrum (between the $V^1\Sigma^+(v' = m + 6)$ and $V^1\Sigma^+(v' = m + 8)$ states). It shows medium to strong H^+ and I^+ signals and weak to very weak HI^+ signals as to be expected for an ion-pair state spectrum [25,27–29,35,36]. Spectral analysis give a small rotational constant ($B_v = 2.95\ cm^{-1}$; see Table 3) of the same order of magnitude as for other ion-pair states. We therefore, assign this newly observed structure to the $V^1\Sigma^+$ ($v' = m + 7$) ion-pair state. As mentioned before, the $V^1\Sigma^+$ ($v' = m + 7$) state will experience off-resonance interactions with the $O^1\Sigma^+$ ($v' = 0$) Rydberg state, which will result in upwards energy level shifts for $V(v' = m + 7)$. Furthermore, the $V(v' = m + 7)$ state must be the perturbing state for the near-resonance interaction effects observed for the $k^3\Pi_1(v' = 1)$ state. $J' = 8 - 11$, mentioned before (see Section 3.3 and Fig. 4).

4. Conclusions

Several spectra features, observed in (2 + n) REMPI of HI, for the excitation region 69 600–71 500 cm^{-1}, were assigned and analyzed. Perturbation effects, seen as line-shifts and/or intensity anomalies, due to interactions between Rydberg states and ion-pair states or repulsive states, proved to be helpful in assigning spectra. Rotational parameters and band origins were determined. Previously observed spectra due to resonance transitions to the $E^1\Sigma^+$ and $H^1\Sigma^+$ Rydberg states were reassigned and the band spectrum centered at $\nu^0 = 71\,295\ cm^{-1}$ was assigned to the $O^1\Sigma^+$ ($v' = 0$), $(\sigma^2\pi^3)4f\pi$ state. Several new spectra were identified and assigned. (i) Firstly, spectra due to resonance transitions to the Rydberg states $k^3\Pi_0(v' = 1)$ and $k^3\Pi_1(v' = 1)$, not previously observed in REMPI,

were identified. Near-resonance interactions are identified for the $k^3\Pi_0(v' = 1)$ state. (ii) Secondly, a new spectrum at $v^0 = 70988.2\ cm^{-1}$, not previously observed, showing characteristics of predissociating Π Rydberg states is assigned to the $d^3\Pi_0(v' = 1)$, $(\sigma^2\pi^3)6p\sigma$ state. (iii) Thirdly, two vibrational bands of the ion-pair state $V^1\Sigma^+$, $V(v' = m + 8)$ and $V(v' = m + 9)$, which have not been detected in REMPI before, were identified and (iv) finally, a new spectrum due to resonance transition to the $V(v' = m + 7)$ vibrational state was observed. All the V state spectra in (iii) and (iv) ($v' = m + 7$, $m + 8$, $m + 9$) show characteristic effects of strong off-resonance interactions with the $E^1\Sigma^+$ ($v' = 2$) and the $O^1\Sigma^+$ ($v' = 0$) states.

Acknowledgments

The financial support of the University Research Fund, University of Iceland and the Icelandic Science Foundation (Project No. 130259-051) is gratefully acknowledged.

References

[1] W.C. Price, Proc. Roy. Soc. Ser. A 167 (1938) 216.
[2] S.G. Tilford, M.L. Ginter, J.T. Vanderslice, J. Mol. Spectrosc. 33 (1970) 505–519.
[3] S.G. Tilford, M.L. Ginter, J. Mol. Spectrosc. 40 (1971) 568–579.
[4] D.S. Ginter, M.L. Ginter, J. Mol. Spectrosc. 90 (1981) 177–196.
[5] D.S. Ginter, M.L. Ginter, S.G. Tilford, J. Mol. Spectrosc. 90 (1981) 152.
[6] J.B. Nee, M. Suto, L.C. Lee, J. Chem. Phys. 85 (1986) 719–724.
[7] T.A. Spiglanin, D.W. Chandler, D.H. Parker, Chem. Phys. Lett. 137 (1987) 414–420.
[8] D.S. Green, G.A. Bickel, S.C. Wallace, J. Mol. Spectrosc. 150 (1991) 303–353.
[9] D.S. Green, G.A. Bickel, S.C. Wallace, J. Mol. Spectrosc. 150 (1991) 354–387.
[10] D.S. Green, G.A. Bickel, S.C. Wallace, J. Mol. Spectrosc. 150 (1991) 388–469.
[11] D.S. Green, S.C. Wallace, J. Chem. Phys. 96 (1992) 5857–5877.
[12] E.d. Beer, B.G. Koenders, M.P. Koopmans, C.A.d. Lange, J. Chem. Soc. Faraday Trans. 86 (1990) 2035–2041.
[13] Y. Xie, P.T.A. Reilly, S. Chilukuri, R.J. Gordon, J. Chem. Phys. 95 (1991) 854–864.
[14] E.d. Beer, W.J. Buma, C.A. deLange, J. Chem. Phys. 99 (1993) 3252–3261.
[15] Á. Kvaran, Á. Logadóttir, H. Wang, J. Chem. Phys. 109 (1998) 5856–5867.
[16] Á. Kvaran, H. Wang, Á. Logadóttir, Recent Res. Devel., in: Physical Chem., Transworld Research Network, 1998, pp. 233–244.
[17] Á. Kvaran, H. Wang, Á. Logadóttir, J. Chem. Phys. 112 (2000) 10811–10820.
[18] Á. Kvaran, H. Wang, B.G. Waage, Can. J. Phys. 79 (2001) 197–210.
[19] H. Wang, Á. Kvaran, J. Mol. Struct. 563–564 (2001) 235–239.
[20] Á. Kvaran, H. Wang, Mol. Phys. 100 (2002) 3513–3519.
[21] Á. Kvaran, H. Wang, J. Mol. Spectrosc. 228 (2004) 143–151.
[22] D. Ascenzi, S. Langford, M. Ashfold, A. Orr-Ewing, Phys. Chem. Chem. Phys. 3 (2001) 29–43.
[23] R. Liyanage, R.J. Gordon, R.W. Field, J. Chem. Phys. 109 (1998) 8374–8387.
[24] Á. Kvaran, H. Wang, K. Matthiasson, A. Bodi, E. Jónsson, J. Chem. Phys. 129 (2008) 16313.
[25] A. Kvaran, H.S. Wang, K. Matthiasson, A. Bodi, E. Jonsson, J. Chem. Phys. 129 (2008) 164313.
[26] K. Matthiasson, H.S. Wang, A. Kvaran, J. Mol. Spectrosc. 255 (2009) 1–5.
[27] A. Kvaran, K. Matthiasson, H.S. Wang, J. Chem. Phys. 131 (2009) 044324.
[28] K. Matthiasson, J.M. Long, H.S. Wang, A. Kvaran, J. Chem. Phys. 134 (2011) 164302.
[29] J. Long, H. Wang, Á. Kvaran, J. Chem. Phys. 138 (2013) 044308.
[30] R.F. Barrow, J.G. Stamper, Proc. Roy. Soc. Ser. A 263 (1961) 277–288.
[31] R.F. Barrow, J.G. Stamper, Proc. Roy. Soc. Ser. A 263 (1961) 259–276.
[32] R. Callaghan, R.J. Gordon, J. Chem. Phys. 93 (1990) 4624–4636.
[33] J.B. Nee, M. Suto, L.C. Lee, J. Chem. Phys. 85 (1986) 4919.
[34] Á. Kvaran, B.G. Waage, H. Wang, J. Chem. Phys. (2000).
[35] J. Long, H. Wang, Á. Kvaran, J. Mol. Spectrosc. 282 (2012) 20–22.
[36] J. Long, H.R. Hróðmarsson, H. Wang, Á. Kvaran, J. Chem. Phys. 136 (2012).
[37] S.G. Tilford, M.L. Ginter, A.M. Bass, J. Mol. Spectrosc. 34 (1970) 327.
[38] D.S. Ginter, M.L. Ginter, S.G. Tilford, J. Mol. Spectrosc. 92 (1982) 40.
[39] M.L. Ginter, S.G. Tilford, A.M. Bass, J. Mol. Spectrosc. 57 (1975) 271.
[40] S.A. Wright, J.D. McDonald, J. Chem. Phys. 101 (1994) 238–245.
[41] S.T. Pratt, M.L. Ginter, J. Chem. Phys. 102 (1995) 1882–1888.
[42] D.S. Ginter, M.L. Ginter, S.G. Tilford, A.M. Bass, J. Mol. Spectrosc. 92 (1982) 55.
[43] A.I. Chichinin, C. Maul, K.H. Gericke, J. Chem. Phys. 124 (2006) 224324.
[44] A.I. Chichinin, P.S. Shternin, N. Gödecke, et al., J. Chem. Phys. 125 (2006) 034310.
[45] S. Kauczok, C. Maul, A.I. Chichinin, K.H. Gericke, J. Chem. Phys. 133 (2010) 024301.
[46] C. Romanescu, S. Manzhos, D. Boldovsky, J. Clarke, H. Loock, J. Chem. Phys. 120 (2004) 767–777.
[47] H.P.L.C. Romanescu, J. Chem. Phys. 127 (2007) 124304.
[48] C. Romanescu, H.P. Loock, Phys. Chem. Chem. Phys. 8 (2006) 2940–2949.
[49] Á. Kvaran, K. Matthíasson, H. Wang, Phys. Chem. Ind. J. 1 (2006) 11–25.
[50] Á. Kvaran, Ó.F. Sigurbjörnsson, H. Wang, J. Mol. Struct. 790 (2006) 27–30.
[51] NIST (National Institute of Standards and Technology), http://webbook.nist.gov/chemistry/form-ser.html.en-us.en>.
[52] H.R. Hróðmarsson, Á. Kvaran, H. Wang, unpublished, (2013).

Article 3

Photofragmentations, state interactions, and energetics of Rydberg and ion-pair states: Resonance enhanced multiphoton ionization of HI.

Helgi Rafn Hróðmarsson, Huasheng Wang, and Ágúst Kvaran

Journal of Chemical Physics. **140**. 244304 (2014).

DOI: 10.1063/1.4883900

Helgi Rafn Hróðmarsson developed the research concept along with Ágúst Kvaran, and performed all the experiments along with Huasheng Wang. Helgi performed all of the data analysis and independently wrote the first manuscript. He contributed to editing until publication.

Photofragmentation, state interaction, and energetics of Rydberg and ion-pair states: Resonance enhanced multiphoton ionization of HI

Helgi Rafn Hróðmarsson, Huasheng Wang, and Ágúst Kvaran[a)]
Science Institute, University of Iceland, Dunhagi 3, 107 Reykjavík, Iceland

(Received 9 April 2014; accepted 5 June 2014; published online 24 June 2014)

Mass resolved resonance enhanced multiphoton ionization data for hydrogen iodide (HI), for two-photon resonance excitation to Rydberg and ion-pair states in the 69 600–72 400 cm^{-1} region were recorded and analyzed. Spectral perturbations due to homogeneous and heterogeneous interactions between Rydberg and ion-pair states, showing as deformations in line-positions, line-intensities, and line-widths, were focused on. Parameters relevant to photodissociation processes, state interaction strengths and spectroscopic parameters for deperturbed states were derived. Overall interaction and dynamical schemes to describe the observations are proposed. © *2014 AIP Publishing LLC*. [http://dx.doi.org/10.1063/1.4883900]

I. INTRODUCTION

Spectroscopic and photofragmentation studies of the hydrogen halides have proven to be very valuable to various contemporary fields of photochemistry such as atmospheric chemistry,[1,2] astrochemistry,[3,4] and photochemical synthesis.[5] The UV, VUV, and multiphoton excitation spectroscopy of these compounds is very rich in structure showing clearly resolved rotational bands due to excitation to Rydberg and ion-pair states.[6–11] Spectral perturbations showing as line shifts[7,8,10,12–20] and/or as line intensity fluctuations[7,8,10,12–19,21–23] are frequently observed as effects of state interactions and/or predissociation processes.[7–9,12,13,18,21] These are seen both in absorption[22,24–29] and REMPI spectra.[7,8,10,12–20,23,30–32] Pronounced ion-pair to Rydberg state mixing have been observed experimentally[7–10,12–14,16–20,22,24–26,30,31,33] and predicted theoretically.[21,34] Furthermore, perturbation effects have been shown to be valuable in spectral assignments.[19]

The spectroscopy of the hydrogen halides has proven to highlight clearly the effects of various perturbation terms neglected in the Born-Oppenheimer (BO) approximation, particularly in the cases of interaction between electronically excited Rydberg states ($\Omega = 0, 1, 2, \ldots$) and ion-pair vibrational states ($\Omega = 0$), where both homogeneous ($\Delta\Omega = 0$) and heterogeneous ($\Delta\Omega > 0$) couplings are observed. In the rotational part of the Hamiltonian, $\mathbf{H^{rot}}$, there are three terms that are neglected in the BO approximation, which are responsible for perturbations between different electronic states. These terms are the following:

(i) $(1/2\mu R^2)(\mathbf{L}^+\mathbf{S}^- + \mathbf{L}^-\mathbf{S}^+)$, which causes spin-electronic homogeneous ($\Delta\Omega = 0$) perturbations.
(ii) $-(1/2\mu R^2)(\mathbf{J}^+\mathbf{S}^- + \mathbf{J}^-\mathbf{S}^+)$, which is the S-uncoupling operator.
(iii) $-(1/2\mu R^2)(\mathbf{J}^+\mathbf{L}^- + \mathbf{J}^-\mathbf{L}^+)$, which is the L-uncoupling operator.

The last two terms are responsible for the heterogeneous ($\Delta\Omega > 0$) perturbations.

Interpretations of observed perturbation effects have in turn allowed distinctions between various photodissociation and photoionization pathways.[18,20]

A number of papers have been published, which place emphasis on state interactions, energy transfers, and photodissociation processes, in HCl[16,18,30,31,35–40] and HBr.[18–20] Whereas most of the studies of hydrogen iodide (HI) have focused on the spectral assignments and the energetics of the Rydberg and ion-pair states, little emphasis has been placed on spectral perturbations for HI. Apart from statements concerning perturbation observations,[17,25,33] no detailed analyses of the spectral perturbations for HI have been reported. In this paper we will emphasize the perturbation effects, involving both homogenenous and heterogenenous state interactions, between the following Rydberg and ion-pair states:

(i) The $H^1\Sigma^+(v' = 1)$ and the $m^3\Pi_2(v' = 0)$ Rydberg states and the $V^1\Sigma^+(v' = m + 6)$ ion-pair state.
(ii) The $O^1\Sigma^+(v' = 0)$ and $k^3\Pi_1(v' = 1)$ Rydberg states and the $V^1\Sigma^+(v' = m + 7)$ ion-pair state.
(iii) The $I^1\Delta_2(v' = 0)$ Rydberg state and the $V^1\Sigma^+(v' = m + 9)$ ion-pair state.

Ginter *et al.*[25] have reported perturbation observations in the absorption spectra due to transitions to the $V^1\Sigma^+(v' = m + 6, m + 9)$ and $k^3\Pi_1(v' = 1)$ states and Pratt and Ginter[33] mention intensity anomalies in a REMPI spectrum for a resonance excitation to the $I^1\Delta_2(v' = 0)$ state. (Vibrational levels of the V state are labeled as $v' = m + i$, $i = 0, 1, 2, \ldots$ where m is an unknown integer.) Here line-shifts (LS) as well as line-intensity (LI) and line-width (LW) alterations, hereafter referred to as LS-, LI-, and LW-effects, respectively, are considered. Quantitative and qualitative information, relevant to photodissociation processes, state interaction and spectroscopic parameters for HI are derived.

a)Author to whom correspondence should be addressed. Electronic mail: agust@hi.is. Telephone: +354-525-4672, +354-525-4800. Fax: +354-552-8911.

II. EXPERIMENTAL

Mass resolved REMPI data were recorded for a HI molecular beam, created by jet expansion of a pure gas sample through a pulsed nozzle. Ions were directed into a time-of-flight tube and detected by a microchannel plate (MCP) detector, to record the ion yield as a function of mass and laser radiation wavenumber.

The apparatus used is similar to that described in Refs. 16, 18, 30, 32, and 41–43. Therefore, only a brief description is given here. The radiation was focused onto the HI molecular beam (HI gas sample obtained from Matheson Gas Products, Inc.) by a lens with a 20 cm focal length inside an ionization chamber between a repeller and extractor plates. The number of photons per pulse inside the chamber is estimated to be about 10^{14} and the photon density about 10^{16} cm^{-2}. The gas sample was pumped through a 500 μm pulsed nozzle from a typical backing pressure of about 2.0–2.5 bar. The pressure inside the ionization chamber was around 10^{-6} mbar during experiments. The nozzle was kept open for about 200 μs and the laser beam was typically fired 500 μs after the nozzle was opened. Ions were extracted into a time-of-flight tube and focused on a MCP detector, from which the signals were fed into a LeCroy WaveSurfer 44MXs-A, 400 MHz storage oscilloscope and stored as a function of ion times-of-flight and laser radiation wavenumber. Average signals were evaluated and recorded for a fixed number of laser pulses. The data were corrected for laser power and mass calibrated to obtain ion yield as a function of mass and excitation wavenumber. REMPI spectra for certain ions as a function of excitation wavenumber were obtained by integrating mass signal intensities for the particular ion. Care was taken to prevent saturation effects as well as power broadening by minimizing laser power. Laser calibration was based on observed (2 + 1) iodine atom REMPI peaks.[44] The absolute accuracy of the calibration was typically found to be about ± 2.0 cm^{-1} on the two-photon wavenumber scale.

III. RESULTS AND ANALYSIS

Mass resolved (2 + n) REMPI spectra of HI were recorded for the two-photon resonance excitation region 69 600–72 400 cm^{-1}. Figs. 1(a)–1(c) show spectra for the

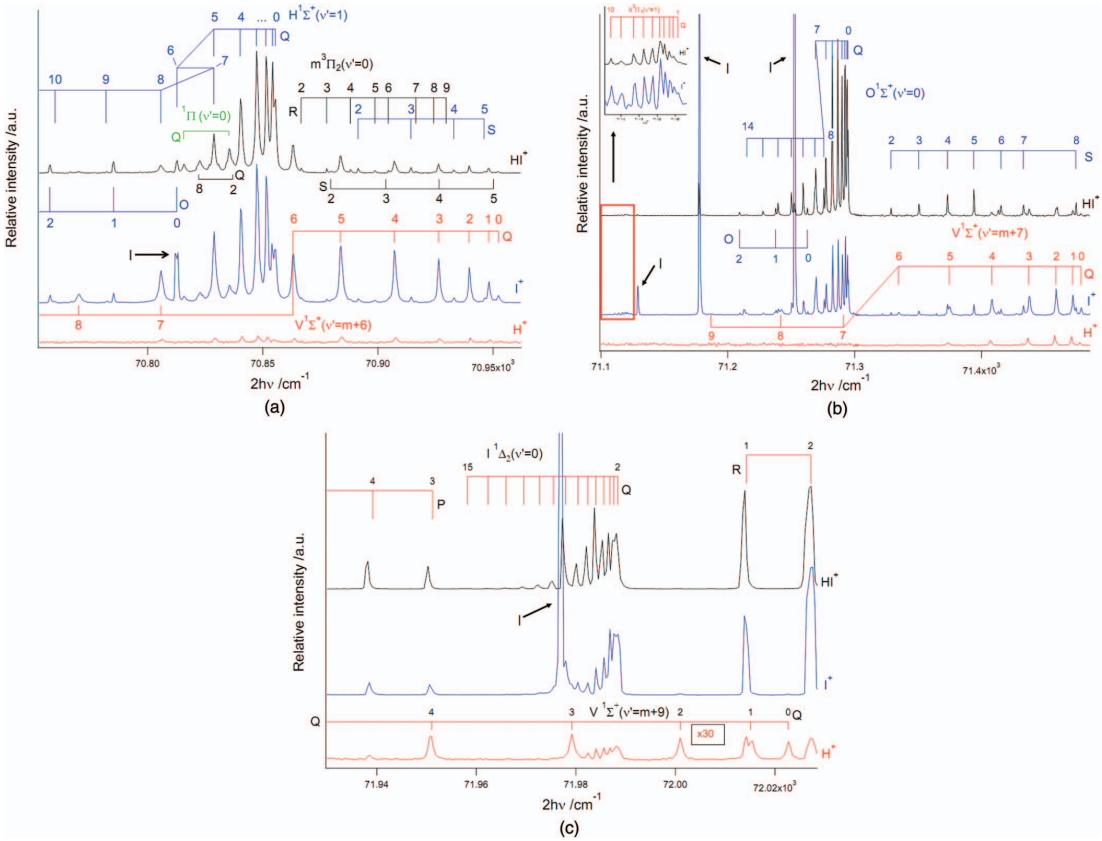

FIG. 1. REMPI spectra for H^+, I^+, and HI^+ and J' assignments of rotational peaks corresponding to two-photon resonance excitation from the ground state to $H^1\Sigma^+(v'=1)$ (a), $V^1\Sigma^+(v'=m+6)$ (a), $m^3\Pi_2(v'=0)$ (a), $O^1\Sigma^+(v'=0)$ (b), $V^1\Sigma^+(v'=m+7)$ (b), $I^1\Delta_2(v'=0)$ (c), $V^1\Sigma^+(v'=m+9)$ (c). (2 + 1) REMPI iodine atomic lines are also marked.[44] The H^+ spectrum in (c) is intensified (×30).

excitation regions 70 710–70 960 cm^{-1}, 71 100–71 490 cm^{-1}, and 71 930–72 030 cm^{-1}, respectively. Peaks due to the two-photon resonance transitions from the ground state $X^1\Sigma^+$ to $H^1\Sigma^+(v'=1)$, $m^3\Pi_2(v'=0)$, $V^1\Sigma^+(v'=m+6)$ (a), $k^3\Pi_1(v'=1)$, $O^1\Sigma^+(v'=0)$, $V^1\Sigma^+(v'=m+7)$ (b), $I^1\Delta_2(v'=0)$, and $V^1\Sigma^+(v'=m+9)$ (c) (hereafter named $H(1)$, $m(0)$, $V(m+6)$, $k(1)$, $O(0)$, $V(m+7)$, $I(0)$, and $V(m+9)$, respectively) are assigned.[17,25] It should be noted that the original assignment of the $H(1)$ state by Ginter *et al.*[25,33] to the $E^1\Sigma^+(v'=0)$ state was reassigned recently.[17] All the major types of spectral perturbations (line-shift (LS), line-intensity (LI), and line-width (LW)-effects) are observed in the spectra. In particular, severe LS-effects are seen in the Q line series for the $H(1)$ and $O(0)$ spectra, where irregular orders of J' quantum numbers are observed (see 1(a) and 1(b)). Analogous effects have been observed for HCl.[15,16] Less severe but clear LS-effects are seen in the Q line series for the $V(m+6)$ spectrum (Fig. 1(a)) and in the S line series for the $O(0)$ spectrum (Fig. 1(b)). Other spectral perturbations, which will be dealt with in more detail below, are less obvious, but significant.

LS-effects refer to deviation of line positions from regular patterns due to rotational energy level shifts because of excited state interactions. This typically shows as nonlinearity in plots of the energy level spacing ($\Delta E_{J',J'-1} = E(J') - E(J'-1)$) vs. J'.[16,18–20] Regular patterns of rotational line positions are determined by transitions to regularly arranged rotational energy levels according to standard energy expressions for unperturbed states, depending on rotational (B_v) and centrifugal distortion (D_v) constants as well as on J' quantum numbers. As an attempt to evaluate the spectroscopic constants, hence the unperturbed energy levels, as well as state interaction strengths (W), from the observed data, simplified deperturbation calculations were performed. Either interactions between one Rydberg vibrational state (1) and one ion-pair vibrational state ($V(v')$; (2)) closest in energy or between two Rydberg states (1a and 1b) and one ion-pair state (2) were considered. The diagonal matrix elements were expressed by the standard energy expressions for the unperturbed energy levels depending on the spectroscopic parameters (see Table I).[45,46] The off-diagonal matrix elements are the interaction strengths (the W's; Table I). The perturbed energy levels were derived from the observed spectral lines and known energy levels for the ground state. The spectroscopic parameters for the states involved as well as the W's were searched for in the deperturbation procedure. In the cases of homogeneous ($\Delta\Omega = 0$) interactions, the W's were assumed to be independent of J', whereas for heterogeneous ($\Delta\Omega \neq 0$) interactions, $W = W'\,(J'\,(J'+1))^{1/2}$, where W' is a constant.

LI-effects appear as abnormal enhancements or drops in ion signal intensities as a function of the J' quantum number. Frequently, "mirror effects" have been observed in the intensity alterations for HCl and HBr,[18,20] in such a way that the ion signal intensity via resonance excitation to one interacting state decreases whereas the ion signal intensity via excitation to the other interacting state increases. This is associated with different ionization processes for the two interacting states. Therefore, ionization of Rydberg states is dominantly found to produce parent molecular ions, whereas ionization of ion-pair states mainly forms fragment ions.[20,30,31] Therefore, ion signal intensity ratios, such as $I(X^+)/I(HX^+)$ vs. J' (X = Cl, Br), have proven to be very useful measures of the J' dependent Rydberg to ion-pair state interactions.[16,18,20,30,31] Furthermore, constant ratio values, independent of J', for the Rydberg states are found to be indicative of dissociation channels.[16–20,25,30,31,33,35–40] An approximation expression for the ion signal intensity ratio in the case of level-to-level interactions for two states (1 and 2) has been derived.[16,18,20,30] The expression depends on the fractional state mixing (c_1^2/c_2^2), state interaction strength (W_{12}), and J' dependent energy level differences ($\Delta E_{J'}$) for the two states as

$$\frac{I(X^+)}{I(HX^+)} = \alpha\frac{\left[\gamma + c_2^2(1-\gamma)\right]}{\left(1-c_2^2\right)}, \tag{1a}$$

$$c_2^2 = \frac{1}{2} - \frac{\sqrt{(\Delta E_{J'})^2 - 4(W_{12})^2}}{2|\Delta E_{J'}|}; \quad c_1^2 = 1 - c_2^2, \tag{1b}$$

and

$$I(X^+) = \alpha_2 c_2^2 + \beta_1 c_1^2; \qquad I(HX^+) = \alpha_1 c_1^2 + \beta_2 c_2^2;$$
$$\alpha = \alpha_2/\alpha_1; \qquad \gamma = \beta_1/\alpha_2; \qquad \alpha\gamma = \beta_1/\alpha_1,$$

where α_1, β_1, α_2, and β_2 are the ionization rate coefficients. γ and $\alpha\gamma$ are measures of X^+ ion formations via dissociation of the Rydberg state, relative to that of the formations of X^+ via excitation of the ion-pair state (γ) and relative to that of the formation of HX^+ via excitation of the Rydberg state ($\alpha\gamma$). Fits of this expression to ion signal intensity ratios vs. J' have allowed evaluation of fractional state mixing as well as the parameters γ and α.[16,18,20,30]

The LS- and LI-effects are found to measure the same effects, namely, bound-to-bound state interactions. The LI-effects, however, are much more sensitive to weak interactions compared to the LS-effects. Thus, weak interaction of

TABLE I. Hamiltonian matrix elements used to derive interaction strengths (W) and spectroscopic parameters (v^0, B', and D') by diagonalization for two-state interaction (a) and a three-state interaction (b). In (a), **1** is a Rydberg vibrational state and **2** is an ion-pair vibrational state ($V^1\Sigma^+(v')$) (see text). v_1^0 and v_1^0 are the relevant term values (band origins). B'_1 and B'_2 are the rotational constants and D'_1 and D'_2 are the centrifugal distortion constants. W_{12} are the interaction parameters. In (b), **1a** and **1b** are Rydberg vibrational states and **2** is an ion-pair vibrational state ($V^1\Sigma^+(v')$) (see text). v_{1a}^0, v_{1b}^0, and v_2^0 are the relevant term values (band origins). B'_{1a}, B'_{1b}, and B'_2 are the rotational constants and D'_{1a}, D'_{1b}, and D'_2 are the centrifugal distortion constants. $W_{1a,2}$ and $W_{1b,2}$ are the interaction parameters.

(a)

	1	**2**
1	E_1^0	W_{12}
2	W_{12}	E_2^0

(b)

	1a	**1b**	**2**
1a	E_{1a}^0	0	$W_{1a,2}$
1b	0	E_{1b}^0	$W_{1b,2}$
2	$W_{1a,2}$	$W_{1b,2}$	E_2^0

$$E_1^0 = v_1^0 + B'_1J'(J'+1) - D'_1J'^2(J'+1)^2$$
$$E_2^0 = v_2^0 + B'_2J'(J'+1) - D'_2J'^2(J'+1)^2$$
$$E_{1a}^0 = v_{1a}^0 + B'_{1a}J'(J'+1) - D'_{1a}J'^2(J'+1)^2$$
$$E_{1b}^0 = v_{1b}^0 + B'_{1b}J'(J'+1) - D'_{1b}J'^2(J'+1)^2$$
$$E_2^0 = v_2^0 + B'_2J'(J'+1) - D'_2J'^2(J'+1)^2$$

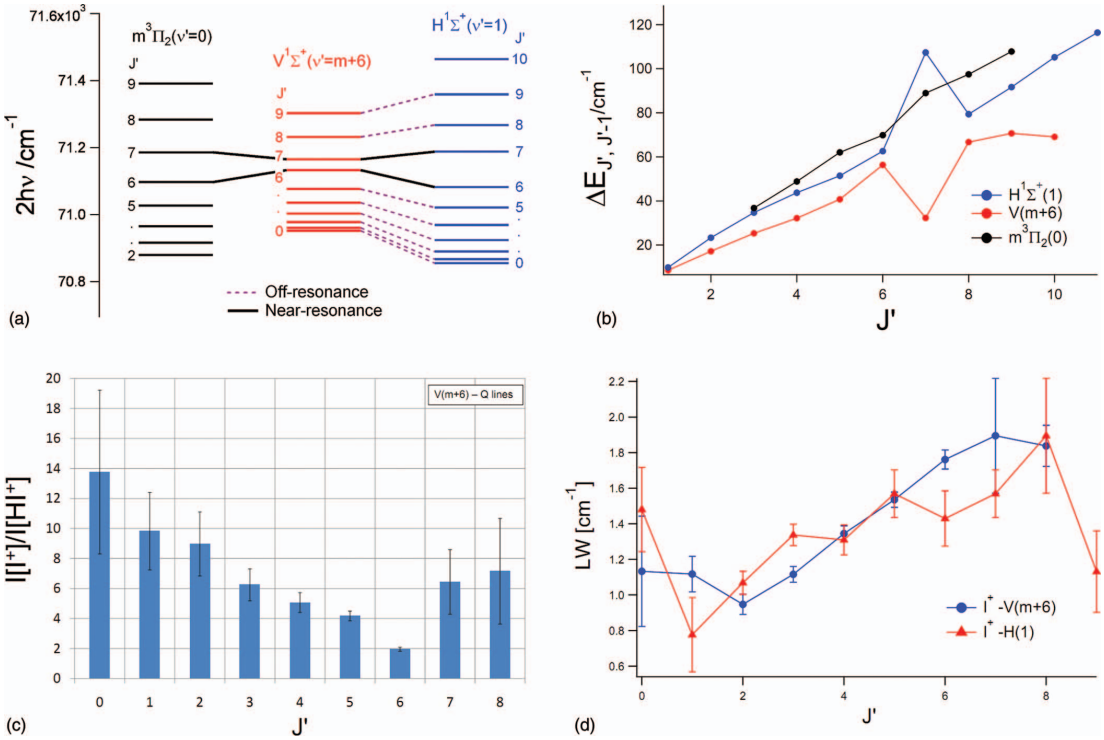

FIG. 2. Figures derived from analysis of REMPI spectra for the $H^1\Sigma^+(v'=1)$, $V^1\Sigma^+(v'=m+6)$, and $m^3\Pi_2(v'=0)$ states (Fig. 1(a)): (a) Rotational energy levels; near- and off-resonance interactions are indicated. (b) Spacing between rotational levels ($\Delta E_{J',J'-1}$) as a function of J'; experimental values. (c) Relative ion-signal intensities ($I(I^+)/I(HI^+)$) vs. J' derived from the Q rotational lines for the $V(m+6)$ state. (d) Rotational line-widths vs. J' derived from the Q lines of the I^+ signals for the $H(1)$ and $V(m+6)$ states.

triplet states and ion-pair states in HCl were found to show clear LI-effects but no significant LS-effects.[30]

The LW-effects appear as J' dependent bandwidths of the ion signals independent of whether it is a parent or a fragment ion. The effects are primarily due to J' dependent lifetimes associated with predissociation processes of Rydberg states.[18,20] These can involve one or more predissociating gateway states in which case the LW-effects also will depend on bound-to-bound state interactions. Thus ion-pair states, which do not predissociate easily, directly,[18–20] can show dramatic LW-effects due to interactions with one or more predissociating Rydberg states in which case the lifetime, hence the line-width, will depend on the Rydberg to ion-pair (bound-to-bound) state interactions as well as predissociation processes of the Rydberg states.[20] Therefore, the rate of dissociation ($1/\tau_2$) of an ion-pair vibrational state (2) has been expressed as a sum of terms, each of which is assumed to be a product of a predissociation rate ($1/t_{1i}$) for a particular Rydberg state (1i) and a J' dependent coupling rate ($f_{1i}(J')$) for the Rydberg to ion-pair state interaction,[20] i.e.,

$$\frac{1}{\tau_2} = \sum_i f_{1i}(J')\frac{1}{\tau_{1i}}. \quad (2)$$

Lower limit lifetimes ($\tau_{\min}$) can be derived from the line-widths (Γ) by[20]

$$\tau_{\min}(\text{ps}) = 5.3/\,\Gamma(\text{cm}^{-1}). \quad (3)$$

A. Off- and near-resonance interactions between the $H^1\Sigma^+(v'=1)$ and $m^3\Pi_2(v'=0)$ Rydberg states and the $V^1\Sigma^+(v'=m+6)$ ion-pair state

The clear LS-effects seen in the spectra of the $H(1)$ Rydberg state and the $V(m+6)$ ion-pair state, mentioned before, where the Q lines for $H(1)$, $J'=6$ and 7 are found to be "clenched" between the corresponding lines for the $V(m+6)$ state (Fig. 1(a)) is indicative of near-resonance interactions. Fig. 2(a) shows the energy levels derived from the rotational lines. Since the $H(1)$ and $V(m+6)$ states share the same symmetry ($^1\Sigma^+$), off-resonance perturbations are also to be expected. Since the band origin (ν^0) of the $V(m+6)$ ion-pair state is higher than that for the $H(1)$ state and that the rotational constant for the ion-pair state is smaller, the energy levels of the Rydberg state ($H(1)$) "catch up" with those of the ion-pair state to exhibit the near-resonance interactions for $J'=6$ and 7 (see Fig. 2(a)). The overall interaction

TABLE II. Parameter values, relevant to state mixing, derived from peak intensity-shifts and intensity-ratios ($I(I^+)/I(HI^+)$) as a function of J' (see text), as well as spectroscopic parameters (see Table I) for the state systems $H(1)$, $V(m+6)$, and $m(0)$ (a), $O(0)$ and $V(m+7)$ (b), and $I(0)$ and $V(m+9)$ (c).

(a)

	$H^1\Sigma^+(v'=1)$ Rydberg state/**1a**	$V^1\Sigma^+(v'=m+6)$ ion-pair state/**2**	$m^3\Pi_2(v'=0)$ Rydberg state/**1b**
J'_{res}[a]	6/7	6 /7	6/7
$\lvert\Delta E_{J'}\rvert(cm^{-1})$ for J'_{res}	50.4/23.0	...	35.6/21.0
$W_{1a,2}/W_{1b,2}(cm^{-1})$	12.3	...	3.3
$c_1^2\ (c_2^2)$ for J'_{res}	0.93 (0.07)/0.67 (0.33)	...	0.98 (0.02)/0.95 (0.05)
$v^0(cm^{-1})$	70855.5[b]	70952.3[b]	70841.5[b]
	70854.0[c]	70954.0[c]	70840.0[c]
	70850.5[d]	70948.6[d]	70837.6[d]
$B_v(cm^{-1})$	5.77[b]	4.16[b]	6.32[b]
	5.94[c]	3.56[c]	6.21[c]
	6.00[d]	4.09[d]	6.11[d]
$D_v(cm^{-1})$	0.0022[b]	0.0031[b]	0.0025[b]
	−0.0011[c]	0.0024[c]	0.0012[c]
	0.0128[d]	0.0044[d]	0.00019[d]

(b)

	$O^1\Sigma^+(v'=0)$ Rydberg state/1	$V^1\Sigma^+(v'=m+7)$ ion-pair state/2
J'_{res}[a]	7/8	
$\lvert\Delta E_{J'}\rvert(cm^{-1})$ for J'_{res}	32.8/32.8	
$W_{12}(cm^{-1})$	11.0	
$c_1^2\ (c_2^2)$ for J'_{res}	0.86 (0.14)/0.86 (0.14)	
γ	0.93	
α	0.52	
$v^0(cm^{-1})$	71294.7[b]	71478.4[b]
	71290.0[c]	71478.0[c]
	71301.9[e]	
$B_v(cm^{-1})$	6.25[b]	2.95[b]
	6.31[c]	2.96[c]
	5.82[e]	
$D_v(cm^{-1})$	0.0023[b]	−0.0023[b]
	−0.0017[c]	0.0022[c]

(c)

	$I^1\Delta_2(v'=0)$ Rydberg state/1	$V^1\Sigma^+(v'=m+9)$ ion-pair state/2
J'_{res}[a]	2/3	
$\lvert\Delta E_{J'}\rvert(cm^{-1})$ for J'_{res}	12.5/8.5	
$W_{12}(cm^{-1})$	1,1[f]	
	1,3[f]	
$c_1^2\ (c_2^2)$ for J'_{res}	0.99.(0.01)/0.98 (0.02)	
	0.99 (0.01)/0.97 (0.03)	
γ	0.0040	
α	69	
$v^0(cm^{-1})$	71989.4[b]	72023.2[b]
	71990.0[c]	72023.0[c]
	71989.1[e]	72022.4[d]
$B_v(cm^{-1})$	6.31[b]	2.84[b]
	6.306[c]	2.85[c]
	6.312[e]	2.792[c]
$D_v(cm^{-1})$	0.00024[b]	0.0001[b]
	−0.00024[c]	−0.0002[c]
	0.00027[e]	−0.00046[d]

[a] $J'_{res} = J'$ levels closest to resonance interactions (see Figs. 2–4).
[b] Deperturbed values; this work.
[c] Undeperturbed (perturbed) values; this work.
[d] From Ref. 25.
[e] From Ref. 33.
[f] Since the interaction strength, W_{12}, is J' dependent (see text), we present the values obtained from both rotational levels that experience the near-resonance interaction.

effect shows very clearly by the graphs of $\Delta E_{J',J'-1}$ vs. J' for the states involved (see Fig. 2(b)). These show "near-mirror image" effects, such that an increase in $\Delta E_{J',J'-1}$, for one of the states, results in a decrease in the corresponding $\Delta E_{J',J'-1}$ value for the other state and vice versa. This can be explained in the following way with a reference to Fig. 2(a). For the low J's the rotational energies of the $V(m+6)$ ion-pair state are "pushed" upwards and the rotational energies of the $H(1)$ Rydberg state are "pushed" downwards. For $J' = 7$, however, where the energy of the $H(1)$ state exceeds that of the $V(m+6)$ ion-pair state, the Rydberg state experiences a significant increase in energy and the ion-pair state a corresponding lowering in energy resulting in increases and decreases in the corresponding $\Delta E_{7,6}$ values, respectively. For $J' \geq 8$, off-resonance interactions cause the $H(1)$ levels to be "pushed" upwards and the $V(m+6)$ levels to be "pushed" downwards. Energy levels for the $m(0)$ state, derived from the R spectral lines, are shown in Fig. 2(a) and a corresponding $\Delta E_{J',J'-1}$ vs. J' plot is shown in Fig. 2(b). These also show weak but clear effects of near-resonance interactions between the $m(0)$ and the $V(m+6)$ states for $J' = 6$ and 7. Since the total electronic angular moment quantum numbers (Ω) of these states differ by two ($\Delta\Omega = 2$) the interaction must involve a mixing with an $\Omega = 1$ state.[12,23,31] Deperturbation analysis for three states interactions, based on the assignments shown in Fig. 1(a), hence the energy level structure presented in 2(a) and 2(b), gave the rotational constants, B_v, and D_v shown in Table II.

The presence of LI-effects further evidences these state interactions. The largest ion intensity ratios, $(I(I^+)/I(HI^+))$, are observed for the Q lines of the $V(m+6)$ state, showing characteristic lowering in the values as the J's increase from 0 to 6 and an increase for $J' = 7$–8 (Fig. 2(c)). The corresponding ratios for the R lines of the $m(0)$ state are much smaller and constant for $J' = 2$–5 whereas the value for $J' = 7$ is significantly larger.[44] The intensity ratios derived from the Q lines of the $H(1)$ state for $J' = 0$–4 are found to be close to constant. Due to severe peak overlaps in the region of the Q lines for the $H(1)$ state, it is difficult to determine the ion intensity ratios $(I(I^+)/I(HI^+))$ for those J' levels which exhibit near-resonance interactions, quantitatively. Nevertheless, there is a qualitative indication of enhanced ratio values with J' for the $J' = 5$–8 peaks. All in all, these observations are indicative of near-resonance interactions for the $J' = 6$–7 levels and gradually decreasing mixing of the $V(m+6)$ state with Rydberg states as the J' numbers deviate from $J' = 6$ and 7. Furthermore, the constant intensity ratio values, independent of J', for $H(1)$ and $m(0)$ suggests that predissociation of both Rydberg states is important (see above).

Line-widths derived from the Q lines for the $H(1)$ and $V(m+6)$ spectra are shown in Fig. 2(d). Line-widths for the $m(0)$ state (R and S series), were found to be constant,

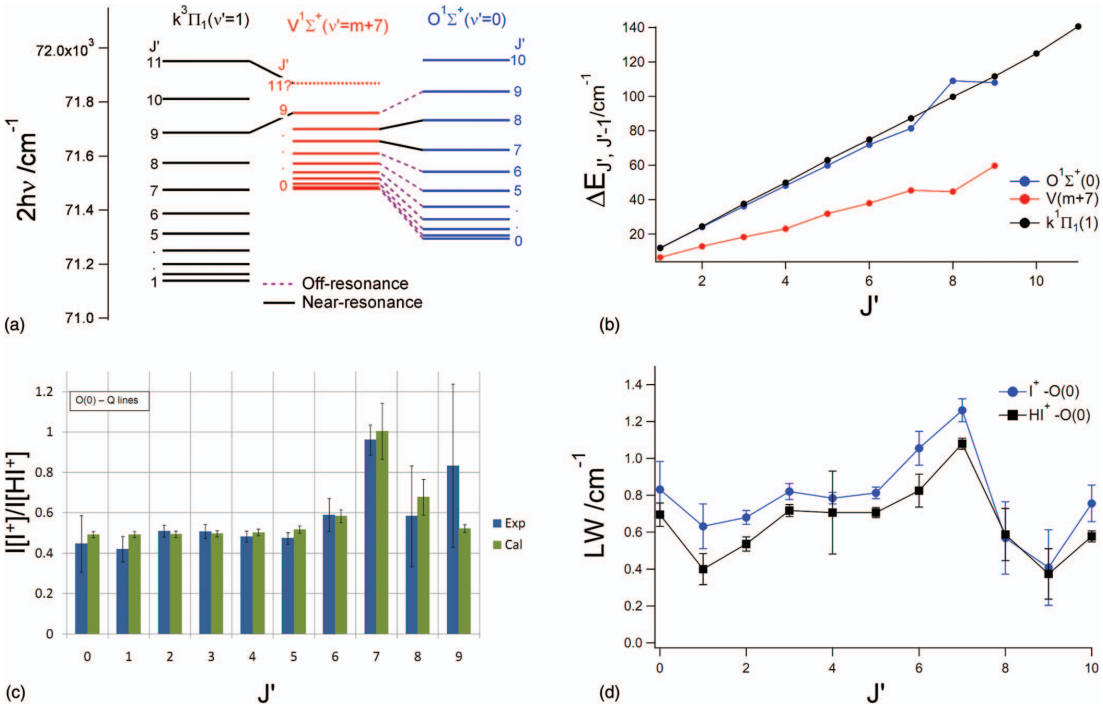

FIG. 3. Figures derived from the analysis of the REMPI spectra for the $k^3\Pi_1(v'=1)$, $O^1\Sigma^+(v'=0)$, and $V^1\Sigma^+(v'=m+7)$ states (Fig. 1(b)). (a) Rotational energy levels. Near- and off-resonance interactions are indicated. (b) Spacing between rotational levels ($\Delta E_{J',J'-1}$) as a function of J'; experimental values. (c) Relative ion-signal intensities $(I(I^+)/I(HI^+))$ vs. J' derived from the Q rotational lines for the $O(0)$ state. (d) Rotational line-widths vs. J' derived from the Q lines of the I^+ and HI^+ signals for the $O(0)$ state.

independent of J', within experimental error, with an average value of about 0.5 cm^{-1}.[44] The line-widths, hence the lifetimes, of the $H(1)$ and $V(m+6)$ states are comparable in terms of the absolute values (0.6–1.9 cm^{-1}) and its J' dependence. By analogy with previous observations for HBr[18] this suggests that the lifetime of the $H(1)$ state is primarily determined by that of the $V(m+6)$ state following its state interaction. Whereas the large average internuclear distance of the V state makes crossing to repulsive states, hence predissociation, highly improbable,[18,20] Rydberg states, on the other hand, are either in close vicinity of, or crossed by, repulsive states to make predissociation processes more probable. Therefore, predissociation of the $V(m+6)$ state is believed to occur via gateway Rydberg states. The predissociating $m(0)$ state is likely to be an important gateway state for the overall $H(1)$ and $V(m+6)$ states predissociation.

B. Off- and near-resonance interactions between the $O^1\Sigma^+(v'=0)$ and $k^3\Pi_1(v'=1)$ Rydberg states and the $V^1\Sigma^+(v'=m+7)$ ion-pair state

In a previous work by Pratt and Ginter,[33] a new Rydberg state was observed at about 71 300 cm^{-1} with the $^1\Sigma^+$ symmetry showing evidence of perturbation effects. This state has been deduced to have a $(\sigma^2\pi^3)4f\pi$ Rydberg orbital and was given the notation $O^1\Sigma^+(v'=0)$. It should be noted that the Rydberg parentage of all of the states mentioned in this paper has been addressed before.[17] It was noted that this Rydberg state was experiencing some perturbation effects due to interactions with the $V(m+7)$ ion-pair state.[17] Here, we will clarify, qualitatively and quantitatively, the nature of this interaction. Furthermore, we will consider evidences for a possible interaction involvement of the $k^3\Pi_1(v'=1)$ state, which is close in energy.

The REMPI spectra of the $O(0)$ and the $k(1)$ Rydberg states as well as the $V(m+7)$ ion-pair state are displayed in Fig. 1(b). The severe LS-effects seen in the spectrum of the $O(0)$ Rydberg state for the Q lines, $J'=7$–8, which are found to be "clenched" between the corresponding Q lines of the $V(m+7)$ state are indicative of near-resonance interactions. Fig. 3(a) shows the energy levels derived from the rotational lines. It shows that a slight enhancement in the energy gap, $\Delta E_{8,7}$, of the $O(0)$ state matches a decrease in the corresponding analogous gap for the $V(m+7)$ state. Slight off-resonance interaction effects are also experienced between levels for different J' values. These effects are clearly seen by the plots of $\Delta E_{J',J'-1}$ vs. J' for the $O(0)$ and $V(m+7)$ states in Fig. 3(b), which exhibit "near-mirror image" effects. Closer inspection of the plots reveals larger enhancement of the $\Delta E_{9,8}$ value for the $V(m+7)$ state compared to that of its corresponding lowering for the $O(0)$ state. This could be due to a near-resonance interaction between the $J'=9$ levels

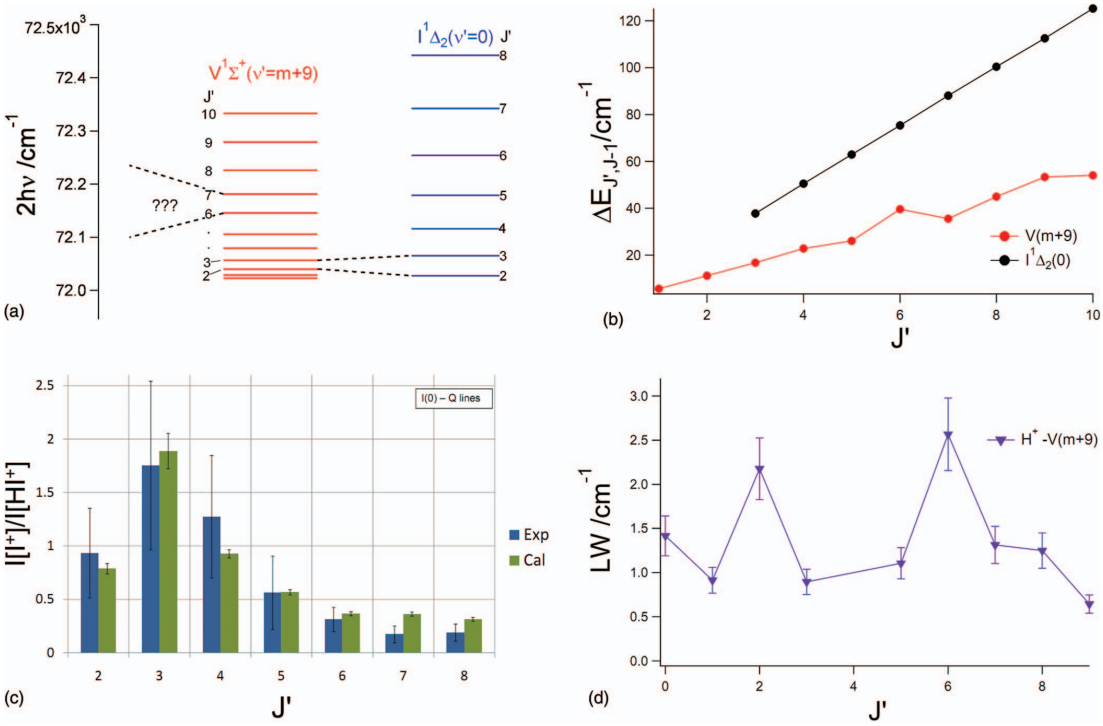

FIG. 4. Figures derived from the analysis of the REMPI spectra for the $I^1\Delta_2(v'=0)$ and $V^1\Sigma^+(v'=m+9)$ states. (a) Rotational energy levels. Near-resonance interactions are indicated. (b) Spacing between rotational levels ($\Delta E_{J',J'-1}$) as a function of J'; experimental values. (c) Relative ion signal intensities ($I(I^+)/I(HI^+)$) vs. J' derived from the Q rotational lines for the $I(0)$ and $V(m+9)$ states. (d) Rotational line-widths vs. J' derived from the Q lines of the H^+ signals for the $V(m+9)$ state.

of the $V(m+7)$ and the $k(1)$ states[17] resulting in still larger energy-gap, $\Delta E_{9,8}$, for the $V(m+7)$ state (see Fig. 3(a)) as well as a lowering in $\Delta E_{9,8}$ for the $k(1)$ state.[17] Furthermore, the drop in $\Delta E_{9,8}$ for the $k(1)$ state is found to be compensated by enhancements in $\Delta E_{10,9}$ and $\Delta E_{11,10}$ for $k(1)$.[17] Due to the lack of observed Q rotational lines for the $V(m+7)$ spectrum for $J' > 9$ the effect of a near-resonance interaction with the $k(1)$ state could not be taken into account in a deperturbation analysis. Deperturbation analysis for two-state interactions, $O(0)$ and $V(m+7)$, based on the assignment shown in Fig. 1(b), hence the energy level structure presented in Figs. 3(a) and 3(b), gave the rotational constants, B_v and D_v, shown in Table II.

The near-resonance interactions between the $O(0)$ and the $V(m+7)$ states are further evidenced by LI-effects. The ion intensity ratios, $I(I^+)/I(HI^+)$, as a function of J' (Fig. 3(c)) for the $O(0)$ state show slight but significant enhancements for $J' = 7$–8. The calculated values, acquired from fitting the data points, are presented in Table II. The relatively large nonzero value derived for γ indicates the importance of a predissociation for the $O(0)$ state, either direct or indirect via gateway Rydberg state(s).

Finally, we consider LW-effects. The line-widths of the Q lines of the $O(0)$ state, derived from the I^+ and HI^+ spectra, are presented in Fig. 3(d). The line-widths for the $k(1)$ state are found to be virtually unchanged with J', within experimental error and comparable in magnitudes to those for the $O(0)$ state.[44] The line-widths of the ion-pair state are found to be larger,[44] hence lifetimes shorter, than those for the Rydberg state. The line-widths of the $O(0)$ system show resemblance to that of the intensity ratios as a function of J' (Fig. 3(c)), both showing a maxima for $J' = 7$. These observations, along with the LI-effects suggest that the predissociation of the $O(0)$ state is partly determined by that of the $V(m+7)$ state[18] following the state interactions as described above. Predissociation of the $V(m+7)$ state will occur via gateway Rydberg states among which the $k(1)$ state is likely to be important.

C. Near-resonance interactions between the $I^1\Delta_2(v' = 0)$ Rydberg state and $V^1\Sigma^+(v' = m+9)$ ion-pair state

REMPI spectra of the $I(0)$ Rydberg state and the $V^1\Sigma^+(m+9)$ ion-pair state show the $J' = 2$ and 3 Q lines of the $I(0)$ state to be "clenched" between the corresponding

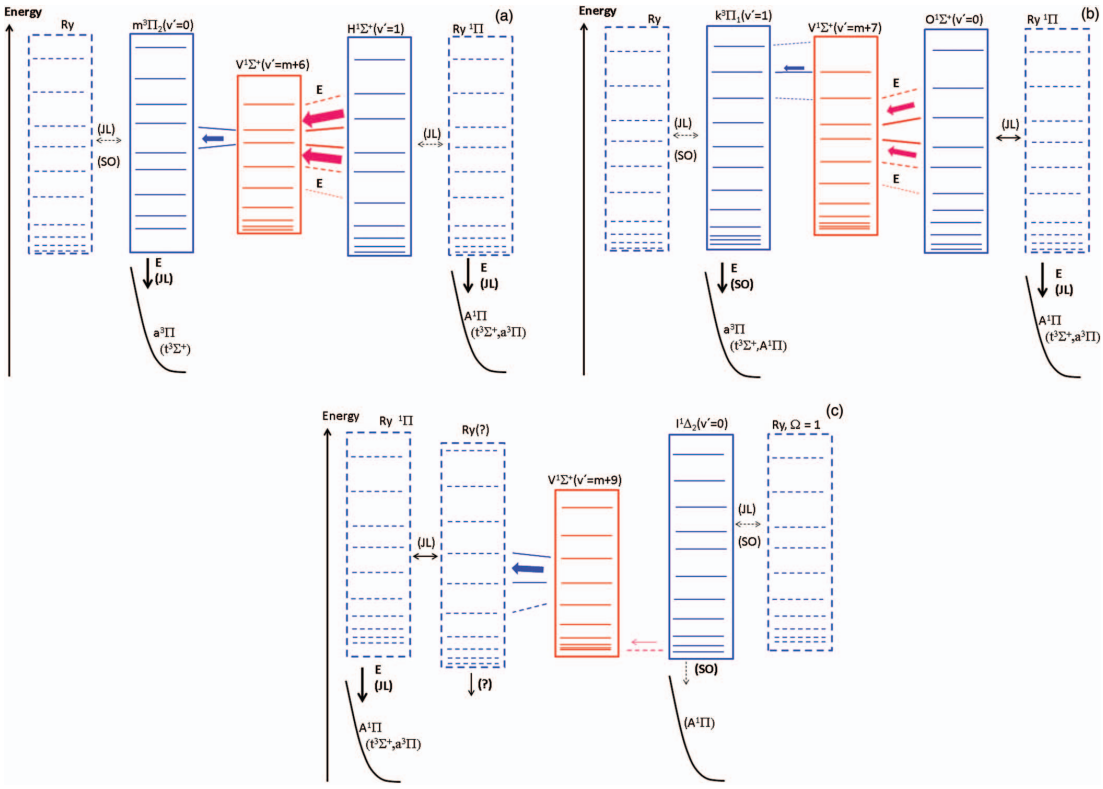

FIG. 5. Semi-schematic figures showing the HI energetics, state interactions, and energy transfers of relevance to the data presented in this paper (see text) for the $H^1\Sigma^+(v'=1)$, $V^1\Sigma^+(v'=m+6)$, and $m^3\Pi_2(v'=0)$ states (a), the $O^1\Sigma^+(v'=0)$, $V^1\Sigma^+(v'=m+7)$, and $k^3\Pi_1(v'=1)$ states (b) and the $I^1\Delta_2(v'=0)$ and $V^1\Sigma^+(v'=m+9)$ states (c). Electrostatic, rotational, and spin orbit couplings are marked *E*, *JL*, and *SO*, respectively. Red boxes represent the ion-pair states. Blue boxes are Rydberg states and black curves are repulsive states. The boxes with solid lines represent Rydberg states, which couple with the ion-pair states. The boxes with broken lines are gateway states with respect to predissociation. Relative importance of couplings and transfers is indicated by different boldness of arrows and broken lines as well as by the use of brackets or not. The colored arrows indicate the major paths towards predissociation.

Q lines of the $V(m+9)$ state.[17] Energy levels derived from the spectra are displayed in Fig. 4(a) and plots of $\Delta E_{J',J'-1}$ vs. J' are shown in Fig. 4(b). Although $\Delta\Omega = 2$ for these states near-resonance interactions might be expected to be found for those levels in the case of a mixing with an $\Omega = 1$ state, by analogy with the observation discussed in Sec. III A. No significant line-shifts due to near-resonance interaction for $J' = 2$–3 are observed, however, whereas an indication of near-resonance interactions with the $V(m+9)$ state, $J' = 5$–7, is clearly found. Since no Rydberg state with near-resonances for $J' = 5$–7 have been observed,[17,25,33] the corresponding LS-effects must belong to an interaction between the $V(m+9)$ state and a hidden state. The hidden state could be either a non-observable state due to selection rules for one- and two-photon transitions or a state experiencing weak transition probabilities for transitions from the ground state. Whereas no significant LS-effects are observed for $J' = 2$–3 due to $V(m+9)$ and $I(0)$ interactions (Fig. 4(a)), LI-effects show as clear ion intensity ratio ($I(H^+)/I(HI^+)$) alternation with J' for $I(0)$ (Fig. 4(c)) indicating weak state interactions. This demonstrates nicely the larger sensitivity of LI-effects compared to that of LS-effects to weak state interactions (see above). Analysis of the intensity ratios, reveal weak interaction strength (W_{12}) and small γ value (see Table II) compared to that derived for the $O(0)$ state (see Sec. III B). The small γ value suggests that predissociation of $I(0)$, either direct or indirect via gateway Rydberg state(s), is of minor importance. Furthermore, there are indications of a slight decrease in the linewidths with J' for $J' \geq 2$ in the case of the $I(0)$ state,[44] suggesting that the lifetime of the $I(0)$ state is primarily determined by these states coupling and by an indirect predissociation of the $V(m+9)$ state. Furthermore, there are also evidences for enhancements in the linewidths of the H^+ ion signals for the $V(m+9)$ state as a function of J' for $J' = 2$ as well as for $J' = 6$ (Fig. 4(d)) further indicating the importance of the state interactions in determining the lifetime of the ion-pair state.

IV. SUMMARY AND CONCLUSIONS

Mass resolved REMPI spectra for HI, showing resonance excitation to Rydberg states and ion-pair vibrational states in the two-photon resonance excitation region 69 600–72 400 cm^{-1}, were recorded and analyzed. Three systems of states, all of which have been shown to involve perturbations,[17,25,33] were addressed independently in terms of state interactions. This was done by interpreting observed line-shifts, line-intensity alterations, and line-width effects. In cases when the different observations depend on the same dynamical properties, the analysis results were found to be supportive in nature. Quantitative analysis revealed interaction strengths and spectroscopic parameters for deperturbed states derived from analysis of the line-shifts and parameters (γ and α) relevant to photodissociation processes derived from the line-intensity alterations. Small but significant changes are derived for the spectroscopic parameters, since observed line-shifts are near-resonance in nature, showing as localized shifts of lines and energy levels but limited alterations in overall trends. Nonzero γ values, derived, are measure of the significance of dissociation channels.[16–20,25,30,31,33,35–40] These analyses as well as interpretation of spectral linewidths, hence state lifetimes, allow proposition of state interactions and energy transfers involved in photofragmentation processes for the three energy systems, with reference to Fig. 5,[46,47] as follows:

(i) Fig. 5(a): The $H(1)$ Rydberg state couples mainly with the $V(m+6)$ state by a strong electrostatic (E) interaction to result in an effective energy transfer from the $H(1)$ state to the $V(m+6)$ state, followed by further transfer to a manifold of predissociating Rydberg states. Among those is the blended $m(0)$ state, which can predissociate via a strong electrostatic interaction with the repulsive $a^3\Pi$ valence state. Energy flow via direct coupling of the $H(1)$ state with Rydberg states is small.

(ii) Fig. 5(b): The $O(0)$ state couples moderately with the $V(m+7)$ state by an electrostatic interaction (E) as well as with a Rydberg state close in energy by a rotational coupling (JL). Energy transfer from the $O(0)$ state mainly occurs via the $V(m+7)$ state to a manifold of predissociating Rydberg states including the $k(1)$ state which predissociates via an electrostatic interaction with the repulsive $a^3\Pi$ state. The direct coupling of the $O(0)$ state with a Rydberg state is likely to involve the $a^1\Pi$ Rydberg state which can couple strongly to the repulsive $A^1\Pi$ state.

(iii) Fig. 5(c): The blended $I(0)$ Rydberg state couples weakly to the $V(m+9)$ ion-pair state whose lifetime is determined by further coupling to predissociating Rydberg states. A near-resonance interaction between the $V(m+9)$ state and a hidden Rydberg state is observed.

ACKNOWLEDGMENTS

The financial support of the University Research Fund, University of Iceland and the Icelandic Science Foundation (Grant No. 130259-051) is gratefully acknowledged. We would also like to thank Dr. Jingming Long for useful assistance with the perturbation analysis work.

[1] M. J. Simpson *et al.*, J. Chem. Phys. **130**(19), 194302 (2009).
[2] J. H. Seinfeld and S. N. Pandis, *Atmospheric Chemistry and Physics: From Air Pollution to Climate Change* (John Wiley & Sons, 2006).
[3] J. I. Lunine, *Astrobiology* (Pearson/Addison Wesley, 2005).
[4] A. M. Shaw, *Astrochemistry: From Astronomy to Astrobiology* (Wiley, 2006).
[5] N. Hoffmann, Chem. Rev. **108**(3), 1052 (2008).
[6] A. E. Douglas and F. R. Greening, Can. J. Phys. **57**(10), 1650 (1979).
[7] D. S. Green, G. A. Bickel, and S. C. Wallace, J. Mol. Spectrosc. **150**(2), 303 (1991).
[8] D. S. Green, G. A. Bickel, and S. C. Wallace, J. Mol. Spectrosc. **150**(2), 354 (1991).
[9] D. S. Green, G. A. Bickel, and S. C. Wallace, J. Mol. Spectrosc. **150**(2), 388 (1991).
[10] D. S. Green and S. C. Wallace, J. Chem. Phys. **96**(8), 5857 (1992).
[11] D. Ascenzi *et al.*, Phys. Chem. Chem. Phys. **3**(1), 29 (2001).
[12] Á. Kvaran, H. Wang, and Á. Logadóttir, J. Chem. Phys. **112**(24), 10811 (2000).
[13] Á. Kvaran, Á. Logadóttir, and H. Wang, J. Chem. Phys. **109**(14), 5856 (1998).
[14] Á. Kvaran, H. Wang, and Á. Logadóttir, *Recent Research Developments in Physical Chemistry* (Transworld Research Network, 1998), p. 233.
[15] Á. Kvaran and H. Wang, J. Mol. Spectrosc. **228**(1), 143 (2004).
[16] K. Matthiasson *et al.*, J. Chem. Phys. **134**(16), 164302 (2011).

[17]H. R. Hróðmarsson, H. Wang, and Á. Kvaran, J. Mol. Spectrosc. **290**, 5 (2013).
[18]J. Long, H. Wang, and Á. Kvaran, J. Chem. Phys. **138**(4), 044308 (2013).
[19]J. Long, H. Wang, and Á. Kvaran, J. Mol. Spectrosc. **282** (1), 20 (2012).
[20]J. Long *et al.*, J. Chem. Phys. **136**(21), 214315 (2012).
[21]R. Liyanage, R. J. Gordon, and R. W. Field, J. Chem. Phys. **109**(19), 8374 (1998).
[22]D. S. Ginter, M. L. Ginter, and S. G. Tilford, J. Mol. Spectrosc. **90**(1), 152 (1981).
[23]Y. Xie *et al.*, J. Chem. Phys. **95**(2), 854 (1991).
[24]D. S. Ginter *et al.*, J. Mol. Spectrosc. **92**(1), 55 (1982).
[25]D. S. Ginter, M. L. Ginter, and S. G. Tilford, J. Mol. Spectrosc. **92**(1), 40 (1982).
[26]D. S. Ginter and M. L. Ginter, J. Mol. Spectrosc. **90**(1), 177 (1981).
[27]M. L. Ginter, S. G. Tilford, and A. M. Bass, J. Mol. Spectrosc. **57**(2), 271 (1975).
[28]S. G. Tilford and M. L. Ginter, J. Mol. Spectrosc. **40**(3), 568 (1971).
[29]J. B. Nee, M. Suto, and L. C. Lee, J. Chem. Phys. **85**(2), 719 (1986).
[30]A. Kvaran, K. Matthiasson, and H. S. Wang, J. Chem. Phys. **131**(4), 044324 (2009).
[31]Á. Kvaran *et al.*, J. Chem. Phys. **129**(16), 164313 (2008).
[32]K. Matthíasson, H. Wang, and Á. Kvaran, J. Mol. Spectrosc. **255**(1), 1 (2009).
[33]S. T. Pratt and M. L. Ginter, J. Chem. Phys. **102**(5), 1882 (1995).
[34]M. Bettendorff *et al.*, Zeitschrift Fur Physik a-Hadrons and Nuclei **304**(2), 125 (1982).
[35]A. I. Chichinin, C. Maul, and K. H. Gericke, J. Chem. Phys. **124**(22), 224324 (2006).
[36]A. I. Chichinin, P. S. Shternin, N. Gödecke *et al.*, J. Chem. Phys. **125**(3), 034310 (2006).
[37]S. Kauczok *et al.*, J. Chem. Phys. **133**(2), 024301 (2010).
[38]C. Romanescu *et al.*, J. Chem. Phys. **120**(2), 767 (2004).
[39]C. Romanescu and H.-P. Loock, J. Chem. Phys. **127**(12), 124304 (2007).
[40]C. Romanescu and H.-P. Loock, Phys. Chem. Chem. Phys. **8**(25), 2940 (2006).
[41]Á. Kvaran, K. Matthíasson, and H. Wang, Phys. Chem.: An Ind. J. **1**(1), 11 (2006).
[42]Á. Kvaran, Ó. F. Sigurbjörnsson, and H. Wang, J. Mol. Struct. **790**(1–3), 27 (2006).
[43]A. Kvaran and H. Wang, Mol. Phys. **100**(22), 3513 (2002).
[44]See supplementary material at http://dx.doi.org/10.1063/1.4883900 for iodine atomic lines, intensity ratios, lifetimes, line-shifts, and line-widths.
[45]J. T. Hougen, *NBS Monograph 115* (National Institute of Standards and Technology, Gaithersburg, MD, 1970).
[46]H. Lefebvre-Brion, and R. W. Field, *Perturbations in the Spectra of Diatomic Molecules* (Academic Press, Inc., London, 1986).
[47]M. H. Alexander *et al.*, Chem. Phys. **231**(2–3), 331 (1998).

6.3.1 Supplementary Material

Photofragmentations, stateinteractions and energetics of Rydberg and ion-pair states: Resonance enhanced multiphoton ionization of HI

Helgi Rafn Hróðmarsson, Huasheng Wang, and ÁgústKvaran*

Supplemental Material

Content:

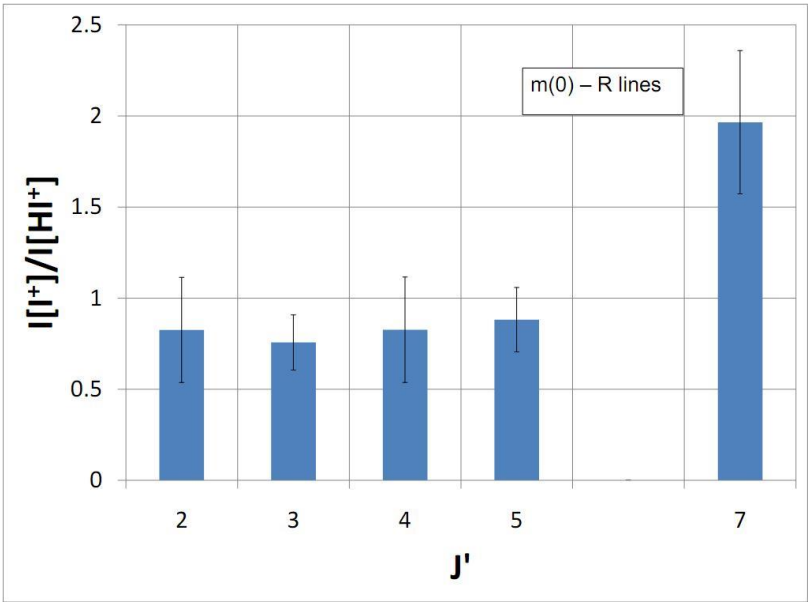

Fig.S2: Relative ion signal intensities, $I(I^+)/I(HI^+)$ vs. J', derived from the *R* rotational lines of the REMPI spectra due to two-photon resonance transition to the Rydberg state $m^3\Pi_2(v' = 0)$.

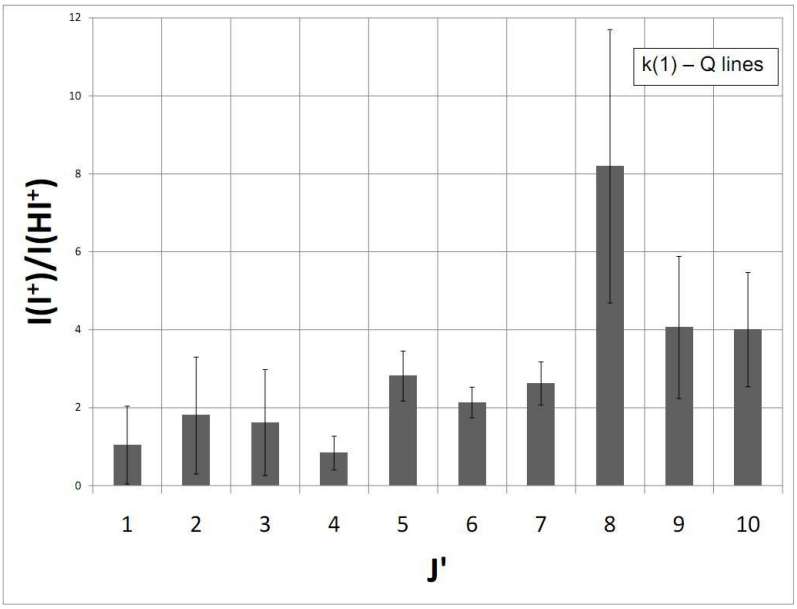

Fig.S3: Relative ion signal intensities, $I(I^+)/I(HI^+)$ vs. J', derived from the *Q* rotational lines of the REMPI spectra due to two-photon resonance transition to the Rydberg state $k^3\Pi_1(v' = 1)$.

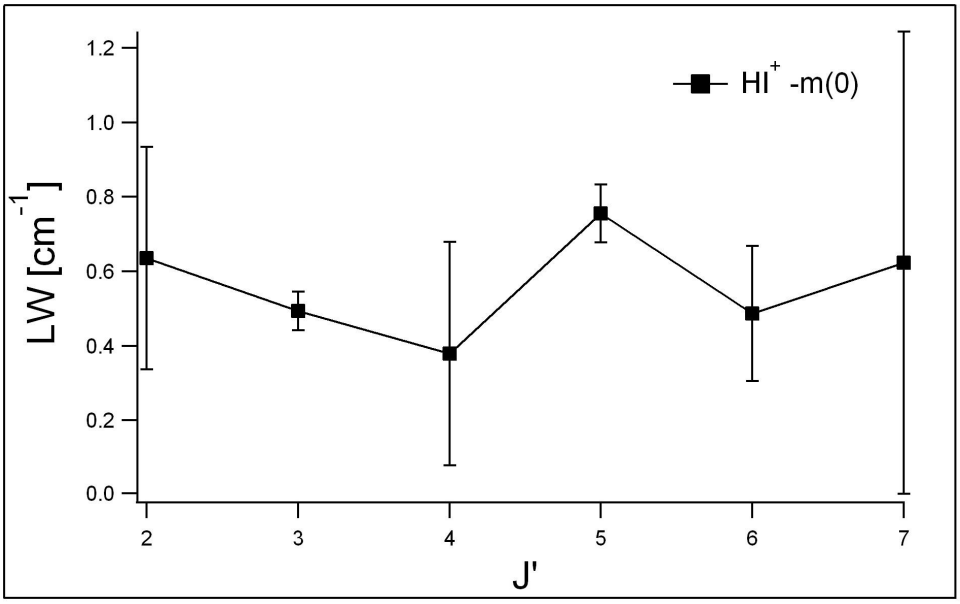

Fig.S4: Rotational line-widths vs. *J´* derived from the *R* lines of the HI^+ REMPI spectrum for the $m^3\Pi_2(v' = 0)$ state.

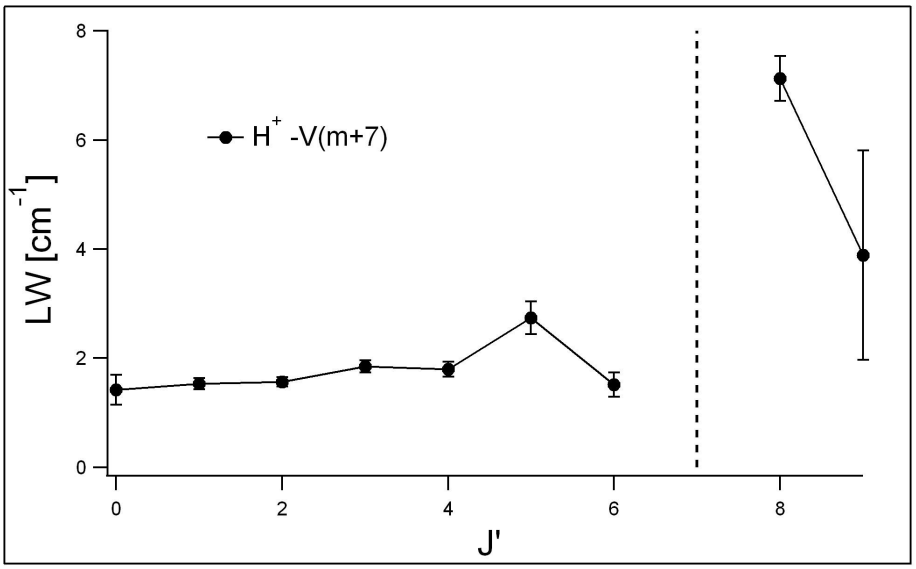

Fig.S5: Rotational line-widths vs. *J´* derived from the *Q* lines of the H^+ REMPI spectrum for the $V^1\Sigma^+(v' = m + 7)$ state. The line-width for $J' = 7$ could not be valuated due to an overlap with *Q* lines of the $O^1\Sigma^+(v' = 0)$ Rydberg state spectrum.

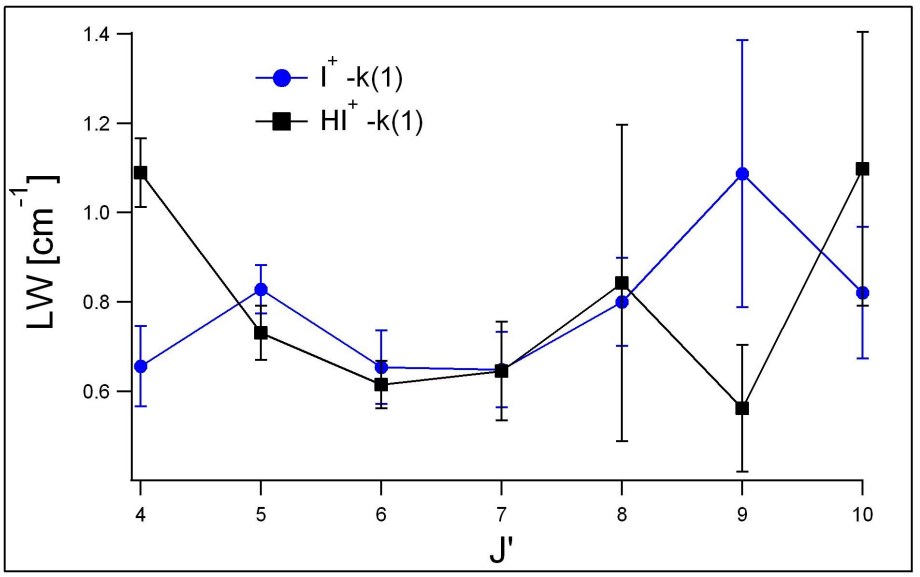

Fig.S6: Rotational line-widths vs. J' derived from the Q lines of the HI^+ and I^+ REMPI spectra for the$k^3\Pi_1(v' = 1)$ state.

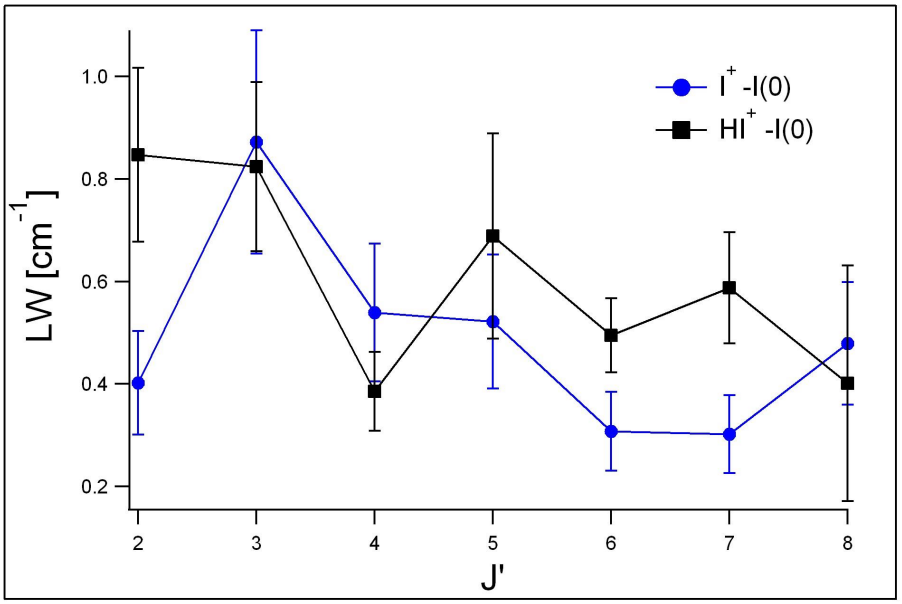

Fig.S7: Rotational line-widths vs. J' derived from the Q lines of the HI^+ and I^+ REMPI spectra for the$I^1\Delta_2(v' = 0)$ state.

Table S1: Observed iodine atomic lines in the REMPI spectra of HI.

Figure	Line position [cm^{-1}]	Ground state	Excited state Configuration	Excited state/Term	Excited state / J
1a	70811.88 – 70813.11	$^2P_{3/2}$ $^2P_{1/2}$ $^2P_{1/2}$	$5s^25p^4(^3P_0)6p$ $5s^25p^4(^1D_2)6p$ $5s^25p^4(^3P_0)7s$	$^2[1]°$ $^2[1]°$ $^2[0]$	1/2 3/2 1/2
1b	71128.95	$^2P_{1/2}$	$5s^25p^4(^3P_2)8p$	$^2[2]°$	5/2
1b	71177.07	$^2P_{1/2}$	$5s^25p^4(^3P_2)8p$	$^2[1]°$	1/2
1b	71251.79	$^2P_{1/2}$	$5s^25p^4(^3P_2)8p$	$^2[3]°$	5/2
1c	71976.78	$^2P_{3/2}$	$5s^25p^4(^3P_0)6p$	$^2[1]°$	3/2

References

[1]Á. Kvaran, K. Matthiasson, and H. Wang, J. Chem. Phys. **131**(4), 044324 (2009).
[2]J. Long *et al.*, J. Chem. Phys. **136**(21), 214315 (2012).

Article 4

Rydberg and valence state excitation dynamics: A velocity map imaging study involving the E-V state interaction in HBr

Dimitris Zaouris, Andreas Kartakoullis, Pavle Glodic, Peter C. Samartzis, Helgi Rafn Hróðmarsson, and Ágúst Kvaran

Physical Chemistry Chemical Physics. **17**. 10468 (2015).

DOI: 10.1039/c5cp00748h

Helgi Rafn Hróðmarsson actively participated in the development of the „two-step“ analysis for anisotropy parameters and performed the data analysis relevant to alignments. Helgi contributed to editing until publication.

PCCP

PAPER

Cite this: *Phys. Chem. Chem. Phys.*, 2015, **17**, 10468

Rydberg and valence state excitation dynamics: a velocity map imaging study involving the E–V state interaction in HBr

Dimitris Zaouris,[a] Andreas Kartakoullis,[a] Pavle Glodic,[a] Peter C. Samartzis,[a] Helgi Rafn Hróðmarsson[b] and Ágúst Kvaran*[b]

Received 5th February 2015,
Accepted 9th March 2015

DOI: 10.1039/c5cp00748h

www.rsc.org/pccp

Photoexcitation dynamics of the E($^1\Sigma^+$) (v' = 0) Rydberg state and the V($^1\Sigma^+$) (v') ion-pair vibrational states of HBr are investigated by velocity map imaging (VMI). H^+ photoions, produced through a number of vibrational and rotational levels of the two states were imaged and kinetic energy release (KER) and angular distributions were extracted from the data. In agreement with previous work, we found the photodissociation channels forming H*(n = 2) + Br($^2P_{3/2}$)/Br*($^2P_{1/2}$) to be dominant. Autoionization pathways leading to H^+ + Br($^2P_{3/2}$)/Br*($^2P_{1/2}$) *via* either $HBr^+(^2\Pi_{3/2})$ or $HBr^{+*}(^2\Pi_{1/2})$ formation were also present. The analysis of KER and angular distributions and comparison with rotationally and mass resolved resonance enhanced multiphoton ionization (REMPI) spectra revealed the excitation transition mechanisms and characteristics of states involved as well as the involvement of the E–V state interactions and their v' and J' dependence.

I. Introduction

In recent years there has been growing interest and emphasis on studies of higher energy valence and Rydberg states, complementing the vast amount of information on molecular ground and low energy valence states. As the excitation energy increases, the higher density of states gives rise to more complex spectroscopy and dynamics involving state mixing, predissociation, autoionization and other interesting state interaction phenomena worth further study.

The hydrogen halides have turned out to be ideal candidates for fundamental spectroscopy and photofragmentation studies involving higher energy valence and Rydberg states.[1–36] Since the original work by Price on the hydrogen halides (HX),[1] a wealth of spectroscopic data has been derived from absorption spectroscopy for HCl,[2,5,6,8] HBr,[3,7,9] and HI[4] and from resonance enhanced multiphoton ionization (REMPI) studies (HCl,[10–12,16,17,19–22] HBr,[13,16–19,23] and HI[14–16,24]). Extensive perturbations observed in spectra are clear indications of the importance of state interactions involved. Photofragmentation studies based on velocity map imaging (VMI) of H^+ following one-colour resonance excitations in HCl**(v', J')[25–27,29,30,37] and HBr[26,27] have been performed. Recently Kvaran and coworkers have used mass resolved REMPI spectra to determine quantitative and qualitative information relevant to state interaction, photofragmentation as well as energetics of HCl,[31–33,35] HBr,[34,35] and HI.[36] The analyses are based on spectral perturbations seen as alterations or irregularities in line-shifts, line-intensities or line-widths. VMI studies and mass-resolved REMPI spectra analysis have been found to give complementary results in terms of Rydberg to ion-pair state interactions for resonance states in HCl.[29,31] Particular emphasis has been laid on studies of the strong homogenenous ($\Delta\Omega$ = 0) state interaction between the $E^1\Sigma^+$ (Ω = 0) Rydberg state and the $V^1\Sigma^+$ (Ω = 0) ion-pair state, which, together, form an adiabatic double-well potential ($B^1\Sigma^+$) (see Fig. 1 for HBr).[25–27,30,35,37] Both photoionization and photodissociation processes are found to be largely affected by this state mixing.

The above studies revealed the following major paths for H^+ formation of the hydrogen halides (HX) following and depending on the resonance excitation.

(i) HX** photolysis followed by fragment ionization:

$$HX^{**}(v', J') + h\nu \rightarrow H^* + X/X^*; \quad \text{photolysis}$$

$$H^* + h\nu \rightarrow H^+ + e^-; \quad \text{photoionization}$$

(ii) HX** ionization followed by ion photolysis:

$$HX^{**}(v', J') + h\nu \rightarrow HX^{\#}; \quad \text{photoexcitation}$$

$$HX^{\#} \rightarrow HX^+(v^+)/HX^{+*}(v^+) + e^-; \quad \text{autoionization}$$

$$HX^+(v^+)/HX^{+*}(v^+) + h\nu \rightarrow H^+ + X/X^*; \quad \text{ion photolysis}$$

[a] *Institute of Electronic Structure and Laser, Foundation for Research and Technology-Hellas, Vassilika Vouton, 71110 Heraklion, Greece*
[b] *Science Institute, University of Iceland, Dunhagi 3, 107 Reykjavík, Iceland. E-mail: agust@hi.is; Fax: +354-552-8911; Tel: +354-525-4672, +354-525-4800*

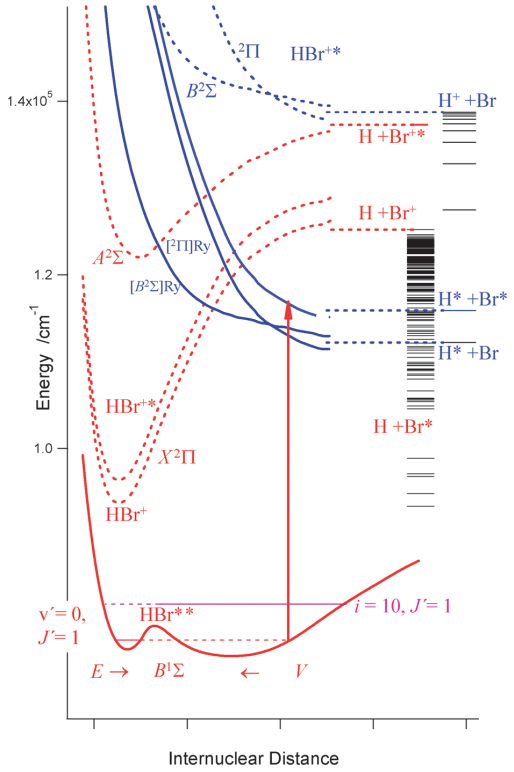

Fig. 1 Potential curves of the states involved in H^+ formation following two-photon excitation of HBr to the E and V states (mixed $B^1\Sigma^+$ state), including asymptotic energies of fragments[42] (right). Potential curves for the ion states (broken curves) are derived from ref. 38. The repulsive Rydberg states, [$B^2\Sigma$]Ry and [$^2\Pi$]Ry (solid blue curves) which correlate to H*(n = 2) + Br and H*(n = 2) + Br* are similar in shape to the ion curves, $B^2\Sigma$ and $^2\Pi$, (ref. 38) but shifted to the respective asymptotes. The potential curve for the B state was derived from Fig. 1 in ref. 26. The vertical arrow represents a possible transition following a resonance excitation to the E(v' = 0) state (see text).

(iii) Ion-pair formation:

$$HX^{**}(v', J') + h\nu \rightarrow H^+ + X^- \quad \text{ion-pair formation}$$

Here X and X* (and HX^+ and HX^{+}*) denote the ground ($X(^2P_{3/2})$/$HX^+(^2\Pi_{3/2})$) and spin–orbit excited ($X^*(^2P_{1/2})$/$HX^{+}*(^2\Pi_{1/2})$) species, respectively. H* is the first excited state of hydrogen, H*(n = 2). In the case of HBr the photoexcitation steps (i) to form H* + Br and H* + Br* involve excitation to repulsive Rydberg states which converge to the repulsive molecular ion states $B^2\Sigma^+(\sigma^2(\pi_x^1\pi_y^1)\sigma^{*1})$ and $^2\Pi(\sigma^1\pi^3\sigma^{*1})$[27,38] labelled, in a simplified form, as [$B^2\Sigma^+$]Ry and [$^2\Pi$]Ry (see Fig. 1), where the details inside the bracket characterize the ion core and "Ry" represents the Rydberg electron. The [$B^2\Sigma^+$]Ry state and the lower energy component of two [$^2\Pi$]Ry states correlate to the assymptotic atom pair, H* + Br, whereas the higher energy component of the [$^2\Pi$]Ry states correlates to H* + Br* as shown in Fig. 1. Considering one-electron transitions from the mixed E/V$^1\Sigma^+$(*i.e.* $B^1\Sigma^+$) state(s), based on the principal electron configurations of the E($[\sigma^2\pi^3]5p\pi^1$) and the V($\sigma^1\pi^4\sigma^{*1}$) states, the Rydberg electron must occupy a 5pπ orbital in which case, the possible Rydberg states characteristics could be $^{1,3}\Pi([B^2\Sigma^+;\sigma^2(\pi_x^1\pi_y^1)\sigma^{*1}]5p\pi^1)$ and $^{1,3}\Sigma([^2\Pi;\sigma^1\pi^3\sigma^{*1}]5p\pi^1)$ (Fig. 1). Although the selection rule for spin conservation favours the involvement of singlet Rydberg states triplet states cannot be ruled out (hence the notations $^{1,3}\Pi$ and $^{1,3}\Sigma$). Three one-electron transitions, two parallel ($\pi \rightarrow p\pi$; $\sigma \rightarrow \sigma^*$) and one perpendicular ($\pi \rightarrow \sigma^*$) transitions, could be involved, *i.e.*

(a) $HBr^{**}\{V^1\Sigma(\sigma^1\pi^4\sigma^{*1})\} + h\nu$
$\rightarrow HBr^{\#}\{^{1,3}\Sigma([^2\Pi;\sigma^1\pi^3\sigma^{*1}]5p\pi^1)\}$; parallel transition

(b) $HBr^{**}\{E^1\Sigma([^2\Pi;\sigma^2\pi^3]5p\pi^1)\} + h\nu$
$\rightarrow HBr^{\#}\{^{1,3}\Sigma([^2\Pi;\sigma^1\pi^3\sigma^{*1}]5p\pi^1)\}$; parallel transition

(c) $HBr^{**}\{E^1\Sigma([^2\Pi;\sigma^2\pi^3]5p\pi^1)\} + h\nu$
$\rightarrow HBr^{\#}\{^{1,3}\Pi([B^2\Sigma^+;\sigma^2(\pi_x^1\pi_y^1)\sigma^{*1}]5p\pi^1)\}$;
perpendicular transition

one of which (a) involves the ion-pair component (*i.e.* largest ion-pair/V state character) of the mixed (B) state. The weight of the ion-pair (V) character will increase (hence the Rydberg (E) character will decrease) gradually from the inner well of the mixed/B state as the internuclear distance increases to reach a maximum near the outer turning point of the outer well.

In this paper we present the results of a VMI investigation involving the interactions between the $E^1\Sigma^+$ Rydberg state and the $V^1\Sigma^+$ ion-pair valence state in HBr. KER and angular distributions data are extracted from images of H^+ originating from the $E^1\Sigma^+(v' = 0; J' = 1\text{–}9)$, $V^1\Sigma^+$ ($v' = m + 4; J' = 0\text{–}8$), $V^1\Sigma^+$ ($v' = m + 5; J' = 0\text{–}4$) and $V^1\Sigma^+$ ($v' = m + i$, i = 6–10; $J' = 0$) states of HBr for $J' = J''$ (*i.e.* Q rotational lines). m is an unknown integer, since the zero vibrational energy ($v' = 0$) is not known for the $V^1\Sigma^+$ state.[13] The contributions of paths (i) and (ii) above were quantified, whereas channel (iii) was not detected. The relative ratio of the two steps in (i) as well as the angular distributions are found to change with J'/v'. Trends coincide with the E–V interaction strength measured in REMPI studies, indicating a possible connection.

II. Experimental

The VMI setup used in this work has been described previously[39,40] and only a brief description will be given here. A supersonic molecular beam of HBr seeded in He is formed by a 15–30% HBr mixture in He supersonically expanding through a homemade piezoelectrically actuated nozzle valve (1 mm diameter) and being skimmed before entering the detection chamber where the ion optics are positioned. After passing through a ~2 mm diameter hole in the repeller electrode, the molecular beam is intersected at right angles by a laser beam focused at the geometric focus position of a single-electrode repeller-grid arrangement. The laser beam is

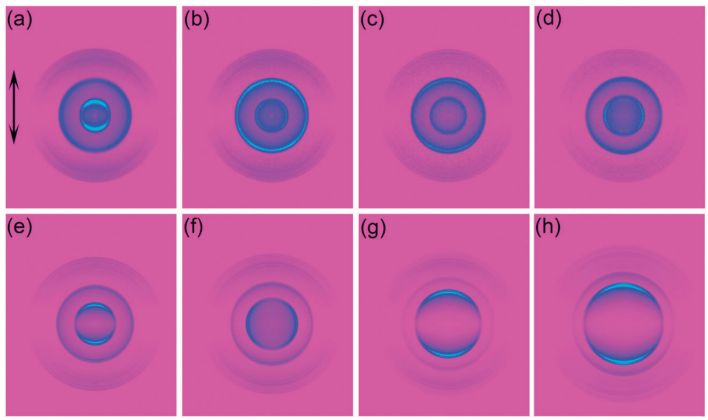

Fig. 2 H^+ velocity map images for (a) $J' = 1$, (b) $J' = 4$, (c) $J' = 7$, (d) $J' = 9$ levels of the E($v' = 0$) and for (e) $v' = m + 5$ (f) $v' = m + 6$ (g) $v' = m + 8$ and (h) $v' = m + 10$ levels of the V($v' = m + i$) states of HBr. The laser polarization is indicated by the double arrow. All the images show two intense rings for low and medium kinetic energy releases and number of weaker rings for higher kinetic energy release.

generated by an Nd^{3+}:YAG pumping a master oscillator power oscillator system (Spectra Physics MOPO).

For the VMI experiments reported here, the repeller is always ON, *i.e.* the apparatus is operated in "VMI mode". The photofragments traverse a field-free time-of-flight region (45 cm) and a gated, position-sensitive detector (dual, imaging-quality MCP array coupled to a phosphor screen) images the photofragment sphere. The image frame is recorded asynchronously every second ($\sim$10 laser shots) by a CCD camera and several thousand frames are averaged to form images such as those shown in Fig. 2. The 2D slice of the 3D ion distribution from each final image is extracted by inverse Abel transformation and integrated from its center over angle to extract the speed and over radius to extract the angular distributions of the photofragments.

H^+ photoion images are recorded following HBr excitation to different intermediate valence and ion-pair electronic and rovibrational levels by appropriate tuning of the laser wavelength (Table 1). Background images are recorded with the laser on and the molecular beam off and subtracted from the signal images.

III. Results

A. H^+ images and kinetic energy release (KER) spectra

H^+ images were recorded for two-photon resonance excitation from the ground state $X^1\Sigma^+(v' = 0; J'')$ to the $E^1\Sigma^+(v' = 0; J' = 1\text{–}9)$ Rydberg and the $V^1\Sigma^+(v' = m + 4; J' = 0\text{–}8)$, $V^1\Sigma^+(v' = m + 5; J' = 0\text{–}4)$ and $V^1\Sigma^+(v' = m + i; i = 4\text{–}10; J' = 0)$ ion-pair states of HBr for $J' = J''$ (*i.e.* Q rotational lines). The majority of the images feature two intense rings surrounded by a number of weaker ones at higher kinetic energy release (KER) as shown in Fig. 2. Fig. 3(a) shows the H^+ KER distributions for the E state as a function of rotational level ($J' = 1\text{–}9$) of $v' = 0$, whereas Fig. 3(b) shows the V state KER distributions as a function of vibrational level ($v' = m + i$, $i = 4\text{–}10$) for $J' = 0$. The two KER peaks around 0.1 eV and 0.5 eV, in the case of the E($v' = 0$) state correspond to the two intense rings in each image. The weaker rings in those images have KERs in the 1.0–2.2 eV region.

Table 1 HBr resonance excited states (term symbols, vibrational quantum numbers (v') and rotational quantum numbers (J')) and two-photon excitation wavenumber (ν). NB: m is an unknown integer number

State	v'	J'	Q lines; ν/cm^{-1}	Ref./comment
$E^1\Sigma^+$	0	1	77938.8	13
		2	77935.6	13
		3	77931.6	13
		4	77926.5	13
		5	77920.6	13
		6	77913.5	13
		7	77905.4	13
		8	77895.6	13
		9	77883.0	13
$V^1\Sigma^+$	$m + 4$	0	77830.0	This work
		1	77821.0	This work
		2	77803.0	This work
		3	77778.7	Derived from ref. 9
		4	77743.6	Derived from ref. 9
		5	77700.1	Derived from ref. 9
		6	77648.2	Derived from ref. 9
		7	77587.9	Derived from ref. 9
		8	77520.0	Derived from ref. 9
$V^1\Sigma^+$	$m + 5$	0	78388.8	13
		1	78380.2	13
		2	78362.4	13
		3	78338.6	13
		4	78300.6	This work
$V^1\Sigma^+$	$m + 6$	0	78940.2	13
$V^1\Sigma^+$	$m + 7$	0	79480.3	13
$V^1\Sigma^+$	$m + 8$	0	80029.7	13
$V^1\Sigma^+$	$m + 9$	0	80638.0	This work
$V^1\Sigma^+$	$m + 10$	0	81197.2	13

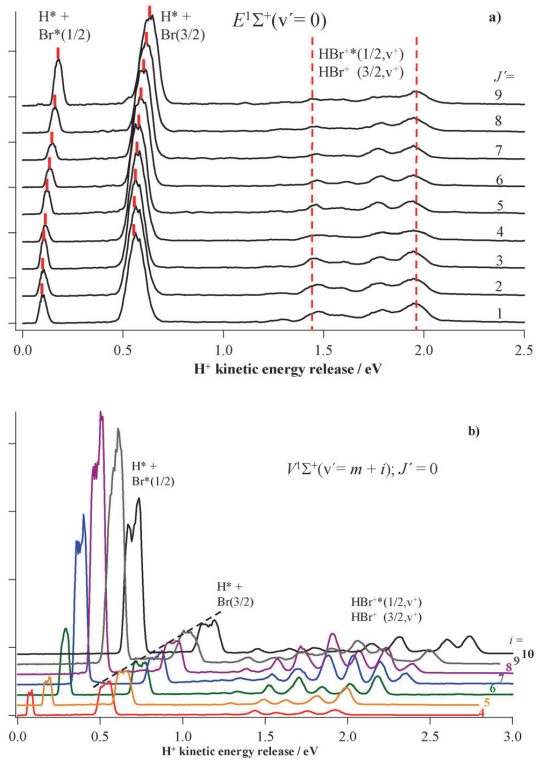

Fig. 3 (a) H^+ kinetic energy release curves (KER's) for resonance excitation from the ground states X(v' = 0, J'') to the E(v' = 0; J' = 1–9) states for J' = J'' (Q lines). Br, Br* and ionic channel peaks are marked (see H* + Br*, H* + Br and HBr^{+}*/HBr^{+}). The curves are normalized to the height of the Br peak. Predicted KER's for the Br and Br* channels are shown as red bars. Horizontal red broken lines in the region for the ionic channels are to guide the eye. (b) H^+ kinetic energy release curves for resonance excitation from the ground states X(v' = 0, J'') to the V(v' = m + i; i = 4–10) states for J' = J'' = 0 (Q lines). The curves are normalized to the height of the peaks for the Br (*i.e.* H* + Br) channel.

In order to assign each KER peak, we calculated the expected KER's for the various channels presented in Section I as follows:

$$\mathrm{KER}(\text{“Br”}) = 3h\nu + E(J'') - D_0(\mathrm{HBr}) - E(\mathrm{H}^*) \quad \text{for channel “H* + Br”; (i)} \tag{1a}$$

$$\mathrm{KER}(\text{“Br*”}) = 3h\nu + E(J'') - D_0(\mathrm{HBr}) - E(\mathrm{H}^*) - \mathrm{SO}(\mathrm{Br}^*) \quad \text{for channel “H* + Br*”; (i)} \tag{1b}$$

$$\mathrm{KER}(\text{“}HBr^{+}\text{”}) = h\nu + \mathrm{IE}(HBr^{+}(3/2)) + G_0(HBr^{+}(3/2),v^{+}) - D_0(\mathrm{HBr}) - \mathrm{IE}(\mathrm{H}) \quad \text{for channel “}HBr^{+}(v^{+})\text{”; (ii)} \tag{1c}$$

$$\mathrm{KER}(\text{“}HBr^{+}{}^{*}\text{”}) = h\nu + \mathrm{IE}(HBr^{+}(1/2)) + G_0(HBr^{+}(1/2),v^{+}) - D_0(\mathrm{HBr}) - \mathrm{IE}(\mathrm{H}) - \mathrm{SO}(\mathrm{Br}^*) \quad \text{for channel “}HBr^{+}{}^{*}(v^{+})\text{”; (ii)} \tag{1d}$$

where $h\nu$ is the photon excitation energy.[9,13,34] D_0(HBr) is the bond energy for HBr (30 210 ± 40 cm^{-1} [27,41]), E(H*) is the electronic energy of H*(n = 2) (82258.95 cm^{-1} [27,42]) and SO(Br*) is the spin–orbit energy of Br (3685.24 cm^{-1} [27,42]). IE(HBr^{+}(3/2)) and IE(HBr^{+}*(1/2)) are the ionization energies of HBr with respect to the formation of HBr^{+}(3/2) (94150.672 cm^{-1}) and HBr^{+}*(1/2) (96796.17 cm^{-1}) respectively.[43] IE(H) is the ionization energy of H (109677.61 cm^{-1} [27,42]). $E(J'')$ is the rotational energy for the rotational level of the ground state, J'', expressed as

$$E(J'') = B''(J''(J''+1)) - D''J''^2(J''+1)^2 \tag{2}$$

where B'' = 8.348244 cm^{-1} and D'' = 3.32 × 10^{-4} cm^{-1}.[19,44] $G_0(HBr^{+}(3/2),v^{+})$ and $G_0(HBr^{+}{}^{*}(1/2),v^{+})$ are the vibrational energies of the v^{+} vibrational levels for HBr^{+}(3/2) and HBr^{+}*(1/2), respectively, expressed as

$$G_0 = \omega_e(v^{+}+1/2) - \omega_e x_e(v^{+}+1/2)^2 + \omega_e y_e(v^{+}+1/2)^3 - (\omega_e(1/2) - \omega_e x_e(1/2)^2 + \omega_e y_e(1/2)^3) \tag{3}$$

where ω_e = 2439.10 cm^{-1}, $\omega_e x_e$ = 45.18 cm^{-1}, $\omega_e y_e$ = 0.126 cm^{-1} and ω_e = 2431.35 cm^{-1}, $\omega_e x_e$ = 44.05 cm^{-1}, $\omega_e y_e$ = 0.0472 cm^{-1} for HBr^{+}(3/2) and HBr^{+}*(1/2) respectively.[43]

Based on the calculations above, the peak around 0.1 eV for the E(v' = 0) state and from 0.1 to 0.7 eV (depending on v') for the V state is due to the H*(n = 2) + Br*($^2P_{1/2}$) formation followed by photoionization of H*(n = 2). We will henceforth refer to this channel as the Br* channel. The peak at ~0.6 eV for the E(v' = 0) state and from 0.5 eV to ~1.2 eV for the V state is assigned to the formation of H*(n = 2) + Br($^2P_{3/2}$) followed by H*(n = 2) photoionization and will henceforth be referred to as the Br channel. Finally, the “multi-peak structure” ranging from 1.0 eV to 2.2 eV for the E(v' = 0) state and from ~1.0 eV to 3.0 eV for the V state is due to photodissociation of several vibrational levels, v^{+}, of the ground $HBr^{+}(^2\Pi_{3/2})$ and the spin–orbit excited $HBr^{+}{}^{*}(^2\Pi_{1/2})$ molecular ions, formed after photoionization of HBr**(v', J'). Those H^+ photofragments are produced with either a Br or a Br* co-fragment. This KER feature corresponds to pathway (ii) of Section I and will henceforth be referred to, collectively, as the “ionic channels” (or the “HBr^{+} ionic channel” and the “HBr^{+}* ionic channel” when referred to separately). The above assignments are in agreement with the work by Loock and coworkers.[27] We note here that we scanned the laser over a broad range of wavelengths in this excitation region looking for Br^- (negative) ions that would confirm the existence of an ion-pair pathway (path iii in Section I), but without success.

The Br and Br* channel KER positions show only a slight increase with J' for the E(v' = 0) state but a clear upwards shift with v' = m + i for the V state. The slight increase with J' in the E(v' = 0) state can be explained by the increase in $E(J'')$ which dominates over a decreasing photon energy ($h\nu$)[9,13,34] (see eqn (1a) and (1b)), whereas the clear shift for the V state is due to the increasing photon energy. We note that the “double” or “split” intense rings observed in some of the images that result in “splitting” of the corresponding KER peaks, for the Br

and Br* channels, for the V($v' = m + i$) states in particular, are due to the recoil effect as the hydrogen atoms H* ionize to form $H^+ + e^-$.[45]

Comparing the various peak intensities in the E (Fig. 3(a)) and the V (Fig. 3(b)) state KER distributions, it is evident that the Br and Br* channels dominate the H^+ production in both states over the ionic channels. For the E($v' = 0$) resonance state, the strongest H^+ signals are observed in the Br channel and the Br*/Br ratio (Fig. 4(a)) reaches a minimum at $J' = 6$–7. For the V($v' = m + i$) resonance states, the relative intensities of the various ion signals vary with v'. The Br channel dominates at low $v' = m + i$ ($i = 4$, 5) whereas the Br* channel dominates at higher v'. The integrated signal intensities reveal that for the V state the Br channel contribution is smallest for $i = 8$ (not shown).

Whereas the Br and Br* channels produce the majority of H^+, the ionic channels feature a number of HBr^+ vibrational peaks. These peak positions remain virtually unchanged with J' for the E($v' = 0$) state, whereas, for the V state they exhibit beat structures with increasing number of peaks as $v' = m + i$ increases. The calculated KER peak positions for the ionic channels (Section I, path (ii) and eqn (1c) and (1d)) are shown above the respective peaks in Fig. 5. Furthermore, the energies of the maximum vibrational levels observed in each spectra ($E(v^+_{max})$) are found to match closely the sum of the molecular ground state internal energy (rotational energy) and the three-photon excitation energy, *i.e.*

$$E(v^+_{max}) \approx E(J'') + 3h\nu \quad (4)$$

The intensity fluctuations observed in KERs for the ionic channel are partly due to the effect of changing Franck–Condon overlaps of the wavefunctions involved and partly due to overlapping of different peaks in the two vibrational progressions for the $H^+ + Br(^2P_{3/2}) \leftarrow HBr^+(^2\Pi_{3/2})$ and $H^+ + Br(^2P_{1/2}) \leftarrow HBr^+(^2\Pi_{1/2})$ transitions. The peak structure gradually fades away as v^+ decreases. The vibrational structures could easily be fitted by sum of Gaussian functions, suggesting that each v^+ peak corresponds to a single or few rotational transitions from the resonance excited states (see Fig. 5(c)). Generally the bandwidths were found to be larger for the E Rydberg state than for the V ion-pair state.

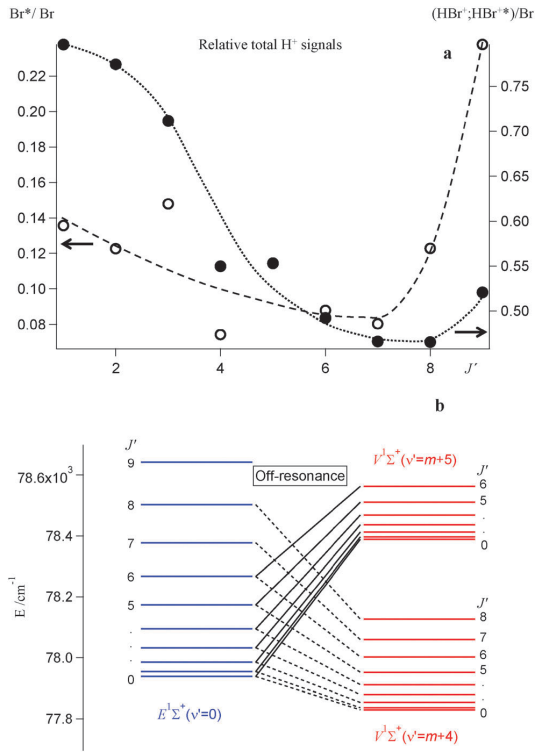

Fig. 4 (a) Ratios of integrated H^+ signal intensities as a function of J': signals for the Br* channel over signals for the Br channel (see (i) in Section I; open circles, dashed fit curve; left axis) and signals for the ionic (HBr^+/HBr^{+*}) channels over signals for the Br channel (see (ii) in Section I; filled circles, dotted fit curve; right axis). (b) Rotational energy levels, derived from observed REMPI rotational peaks for the E($v' = 0$) and the V($v' = m + i$); $i = 4$, 5 states. Level-to-level off-resonance interactions between the V($v' = m + i$) ion-pair states and the E($v' = 0$) Rydberg state are indicated by broken and unbroken lines.

B. Angular distributions of H^+

Significant angular distribution variations of the H^+ ions for the E state *vs.* J' and for the V state *vs.* v' can be seen in Fig. 2. As J' increases from $J' = 1$ to $J' = 9$ for the E state, the Br* channel distribution changes gradually from a shape corresponding to a parallel transition towards a perpendicular one. The opposite effect is observed for the Br channel. For the $v' = m + i$ vibrational levels of the V state, the Br* channel exhibits a parallel character for all i's except for $i = 6$. The same is observed for the Br channel with the exception of $i = 5, J' = 0$–4. The ionic channel angular distribution shapes do not exhibit any significant change as the excitation energy changes both for the E and the V states.

In extracting quantitative information from the angular distributions above, we were faced with a difficult dilemma. In the simple case of a single-photon photolysis, followed by photofragment ionization, the angular distribution ($P(\theta)$) can be expressed[46] as

$$P(\theta) = A(1 + \beta_2 P_2(\cos(\theta)) + \beta_4 P_4(\cos(\theta)) + \beta_6 P_6(\cos(\theta))) \quad (5)$$

where P_2, P_4 and P_6 are the second, fourth and sixth order Legendre polynomials. β_2, β_4 and β_6 are the corresponding anisotropy beta parameters and A is a scaling factor. The three beta parameters can then be related to the transition state symmetry and dynamics including vector correlation phenomena such as alignment and orientation.

Whereas most angular distribution treatments associated with VMI studies are based on such one-step direct process analysis, some work on HCl and HBr has been based on two-step processes, *i.e.* a one-step resonance excitation followed by

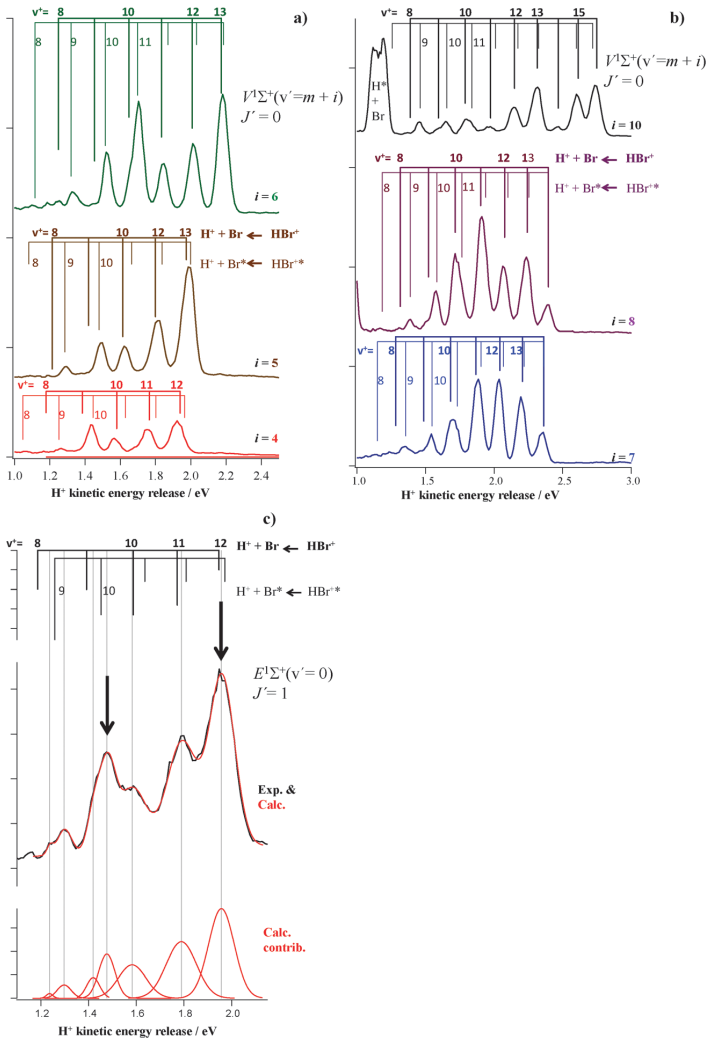

Fig. 5 Assignment and analysis of H^+ kinetic energy release curves for the ionic (HBr^{+}* and HBr^+) channels (see (ii) in Section I) for resonance excitation from the ground states X(v' = 0, J'') to V(v' = m + i; i = 4, 5, 6), J' = J'' = 0 (a), to V(v' = m + i; i = 7, 8, 10), J' = J''= 0 (b) and to E(v' = 0) J' = J'' = 1 (c). Predicted peak positions/peak assignments due to v^+ excitations are shown above spectra (a–c). Gaussian multi-peak fit of the spectral structure for the resonance excited state E(v' = 0) J' =1 is shown in (c). Arrows in (c) indicate peaks which are dominantly due to HBr^+ (v^+ = 12; right) and HBr^+* (v^+ = 10; left) formation.

a second ionization step.[47,48] Here, HBr absorbs two photons to reach a specific v', J' level of the E or the V resonance states, followed by two photons to produce H^+ *via* the pathways described in Sections I and IIIA. Thus the overall process involves the absorption of four photons. Hence, fitting the angular distributions with a function such as eqn (5), will result in "effective" beta parameters, which can be only loosely related to the ones the reader is familiar with in single-photon cases. On the other hand, the obvious change in the angular distribution of the Br and Br* channels for the E resonance state, requires some kind of quantification. We finally ended up using a form of eqn (5) limiting the fit to the β_4 term and we discuss the resulting "effective" beta parameters taking into account the multiphoton nature of the H^+ production processes. Where possible, we attempted a two-step analysis. The beta parameters resulting from both approaches for the Br and Br* channels are plotted in Fig. 6.

The β_2 values for the Br* channel of the E state follow a decreasing trend starting positive around 0.5 for J' = 1, changing sign at J' = 4 and reaching −0.6 for J' = 9. The opposite trend is observed for the Br channel starting at −0.4 for J' = 1, changing sign at J' = 4 and ending up at 0.27 for J' = 9 (Fig. 6(a)).

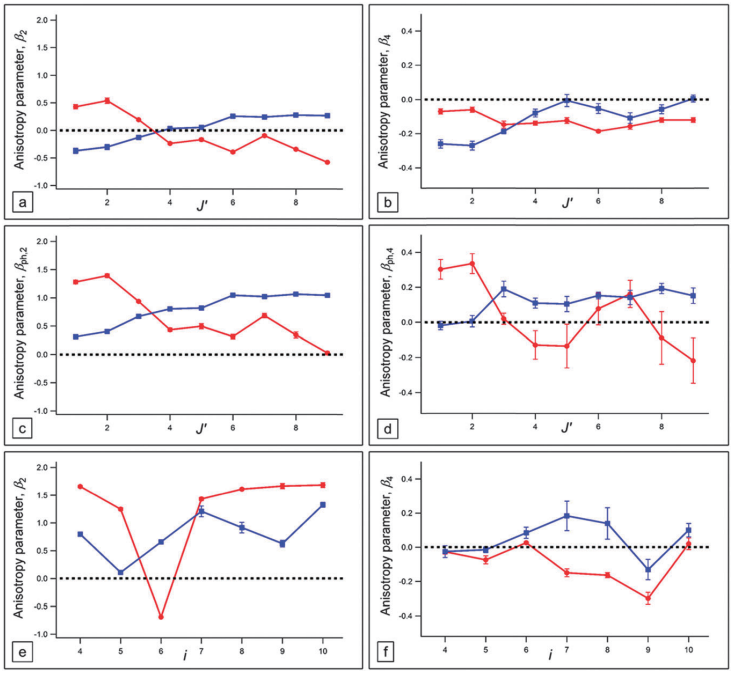

Fig. 6 Anisotropy parameters extracted for the E(v' = 0) and V(v' = m + i) states. Top: β_2 (a) and β_4 (b) derived by "single step analysis" (see text) for the H* + Br (blue) and H* + Br* (red) channels of the E(v' = 0) state *vs.* J'. Middle: $\beta_{ph,2}$ (c) and $\beta_{phi,4}$ (d) derived by "two-step analysis" (see text) for the H* + Br (blue) and H* + Br* (red) channels of the E(v' = 0) state *vs.* J', bottom: β_2 (e) and β_4 (f) derived by "single step analysis" for the H* + Br (blue) and H* + Br* (red) channels of the V(v' = m + i) state *vs.* i.

The fourth Legendre polynomial coefficient (β_4) was used more in order to improve fits rather than to evaluate vector correlation effects. It has mostly negative values, which fluctuate around zero (ranging from −0.3 to 0) as J' changes from 1 to 9 for both Br* and Br channel (Fig. 6(b)). The Br and Br* channels for the V(m + 4) state both exhibit a downward trend in β_2 as J' increases, with Br* having more positive values than Br at any given J'.

To evaluate how much the crude beta parameters differ from a more appropriate analysis taking into account the multi-photon nature of the processes involved the data for the angular distributions derived for the resonance excitation to E(v' = 0, J') were analysed according to a more appropriate two-step photoexcitation formalism given by Chichinin *et al.*[48] corresponding to two-photon excitation to the E(v' = 0, J') states followed by one-photon excitation to superexcited states. The observed angular distribution of the photoproduct, $P(\theta)$, is expressed as

$$P(\theta) = AP_f(\theta)\, P_{ph}(\theta) \tag{6}$$

where $P_f(\theta)$ is the angular distribution of the axes in the resonance intermediate state and $P_{ph}(\theta)$ is the photofragment angular distribution produced by the photolysis of the unpolarised intermediate state. $P_f(\theta)$ and $P_{ph}(\theta)$ are expressed as

$$P_f(\theta) = 1 + \beta_{f,2}P_2(\cos(\theta)) + \beta_{f,4}P_4(\cos(\theta)) \tag{7a}$$

$$P_{ph}(\theta) = 1 + \beta_{ph,2}P_2(\cos(\theta)) + \beta_{ph,4}P_4(\cos(\theta)) \tag{7b}$$

Expression (6) was used to fit the angular distributions for A, $\beta_{f,4}$, $\beta_{ph,2}$ and $\beta_{ph,4}$ as variables and for $\beta_{f,2}$ estimated from

$$\beta_{f,2} = \frac{2 - 20\mathrm{Re}[b]}{2 + 25|b|^2}; \tag{8}$$

where Re[b] represents the real part of the parameter b which can be derived from intensity ratios of Q over S (*i.e.* I_Q/I_S) and Q over O (I_Q/I_O) rotational lines from

$$\begin{aligned} \frac{I_Q}{I_S} &= \frac{10}{3}\frac{(2J''+1)}{(J''+2)}\left[|b|^2\frac{(2J''+3)}{(J''+1)} + \frac{1}{5}\frac{J''}{(2J''-1)}\right] \\ \frac{I_Q}{I_O} &= \frac{10}{3}\frac{(2J''+1)}{(J''-1)}\left[|b|^2\frac{(2J''-1)}{J''} + \frac{1}{5}\frac{(J''+1)}{(2J''+3)}\right] \end{aligned} \tag{9}$$

where J'' is the rotational quantum number for the ground state. Furthermore, the alignment parameter, A_{20}, for J' = 1 can be derived from

$$A_{20} = \frac{10\mathrm{Re}[b] - 1}{25|b|^2 + 2} \tag{10}$$

Based on line intensity ratios evaluated from mass resolved (2 + n) REMPI spectra of HBr, for the E(v' = 0) state, b^2 = 1.2 (b = 1.1)

was obtained by eqn (9). This gave $A_{20} = +0.31$ for $J' = 1$ by eqn (10) and $\beta_{f,2} = -0.62$ by eqn (8). The A_{20} value (+0.31) can be compared with the extreme values of $A_{20}^{max} = +0.5$ and $A_{20}^{min} = -1$ for dominating perpendicular and parallel transitions respectively[48,49] and the $\beta_{f,2}$ value (−0.62) can be compared with the corresponding extreme values of −1 (perpendicular) and +2 (parallel). The results are plotted in Fig. 6(a) and (b). The $\beta_{ph,2}$ parameters for both Br and Br* exhibit similar trends as in the one-step analysis, however, their values are all positive, ranging from 0 to ∼1.4 (Fig. 6(c)). The $\beta_{ph,4}$ parameters fluctuate around 0 (Fig. 6(d)).

IV. Discussion

The trend seen in Fig. 4(a) for the Br*/Br ratio is similar to what has been found in REMPI work[35] for the total ion signal intensities of $Br^+(I(Br^+))$ over that for the total ion signal intensities of $HBr^+(I(HBr^+))$ (*i.e.* $I(Br^+)/I(HBr^+)$) as well as linewidths of ion signal intensities. Both, have been explained to be associated with J' dependent state mixing between the $E(v' = 0)$ Rydberg state and the $V(v' = m + 4)$ and $V(v' = m + 5)$ ion-pair states.[35] This similarity suggests that the relative ion signals for the Br* and Br channels are also indicative of the state mixing. The state mixing between a Rydberg state and an ion-pair vibrational state depends on the state interaction strength, which, to a first approximation, is proportional to the vibrational wavefunction overlap. Furthermore, the mixing, which holds for J' levels of equal values only, increases as the energy difference between the energy levels decreases (see Fig. 4(b)). Thus, the mixing between the $E(v' = 0)$ and the $V(v' = m + 4)$ states decreases as J' increases whereas the mixing between $E(v' = 0)$ and $V(v' = m + 5)$ increases with J'. By comparison, therefore, we conclude that enhanced H^+ signals due to the Br* channel (and also the ionic channels (Fig. 4(a))) relative to that for the Br channel is an indication of a mixing of the $E(v' = 0)$ and V ($V(v' = m + 4)$ and $V(v' = m + 5)$) states or, in other words, that an increased ion-pair character of the $E(v' = 0)$ state favours the Br* and the ionic channels over the Br channel.

As can be seen in Fig. 1, favourable (Franck–Condon wise) transitions to the Rydberg state(s) which correlate with H* + Br* (Br* channel) might in fact occur close to the outer turning point of the V well, *i.e.* to the higher energy component of the $^{1,3}\Sigma([^2\Pi;\sigma^1\pi^3\sigma^{*1}]5p\pi^1)$ states. This could explain why the Br* channel is favoured over the Br channel as the ion-pair character increases. Transitions from shorter internuclear distances (hence smaller V state character) to the $^{1,3}\Pi([B^2\Sigma^+;\sigma^2(\pi_x^1\pi_y^1)\sigma^{*1}]5p\pi^1)$ Rydberg state correlating with H* + Br, on the other hand, might play an important role in the Br channel (see Fig. 1). Considering the close correlation seen in the behaviour of the H^+ signals for the Br* and ionic channels (Fig. 4(a)), there is a reason to believe that these channels originate from the same intermediate state(s). We, therefore, propose that the major contribution to the stepwise ionization *via* the ionic channel formations involves excitation to the higher energy component of the $^{1,3}\Sigma([^2\Pi;\sigma^1\pi^3\sigma^{*1}]5p\pi^1)$ state by excitation (a) in Section I ((b) to a lesser extent) followed by autoionization according to the Auger effect, where the Rydberg electron is removed and the σ* electron transfers back to the σ orbital to form HBr^+ and $HBr^{+*}/^2\Pi_{3/2,1/2}(\sigma^2\pi^3)$, *i.e.*

$$HBr^{\#}\{^{1,3}\Sigma([^2\Pi;\sigma^1\pi^3\sigma^{*1}]5p\pi^1)\} \rightarrow HBr^+/HBr^{+*}\{^2\Pi_{3/2,1/2}(\sigma^2\pi^3)\} + e^-;$$
autoionization

As mentioned in the results section, the $\beta_{f,2}$ value (−0.62) can be compared with the corresponding extreme value of −1 for a perpendicular transition. This suggests that the resonance transition corresponds to a dominating perpendicular two-photon transition (*i.e.* $\Sigma \leftarrow \Pi \leftarrow \Sigma$).[48] This is in agreement with earlier observations by Loock and coworkers who came to the conclusion that the transition involved about 20% contribution of the parallel excitation pathway ($\Sigma \leftarrow \Sigma \leftarrow \Sigma$).[27] Comparison of the β_2 and $\beta_{ph,2}$ values of Fig. 6 shows the effect of performing a two-step excitation analysis rather than an analysis based on a one-step excitation process only. Thus, the β_2's, for the overall process, (Fig. 6(a)) for the signals derived for the Br* and Br channels cross the border value of zero which separates mostly parallel transitions ($0 < \beta_2 < 2$) from mostly perpendicular ones ($-1 < \beta_2 < 0$) as J' changes, whereas the $\beta_{ph,2}$'s, for the second excitation steps are larger than zero in all cases, corresponding to mostly parallel transitions for all J's. Clearly the contribution of a perpendicular transition increases for Br* but decreases for Br in the second excitation step as J' increases, whereas the corresponding transitions *via* HBr^+ and HBr^{+*} are virtually purely parallel in nature, independent of J'. Judging from this and the arguments above, the parallel transitions (Section I(a) and (b)) corresponding to the excitations to the $^{1,3}\Sigma([^2\Pi;\sigma^1\pi^3\sigma^{*1}]5p\pi^1)$ states to form mainly H* + Br* but to a lesser extent H* + Br, are dominant for $J' = 1$–9. The J' dependence of the $\beta_{ph,2}$ values, however, suggests that the contribution of the perpendicular transition (Section I(c)) to $^{1,3}\Pi([B^2\Sigma^+;\sigma^2(\pi_x^1\pi_y^1)\sigma^{*1}]5p\pi^1)$ to form H* + Br increases with J'. Increasing contribution of a perpendicular transition associated with the formation of H* + Br* as J' increases must be associated with curve crossings.

Due to low rotational line intensities for the $V(v' = m + i)$; $i = 4$–10 states, hence inaccuracy in the evaluation of intensity ratios I_Q/I_S and I_Q/I_O (eqn (9)), the corresponding angular distributions could not be analysed according to the two-step formalism described above and used for $E(v' = 0)$. Instead they were analysed by the single step approximation method (eqn (5)). There is, however, a reason to believe that the first step involves a dominating parallel transition as in the case of the resonance excitation to the $E(v' = 0)$ state. Therefore, based on the comparison of the two methods of analysis for the $E(v' = 0)$ state, the β_2 parameters derived for the $V(v' = m + i)$ states can be viewed as lower limit values for the corresponding dissociation steps ($\beta_{ph,2}$). β_2 and β_4 values are plotted in Fig. 6 as a function of i for $J' = 0$. The plot of the anisotropy parameter, β_2 *vs.* i (Fig. 6) for the Br channel reveals two minima (enhanced perpendicular transition contributions) for $i = 5$ and 9. These correspond to the V vibrational states, which, along with the $i = 4$ and 8 states, are closest in energy to the $E(v' = 0)$ and $E(v' = 1)$

states respectively.[16,17] This could be associated with an enhanced E state character, hence increased contribution of the perpendicular transition to the $^{1,3}\Pi([B^2\Sigma^+;\sigma^2(\pi_x^1\pi_y^1)\sigma^{*1}]5p\pi^1)$ state. The sudden drop in β_2 *vs.* i observed for i = 6, (Br* channel), was a bit of a surprise. REMPI spectra of HBr show weak peak structure close to the V(v' = m + 6; J' = 0) band which must be Q lines of a Rydberg state. Ginter *et al.*[9] as well as Callaghan and Gordon[13] have assigned spectra in this region to the f $^3\Delta_1$ Rydberg state. Most likely, therefore, the "sudden" enhanced perpendicular transition contribution observed is associated with a V(v' = m + 6) to Rydberg state interaction, either directly or *via* a gateway Rydberg state. Finally, the transitions *via* HBr^+ and $HBr^{+}*$ are found to be virtually purely parallel in nature analogous to that found for E(v' = 0).

V. Conclusions

Proton photoion images were recorded following (2 + n) REMPI of HBr *via* the mixed E($^1\Sigma^+$) Rydberg and V($^1\Sigma^+$) ion-pair states (the mixed B($^1\Sigma^+$) state) for v' = 0 in the E state and v' = m + i; i = 4–10 in the V state, for a number of rotational levels (J' = J''/Q lines). Kinetic energy release and angular distributions were derived from the data. Four major dissociation channels were detected:

(ia) $HBr^{**}(B,v',J') + h\nu \rightarrow H^* + Br$; Br channel

(ib) $HBr^{**}(B,v',J') + h\nu \rightarrow H^* + Br^*$; Br* channel

(iia) $HBr^{**}(B,v',J') + h\nu \rightarrow HBr^{\#} \rightarrow HBr^{+}*(v^+)$;

$HBr^+(v^+) + h\nu \rightarrow H^+ + Br$ HBr^+ ionic channel

(iib) $HBr^{**}(B,v',J') + h\nu \rightarrow HBr^{\#} \rightarrow HBr^{+}*(v^+)$;

$HBr^{+}*(v^+) + h\nu \rightarrow H^+ + Br^*$ $HBr^{+}*$ ionic channel

The KER and angular distributions for the different channels vary largely, depending on v' and J' for excitations to the V and the E states. The KER spectra were assigned and found to agree with previous work. Br*/Br KER peak ratios in comparison with mass resolved REMPI spectra data suggest that channel (ia) is largely associated with the E Rydberg state character of the mixed state whereas the other channels (ia, iia and iib) are to a large extent associated with the V ion-pair state character. Angular distributions were analyzed to determine anisotropy parameters by a single as well as a two-step photoexcitation formalism[48] where possible. The analysis revealed a dominating perpendicular transition for the resonance excitation steps, but mostly parallel transitions for the dissociation steps with some perpendicular contribution character for the dissociation steps, varying with J' for the E(v' = 0) state and with v' for the V(v' = m + i) states for channels (ia) and (ib). Our results suggest that the corresponding major parallel and perpendicular photoexcitation transitions, following the resonance excitations, involve transitions to singlet or triplet superexcited Rydberg states, which converge to the excited ionic states $B^2\Sigma^+$ and $^2\Pi_{3/2,1/2}$ and which correlate to the neutral fragments H*(n = 2) + Br($^2P_{3/2}$) and H*(n = 2) + Br*($^2P_{1/2}$), *i.e.*

$$HBr^{**}\{V^1\Sigma(\sigma^1\pi^4\sigma^{*1})\} + h\nu \rightarrow HBr^{\#}\{^{1,3}\Sigma([^2\Pi;\sigma^1\pi^3\sigma^{*1}]5p\pi^1)\}$$

parallel transition (ib, iia, iib)

$$HBr^{**}\{E^1\Sigma([^2\Pi;\sigma^2\pi^3]5p\pi^1)\} + h\nu \rightarrow HBr^{\#}\{^{1,3}\Pi([B^2\Sigma^+;\ \sigma^2(\pi_x^1\pi_y^1)\sigma^{*1}]5p\pi^1)\};$$ perpendicular transition (ia)

The major formation of $HBr^+(3/2,v^+)$ and $HBr^{+}*(1/2,v^+)$ (iia, iib) then involves autoionization according to the Auger effect,

$$HBr^{\#}\{^{1,3}\Sigma([^2\Pi;\sigma^1\pi^3\sigma^{*1}]5p\pi^1)\} \rightarrow HBr^+/HBr^{+}*\{^2\Pi_{3/2,1/2}(\sigma^2\pi^3)\} + e^-$$

Acknowledgements

The financial support of the University Research Fund, University of Iceland and the Icelandic Science Foundation (Grant No. 130259-051) is gratefully acknowledged. This work was supported by Greek Secretariat for Research and Technology programs ERC03:ITSSUED and THALIS:ISEPUMA, co-financed by EU (European Social Fund) and national funds under NSRF2007-2013. PS gratefully acknowledges support from an EU Marie Curie Reintegration Grant (GPSDI, Grant No. PIRG07-GA-2010-268305). DZ gratefully acknowledges EU Marie Curie IAPP program SOFORT (GA 251598). The research leading to these results has also received funding from LASERLAB-EUROPE (grant agreement no. 284464, EC's Seventh Framework Programme). We wish to thank Andri Þór Jóhannsson for execution of the graphical abstract.

References

1 W. C. Price, *Proc. R. Soc. London, Ser. A*, 1938, **167**, 216.
2 S. G. Tilford, M. L. Ginter and J. T. Vanderslice, *J. Mol. Spectrosc.*, 1970, **33**, 505.
3 M. L. Ginter and S. G. Tilford, *J. Mol. Spectrosc.*, 1970, **34**, 206.
4 S. G. Tilford, M. L. Ginter and A. M. Bass, *J. Mol. Spectrosc.*, 1970, **34**, 327.
5 S. G. Tilford and M. L. Ginter, *J. Mol. Spectrosc.*, 1971, **40**, 568.
6 J. B. Nee, M. Suto and L. C. Lee, *J. Chem. Phys.*, 1986, **85**, 719.
7 J. B. Nee, M. Suto and L. C. Lee, *J. Chem. Phys.*, 1986, **85**, 4919.
8 D. S. Ginter and M. L. Ginter, *J. Mol. Spectrosc.*, 1981, **90**, 177.
9 D. S. Ginter, M. L. Ginter and S. G. Tilford, *J. Mol. Spectrosc.*, 1981, **90**, 152.
10 D. S. Green, G. A. Bickel and S. C. Wallace, *J. Mol. Spectrosc.*, 1991, **150**, 303.
11 D. S. Green, G. A. Bickel and S. C. Wallace, *J. Mol. Spectrosc.*, 1991, **150**, 354.

12 D. S. Green, G. A. Bickel and S. C. Wallace, *J. Mol. Spectrosc.*, 1991, **150**, 388.
13 R. Callaghan and R. J. Gordon, *J. Chem. Phys.*, 1990, **93**, 4624.
14 S. T. Pratt and M. L. Ginter, *J. Chem. Phys.*, 1995, **102**, 1882.
15 S. A. Wright and J. D. McDonald, *J. Chem. Phys.*, 1994, **101**, 238.
16 Á. Kvaran, Á. Logadóttir and H. Wang, *J. Chem. Phys.*, 1998, **109**, 5856.
17 Á. Kvaran, H. Wang and Á. Logadóttir, *J. Chem. Phys.*, 2000, **112**, 10811.
18 Á. Kvaran, B. G. Waage and H. Wang, *J. Chem. Phys.*, 2000, **113**, 1755.
19 Á. Kvaran, H. Wang and B. G. Waage, *Can. J. Phys.*, 2001, **79**, 197.
20 Á. Kvaran and H. Wang, *Mol. Phys.*, 2002, **100**, 3513.
21 Á. Kvaran and H. Wang, *J. Mol. Spectrosc.*, 2004, **228**, 143.
22 K. Matthiasson, H. S. Wang and A. Kvaran, *J. Mol. Spectrosc.*, 2009, **255**, 1.
23 J. Long, H. Wang and A. Kvaran, *J. Mol. Spectrosc.*, 2012, **282**, 20.
24 H. R. Hrodmarsson, H. S. Wang and A. Kvaran, *J. Mol. Spectrosc.*, 2013, **290**, 5.
25 C. Romanescu, S. Manzhos, D. Boldovsky, J. Clarke and H. Loock, *J. Chem. Phys.*, 2004, **120**, 767.
26 C. Romanescu and H. P. Loock, *Phys. Chem. Chem. Phys.*, 2006, **8**, 2940.
27 C. Romanescu and H. P. Loock, *J. Chem. Phys.*, 2007, **127**, 124304.
28 A. I. Chichinin, C. Maul and K. H. Gericke, *J. Chem. Phys.*, 2006, **124**, 224324.
29 S. Kauczok, C. Maul, A. I. Chichinin and K. H. Gericke, *J. Chem. Phys.*, 2010, **133**, 24301.
30 C. Maul, A. I. Chichinin and K.-H. Gericke, *J. At., Mol., Opt. Phys.*, 2011, **2011**, 410108.
31 Á. Kvaran, K. Matthíasson, H. Wang, A. Bodi and E. Jonsson, *J. Chem. Phys.*, 2008, **129**, 164313.
32 A. Kvaran, K. Matthiasson and H. Wang, *J. Chem. Phys.*, 2009, **131**, 044324.
33 K. Matthiasson, J. Long, H. Wang and A. Kvaran, *J. Chem. Phys.*, 2011, **134**, 164302.
34 J. Long, H. R. Hrodmarsson, H. Wang and A. Kvaran, *J. Chem. Phys.*, 2012, **136**, 214315.
35 J. Long, H. Wang and A. Kvaran, *J. Chem. Phys.*, 2013, **138**, 044308.
36 H. R. Hróðmarsson, H. Wang and Á. Kvaran, *J. Chem. Phys.*, 2014, **140**, 244304.
37 M. Poretskiy, A. I. Chichinin, C. Maul and K.-H. Gericke, *Phys. Chem. Chem. Phys.*, 2014, **16**, 19741.
38 A. Banichevich, R. Klotz and S. D. Peyerimhoff, *Mol. Phys.*, 1992, **75**, 173.
39 C. R. Gebhardt, T. P. Rakitzis, P. C. Samartzis, V. Ladopoulos and T. N. Kitsopoulos, *Rev. Sci. Instrum.*, 2001, **72**, 3848.
40 V. Papadakis and T. N. Kitsopoulos, *Rev. Sci. Instrum.*, 2006, **77**, 5.
41 P. M. Regan, S. R. Langford, A. J. Orr-Ewing and M. N. R. Ashfold, *J. Chem. Phys.*, 1999, **110**, 281.
42 NIST (National Institute of Standards and Technology).
43 A. J. Yencha, A. J. Cormack, R. J. Donovan, K. P. Lawley, A. Hopkirk and G. C. King, *Chem. Phys.*, 1998, **238**, 133.
44 *NIST Chemistry WebBook*; NIST (National Institute of Standards and Technology) Chemistry WebBook.
45 F. Aguirre and S. T. Pratt, *J. Chem. Phys.*, 2004, **121**, 9855.
46 T. P. Rakitzis, *Chem. Phys. Lett.*, 2001, **342**, 121.
47 S. Manzhos, C. Romanescu, H. P. Loock and J. G. Underwood, *J. Chem. Phys.*, 2004, **121**, 11802.
48 A. I. Chichinin, P. S. Shternin, N. Godecke, S. Kauczok, C. Maul, O. S. Vasyutinskii and K. H. Gericke, *J. Chem. Phys.*, 2006, **125**, 034310.
49 R. N. Zare, *Angular momentum: Understanding spatial aspects in chemistry and physics*, Wiley, 1988.

Article 5

State interactions and illumination of hidden states through perturbations and observations of new states: High energy resonance enhanced multiphoton ionization of HI.

Helgi Rafn Hróðmarsson, Huasheng Wang, and Ágúst Kvaran

Journal of Chemical Physics. **142**. 244312 (2015).

DOI: 10.1063/1.4922892

Helgi Rafn Hróðmarsson independently developed the research concept and performed all the experiments along with Huasheng Wang. Helgi performed all of the data analysis and independently wrote the first manuscript. He contributed to editing until publication.

State interactions and illumination of hidden states through perturbations and observations of new states: High energy resonance enhanced multiphoton ionization of HI

Helgi Rafn Hróðmarsson, Huasheng Wang, and Ágúst Kvaran[a)]
Science Institute, University of Iceland, Dunhagi 3, 107 Reykjavík, Iceland

(Received 24 March 2015; accepted 12 June 2015; published online 30 June 2015)

Hydrogen iodide, a Hund's case (c) molecule, serves as a benchmark compound for studying rich molecular state interactions between Rydberg and valence states as well as between Rydberg states at high energies (72 300–74 600 cm^{-1}) by mass resolved resonance enhanced multiphoton ionization (REMPI). Perturbations in the spectra appearing as deformations in line-positions, line-intensities, and linewidths are found to be either due to near-degenerate or non-degenerate interactions, both homogeneous and heterogeneous in nature. Perturbation analyses allow indirect observation as well as characterization of "hidden states" to some extent. Furthermore, new observable spectral features are assigned and characterized. © *2015 AIP Publishing LLC.* [http://dx.doi.org/10.1063/1.4922892]

I. INTRODUCTION

The electronic spectra of the hydrogen halides are of particular interest within the spectroscopic community due to the clarity and resolution of their spectral structures as well as the state interactions embedded within as perturbation effects. The spectra provide clear examples of interactions between Rydberg and valence states of varying strength and nature. They provide information about various photofragmentation and photoionization pathways which are of interest to a variety of other related fields such as atmospheric chemistry,[1,2] astrochemistry,[3,4] and photochemical syntheses.[5]

In addition to standard absorption spectroscopic studies of the hydrogen halides,[6–15] resonance enhanced multiphoton ionization (REMPI) analyses have been widely used, allowing states, which are regularly inaccessible by single photon selection rules to be formed. Most REMPI experiments have been conducted on HCl,[16–33] whereas a handful of studies of HBr[26,27,33–39] and HI[40–45] have been performed. Furthermore, some REMPI coupled velocity map imaging (VMI) studies have been performed on the hydrogen halides, highlighting various photoionization and photofragmentation pathways.[46–52]

The large atomic mass of iodine makes HI particularly interesting amongst the hydrogen halides due to its strong spin-orbit interactions. For the lighter hydrogen halides, such as HF and HCl, the spin and electronic orbital motions are coupled strongly to the molecular axis to give well defined projections on the internuclear axis, which along with the angular momentum of the nuclear motion (**R**) give the total angular momentum, **J** according the to Hund's case (a) classification. For HI, on the other hand, the coupling between **L** and **S** is stronger than the interaction with the internuclear axis, which makes only Ω well defined, resulting in the Hund's case (c) classification.[53] Nevertheless, it has become a custom in the literature to use analogous and comparable state assignments, more appropriate for Hund's cases (a) and (b), for all the hydrogen halides.[6–15]

The rotational spectroscopy of HI was first studied in the pioneering work by Price.[54] Later absorption experiments constructed a coherent database of excited Rydberg and ion-pair states of HI[13–15] as well as DI[14,15,55] and addressed several observed perturbations seen in the spectra. The first REMPI spectra of HI were published in 1994–1995.[40,41] These studies included new observations of spectral structures, but with some tentative assignments. These have recently been revisited with an emphasis placed on new observations as well as state interactions between Rydberg and valence (ion-pair and repulsive) states.[44,45] Among recent findings, the utilization of perturbation effects was used to illuminate interactions between an ion-pair state and a state that was "hidden" from REMPI detection.[45] The "hidden" state could either be a non-observable state due to selection rules or a state experiencing weak transition probabilities, which could possibly be detectable by other means, such as in standard absorption.

We will now present REMPI data of HI for the high energy two-photon excitation region of 72 300–74 600 cm^{-1} and analyses relevant to state interactions between Rydberg and valence states as well as between Rydberg states. Furthermore, new observations both for observable and "hidden" states are presented.

II. EXPERIMENTAL

The experimental apparatus as well as relevant equipment parameters are similar to that described in previous publications.[39,44,45] Therefore, only a brief experimental discussion will be given here.

Mass resolved REMPI data for a HI molecular beam were recorded. The beam was created by a jet expansion of a pure gas sample through a pulsed nozzle and ions

a)Author to whom correspondence should be addressed. Electronic mail: agust@hi.is. Telephone: +354-525-4672 and +354-525-4800. Fax: +354-552-8911.

TABLE I. Observed (2 + 1) REMPI iodine atomic lines used for laser calibration.

Configuration	Term	J	Ion core	Positions (cm^{-1})[64]
$5s^25p^4(^1D_2)6p$	$^2[1]^\circ$	1/2	$^2P_{1/2}$	72 098.6
$5s^25p^4(^3P_2)5g$	$^2[5]$	11/2 and 9/2	$^2P_{1/2}$	72 285.0
$5s^25p^4(^3P_2)5g$	$^2[4]$	9/2 and 7/2	$^2P_{1/2}$	72 285.1
$5s^25p^4(^1D_2)6p$	$^2[2]^\circ$	3/2	$^2P_{1/2}$	72 436.8
$5s^25p^4(^3P_1)6p$	$^2[2]^\circ$	5/2	$^2P_{3/2}$	72 529.2
$5s^25p^4(^3P_1)6p$	$^2[2]^\circ$	3/2	$^2P_{3/2}$	72 806.4
$5s^25p^4(^3P_2)9p$	$^2[2]^\circ$	3/2	$^2P_{1/2}$	73 013.2
$5s^25p^4(^3P_2)9p$	$^2[2]^\circ$	5/2	$^2P_{1/2}$	73 021.5
$5s^25p^4(^3P_2)9p$	$^2[3]^\circ$	5/2	$^2P_{1/2}$	73 056.1
$5s^25p^4(^3P_2)9p$	$^2[3]^\circ$	7/2	$^2P_{1/2}$	73 058.3
$5s^25p^4(^3P_2)8d$	$^2[1]$	3/2	$^2P_{1/2}$	73 088.0
$5s^25p^4(^3P_2)8d$	$^2[1]$	1/2	$^2P_{1/2}$	73 091.0
$5s^25p^4(^3P_2)9p$	$^2[1]^\circ$	1/2	$^2P_{1/2}$	73 117.9
$5s^25p^4(^3P_1)6p$	$^2[1]^\circ$	1/2	$^2P_{3/2}$	73 387.2

were directed into a time-of-flight tube and detected by a microchannel plate (MCP) detector to record the ion yield as a function of mass and laser radiation wavenumber. Mass signals were recorded by a LeCroy Wavesurfer 44MXs-A, 400 MHz storage oscilloscope. Tunable excitation radiation was generated by an excimer laser-pumped dye laser system, using a Lambda Physik COMPex 205 excimer laser and a Coherent ScanMatePro dye laser, applying a C-540 dye. Laser power was minimized to prevent saturation effects and power broadening. Laser calibration was based on observed (2 + 1) REMPI iodine peaks (see Table I). The accuracy of the calibration was found to be about $\pm 1.0\ cm^{-1}$ on a two-photon wavenumber scale.

III. PERTURBATIONS

For molecular systems, evaluation of the total Hamiltonian can be very onerous. In order to simplify its expression, the Born-Oppenheimer approximation is commonly utilized which involves omitting terms which are the source of observed perturbations in recorded spectra.[56] These are the electronic operator, $\mathbf{H^{el}}$, which is representative of interactions between electronic states, the vibrational operator, $\mathbf{T^N}$, which is representative of interactions between vibrational states, and the spin-orbit operator, $\mathbf{H^{SO}}$, which is representative of interactions between the electron spin and its orbital motion, all of which are homogeneous ($\Delta\Omega = 0$) in nature. The L-uncoupling operator, $(-1/2\mu R^2)(\mathbf{J^+L^-} + \mathbf{J^-L^+})$, and the S-uncoupling operator, $(-1/2\mu R^2)(\mathbf{J^+S^-} + \mathbf{J^-S^+})$, are responsible for heterogeneous ($\Delta\Omega \neq 0$) interactions. The state interaction strength (i.e., the perturbation matrix element, W_{12}, for electronic states, 1 and 2)[57] is independent of the total angular momentum quantum number, J', for homogeneous interactions, but J' dependent for heterogeneous interactions.[56] Such interactions appear as energy level repulsion effects for levels of the interacting states with the same J' values, the degree of which depends on the interaction strength (W_{12}) and the energy mismatch ($\Delta E_{J'}$) of the interacting J' levels,[29,31–33,45,56,58]

$$\Delta E_{J'} = E_{J'}(1) - E_{J'}(2) \tag{1a}$$

for

$$E_{J'}(i) = \frac{1}{2}\left(E^0_{J'}(1) + E^0_{J'}(2)\right) \pm \frac{1}{2}\left[4\,|W_{12}|^2 + \left(E^0_{J'}(1) - E^0_{J'}(2)\right)^2\right]^{1/2}, \quad i = 1,2, \tag{1b}$$

where $E^0_{J'}(1)$ and $E^0_{J'}(2)$ are the zero-order energy levels for the unperturbed states 1 and 2. Furthermore, the interaction involves mixing of the states, fraction of which (c^2(i)) also depends on W_{12} and $\Delta E_{J'}$[29,31,32,45,56,58] as

$$c^2(i) = \frac{1}{2} \pm \frac{\sqrt{|\Delta E_{J'}|^2 - 4|W_{12}|^2}}{2\,|\Delta E_{J'}|}, \quad \mathrm{i} = 1,2. \tag{2}$$

Repulsion effects and the level of state mixing increase with increasing W_{12} and decreasing $\Delta E_{J'}$. In the limit of $\Delta E_{J'} \approx 0$ where solutions are approximated by "degenerate state perturbation theory"[59,60] which yields very large energy level shifts and state mixings, characteristic for the "near-degenerate" J' levels. Hereby, we shall refer to such cases as "near-degenerate interactions." Furthermore, to distinguish between such cases and cases where interacting levels are non-degenerate[59,60] and perturbations will be less sharply J' dependent, we shall refer to "non-degenerate interactions." We wish to use these expressions to replace the less clear expressions "near-resonance-" and "off-resonance-" interactions, respectively, which have been used before.[29,31–33,39,44–46,58,61]

Interactions between Rydberg and ion-pair states of the hydrogen halides appear distinctively as perturbations in rotationally resolved REMPI spectra, i.e., as deviations in the expected spectral structure of unperturbed states. These deviations can show as line shifts (LS-effects) as a result of the energy level shifts and/or as line-intensity alterations (LI-effects) due to the state mixing which can cause alterations in ion formation paths.[45] Furthermore, perturbations can result in alterations in linewidths on account of different predissociation processes of the mixed states (LW-effect). Observed perturbations, in the spectra of the hydrogen halides, can be classified in the following way:

(a) Weakest effects are found for heterogeneous ($\Delta\Omega \neq 0$), spin forbidden ($\Delta\Sigma \neq 0$) interactions resulting in LI-effects for near-degenerate interactions.[39,44,45,58]
(b) Intermediately strong effects are observed for heterogeneous ($\Delta\Omega \neq 0$), spin conserved ($\Delta\Sigma = 0$) interactions, which typically result in LS-effects for near-degenerate interactions and LI-effects for both near- and non-degenerate interactions.[39,44,45,58]
(c) Strongest effects are seen among homogeneous interactions ($\Delta\Omega = 0$), which show both as LS- and LI- effects both for near-degenerate and non-degenerate interactions.[44,45,58]

Rotational constants for ion-pair vibrational states generally are smaller than those for the interacting Rydberg states. Hence, the energy spacing between J' levels ($\Delta E_{J',J'-1}$) for the Rydberg states is larger than corresponding levels for the ion-pair states.[31–33,44–46,58,61,62] Therefore, near-degenerate interactions, for $\Delta E_{J'} \approx 0$, typically, are observed for one or two J' levels only, whereas non-degenerate interactions can

be observed for a range of J' levels both to higher and lower energies with increasing $|\Delta E_{J'}|$ as J' deviates further away from the near-degenerate levels.[62] Therefore, the non-degenerate interactions show as gradually decreasing LS- and LI-effects, as the J's deviate further away from the near-degenerate J's.

A. LS-effects

To a first approximation, a linear behavior is expected for plots of energy level spacing ($\Delta E_{J',J'-1} = E(J') - E(J'-1)$) vs. J'. Such linearity with a slope of $2B_{v'}$, where $B_{v'}$ is the v′ dependent rotational constant, implies an unperturbed state. Deviations from linearity constitute LS-effects, which are prevalent in (b) and (c) cases mentioned above. The presence of curvatures or irregular shapes in such plots indicates medium to strong state interactions. In order to visualize irregular shapes due to effects of possible near-degenerate interactions more clearly, "reduced term value plots" were also made.[62] These show the difference between observed level energies ($E_{J'}$) and energies, $E^0_{J'}$, given by the expression

$$E^0_{J'} = \nu^0 + B'J'(J'+1) - D'J'^2(J'+1)^2 \qquad (3)$$

for parameters ν^0, B', and D' derived either by deperturbation analysis or by the functional (Eq. (3)) fit to the data points.

B. LI-effects

The REMPI data of the hydrogen halides for resonance excitations to Rydberg or ion-pair states consist of ion signals from both the parent molecule (HX^+) and the atomic fragments (X^+ and H^+). The integrated signals of each respective ion mass reveal relative fractions of the respective formation pathways. The strengths of the ion signals are determined by rates of formation of the resonance excited states, which can involve interference effects as well as the rates of ionization. In the case of a Rydberg to ion-pair state interaction, a relatively large HX^+ signal evidences a large Rydberg state character of the resonance state, whereas a relatively large X^+ signal evidences its large ion-pair state character or an affinity for dissociation. By exploring alterations in the intensity ratio, $I[X^+]/I[HX^+]$ rather than the absolute ion signals ($I[X^+], I[HX^+]$) as a function of J', mixing/interactions of Rydberg and ion-pair states, can be highlighted. Thus, an enhanced intensity ratio, $I[X^+]/I[HX^+]$, with J', for Rydberg resonance states, gives an indication of increased mixing/interactions with an ion-pair state, whereas significant lowering in the ratio would, on the other hand, evidence the opposite, i.e., decreased mixing/interactions with an ion-pair state. It has been found that the overall sensitivity of the LI-effects generally is greater than LS-effects. Thus, for weakly interacting states, there may be a distinctive lack of LS-effects, whereas significant LI-effects may be observed.[31,32,45,61]

C. LW-effects

LW-effects appear as J' dependent alterations in the linewidth of ion signals. To a first approximation, linewidths are inversely proportional to the lifetimes of the resonance excited states and provide a lower limit to their lifetimes. Thus, LW-effects can give indications of lifetimes of rotational levels prior to predissociation. Such predissociation is mainly determined by the rates of crossing from bound to repulsive states. Rydberg states are usually in close proximity to or are crossed by one or more repulsive states whereas the internuclear distance of ion-pair states is too large for curve crossings between ion-pair states and repulsive states to be possible. Therefore, ion-pair states require interactions with Rydberg states, which act as gateway states prior to predissociation.[45,58] Linewidths of ion-pair state spectra are frequently found to be larger (hence lifetimes shorter) than those of Rydberg states, close in energy, suggesting that effective predissociation of ion-pair states can involve several gateway Rydberg states. In REMPI studies of HI,[40,41,44,45] there is a distinct lack of appearances of Rydberg states with $\Omega = 1$. It has been suggested that these states play an important role as gateway states for predissociation processes,[45] acting as dark perturbers or hidden states.

It has been shown that the appearance of LW-effects is intrinsically linked with the appearance of LS- and LI-effects for HBr[58] and HI.[44,45] Thus, the LW-effects are found to show close, but not necessarily equivalent, correspondence to that observed from LS- and LI-effects in terms of J' quantum level dependences.

IV. RESULTS AND ANALYSIS

A. Spectral observations

Figure 1 shows assigned REMPI spectra for HI in the two-photon resonance excitation region of 72 300–74 600 cm^{-1}. A number of new and reassigned Rydberg and ion-pair vibrational states have been detected and analyzed (see details below). The states' characteristics are listed in Tables II and III. $nl\lambda$ type labels are used to characterize the Rydberg electrons, where n is the principal quantum number and the l and λ quantum numbers are replaced by the relevant atomic and molecular orbital letters, respectively. The ion core ($\sigma^2\pi^3$) involves two spin-orbit states, i.e., $\Omega = 1/2, 3/2$.

New Rydberg states were observed with band origins at 72 324.0 cm^{-1} and 73 081.7 cm^{-1} where weak, previously unreported structures, were found in the HI^+ ion spectra (see Figs. 1(a) and 1(b)). These are assigned to the $F^1\Delta_2(v' = 1)$ and $P^1\Delta_2(v' = 0)$ states, respectively. At 72 945.0 cm^{-1} (see Fig. 1(c)), another weak structure was observed in the I^+ spectra. This structure is assigned to the $m^3\Pi_1(v' = 1)$ state. Whereas, it has been detected in absorption,[13] it has not been seen in REMPI before. At 73 384.2 cm^{-1}, a strong, clearly resolved, rotational feature is observed. This feature has previously been reported, unassigned in REMPI,[41] and is here assigned to the $O^1\Sigma^+(v' = 1)$ state (Fig. 1(d)). At 72 923.0 cm^{-1} and 73 110.8 cm^{-1}, new spectral structures were observed mainly in the I^+ and H^+ spectra. Both reveal small rotational constants, $B_{v'}$, and have been assigned to the $V^1\Sigma^+(v' = m + 11)$ and $V^1\Sigma^+(v' = m + 12)$ ion-pair states (see Figs. 1(b) and 1(c)). It should be noted that m denotes an unknown positive integer, since the absolute values of the v′s are uncertain. All other subsequent numberings of previously

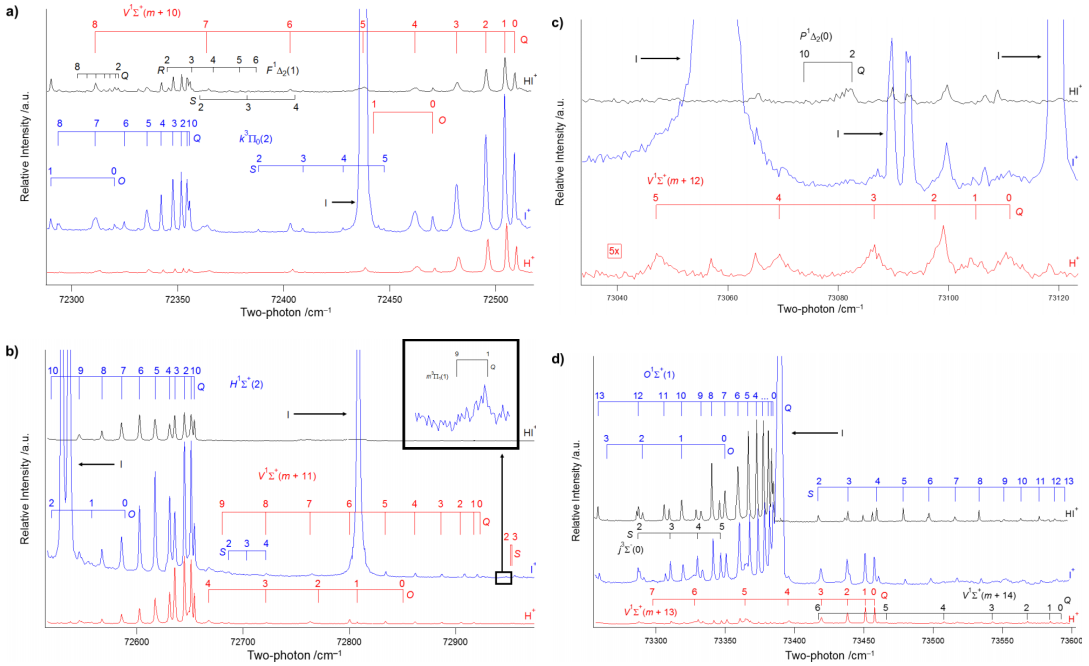

FIG. 1. REMPI spectra for H^+, I^+, and HI^+ and J' assignments of rotational peaks corresponding to two-photon resonance excitation from the ground state to $F^1\Delta_2(v'=1)$ (a), $k^3\Pi_0(v'=2)$ (a), $V^1\Sigma^+(v'=m+10)$ (a); $H^1\Sigma^+(v'=2)$ (b), $V^1\Sigma^+(v'=m+11)$ (b), $m^3\Pi_1(v'=1)$ (b); $P^1\Delta_2(v'=0)$ (c), $V^1\Sigma^+(v'=m+12)$ (c); $j^3\Sigma^-(v'=0)$ (d), $O^1\Sigma^+(v'=1)$ (d), $V^1\Sigma^+(v'=m+13)$ (d), and $V^1\Sigma^+(v'=m+14)$ (d). (2+1) REMPI iodine atomic lines are indicated (see Table I). The H^+ portion of the REMPI spectrum in (c) is magnified (×5).

assigned ion-pair states,[13] upwards from and including the previously assigned $V(m+11)$ ion-pair state, are, therefore, re-assigned as $V(m+i+2)$, where "i" is a positive integer, representing the previous vibrational assignment made by Ginter *et al.*,[13] e.g., $V(m+11)$ is re-assigned as $V(m+13)$ and $V(m+12)$ is re-assigned as $V(m+14)$. Peak positions in the REMPI spectra of all newly observed states are listed in Table IV.

For the subsequent analyses of our observations, the excited states, whose spectra display various types of state interactions, are grouped into four interacting systems. These are the following:

1. The $F^1\Delta_2(v'=1)$, $k^3\Pi_0(v'=2)$, $V^1\Sigma^+(v'=m+10)$ system.
2. The $V^1\Sigma^+(v'=m+10)$, $H^1\Sigma^+(v'=2)$, $V^1\Sigma^+(v'=m+11)$, $m^3\Pi_1(v'=1)$ system.
3. The $P^1\Delta_2(v'=0)$ and $V^1\Sigma^+(v'=m+12)$ states.
4. The $O^1\Sigma^+(v'=1)$, $V^1\Sigma^+(v'=m+13)$, $V^1\Sigma^+(v'=m+14)$, $V^1\Sigma^+(v'=m+15)$ system.

1. The $F^1\Delta_2(v'=1)$, $k^3\Pi_0(v'=2)$, $V^1\Sigma^+(v'=m+10)$ system

Fig. 1(a) shows assigned REMPI spectra for the states of concern. Fig. 2(a) shows the rotational energy levels derived from the spectra. The reasoning behind the assignment of the 72 324.0 cm^{-1} band to the $F^1\Delta_2(1)$ Rydberg state, as mentioned above, is manifold. First, the rotational structure, showing clear Q, R, and S lines for the lowest J' quantum

TABLE II. MO configurations, term symbols, ion core configurations, band origins, rotational parameters, quantum defects, and relative intensities for all Rydberg states observed in the 72 300–74 600 cm^{-1} region.

MO configuration	Term symbols	Ion core	ν^0 (cm^{-1})		$B_{v'}$ (cm^{-1})		$D_{v'}$ (cm^{-1})		Quantum defect, δ_l	Intensity
			This work	Others[13]	This work	Others[13]	This work	Others[13]		
$(\sigma^2\pi^3)6p\pi$	$F^1\Delta_2(1)$	$^2\Pi_{1/2}$	72 324.0	…	6.13	…	0.000 3	…	3.16	w
$(\sigma^2\pi^3)5d\delta$	$k^3\Pi_0(2)$	$^2\Pi_{3/2}$	72 355.6	72 353.1	5.86	5.650	0.004 2	0.000 549	2.35	s
$(\sigma^2\pi^3)5d\pi$	$H^1\Sigma^+(2)$	$^2\Pi_{3/2}$	72 654.3	72 650.8	5.19	5.29	0.000 0	0.000 396	2.32	vs
$(\sigma^2\pi^3)7s\sigma$	$m^3\Pi_1(1)$	$^2\Pi_{3/2}$	72 945.0	72 924.8	6.16	6.205	−0.001 6	0.000 463	4.09	vw
$(\sigma^2\pi^3)4f\pi$	$P^1\Delta_2(0)$	$^2\Pi_{1/2}$	73 081.7	…	6.35	…	0.000 22	…	0.80	vw
$(\sigma^2\pi^3)5d\delta$	$k^3\Pi_1(2)$	$^2\Pi_{3/2}$	73 176.7	73 180.7	6.13	6.034	0.002 3	0.000 872	2.27	m
$(\sigma^2\pi^3)5d\pi$	$j^3\Sigma^-(0)$	$^2\Pi_{1/2}$	73 252.0	73 254.9	5.63	5.706	0.004 6	0.004 75	1.77	vs
$(\sigma^2\pi^3)4f\pi$	$O^1\Sigma^+(1)$	$^2\Pi_{3/2}$	73 384.2	73 383.6	5.70	5.819	0.000	0.000 446	1.04	s

TABLE III. Band origins, rotational parameters, and relative intensities for all ion-pair states observed in the 72 300–74 600 cm^{-1} region.

Ion-pair state,	ν^0 (cm^{-1})		$B_{v'}$ (cm^{-1})		$D_{v'}$ (cm^{-1})		
$V(m+i)$	This work	Others[13]	This work	Others[13]	This work	Others[13]	Intensity
$i=10$	72 508.8	72 506.0	4.25	4.106	0.008 0	0.001 47	s
$i=11$	72 923.0	...	3.43	...	0.001 9	...	m
$i=12$	73 110.8	...	4.34	...	0.001	...	vw
$i=13$	73 459.1	73 457.8	4.52	3.177	0.008 9	−0.002 37	m
$i=14$	73 590.8	73 589.5	2.23	2.294	0.000	−0.001 15	m
$i=15$	73 831.8	73 822.7	4.14	3.769	0.009	−0.000 225	m

level, $J'=2$, is a clear indication of an $\Omega=2$ state. Second, its band origin is 2100.4 cm^{-1} higher than that for the $F^1\Delta_2(0)$ state,[44] which is close to that to expect for an energy difference between $v'=0$ and 1 levels of a pure Rydberg state. For comparison, the energy difference between the $v'=0$ and 1 levels of the ground state ion is 2140 cm^{-1}.[63] Third, spectral analyses give a rotational constant $B_{v'}$ (6.13 cm^{-1}) close to that for the ground state (6.43 cm^{-1})[64] and slightly less than that for the $F^1\Delta_2(0)$ state.[44] Finally, the REMPI spectral structure was mainly found for the HI^+ ions, further supporting the claim of a pure Rydberg state (see Sec. III).

a. LS-effects. Fig. 2(b) shows the spacing between the rotational levels ($\Delta E_{J',J'-1}$) for the $F^1\Delta_2(1)$ and $k^3\Pi_0(2)$ Rydberg states as a function of J' (see also supplementary material in Ref. 62). Whereas no significant deviation from linearity is seen in the plot for the $F^1\Delta_2(1)$ state, a negative curvature is observed for the $k^3\Pi_0(2)$ state. This suggests that the $F^1\Delta_2(1)$ state experiences negligible or very small state interactions, whereas the $k^3\Pi_0(2)$ state undergoes increasing non-degenerate interactions with J'. An inspection of the energy level diagram (Fig. 2(a)) reveals that such an effect is to be expected for an interaction with the $V(m+10)$ state as the spacing between quantum levels with equal J' quantum numbers gradually decreases as J' increases from 0 to 8.

b. LI-effects. The intensity ratio, $I[I^+]/I[HI^+]$, derived from the Q lines for the $k^3\Pi_0(2)$ state, shows a gradual increase with J' from $J'=0$ to 8 with the exception of $J'=7$ (Fig. 2(c)). This indicates that the $k^3\Pi_0(2)$ state experiences increased mixing with the $V(m+10)$ state as J' increases. Furthermore, based on the rotational energy level diagram (see Fig. 2(a)), a near-degenerate interaction between the $k^3\Pi_0(2)$ and the $F^1\Delta_2(1)$ states might be expected for $J'=7$ (and for $J'=8$). Therefore, the drop in the intensity ratio for $J'=7$ is most probably due to mixing of the $k^3\Pi_0(2)$ and $F^1\Delta_2(1)$ states, resulting in changed formation rates of the I^+ and/or HI^+ ions, thus allowing weak near-degenerate interactions, not detectable by line shifts, to be observed. An interaction between the $k^3\Pi_0(2)$ ($\Omega=0$) and the $F^1\Delta_2(1)$ ($\Omega=2$) states, however, requires mixing with an $\Omega=1$ state to fulfill the requirement of $|\Delta\Omega|=1$ state interactions.[56]

c. LW-effects. Fig. 3 shows linewidths of Q rotational lines of spectra for the $k^3\Pi_0(2)$ state (for I^+ ions) and the $V(m+10)$ state (H^+). Similar looking graphs were obtained for other ions (HI^+ for $k^3\Pi_0(2)$, and HI^+ and I^+ for $V(m+10)$). Significant line broadenings are observed for $J'=5$ and $J'=7$–8 in the case of $k^3\Pi_0(2)$, and for $J'\sim4$ and $J'=7$–8 in the case of $V(m+10)$. Generally, the linewidths of the $V(m+10)$ state are larger than the linewidths of the $k^3\Pi_0(2)$ state for $J'=0$–6. They are, however, comparable for $J'=7$–8 within experimental error. These observations can be interpreted in the following way, assuming that variations in the linewidths are determined by a combination of bound state interactions and/or predissociation effects (see above in Sec. III). First, based on the above interpretations of the LS- and LI-effects, the enhanced linewidth for $J'=7(8)$ is most probably associated with the $J'=7$ near-degenerate interaction between the $k^3\Pi_0(2)$ and $F^1\Delta_2(1)$ Rydberg states via a mixed $\Omega=1$ state. Furthermore, as seen from Fig. 2(a),

TABLE IV. Rotational lines for HI due to two-photon resonance transitions to $F^1\Delta_2(v'=1)$, $P^1\Delta_2(v'=0)$, $V^1\Sigma^+(v'=m+12)$, and $V^1\Sigma^+(v'=m+13)$ states.

	$F^1\Delta_2(1)$ (cm^{-1})			$m^3\Pi_1(1)$ (cm^{-1})	$P^1\Delta_2(0)$ (cm^{-1})	$V^1\Sigma^+(m+11)$ (cm^{-1})			$V^1\Sigma^+(m+12)$ (cm^{-1})
J'	Q	R	S	Q	Q	O	Q	S	Q
0						72 850.5	72 923.0		73 110.8
1				72 944.0		72 807.6	72 917.0		73 104.6
2	72 321.7	72 345.3	72 360.4	72 943.2	73 081.1	72 771.2	72 904.5	72 951.3	73 097.2
3	72 320.1	72 356.8	72 382.8	72 942.0	73 080.4	72 721.6	72 886.3	72 952.9	73 086.2
4	72 317.7	72 367.1	72 405.2	72 939.6	73 079.6	72 667.8	72 861.5		73 069.0
5	72 315.0	72 379.3		72 937.6	73 078.6		72 833.7		73 046.7
6	72 311.0	72 387.2		72 936.8	73 077.5		72 800.4		
7	72 306.7			72 935.5	73 076.0		72 762.8		
8	72 302.3			72 934.3	73 074.9		72 721.6		
9					73 073.1		72 680.6		
10							72 644.7		

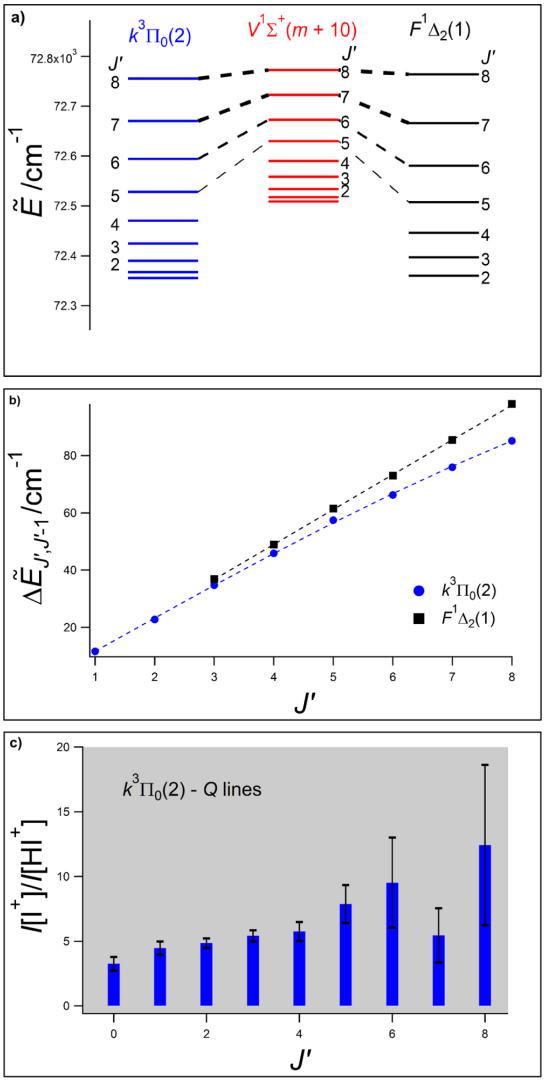

FIG. 2. (a) Rotational energy levels of the $F^1\Delta_2(v'=1)$, $k^3\Pi_0(v'=2)$, and $V^1\Sigma^+(v'=m+10)$ states, derived from the observed REMPI spectra. J' dependent state interactions are also indicated. (b) Spacing between rotational levels ($\Delta E_{J',J'-1}$) as a function of J'; experimental values and fit curves for the $k^3\Pi_0(v'=2)$ and $F^1\Delta_2(v'=1)$ states. (c) Relative ion-signal intensities ($I(I^+)/I(HI^+)$) vs. J' derived from the Q rotational lines for the $k^3\Pi_0(v'=2)$ state.

a relatively large interaction between those states and the $V(m+10)$ state might be expected for $J'=7$–8, since the $J'=8$ levels for all the states (and the $J'=7$ levels to a lesser extent) are near-degenerate. The linewidth increase in $J'=5$ for the $k^3\Pi_0(2)$ state is likely to be associated with near-degenerate interactions. The rotational energy diagram (Fig. 2(a)) signifies, however, that this can neither be due to near-degenerate interactions with the $F^1\Delta_2(1)$ state nor with the $V(m+10)$ state. We, therefore, propose that the $k^3\Pi_0(2)$ state undergoes a near-degenerate interaction, for $J'=5$, with an $\Omega=1$ hidden Rydberg state which plays a pivotal role in the aforementioned interaction between the $k^3\Pi_0(2)$ and $F^1\Delta_2(1)$ states as well as interactions between the $V(m+10)$ ($\Omega=0$) and $F^1\Delta_2(1)$ ($\Omega=2$) states. Thus, the decreased lifetime for $k^3\Pi_0(2)$, $J'=5$ (larger linewidths), will be due to the $\Omega=1$ state's predissociation by one or more of the repulsive valence states, namely, $A^1\Pi_1$, $a^3\Pi_1$, and/or $t^3\Sigma^+$. The $\Omega=1$ state will, then, act as a gateway state towards predissociation of the $k^3\Pi_0(2)$ state. The broader linewidths for $V(m+10)$, $J'\sim4$, could be associated with indirect predissociation of the ion-pair state via interaction with the mixed $k^3\Pi_0(2)$ and $F^1\Delta_2(1)$ states. Finally, large linewidths, hence shorter lifetimes for the $V(m+10)$ levels than for the $k^3\Pi_0(2)$ levels, $J'=0$–6, suggest that interactions of the V state with additional predissociating gateway states are also of importance.

In light of the above observations and interpretations, the hidden Rydberg state characteristics could be guessed. Assuming the $J'=5$ level of the hidden Rydberg state to be close in energy to that of the $J'=5$ level of the $k^3\Pi_0(2)$ state and by using "typical" spectroscopic constants for a HI Rydberg state, its band origin can be estimated to be about $\nu^0\approx72\,400$ cm$^{-1}\pm5$ cm^{-1}. Among singlet or triplet $\Omega=1$ Rydberg states, which could readily interact with the repulsive valence states, higher vibrational levels of any of the previously observed Rydberg states possessing $^1\Pi_1$ or $^3\Pi_1$ symmetry, i.e., $K^1\Pi_1$, $D^1\Pi_1$, $N^1\Pi_1$, $k^3\Pi_1$, $d^3\Pi_1$, and $m^3\Pi_1$ states[44] could be excluded, energetically. We propose that the hidden state, centered near 72 400 cm^{-1} is the $n^3\Pi_1(v'=0)$ ($(\sigma^2\pi^3)5d\sigma$) Rydberg state, which has not been observed before and, furthermore, that the observed perturbation is due to a weak S-uncoupling ($|\Delta\Omega|=1$) interaction.[65]

2. The $V^1\Sigma^+(v'=m+10)$, $H^1\Sigma^+(v'=2)$, $V^1\Sigma^+(v'=m+11)$, $m^3\Pi_1(v'=1)$ system

Fig. 1(b) shows assigned REMPI spectra for the states of concern. Fig. 4(a) shows the rotational energy levels derived from the molecular spectra. The spectrum for the $H^1\Sigma^+(2)$ Rydberg state has been observed before.[13] It should be mentioned that the spectrum was re-assigned in a recent publication.[44] The mass resolved spectra of the Q lines (Fig. 1(b)) all reveal clear perturbations in the form of LS- and/or LI-effects for $J'\sim3$–5. The $m^3\Pi_1(1)$ Rydberg state, previously observed in absorption,[13] is now seen in REMPI for the first time with band origin 72 945.0 cm^{-1}. Only weak Q lines for the I^+ ion are significantly visible. Some weak lines are observed between 72 960 and 73 000 cm^{-1} which could belong to the R and/or S series. These, however, remain unassigned for the time being. With a band origin ν^0 = 72 923.0 cm^{-1} and a rotational constant of $B_{v'}=3.43$ cm^{-1}, a rotational structure was observed mainly for the I^+ and H^+ ions. This system has never been observed before, neither in absorption nor in REMPI. The small rotational constant, the band origin value, the dominating appearance of the structure for the fragment ions, as well as the appearance of O, Q, and S lines, only, make the assignment of the spectrum to the $V(m+11)$ ion-pair state indisputable.

a. LS-effects. Figs. 4(b) and 4(c) show the spacing between the rotational levels for the $H^1\Sigma^+(2)$, $V(m+10)$, and $V(m+11)$ states as a function of J' as well as the correspond-

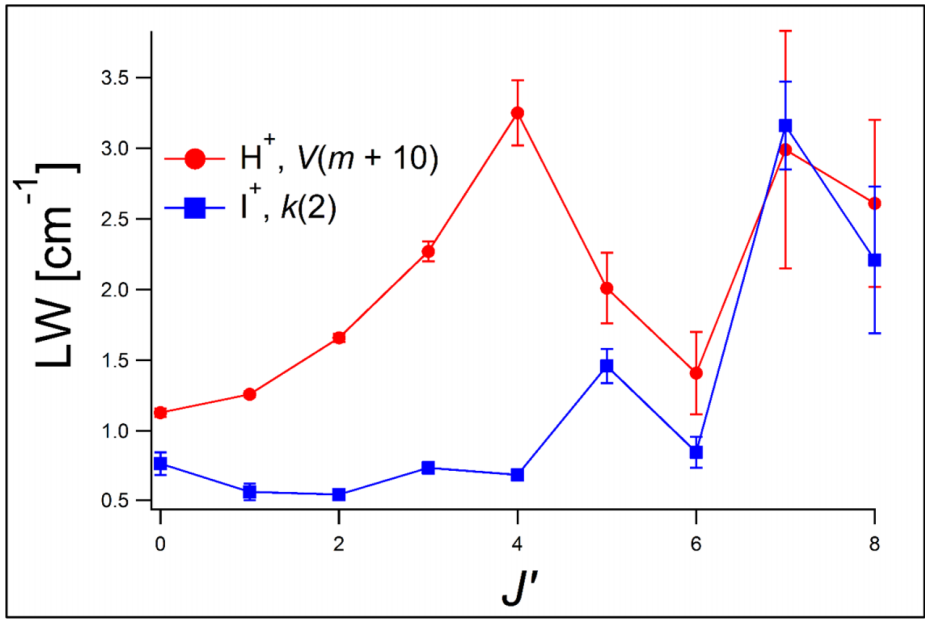

FIG. 3. Rotational linewidths vs. J' derived from the Q lines of the I^+ signal for the $k^3\Pi_0(v' = 2)$ state and of the H^+ signals for the $V^1\Sigma^+(v' = m + 10)$ state.

ing reduced term value plots. First, irregularities in the plots for $H^1\Sigma^+(2)$, appearing as a decrease of the $\Delta E_{3,2}$ and $\Delta E_{5,4}$ values but as an increase of the $\Delta E_{4,3}$ value relative to those of a line fit (unperturbed values), are typical for a near-degenerate interaction. Apart from these irregularities, the $\Delta E_{J',J'-1}$ vs. J' plot for $H^1\Sigma^+(2)$ is close to linear. The corresponding plots for the $V(m + 10)$ and $V(m + 11)$ states, on the other hand, show negative and positive curvatures, respectively, suggesting that the ion-pair states experience non-degenerate interactions with the $H^1\Sigma^+(2)$ Rydberg state, which is of energy in between and close to those of the $V(m + 10)$ and $V(m + 11)$ states (see Fig. 4(a)). Further inspection of the vibrational energies of the ion-pair vibrational states (see Ref. 44 and Fig. 5) reveals larger energy gap between the $V(m + 10)$ and $V(m + 11)$ states, which is to be expected for vibrational states closest in energy to an interacting $\Omega = 0$ Rydberg state.[44] To verify this and to determine the strength of the interaction between the ion-pair states and the $H^1\Sigma^+(2)$ state, a three-state deperturbation analysis was performed, which has been described explicitly in previous publications.[33,45,58] The deperturbation analysis only gave approximate interaction strengths as $W_{H,V(m+11)} = 13 \pm 6$ cm^{-1} and $W_{H,V(m+12)} = 15 \pm 8$ cm^{-1}. The deperturbation results, however, do not explain the interaction effects observed at $J' = 3$–5 in the $H^1\Sigma^+(2)$ state nor can they be ascribed to interaction effects of the $m^3\Pi_1(1)$ state, which is higher in energy. Therefore, we propose that these effects are caused by interaction with a hidden Rydberg state.

b. LI-effect. Fig. 4(d) shows the intensity ratio, $I[I^+]/I[HI^+]$, derived from the Q lines for the $H^1\Sigma^+(2)$ state. Apart from the dip in the ratio for $J' = 3$, it is found to increase with J' from $J' = 0$ to 2 followed by a decrease to $J' = 7$. Comparatively, non-degenerate interactions between $\Omega = 0$ Rydberg states ($E^1\Sigma^+$) and ion-pair states, close in energy, for HCl and HBr,[33] display distinctively dissimilar behaviors than analogous interactions between the $H^1\Sigma^+$ state and the $V(m + 10)$ and $V(m + 11)$ states. The different trends observed in the intensity ratio for $J' = 0$–7 (Fig. 4(d)) as well as the irregularities in the absolute ion signal intensities (see Fig. 1(b) and text above) must be due to interactions between the $H^1\Sigma^+(2)$ state and a hidden Rydberg state. Thus, the state mixing can alter the ionization yield of the otherwise unmixed $H^1\Sigma^+(2)$ Rydberg state to increase the I^+ formation and/or decrease the HI^+ formation for $J' \sim 1$, 2 and $J' \sim 4$, 5 and give the ratios shown in Fig. 4(d). This can be due to different ionization rates of the two interacting states.

c. LW-effects. No significant alterations were observed for the rotational linewidths as a function of J' for all the spectra except for the $V(m + 10)$ ion-pair state as mentioned before (see Sec. IV A 1). The average linewidths for the $V(m + 10)$, $V(m + 11)$, $H^1\Sigma^+(2)$, and $m^3\Pi_1(1)$ states are about 2.1, 1.8, 1.3, and 1.0 cm^{-1}, respectively. Typically, larger linewidths, hence shorter lifetime, are observed for the ion-pair states than for an interacting Rydberg state, again suggesting that interactions of the ion-pair states with more strongly predissociating gateway states are of importance.

Whereas the $m^3\Pi_1(1)$ Rydberg state's $\Omega = 2$ counterpart, $m^3\Pi_2(1)$, has not been observed in REMPI,[33,36] it has been seen in absorption at about $\nu^0 = 72\,697$ cm^{-1}.[13] Therefore, it could interact with the $H^1\Sigma^+(2)$ state ($\nu^0 = 72\,654.3$ cm^{-1}) due to its energetic proximity via mixing with an $\Omega = 1$ state. Furthermore, perturbations have not been observed in the $H^1\Sigma^+(2)$ spectra for $J' < 2$,[13] which might suggest that the perturbing state is an $\Omega = 2$ state. Due to the difference

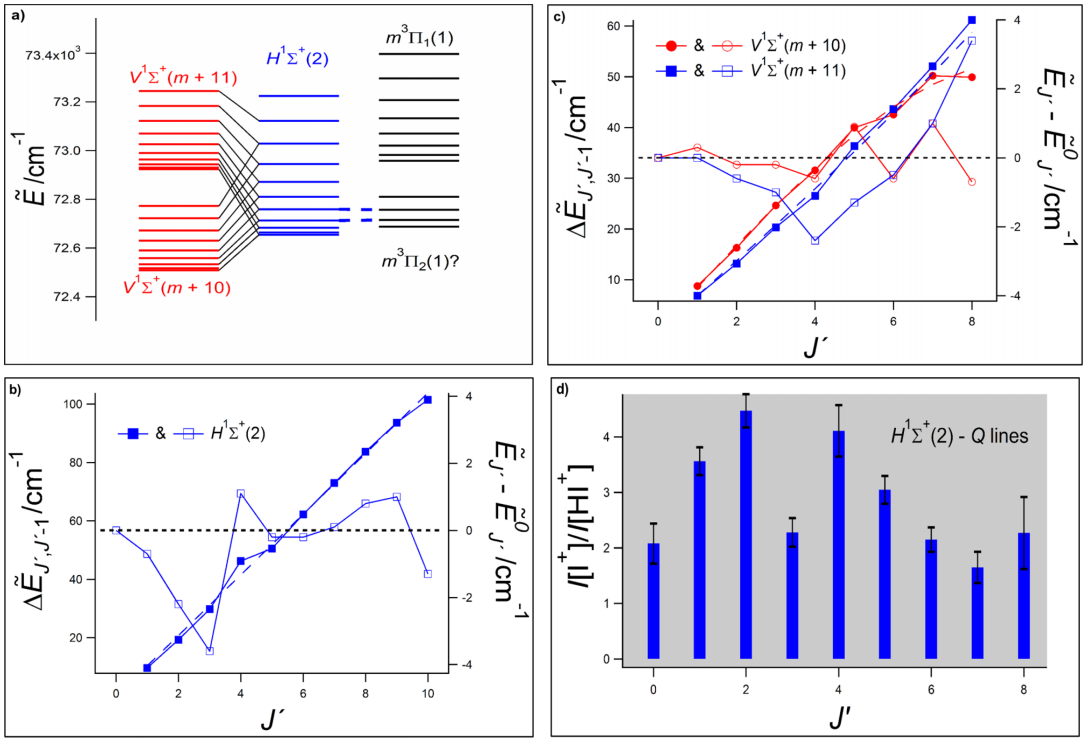

FIG. 4. (a) Rotational energy levels of the $V^1\Sigma^+(v'=m+10)$, $H^1\Sigma^+(v'=2)$, $V^1\Sigma^+(v'=m+11)$ and $m^3\Pi_1(v'=1)$ states derived from the REMPI spectra as well as rotational energy levels of the $m^3\Pi_2(v'=1)$ state derived from Ref. 13. Non-degenerate interactions between the $H^1\Sigma^+(v'=2)$ Rydberg state and the $V^1\Sigma^+(v'=m+10)$ and $V^1\Sigma^+(v'=m+11)$ ion-pair states are marked as well as the near-degenerate interactions between the $J'=3$, 4 rotational levels of the $H^1\Sigma^+(v'=2)$ Rydberg state and the $m^3\Pi_2(v'=1)$ state. (b) Spacing between rotational levels ($\Delta E_{J',J'-1}$) as a function of J' (left vertical axis) and the corresponding reduced term value plot (right vertical axis) for the $H^1\Sigma^+(v'=2)$ state; experimental values (dots joined by lines); and fit curve (dashed blue curve). (c) Spacing between rotational levels ($\Delta E_{J',J'-1}$) as a function of J' (left vertical axis) and the corresponding reduced term value plot (right vertical axis) for the $V^1\Sigma^+(v'=m+10)$ (red) and $V^1\Sigma^+(v'=m+11)$ (blue) states; experimental values (dots joined by lines), and fit curve (dotted line). (d) Relative ion-signal intensities ($I(I^+)/I(HI^+)$) vs. J' derived from the Q rotational lines for the $H^1\Sigma^+(v'=2)$ state.

in the rotational constants for the two states (about 5.19 and 6.16 cm^{-1} for the $H^1\Sigma^+(2)$ and $m^3\Pi_2(1)$ states, respectively), the spacing between the rotational levels of same J' values will increase; hence the mixing will decrease, with J'. On the other hand, the interaction strength (W_{12}) will increase with J' ($W_{12} = W_{12}'(J'(J'+1))^{1/2}$ for $|\Delta\Omega| = 1$ interactions). Therefore, an increase in interaction strength followed by its decrease as J' increases might be expected, analogous to the behaviour observed for the intensity ratio ($I[I^+]/I[HI^+]$) as a function of J', apart from the dip for $J' = 3$. Therefore, we propose that the hidden state is the $m^3\Pi_2(v'=1)$ Rydberg state, being hidden in REMPI but observable in absorption.

3. The $P^1\Delta_2(v'=0)$ and $V^1\Sigma^+(v'=m+12)$ states

Fig. 1(c) shows assigned REMPI spectra for the states of concern. Fig. 5 shows relevant band origins along with other states, close in energy. The reasoning behind the assignment of the weak band at 73 081.7 cm^{-1} to the $P^1\Delta_2(0)$ Rydberg state, as mentioned above, is manifold. First, the absence of Q rotational lines for $J' < 2$ strongly suggests a state with the total angular momentum of $\Omega = 2$. The rotational constant ($B_{v'} = 6.35$ cm^{-1}) derived from the spectrum is relatively large and comparable to those derived from virtually unperturbed (pure) Rydberg states, such as the $F^1\Delta_2(0)$ ($B_{v'} = 6.32$ cm^{-1}) and $I^1\Delta_2(0)$ ($B_{v'} = 6.31$ cm^{-1}) states.[36,37] An observation of, primarily, the HI^+ signal is also a clear indication of a pure Rydberg state. The state can neither be a vibrationally excited $F^1\Delta_2$ ($((\sigma^2\pi^3)6p\pi)$ or $I^1\Delta_2$ ($((\sigma^2\pi^3)5d\pi)$ state, since it does not fit into the corresponding vibrational state series. Simple quantum defect analysis,[44,58] based on the expression for vibrational Rydberg state energies ($E_{v'}([\Omega_c, v^+]nl;\omega)$),

$$E_{v'}([\Omega_c, v^+]nl;\omega) = IE([\Omega_c, v^+]) - R/(n^*)^2, \qquad (4)$$

was performed. In Eq. (4), v' and v^+ are the vibrational quantum numbers for the Rydberg and ionic states, respectively ($v' = v^+$), and $IE([\Omega_c, v^+])$ is the ionization limit of the molecular ion vibrational state, to which the Rydberg series converges. n^* is the effective principal quantum number depending on the Rydberg electron principal quantum number (n) and the l quantum number dependent quantum defect value (δ_l) as $n^* = n - \delta_l$. The analyses revealed a value

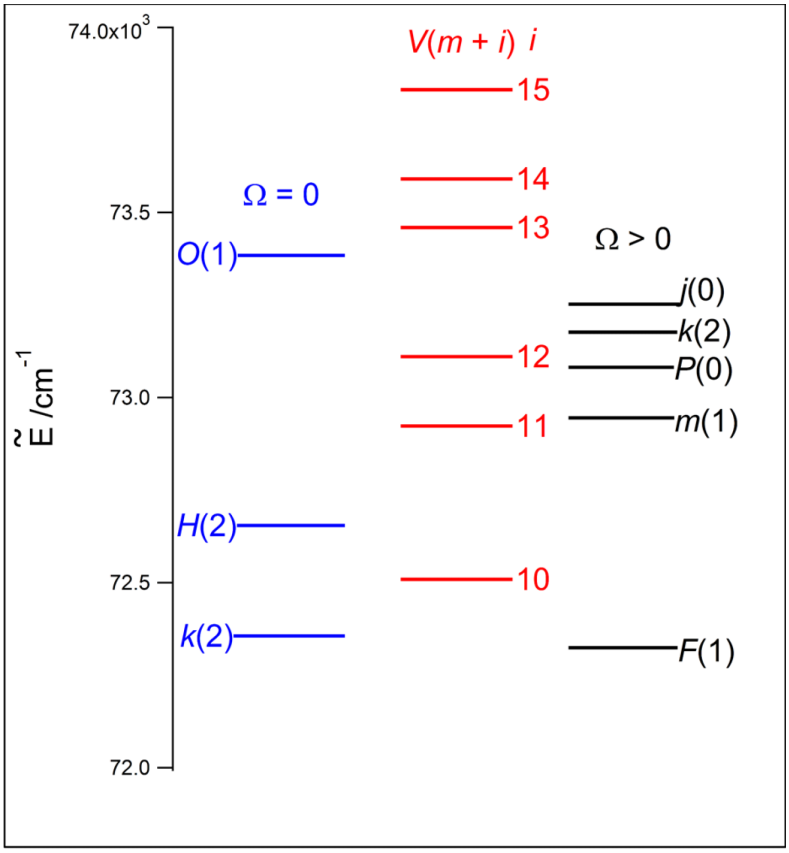

FIG. 5. Energy diagram of the observed electronic states for HI in the two-photon excitation region 72 300–74 600 cm^{-1}. Rydberg states with $\Omega = 0$ total angular momentum are presented in blue to the left, ion-pair states are presented in red (middle) and Rydberg states with $\Omega \neq 0$ total angular momentum are presented in black to the right.

of 0.8 for δ_l, which although quite large, are significantly lower than values derived for d electron Rydberg states (see Table II) and comparable to that previously determined for the $O^1\Sigma^+(v' = 0)$ $((\sigma^2\pi^3)4f\pi)$ state.[44] Therefore, we assign the spectrum centered at 73 081.7 cm^{-1} to the $P^1\Delta_2(v' = 0)$ $((\sigma^2\pi^3)4f\pi)$ Rydberg state. At 73 110.8 cm^{-1}, very weak and broad Q lines are observed for the first time. Analyses gave the rotational constant $B_{v'} = 4.34$ cm^{-1}. The small rotational constant, the band origin value, and a dominating appearance of the structure for the fragment ion H^+ (see Fig. 5) make the assignment of the spectrum to the $V(m + 12)$ ion-pair state indisputable.

a. LS-, LI-, and LW-effects. Although close in energy, there are no indications of interactions between the $P^1\Delta_2(0)$ and $V(m + 12)$ states based on LS- or LI-effects. The linewidths of the Q lines of the $V(m + 12)$ state spectrum are about 3.6 cm^{-1}, on average, whereas the linewidths of the Q lines of the $P^1\Delta_2(0)$ spectrum are close to or just above the detection limit of about 0.3–0.5 cm^{-1}. The linewidths of the $V(m + 12)$ spectrum are found to be larger than those of V-vibrational states closer in energy to neighboring $\Omega = 0$ Rydberg states (see Fig. 5). Thus, the average linewidths of the Q lines for the $V(m + 10)$ and $V(m + 11)$ spectra are about 2.1 and 1.8 cm^{-1}, respectively, and the linewidths of the rotational lines for the lowest J' levels of the $V(m + 13)$ spectrum are less than 1 cm^{-1}. This suggest that interactions of $V(m + 12)$ with the closest in energy $\Omega = 0$ Rydberg states are not the major reason for the broad linewidths observed. More likely, the main reason is a direct heterogeneous interaction with a close in energy $\Omega = 1$ state which acts as a gateway state towards rapid predissociation.

A possible candidate for an $\Omega = 1$ hidden Rydberg state is either of the $M^1\Pi_1$, $(\sigma^2\pi^3)7s\sigma$ or $R^1\Pi_1$, $(\sigma^2\pi^3)7p\sigma$ Rydberg states, both of which have not been observed in absorption or REMPI. Further information, however, are required for a definitive assignment, so for the time being, these proposals are purely conjectured.

4. The $O^1\Sigma^+(v' = 1)$, $V^1\Sigma^+(v' = m + 13)$, $V^1\Sigma^+(v' = m + 14)$, $V^1\Sigma^+(v' = m + 15)$ system

Fig. 1(d) shows assigned REMPI spectra for the states of concern. Fig. 6(a) shows the rotational energy levels derived from the spectra as well as those derived for the $V(m + 15)$ state. The spectrum centered at 73 384.2 cm^{-1} has been assigned before to an $\Omega = 0^+$ Rydberg state.[41] We assign it to the first excited vibrational state of the $O^1\Sigma^+$ state, i.e., the

$O^1\Sigma^+(v' = 1)$ state, since its energy is 2089.5 cm^{-1} higher than that of the $O^1\Sigma^+(v' = 0)$ state, typical for a vibrational energy difference of a Rydberg state.[13,41,44] Furthermore, the quantum defect of the $O^1\Sigma^+(v' = 1)$ state (Table II) equals the quantum defect of the previously reported $O^1\Sigma^+(v' = 0)$ state.[44] The ion-pair state spectra, previously assigned to the $V(m + 11)$, $V(m + 12)$, and $V(m + 13)$ states, now assigned to the $V(m + 13)$, $V(m + 14)$, and $V(m + 15)$ states, respectively (see Secs. IV A 2 and IV A 3), have all been observed in absorption.[13] Perturbation effects, seen in the spectra, have been reported.[13]

a. LS- and LI-effects. Fig. 6(b) shows the spacing between the rotational levels ($\Delta E_{J',J'-1}$) for the $O^1\Sigma^+(1)$ Rydberg state as a function of J' as well as the corresponding reduced term value plot. Irregularities in the plots, for $J' \sim 9$, are typical for near-degenerate interactions. Furthermore, there is an indication of interactions for higher $J's$. Intensity ratios, $I(H^+)/I(HI^+)$ as a function of J', derived from the Q lines for the $O^1\Sigma^+(1)$ state also are indicative of a near-degenerate interaction for $J' = 9$ as well as for $J' = 6$ (Fig. 6(c)). Based on the energy levels of the states involved as well as extrapolated values for higher $J's$ (Fig. 6(a)), these observed perturbations are due to near-degenerate interactions with the $V(m + 13)$ and $V(m + 14)$ states for $J' = 6$ and 9, respectively.

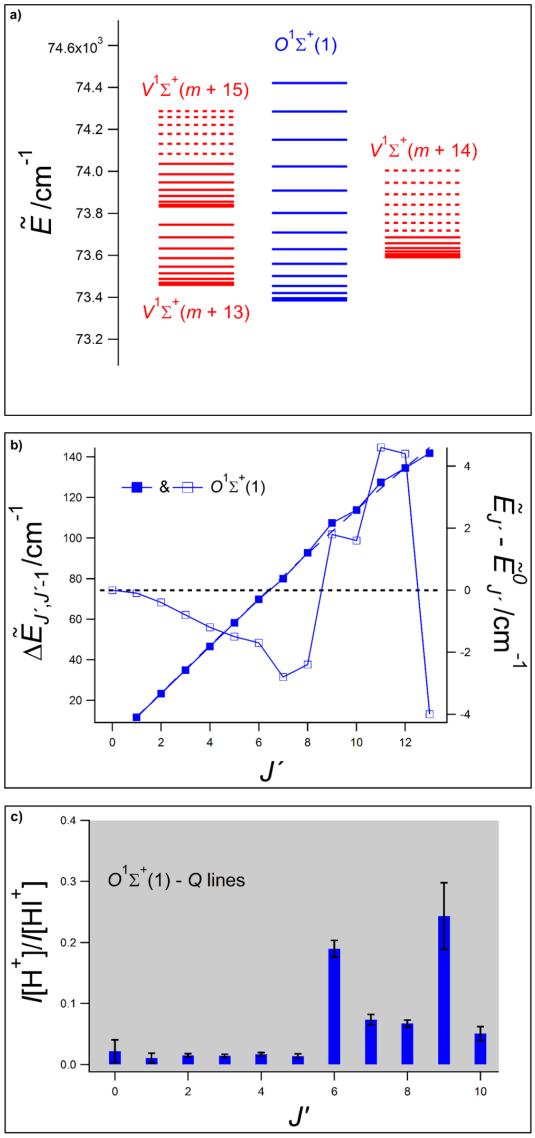

FIG. 6. (a) Rotational energy levels of the $O^1\Sigma^+(v' = 1)$, $V^1\Sigma^+(v' = m + 13)$, $V^1\Sigma^+(v' = m + 14)$, and $V^1\Sigma^+(v' = m + 15)$ states derived from the REMPI spectra. (b) Spacing between rotational levels ($\Delta E_{J',J'-1}$) as a function of J' as well as the corresponding reduced term value plot for the $O^1\Sigma^+(v' = 1)$ Rydberg state; experimental values (dots joined by lines); and fit curve (dotted line). (c) Relative ion-signal intensities ($I(H^+)/I(HI^+)$) vs. J' derived from the Q rotational lines for the $O^1\Sigma^+(v' = 1)$ state.

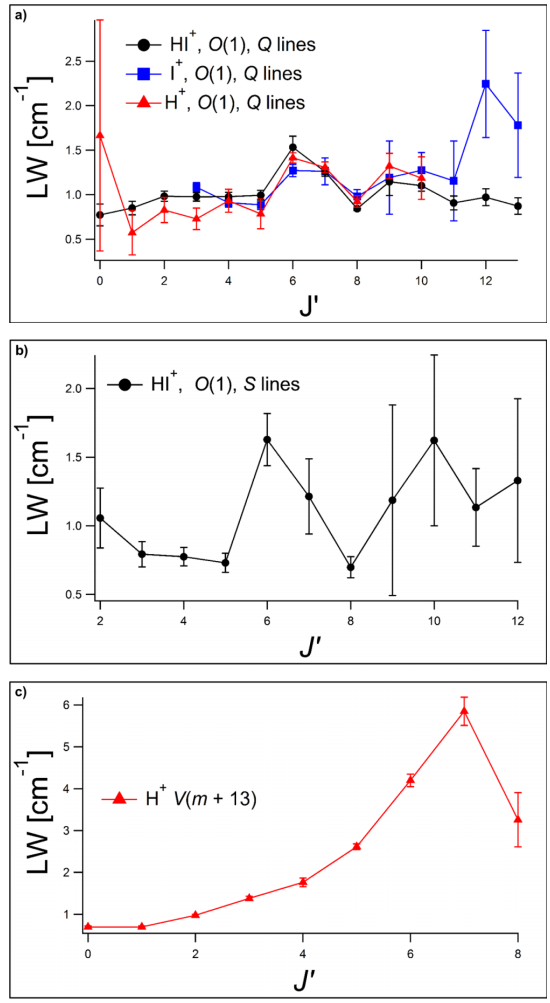

FIG. 7. (a) Rotational linewidths vs. J' derived from the Q lines of the H^+, I^+, and HI^+ signals for the $O^1\Sigma^+(v' = 1)$ state. (b) Rotational linewidths vs. J' derived from the S lines of the HI^+ signals for the $O^1\Sigma^+(v' = 1)$ state. (c) Rotational linewidths vs. J' derived from the Q lines of the H^+ signal for the $V^1\Sigma^+(v' = m + 13)$ ion-pair state.

b. LW-effect. Figs. 7(a)–7(c) show linewidths of rotational lines for the $O^1\Sigma^+(1)$ and $V(m+13)$ spectra. The linewidths for the $O^1\Sigma^+(1)$ state are close to 1 cm^{-1}, on average, whereas those for the $V(m+13)$ state rise with J' from values less than 1 cm^{-1} to about 6 cm^{-1} for $J'=7$. Q and S rotational lines of the $O^1\Sigma^+(1)$ spectrum show line broadening for $J'=6$–7 as well as for $J'=9$–10. Furthermore, the maximum linewidth for $V(m+13)$ is observed for $J'=7$. These observations fit with the LS- and LI-effects seen in the $O^1\Sigma^+(1)$ spectrum (see above), suggesting that it is associated with the coupling between the $O^1\Sigma^+(1)$ state and the $V(m+13)$ and $V(m+14)$ ion-pair states. Considering the larger linewidths of the $J'\sim 5$–8 lines for the $V(m+13)$ state compared with the $O^1\Sigma^+(1)$ state (Figs. 7(a)–7(c)), the lifetime of the coupling states ($J'\sim 6$) must be determined, to some extent, by that of the $V(m+13)$ state which will predissociate via a manifold of gateway Rydberg state(s) (see Sec. III). The rise in the linewidth for the $V(m+13)$ state for $J'\sim 2$–7 is most probably associated with an increasing non-degenerate interaction between the $O^1\Sigma^+(1)$ and $V(m+13)$ states as J' increases.

Whereas the $k^3\Pi_2(v'=0)$ Rydberg state has been observed[13] in this region by absorption at $\nu^0=73\,360.0$ cm^{-1}, it is not seen here. Its lack of appearance might be an indication of the presence of a nearby predissociating $\Omega=1$ hidden Rydberg state, which again could be responsible for the observed "shorter lifetime" of the $V(m+13)$ state.

V. CONCLUSIONS

REMPI spectra of atomic and molecular ions of HI in the two-photon excitation region 72 300–74 600 cm^{-1} were analyzed.

First, the analysis allowed assignments of new spectral structures and characterization of new excited states. New spectral bands at 72 324.0, 73 081.7, 72 923.0, and 73 110.8 cm^{-1} were assigned to the $F^1\Delta_2(1)$ and $P^1\Delta_2(0)$ Rydberg states and the $V^1\Sigma^+(m+11)$ and $V^1\Sigma^+(m+12)$ ion-pair states, respectively. A previously un-assigned spectral structure centered at 73 384.2 cm^{-1} was assigned as the $O^1\Sigma^+(1)$ Rydberg state and the $m^3\Pi_1(1)$ Rydberg state at 72 945.0 cm^{-1} was now observed for the first time in REMPI.

Second, perturbation effects appearing as line shift-, line-intensity-, and linewidth-effects allowed determination of Rydberg to ion-pair as well as Rydberg to Rydberg state interactions both qualitatively and quantitatively. Whereas the line shift and line-intensity effects are primarily indications of bound-to-bound state interactions, the linewidth effects are reflective of direct or indirect (via gateway states) predissociation processes. Generally, it is found that the overall sensitivity of the line-intensity effects is greater than line shift effects. Gradual changes in the various effects as a function of rotational quantum numbers, J', are found to be clear indications of relatively strong homogeneous, non-degenerate interactions between Rydberg and ion-pair states, whereas sudden alterations with J' signals are found to correspond with near-degenerate interactions between Rydberg and ion-pair states or between Rydberg states.

(1) Relatively strong non-degenerate interactions are observed between the states,
   (i) $k^3\Pi_0(v'=2)$ and $V^1\Sigma^+(v'=m+10)$,
   (ii) $H^1\Sigma^+(v'=2)$ and $V^1\Sigma^+(v'=m+10)$,
   (iii) $H^1\Sigma^+(v'=2)$ and $V^1\Sigma^+(v'=m+11)$.

(2) Near-degenerate interactions are observed between the states,
   (i) $k^3\Pi_0(v'=2)$ and $F^1\Delta_2(v'=1)$ ($J'=7$–8),
   (ii) $k^3\Pi_0(v'=2)$ and $V^1\Sigma^+(v'=m+10)$ ($J'=7$–8),
   (iii) $O^1\Sigma^+(v'=1)$ and $V^1\Sigma^+(v'=m+13)$ ($J'=6$),
   (iv) $O^1\Sigma^+(v'=1)$ and $V^1\Sigma^+(v'=m+14)$ ($J'=9$).

Third, the various perturbation effects are found to be indicative of the presence of "hidden states" not observable here, but possibly observable by other technical means. The observed perturbations allowed assignments of these hidden states to some extent.

1. Based on perturbation effects seen in the spectra of the $F^1\Delta_2(1)$, $k^3\Pi_0(2)$ and $V^1\Sigma^+(m+10)$ states, the $n^3\Pi_1(0)$ Rydberg state, centered near 72 400 cm^{-1}, is proposed as a hidden state causing the appearances of LW-effects in the $V^1\Sigma^+(m+10)$ ion-pair state as well as acting as a gateway state to interactions between the $F^1\Delta_2(1)$ Rydberg state and the $k^3\Pi_0(2)$ and $V^1\Sigma^+(m+10)$ states, respectively.
2. The $m^3\Pi_2(1)$ state, centered near 72 697 cm^{-1}, but not observed in REMPI was proposed to be a possible perturber in the $H^1\Sigma^+(2)$ Rydberg state spectrum. Its coupling with the H state would require a mixing with an $\Omega=1$ state, close in energy.
3. Either the $M^1\Pi_1$ or the $R^1\Pi_1$ states are suggested as a possible culprits of rather large linewidths of the $V^1\Sigma^+(m+12)$ ion-pair state.
4. Finally, a hidden $\Omega=1$ Rydberg state, causing the $k^3\Pi_2(0)$ state to be unseen in REMPI due to predissociation, is proposed.

In all the cases (1–4), above, $\Omega=1$ states are believed to be involved, directly or indirectly, as hidden states. This harmonizes with previous findings for the hydrogen halides.[27,29,31–33,45,58] A likely reason for the elusiveness of interacting $\Omega=1$ states is their short lifetimes due to predissociation, but out of six repulsive valence states, which converge to $H(n=1)+I(^2P_{3/2,1/2})$, three are $\Omega=1$ states.

ACKNOWLEDGMENTS

The financial support of the University Research Fund, University of Iceland, and the Icelandic Science Foundation (Grant No. 130259-051) is gratefully acknowledged.

[1]M. J. Simpson, R. P. Tuckett, K. F. Dunn, C. A. Hunniford, and C. J. Latimer, J. Chem. Phys. **130**, 194302 (2009).
[2]J. H. Seinfeld and S. N. Pandis, *Atmospheric Chemistry and Physics: From Air Pollution to Climate Change* (John Wiley & Sons, 2006).
[3]J. I. Lunine, *Astrobiology* (Pearson Addison Wesley, 2005).
[4]A. M. Shaw, *Astrochemistry: From Astronomy to Astrobiology* (Wiley, 2006).
[5]N. Hoffmann, Chem. Rev. **108**, 1052 (2008).
[6]J. B. Nee, M. Suto, and L. C. Lee, J. Chem. Phys. **85**, 719 (1986).
[7]D. S. Ginter and M. L. Ginter, J. Mol. Spectrosc. **90**, 177 (1981).

[8]S. G. Tilford, M. L. Ginter, and J. T. Vanderslice, J. Mol. Spectrosc. **33**, 505 (1970).
[9]J. B. Nee, M. Suto, and L. C. Lee, J. Chem. Phys. **85**, 4919 (1986).
[10]D. S. Ginter, M. L. Ginter, and S. G. Tilford, J. Mol. Spectrosc. **90**, 152 (1981).
[11]R. F. Barrow and J. G. Stamper, Proc. R. Soc. A **263**, 277 (1961).
[12]R. F. Barrow and J. G. Stamper, Proc. R. Soc. A **263**, 259 (1961).
[13]D. S. Ginter, M. L. Ginter, and S. G. Tilford, J. Mol. Spectrosc. **92**, 40 (1982).
[14]M. L. Ginter, S. G. Tilford, and A. M. Bass, J. Mol. Spectrosc. **57**, 271 (1975).
[15]S. G. Tilford, M. L. Ginter, and A. M. Bass, J. Mol. Spectrosc. **34**, 327 (1970).
[16]T. A. Spiglanin, D. W. Chandler, and D. H. Parker, Chem. Phys. Lett. **137**, 414 (1987).
[17]E. de Beer, B. G. Koenders, M. P. Koopmans, and C. A. de Lange, J. Chem. Soc., Faraday Trans. **86**, 2035 (1990).
[18]K. Wang and V. McKoy, J. Chem. Phys. **95**, 8718 (1991).
[19]Y. Xie, P. T. A. Reilly, S. Chilukuri, and R. J. Gordon, J. Chem. Phys. **95**, 854 (1991).
[20]D. S. Green, G. A. Bickel, and S. C. Wallace, J. Mol. Spectrosc. **150**, 303 (1991).
[21]D. S. Green, G. A. Bickel, and S. C. Wallace, J. Mol. Spectrosc. **150**, 354 (1991).
[22]D. S. Green, G. A. Bickel, and S. C. Wallace, J. Mol. Spectrosc. **150**, 388 (1991).
[23]D. S. Green and S. C. Wallace, J. Chem. Phys. **96**, 5857 (1992).
[24]E. de Beer, W. J. Buma, and C. A. deLange, J. Chem. Phys. **99**, 3252 (1993).
[25]P. M. Regan, S. R. Langford, D. Ascenzi, P. A. Cook, A. J. Orr-Ewing, and M. N. R. Ashfold, Phys. Chem. Chem. Phys. **1**, 3247 (1999).
[26]Á. Kvaran, H. Wang, and Á. Logadóttir, J. Chem. Phys. **112**, 10811 (2000).
[27]Á. Kvaran, H. Wang, and B. G. Waage, Can. J. Phys. **79**, 197 (2001).
[28]H. Wang and Á. Kvaran, J. Mol. Struct. **563**, 235 (2001).
[29]Á. Kvaran, H. S. Wang, K. Matthiasson, A. Bodi, and E. Jonsson, J. Chem. Phys. **129**, 164313 (2008).
[30]K. Matthiasson, H. S. Wang, and Á. Kvaran, J. Mol. Spectrosc. **255**, 1 (2009).
[31]Á. Kvaran, K. Matthiasson, and H. S. Wang, J. Chem. Phys. **131**, 044324 (2009).
[32]K. Matthiasson, J. M. Long, H. S. Wang, and Á. Kvaran, J. Chem. Phys. **134**, 164302 (2011).
[33]J. Long, H. Wang, and Á. Kvaran, J. Chem. Phys. **138**, 044308 (2013).
[34]R. Callaghan and R. J. Gordon, J. Chem. Phys. **93**, 4624 (1990).
[35]K. Wang and V. McKoy, J. Chem. Phys. **95**, 7872 (1991).
[36]A. E. Belikov, M. M. Ahern, and M. A. Smith, Chem. Phys. **234**, 195 (1998).
[37]Á. Kvaran, B. G. Waage, and H. Wang, J. Chem. Phys. **113**, 1755 (2000).
[38]D. Ascenzi, S. Langford, M. Ashfold, and A. Orr-Ewing, Phys. Chem. Chem. Phys. **3**, 29 (2001).
[39]J. Long, H. Wang, and Á. Kvaran, J. Mol. Spectrosc. **282**, 20 (2012).
[40]S. A. Wright and J. D. McDonald, J. Chem. Phys. **101**, 238 (1994).
[41]S. T. Pratt and M. L. Ginter, J. Chem. Phys. **102**, 1882 (1995).
[42]Á. Kvaran, Á. Logadóttir, and H. Wang, J. Chem. Phys. **109**, 5856 (1998).
[43]P. M. Regan, D. Ascenzi, E. Wrede, P. A. Cook, M. N. R. Ashfold, and A. J. Orr-Ewing, Phys. Chem. Chem. Phys. **2**, 5364 (2000).
[44]H. R. Hróðmarsson, H. S. Wang, and Á. Kvaran, J. Mol. Spectrosc. **290**, 5 (2013).
[45]H. R. Hróðmarsson, H. S. Wang, and Á. Kvaran, J. Chem. Phys. **140**, 244304 (2014).
[46]D. Zaouris, A. Kartakoullis, P. Glodic, P. C. Samartzis, H. R. Hróðmarsson, and Á. Kvaran, Phys. Chem. Chem. Phys. **17**, 10468 (2015).
[47]S. Kauczok, C. Maul, A. I. Chichinin, and K. H. Gericke, J. Chem. Phys. **133**, 024301 (2010).
[48]C. Romanescu and H. P. Loock, J. Chem. Phys. **127**, 124304 (2007).
[49]C. Romanescu and H. P. Loock, Phys. Chem. Chem. Phys. **8**, 2940 (2006).
[50]C. Romanescu, S. Manzhos, D. Boldovsky, J. Clarke, and H. Loock, J. Chem. Phys. **120**, 767 (2004).
[51]H. P. Loock, C. Romanescu, and S. Manzhos, Abstr. Pap. Am. Chem. Soc. **223**, C19 (2002).
[52]H. P. Loock, B. L. G. Bakker, and D. H. Parker, Can. J. Phys. **79**, 211 (2001).
[53]J. Brown and A. Carrington, *Rotational Spectroscopy of Diatomic Molecules* (Cambridge University Press, Cambridge, United Kingdom, 2003).
[54]W. C. Price, Proc. R. Soc. A **167**, 216 (1938).
[55]D. S. Ginter, M. L. Ginter, S. G. Tilford, and A. M. Bass, J. Mol. Spectrosc. **92**, 55 (1982).
[56]H. Lefebvre-Brion and R. W. Field, *Perturbations in the Spectra of Diatomic Molecules* (Academic Press, Inc., London, 1986).
[57]G. Herzberg, *Molecular Spectra and Molecular Structure: I. Spectra of Diatomic Molecules, Molecular Spectra and Molecular Structure*, 2nd ed. (Van Nostrand Reinhold Company, New York, 1950).
[58]J. Long, H. R. Hróðmarsson, H. Wang, and Á. Kvaran, J. Chem. Phys. **136**, 214315 (2012).
[59]P. A. M. Dirac, *The Principles of Quantum Mechanics* (Oxford University Press, 1930).
[60]D. Bohm, *Quantum Theory* (Dover Publications, New York, 1951).
[61]J. Long, H. Wang, and Á. Kvaran, Acta Phys. Sin. **62**, 163302 (2013).
[62]See supplementary material at http://dx.doi.org/10.1063/1.4922892 for LS- and reduced term value plots and further distinction between near- and non-degenerate perturbations.
[63]N. Böwering, H. W. Klausing, M. Muller, M. Salzmann, and U. Heinzmann, Chem. Phys. Lett. **189**, 467 (1992).
[64]See http://webbook.nist.gov/chemistry/for-ser.html.en-us.en for NIST, 2015.
[65]M. H. Alexander, X. N. Li, R. Liyanage, and R. J. Gordon, Chem. Phys. **231**, 331 (1998).

6.5.1 Supplementary material

State interactions, illumination of hidden states through perturbations and observations of new states:
High energy resonance enhanced multiphoton ionization of HI

Helgi Rafn Hróðmarsson, Huasheng Wang, and Ágúst Kvaran*
Science Institute, University of Iceland, Dunhagi 3, 107 Reykjavik, Iceland.

Supplemental Material

Content: **page:**

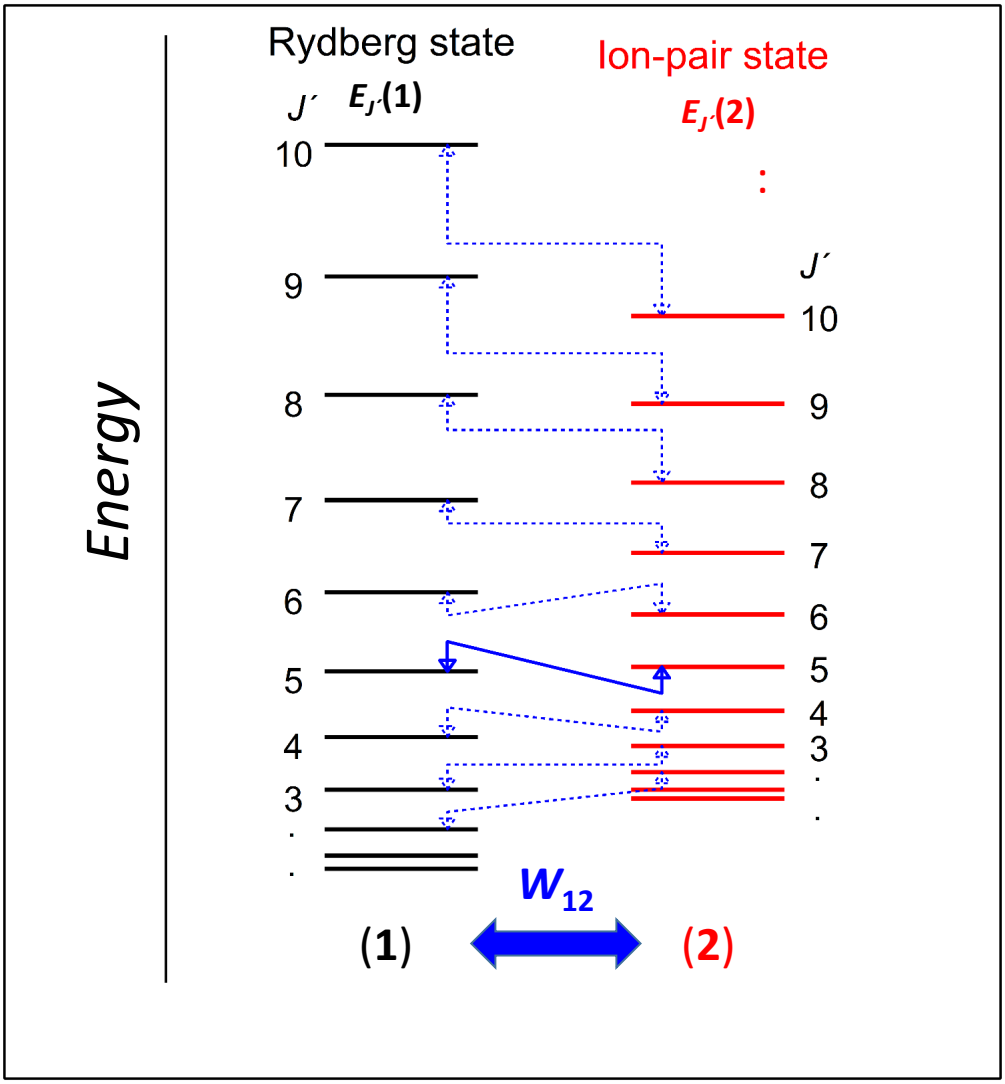

Fig. S1: Schematic figure of J' energy levels for interacting Rydberg ($E_{J'}(1)$; black; left) and ion-pair ($E_{J'}(2)$; red; right) vibrational states and repulsion interaction effects (blue arrows). The interaction involves shifts of energy levels as indicated by the arrows, which increase as the energy difference ($\Delta E_{J'} = |E_{J'}(1) - E_{J'}(2)|$) decreases, to an extent which depends on the interaction strength (W_{12}). A near-degenerate interaction is indicated by a solid blue arrow ($J' = 5$), whereas non-degenerate interactions are shown by dotted arrows.

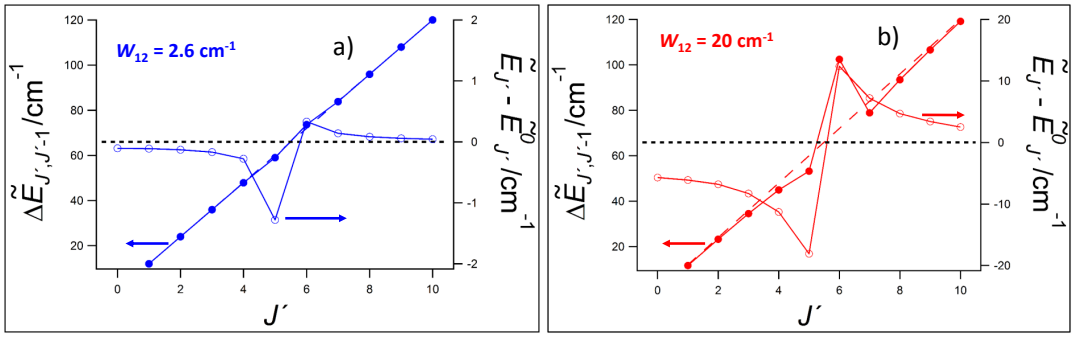

Fig. S2: Effect of Rydberg (1) to ion-pair(2) state interactions (see Fig. S1) on energy level shifts of a Rydberg state (1), for the rotational constants, $B´(1) = 6$ cm^{-1} and $B´(2) = 4$ cm^{-1}, band origin difference, $\Delta\nu^0 = \nu^0(2) - \nu^0(1) = 64$ cm^{-1}, $W_{12} = 2.6$ cm^{-1} (a) and $W_{12} = 20$ cm^{-1} (b). Filled dots, are $\Delta E_{J´,J´-1}$ (= $E_{J´}(1) - E_{J´-1}(1)$) vs. $J´$. Unfilled dots represent the difference between the perturbed and unperturbed energy levels ($E_{J´}(1) - E^0_{J´}(1)$). Broken blue(a) and red(b) curves are for unperturbed energies. Largest energy level shifts are observed for the near-degenerate interaction ($J´ = 5$). Shifts of non-degenerate levels decrease as $J´$ deviates more from the near-degenerate level and to a different degree depending on the interaction strength (W_{12}).

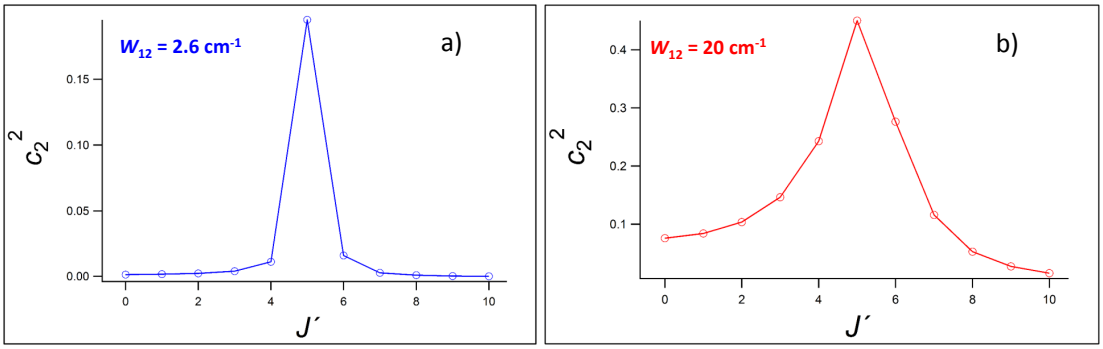

Fig. S3: Fractional contributions (c_2^2) of the ion-pair state (2) character in the Rydberg state(1) as a function of $J´$ in the state interaction described in the figure caption of Fig. S2 (see above). Largest mixing is obtained for the near-degenerate J´level ($J´ = 5$). Mixing of non-degenerate levels decrease as $J´$ deviates more from the near-degenerate level and to a different degree depending on the interaction strength (W_{12}).

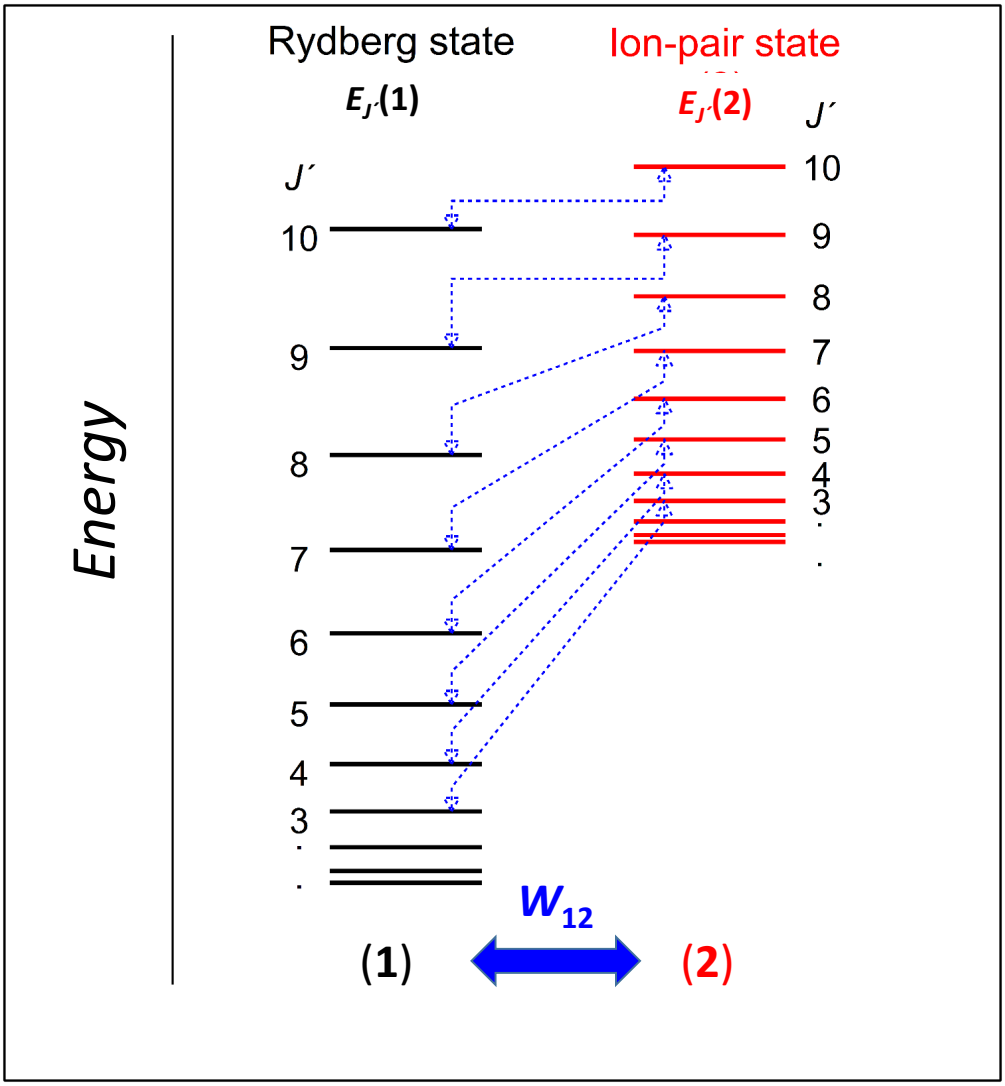

Fig. S4: Schematic figure of J' energy levels for interacting Rydberg ($E_{J'}(1)$; black; left) and ion-pair ($E_{J'}(2)$; red; right) vibrational states and repulsion interaction effects (blue arrows). The interactions are non-degenerate and involve shifts of energy levels as indicated by the arrows and state mixing, both which increase as the energy difference ($\Delta E_{J'} = |E_{J'}(1) - E_{J'}(2)|$) decreases, to an extent which depends on the interaction strength (W_{12}).

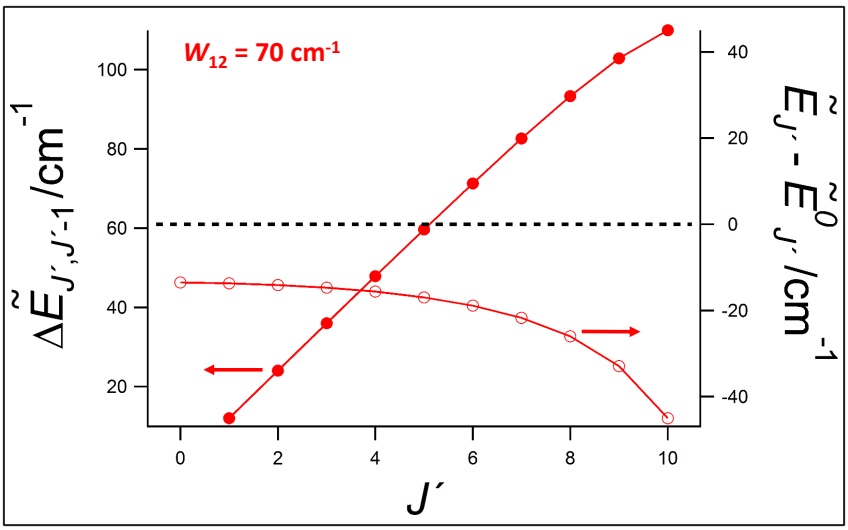

Fig. S5: Effect of Rydberg (1) to ion-pair(2) state interactions (non-degenerate interactions; see Fig. S4) on energy level shifts of a Rydberg state (1), for the rotational constants, $B´(1) = 6.1$ cm^{-1} and $B´(2) = 3.5$ cm^{-1}, band origin difference, $\Delta\nu^0 = \nu^0(2) - \nu^0(1) = 350$ cm^{-1} and $W_{12} = 70$ cm^{-1}. Filled dots, are $\Delta E_{J´,J´-1}$ (= $E_{J´}(1) - E_{J´-1}(1)$) vs. $J´$. Unfilled dots represent the difference between the perturbed and unperturbed energy levels ($E_{J´}(1) - E^0_{J´}(1)$). Broken curves are for unperturbed energies. The plot of $\Delta E_{J´,J´-1}$ vs. $J´$ shows characteristic negative curvature due to the interaction.

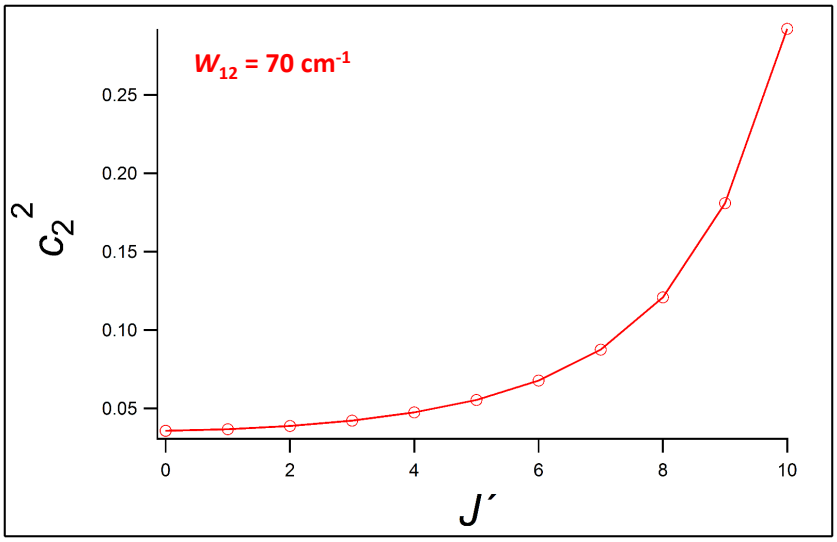

Fig. S6: Fractional contributions (c_2^2) of the ion-pair state (2) character in the Rydberg state(1) as a function of $J´$ in the state interaction described in the figure caption of Fig. S5 (see above). Mixing of non-degenerate levels decrease as $J´$ deviates more from near-degenerate level(s).

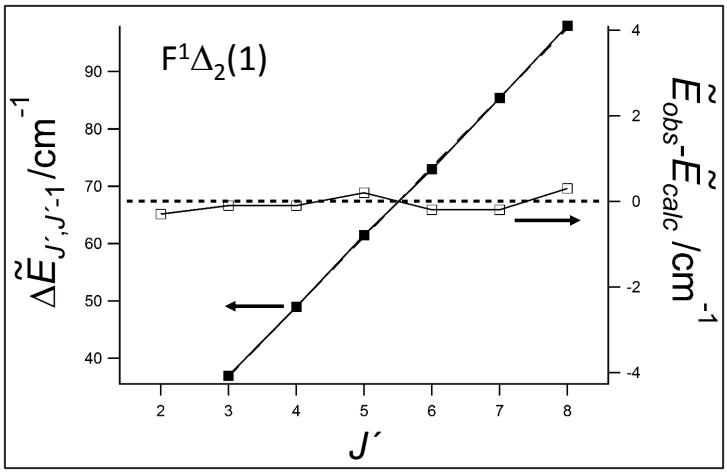

Fig. S7: $F^1\Delta_2$(v´ = 1) in interaction system A. Spacing between rotational levels ($\Delta E_{J',J'-1}$) as a function of J' (filled dots (experimental) and broken curve(fit function); vertical axis to left). Unfilled dots represent the energy difference between the observed energy levels (E_{obs}) and and energy values derived from the fit function (E_{calc}) (vertical right axis).

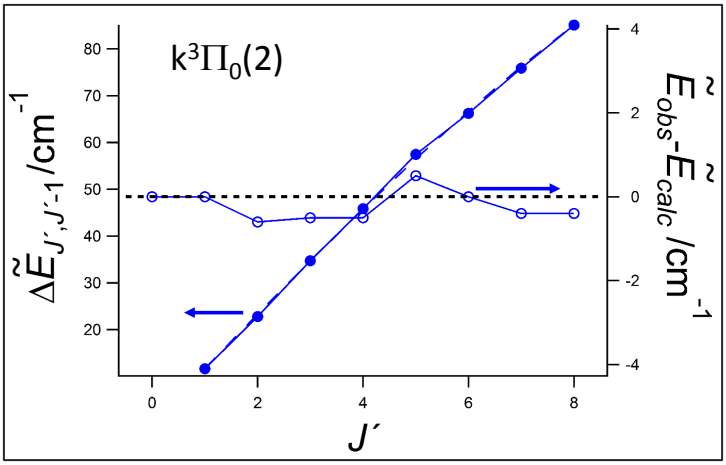

Fig. S8: $k^3\Pi_0$(v´ = 2) in interaction system A. Spacing between rotational levels ($\Delta E_{J',J'-1}$) as a function of J' (filled dots (experimental) and broken blue curve(fit function); vertical axis to left). Unfilled dots represent the energy difference between the observed energy levels (E_{obs}) and and energy values derived from the fit function (E_{calc}) (vertical right axis).

Article 6

Revealing photofragmentation dynamics through interactions between Rydberg states: REMPI of HI as a case study.

Helgi Rafn Hróðmarsson and Ágúst Kvaran

Physical Chemistry Chemical Physics. **17**, 32517 (2015).

DOI: 10.1039/c5cp06185g

Helgi Rafn Hróðmarsson independently developed the research concept. Helgi performed all of the data analysis and independently wrote the first manuscript. He contributed to editing until publication.

PCCP

PAPER

Cite this: *Phys. Chem. Chem. Phys.*, 2015, **17**, 32517

Revealing photofragmentation dynamics through interactions between Rydberg states: REMPI of HI as a case study

Helgi Rafn Hróðmarsson and Ágúst Kvaran*

Received 13th October 2015,
Accepted 11th November 2015

DOI: 10.1039/c5cp06185g

www.rsc.org/pccp

High energy regions of molecular electronic states are largely characterized by the nature and involvement of Rydberg states. Whereas there are a number of observed dynamical processes that are due to interactions between Rydberg and valence states, reports on the corresponding effect of Rydberg–Rydberg state interaction in the literature are scarce. Here we report a detailed characterization of the effects of interactions between two Rydberg states on photofragmentation processes, for a hydrogen halide molecule. Perturbation effects, showing as rotational line shifts, intensity alterations and line-broadenings in REMPI spectra of HI, for two-photon resonance excitations to the $j^3\Sigma^-(0^+; v' = 0)$ and $k^3\Pi_1(v' = 2)$ Rydberg states, are analyzed. The data reveal pathways of further photofragmentation processes involving photodissociation, autoionization and photoionization affected by the Rydberg–Rydberg state interactions as well as the involvement of other states, close in energy. Detailed mechanisms of the involved processes are proposed.

Introduction

Since the original work on the spectroscopy of the hydrogen halides, performed by Price,[1] hydrogen iodide (HI) has been the subject of various studies related to its electronic structure, potential energy surfaces, photodissociation and photofragmentations. Absorption measurements performed by Tilford *et al.*,[2] M. L. Ginter *et al.*,[3] and D. S. Ginter *et al.*,[4] respectfully, provided a comprehensive overview of Rydberg and valence (ion-pair) states observed in the excitation region between 52 610 cm^{-1} and 74 400 cm^{-1}. Assignments of the HI Rydberg states were based on comparison of the observed spectral series and known Rydberg series for xenon.[5] Lower energy states, of repulsive potential curves, in the range 32 000 cm^{-1} to 52 000 cm^{-1}, as well as relevant photodissociation branching ratios have been studied extensively[6–22] and a number of *ab initio* calculations of the relevant potential curves have been performed.[23–30] Studies of competitions between spin–orbit autoionization and predissociation of Rydberg states have been performed[25,31–33] and the ground state of the molecular ion, HI^+, has been explored by a number of experimental techniques.[27,34–42] The first resonance enhanced multiphoton ionization (REMPI) experiments for HI were performed by Wright and McDonald[43] and Pratt and Ginter.[44] Later, the REMPI technique was used complementarily with photolysis for three-photon excitations in the region of 82 050 cm^{-1} and 83 250 cm^{-1},[45] and branching ratios were determined by previous usage of the photolysis technique.[14,19,21,22,29] Velocity map images, following a three-photon excitation scheme at 108 000 cm^{-1} (13.39 eV) and 125 700 cm^{-1} (15.59 eV) were recorded by Loock *et al.*,[46] where iodine fragments were used to derive information regarding interactions between repulsive and super-excited states. Two-dimensional photoelectron spectroscopy studies of HI were performed for the 89 530–119 800 cm^{-1} (11.10–14.85 eV) excitation region by Hikosaka and Mitsuke,[47] to cover the energy range between the ionic ground state ($X^2\Pi$) and the excited ionic state $A^2\Sigma^+$. In recent years, an appreciable amount of REMPI work has been performed on the hydrogen halides, emphasizing interactions between Rydberg and ion-pair states, mostly for HCl[48–51] and HBr.[51,52] The emphasis has, only recently, shifted towards HI for the two-photon excitation region of 69 600–73 500 cm^{-1}, where relevant studies have focused on the assignment of new states,[53] state interactions[54] as well as identifications and assignments of hidden (or dark) states.[55]

Localized level-to-level interactions between Rydberg states and ion-pair states have been investigated to a large extent for the hydrogen halides both qualitatively and quantitatively, whereas analogous interactions between Rydberg states have only been dealt with speculatively. (*e.g.* see ref. 55 and references therein). In this paper we present, for the first time, a characterization of localized level-to-level interactions between two Rydberg states in one of the hydrogen halide molecules (HI). Based on perturbation effects in the REMPI spectra of HI for two-photon

Science Institute, University of Iceland, Dunhagi 3, 107 Reykjavík, Iceland.
E-mail: agust@hi.is; Fax: +354-552-8911; Tel: +354-525-4672, +354-525-4800

resonance excitations to the triplet Rydberg states $j^3\Sigma^-(0^+; v' = 0)$ and $k^3\Pi_1(v' = 2)$, state interactions are determined quantitatively. Furthermore, the impact of the state interactions on photofragmentation pathways upon additional photoexcitation is explored.

Experimental

The experimental apparatus as well as relevant equipment parameters are similar to that described in previous publications.[52–55] Therefore, only a short summary will be addressed.

Mass resolved REMPI data for a HI molecular beam were recorded. The beam was created by a jet expansion of a pure gas sample through a pulsed nozzle and ions were directed into a time-of-flight tube and detected by microchannel plates (MCP) to record the ion yields as a function of mass and laser radiation wavenumber. Signals were recorded by a LeCroy Wavesurfer 44MXs-A, 400 MHz storage oscilloscope. Tunable excitation radiation was generated by an Excimer laser-pumped dye laser system, using a Lambda Physik COMPex 205 Excimer laser and a Coherent ScanMatePro dye laser, with a C-540 dye. Frequency doubling was achieved by using a SIRAH second harmonic generator (SHG). Laser power was minimized to prevent saturation effects and power broadening. Laser calibration was based on observed (2 + 1) REMPI iodine atomic lines.[55] The accuracy of the calibration was found to be about ± 0.5 cm^{-1} on the laser wavenumber scale, hence about ± 1.0 cm^{-1} on the two-photon wavenumber scale.

Theory

Line shift determining factors

In molecular spectra, perturbations give invaluable insight into the mechanisms of various state interactions. State interactions are classified as homogeneous ($\Delta\Omega = 0$) and heterogeneous ($\Delta\Omega \neq 0$) and the resulting perturbations differ in accordance with their nature. Thus, if $\Delta\Omega = 0$, the interactions are independent of rotational quantum numbers, J', whereas if $\Delta\Omega \neq 0$, interactions are J' dependent. In REMPI spectra of the hydrogen halides, these effects have been found to manifest themselves as spectral line shifts (hence energy level shifts) in the cases of interactions between Rydberg and ion-pair states.[48–50,52,54–57]

When dealing with perturbations, caused by two interacting states, (1) and (2), it is customary to utilize the diagonalization of the Hamiltonian matrix elements[58] for interactions between energy levels with the same J' quantum numbers, which depend on the zeroth order unperturbed energies ($E^0_{J'}(1)$ and $E^0_{J'}(2)$) and the interaction strength (W_{12}),

$$\begin{array}{ccc} & 1 & 2 \\ 1 & E^0_{J'}(1) & W_{12} \\ 2 & W_{12} & E^0_{J'}(2) \end{array} \quad (1)$$

for

$$E^0_{J'}(i) = \nu^0(i) + B'(i)J'(J'+1) - D'(i)J'^2(J'+1)^2,\ i = 1, 2 \quad (2)$$

where $\nu^0(i)$ are the band origins, $B'(i)$ are the rotational constants, and $D'(i)$ are the centrifugal distortion constants. This yields the observed, perturbed energy levels ($E_{J'}(1)$ and $E_{J'}(2)$),

$$E_{J'}(i) = \frac{1}{2}\left(E^0_{J'}(1) + E^0_{J'}(2)\right) \pm \frac{1}{2}\left[4|W_{12}|^2 + \left(E^0_{J'}(1) - E^2_{J'}(2)\right)\right]^{1/2}, \quad i = 1, 2 \quad (3)$$

For homogeneous interactions, W_{12} is a constant, whereas for heterogeneous interactions

$$W_{12} = W_{12}{}' \sqrt{(J'(J'+1))} \quad (4)$$

where $W_{12}{}'$ is a constant.

In the limit of $\Delta E_{J'}(= E_{J'}(1) - E_{J'}(2)) \approx 0$, solutions are approximated by the degenerate state perturbation theory[58,59] which yields very large energy level shifts, characteristic for "near-degenerate" J' levels. Hereby, we shall refer to such cases as "near-degenerate interactions" to distinguish them from "non-degenerate interactions".

Line strength determining factors

Several factors govern the rotational line strengths in REMPI spectra. The relative intensities (I_{rel}) are proportional to the product of the cross sections of the resonance excitation step (σ_1) and the photoionization step (σ_2).

$$I_{\mathrm{rel}} \propto \sigma_1\sigma_2 \quad (5)$$

The cross section for the photoionization step (σ_2), is commonly a slowly varying function with photon energy and in the cases where the excitation frequency range is narrow, it can be assumed to be constant, of a value depending on the ionized state ($\sigma_2(\Omega')$). The cross section of the resonance excitation step (σ_1) is expressed as,[60–62]

$$\sigma_1 \sim \left|\sum_i \frac{\langle 1|\boldsymbol{\varepsilon}\cdot\boldsymbol{\mu}|i\rangle\langle i|\boldsymbol{\varepsilon}\cdot\boldsymbol{\mu}|0\rangle}{\Delta E_{0i} - h\nu + C(\Gamma_i)}\right|^2 \quad (6)$$

for a two-photon transition between the states $|0\rangle$ and $|1\rangle$. $h\nu$, is the photon energy, $\boldsymbol{\varepsilon}\cdot\boldsymbol{\mu}$ is the operator representing the interaction between the electric field component of the electromagnetic wave and the molecular charge dipole and $|i\rangle$ is an intermediate state with energy ΔE_{0i}. Based on the Born–Oppenheimer approximation, eqn (6) can be simplified and approached by a product of terms depending on the electron configuration (C_e) and the nuclear motions ($S(\Delta\Omega, J', J'')$ and $\mathrm{FCF}(v', v'')$),

$$\sigma_1 = C_e S(\Delta\Omega, J', J'')\mathrm{FCF}(v', v'') \quad (7)$$

where $\mathrm{FCF}(v', v'')$ is the Franck–Condon-Factor, depending on the vibrational quantum numbers v' and v'' and $S(\Delta\Omega, J', J'')$ is the transition strength, depending on the rotational quantum numbers (J', J'') and the difference in the total electronic angular momentum quantum numbers ($\Delta\Omega = |\Omega' - \Omega''|$). $S(\Delta\Omega, J', J'')$ also depends on the parallel ($\mu_\parallel$) and perpendicular ($\mu_\perp$)

transition dipole moments that correspond to transitions to the virtual intermediary state(s), $|i\rangle$.

$$\mu_{\parallel} = \langle \Omega | \boldsymbol{\varepsilon} \cdot \boldsymbol{\mu} | \Omega \rangle \quad (8a)$$

$$\mu_{\perp} = \langle \Omega \pm 1 | \boldsymbol{\varepsilon} \cdot \boldsymbol{\mu} | \Omega \rangle \quad (8b)$$

The general expression of the two-photon transition strength is[63]

$$S(\Delta\Omega, J', J'') = s_0 {\mu_0}^2 + s_2 {\mu_2}^2 \quad (8c)$$

where s_0 and s_2 are functions of J' and J'' as well as Ω' and Ω'' and are written in terms of Clebsch–Gordan coefficients for zeroth order coefficients (subscript 0) and second order coefficients (subscript 2).[63,64] ${\mu_0}^2$ and ${\mu_2}^2$ are sum and product functions of ($\mu_{\parallel}$) and ($\mu_{\perp}$) which collectively represent the effect of all one-photon transition moments that give rise to parallel and perpendicular transitions.

Furthermore, the relative intensity (I_{rel}) is proportional to the population ($N(v'', J'')$) and the degeneracy ($g(J'')$) of the absorbing state as well as the laser power (P) as P^n, where n represents the total number of photons absorbed.[65]

All in all, I_{rel} can be expressed as

$$I_{\mathrm{rel}} = K(\Omega') P^n [C_e S(\Delta\Omega, J', J'') \mathrm{FCF}(v', v'')][g(J'') N(v'', J'')] \quad (9)$$

where $K(\Omega')$ is a constant depending on the ionized state. For a certain electronic and vibrational ($v' \leftarrow\leftarrow v''$) transition C_e and FCF(v',v'') can be assumed to be constant, to a first approximation.

Line width determining factors

Lower limit lifetimes (τ_{min}) can be derived from spectral line widths (Γ) by[58]

$$\tau_{\mathrm{min}}\ (\mathrm{ps}) = 5.3/\Gamma\ (\mathrm{cm}^{-1}) \quad (10)$$

Line widths of Rydberg state spectra are primarily affected by predissociation processes. Such processes can occur *via* gateway Rydberg states in which cases the lifetimes, hence linewidths, depend on bound-to-bound Rydberg state interactions as well.[52,54,55]

Results

Spectral observations

Fig. 1 shows REMPI spectra in the two-photon excitation region of 73 098–73 261 cm^{-1}. By comparison with the work by Ginter *et al.*[4] the major spectral features were assigned to two-photon resonance transitions to the $j^3\Sigma^-(0^+; v' = 0)$ and $k^3\Pi_1(v' = 2)$ Rydberg states with the electron configurations $(\sigma^2\pi^3)5d\pi$ and $(\sigma^2\pi^3)5d\delta$, respectively. In this respect, it should be mentioned that, whereas, the lighter hydrogen halides have been assigned according to the Hunds case (a) and Hunds case (b) classifications, HI correlates better with the Hunds case (c) classification[2–4,55] and, furthermore, that super-excited states of HI have been shown to display the Hunds case (e) characteristics.[25] Nevertheless, it has been a convention to retain the assignments of HI states according to the Hunds cases (a) and (b).[2–4,43–45,54,55,57,65,66] The observed line positions (Fig. 1) of the $j(0)$ (*i.e.* $j^3\Sigma^-(0^+; v' = 0)$) and

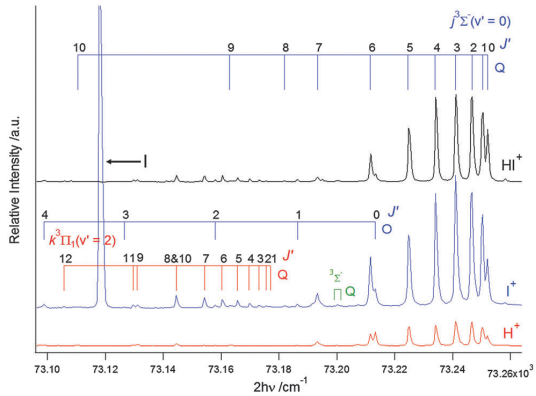

Fig. 1 REMPI spectra of HI for the ions H^+, I^+ and HI^+. *J*-Quantum numbers for the excited states (*J*′) of rotational peaks corresponding to two-photon resonance excitations from the ground state to the $j^3\Sigma^-(0^+; v' = 0)$ and $k^3\Pi_1(v' = 2)$ Rydberg states are indicated. *Q* lines due to transitions to a $^3\Sigma^-(\Omega = 1)$ Rydberg state are marked. An iodine atomic line, at 73 117.9 cm^{-1}, is marked.

Table 1 Rotational lines for HI due to two-photon resonance transitions (cm^{-1}) from the ground state $X^1\Sigma^+(v'' = 0)$ to the $j^3\Sigma^-(0^+; v' = 0)$ and $k^3\Pi_1(v' = 2)$ Rydberg states *vs.* *J*-quantum numbers for the upper states (*J*′)

	$k^3\Pi_1(2)$	$j^3\Sigma^-(0^+; 0)$		
J'	*Q*	*O*	*Q*	*S*
0		73213.3	73252.0	
1	73177.0	73186.4	73250.4	
2	73175.6	73157.9	73246.7	73285.8
3	73173.0	73126.6	73241.0	73309.1
4	73169.7	73098.4	73234.0	73328.7
5	73165.6		73224.7	73345.4
6	73160.3		73211.6	
7	73154.2		73193.3	
8	73144.5		73181.9	
9	73131.0		73105.7	
10	73144.5		73056.6	
11	73129.5			
12	73105.7			

$k(2)$ (*i.e.* $k^3\Pi_1(v' = 2)$) spectra are presented in Table 1. It is clear that level-to-level interactions are taking place for $J' = 9$–10. Thus, the corresponding $j(0)$ lines are found to be significantly spread apart, whereas the $J' = 9$ and 10 lines for the $k(2)$ spectrum are interchanged. The $J' = 10$ line of the $k(2)$ spectrum is shifted upwards in energy, so radically, that it merges with the $J' = 8$ peak. The assignment was adequately reproduced by simulation calculations by use of the PGOPHER program.[67] Analogous effects have been observed in REMPI spectra of hydrogen halides in the cases of Rydberg to ion-pair interactions.[50–52,54,55,57] The quantum energy levels of the $j(0)$ and $k(2)$ states, derived from the spectra, are presented in Fig. 2. These imply near degenerate interactions between the $j(0)$ and $k(2)$ Rydberg states for $J' = 9$–10, which appear as an expansion of the energy level gap for $k(2)$ but a compression of the corresponding levels for $j(0)$. The symmetries of the two Rydberg states suggest that the interaction of concern is L-uncoupling ($\Delta S = 0$, $\Delta\Omega = \pm 1$), *i.e.* a

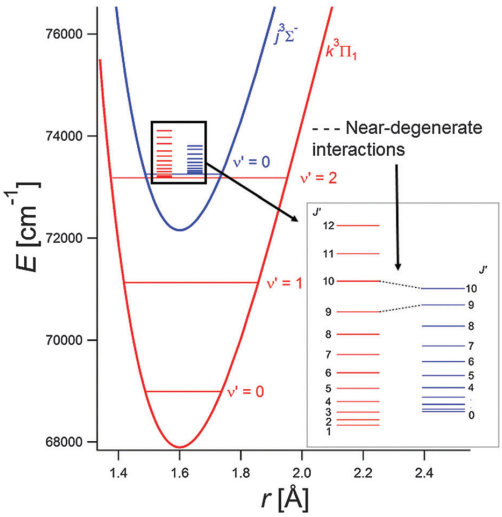

Fig. 2 Potential energy curves and quantum energy levels for the $j^3\Sigma^-(0^+; v' = 0)$ and $k^3\Pi_1(v' = 2)$ Rydberg states. The rotational energy levels were derived from the REMPI spectra (Fig. 1). Near-degenerate interactions between levels $J' = 9$ and 10 are indicated. The potential curve for the $k^3\Pi_1(v' = 2)$ state was derived from available spectroscopic constants.[4,55,57] The shape of the potential curve for the $j^3\Sigma^-(0^+; v' = 0)$ state was approximated by the curve for the $k^3\Pi_1(v' = 2)$ state.

gyroscopic perturbation.[58] In addition to line-shift analysis, the REMPI spectra were explored in terms of signal intensities, and linewidths alterations (see below).

In the region between about 73 196 and 73 210 cm^{-1} weak signals are found in all the spectra. These could not be assigned to either the $j(0)$ or the $k(2)$ state. At 73 117.9 cm^{-1} a strong iodine atomic line is observed. It is a (2 + 1) REMPI of I [$^2P_{1/2}$] for resonance excitation to the atomic Rydberg state $^2[1]^\circ_{1/2}$ ($5s^25p^4(^3P_2)9p$).[68] Furthermore, weak signals close to 73 110 cm^{-1}, are due to a transition to the $V(m + 12)$ (*i.e.* $V^1\Sigma^+(v' = m + 12)$) ion-pair state.[55] A few weak peaks in the region 73 100–73 115 cm^{-1} remain unassigned. These, most likely, belong to the *R* and/or *S* series of the $P(0)$ ($P^1\Delta_2(v' = 0)$) Rydberg state spectrum or possibly high *J*'s of the $V(m + 13)$ ion-pair state.[55] A weak signal observed at 73 200 cm^{-1} is attributed to a transition to a previously unobserved $^3\Sigma^-(\Omega = 1)$ Rydberg state (see Discussion below).

Perturbation analysis

A two-state deperturbation analysis was performed for the $j(0)$ and $k(2)$ Rydberg states. It produced the interaction strengths and spectroscopic constants presented in Tables 2 and 3, respectively. A more detailed discussion of the perturbation analyses procedures follows.

Line shift (LS)-effects

To a first approximation the energy spacing between adjacent rotational levels ($\Delta E_{J',J'-1} = E(J') - E(J' - 1)$) of a non-interacting Rydberg state will display linear behavior as a function of J'. The slope equals $2B_{v'}$, where $B_{v'}$ is the v'-dependent rotational constant. Deviations from linearity are indications of perturbation effects due to state interactions, where rotational levels experience level-to-level repulsions for states with same J' quantum numbers. This effect can be seen more clearly by plotting the difference between the observed level energies ($E_{J'}$), derived from the rotational lines, and the corresponding zeroth order energies derived from eqn (2) (*i.e.* "reduced term value plots"). This has been referred to as line shift (LS)-effects.[54,55]

Table 2 Parameter values (cm^{-1}), level energies (E), energy level differences ($\Delta E_{J'}$) and interaction strengths (W_{12}') relevant to near-degenerate interactions between the $j^3\Sigma^-(0^+; v' = 0)$ and $k^3\Pi_1(v' = 2)$ Rydberg states for $J' = 9$ and 10, derived from perturbation analysis based on peak positions (see text)

J'	$E/k(2)$ state	$E/j(0)$ state	$\Delta E_{J'}$	$\langle W_{12}' \rangle$
9	73707.7	73739.6	−31.9	1.52 ± 0.09
10	73848.9	73814.8	34.1	

Table 3 Spectroscopic parameters (cm^{-1}) for the $k^3\Pi_1(v' = 2)$ and $j^3\Sigma^-(0^+; v' = 0)$ Rydberg states derived from our REMPI spectra and from reported work by Ginter *et al.*[4]

	$k^3\Pi_1(v' = 2)$		$j^3\Sigma^-(0^+; v' = 0)$	
	This work	Others[4]	This work	Others[4]
ν^0	73180.0	73180.7	73252.0	73254.9
$B_{v'}$	6.10 ± 0.06	6.034	5.37 ± 0.06	5.706
$D_{v'}$	0.0014 ± 0.0005	0.000872	0.0007 ± 0.0007	0.00475

LS-effects are clearly apparent in the $j(0)$ and $k(2)$ spectra, as mentioned before. Respective rotational energy level differences, as a function of J', are presented in Fig. 3a along with the corresponding deperturbed curves. The $j(0)$ state displays slight increases in the energy gaps between $J' = 7$ and $J' = 8$ ($\Delta E_{8,7}$) and between $J' = 8$ and $J' = 9$ ($\Delta E_{9,8}$), followed by a significant decrease in the energy gap between $J' = 9$ and $J' = 10$ ($\Delta E_{10,9}$). This effect is "mirrored" in the plot for the $k(2)$ state, which shows significant decreases in $\Delta E_{9,8}$ and $\Delta E_{9,8}$, but an increase in $\Delta E_{10,9}$. It is worth noting that, whereas, the $j(0)$ state is experiencing a significant increase in $\Delta E_{8,7}$ the corresponding decrease in $\Delta E_{8,7}$ for the $k(2)$ state is less. The reduced term value plots shown in Fig. 3b show the LS-effects even clearer. Therein, the $k(2)$ state levels are experiencing slight repulsion effects, downwards, for $J' = 8$ and 9 but a strong repulsion, upwards, for $J' = 10$. This effect is virtually "mirrored" in the $j(0)$ state. In addition, the $j(0)$ state, displays upward shifts of levels $J' = 3$–6, followed by a slight tug downward for $J' = 7$. The additional "non-mirror" effects observed for the $j(0)$ state suggests an additional interaction with another (hidden) state.[55] This will be discussed in more detail below. Furthermore, according to the reduced term value plot (Fig. 3b), levels $J' = 11$ and 12 of the $k(2)$ state display upward repulsion effects.

Line intensity (LI)-effects

The REMPI data for resonance excitations to a Rydberg state of the hydrogen halides (HX) consists of ion signals from the

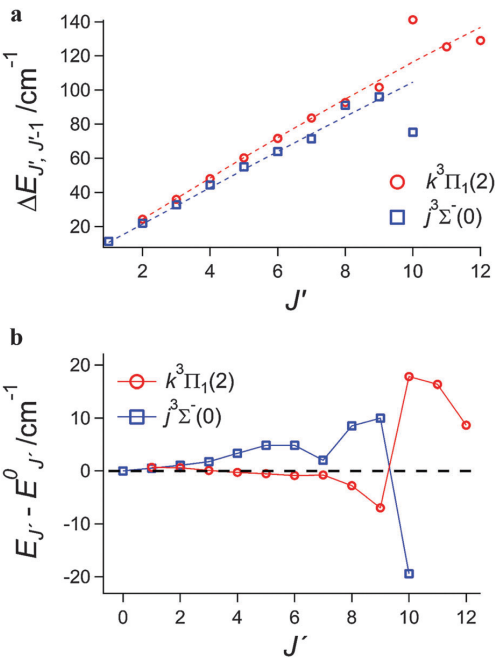

Fig. 3 (a) Spacing between rotational levels ($\Delta E_{J',J'-1}$) as a function of J'; experimental values (dots) and fit curves for the $j^3\Sigma^-(0^+;\ v' = 0)$ and $k^3\Pi_1(v' = 2)$ states and (b) the corresponding reduced term value plots.

parent molecule (HX^+) as well as the ionic fragments (X^+ and H^+). The integrated signals of each respective ion reveal the relative fractions of the various formation pathways, which can depend on state interactions.[48–52,54,55] This has been referred to as line intensity (LI)-effects.[54,55] Thus, in cases of interactions between Rydberg and ion-pair states, the presence of a J' dependent halogen ion signal (X^+) in the REMPI spectrum of a Rydberg state is found to be a strong indication of a Rydberg to ion-pair state mixing.[48,69–72] The intensity ratio, $I[X^+]/I[HX^+]$, (and to a lesser extent $I[H^+]/I[HX^+]$) has been applied to a number of interacting systems to evaluate the level of state mixing.[50,52,54,55,57] Analysis based on LI-effects for Rydberg to Rydberg state interactions, as seen here for the $k(2)$ and $j(0)$ Rydberg states, on the other hand, have not been developed and require a different approach.

According to eqn (9), the relative intensity ratio of the Q rotational lines, of same J' ($= J'' = J$), for the $k(2)$ ($\Omega' = 1$) and $j(0)$ ($\Omega' = 0^+$) spectra in the case of no interaction, simplifies to,

$$\frac{I_{\mathrm{rel}}[k,J]}{I_{\mathrm{rel}}[j,J]} = \frac{K(k)S(k)}{K(j)S(j)} \qquad (11a)$$

where $K(k)$ and $K(j)$ are constants for the two states with values depending on the corresponding ionization cross sections. $S(k)$ and $S(j)$ are the corresponding transition strengths. By using J'-dependent expressions for s_0 and s_2 to determine $S(k)$ ($\Delta\Omega = 1$) and $S(j)$ ($\Delta\Omega = 0$) (eqn (8))[60,63,73] eqn (11a) takes the form,

$$\frac{I_{\mathrm{rel}}[k,J]}{I_{\mathrm{rel}}[j,J]} = \frac{K(k)}{K(j)} \frac{\left(\frac{1}{10}\frac{(2J+1)}{(2J+3)(2J-1)}\right)}{\left(\mu_0^2\left(\frac{1}{9}(2J+1)\right) + \mu_2^2\left(\frac{1}{45}\frac{(J+1)(J+2)}{(2J+3)(2J-1)}\right)\right)} \qquad (11b)$$

for $J = J' = J''$. An investigation of the rotational line intensities of the $j(0)$ and $k(2)$ spectra (Fig. 1 and 4a) shows that the total ion intensities of the $k(2)$ spectrum are relatively large for high J's, whereas the opposite is found for the $j(0)$ spectrum. The corresponding intensity ratio $\frac{I_{\mathrm{rel}}k(2)}{I_{\mathrm{rel}}(j(0))}$, as a function of J' (Fig. 4b) shows close to constant value for low J's but large increases for high J's. The data points for low J's ($J' = 2$–5), where interaction between the two states is found to be negligible (see previous section), were fitted by the expression on the right side of eqn (11b), for μ_0^2, μ_2^2 and $K(k)/K(j)$ as variables. This gave a smooth, slightly varying function of J' for all J's (Fig. 4b). The discrepancy between the data points and the fit curve is a clear indication of state mixing/interaction for high J's ($J' = 8$–10 in particular), which can be partly due to a change in the transition strength (S) and partly because of changes in the ionization cross sections (hence the K's) which manifest as enhanced intensities for high J's in the case of the $k(2)$ spectrum, but as lowered intensities for the $j(0)$ spectrum. This can be referred to as "intensity borrowing".

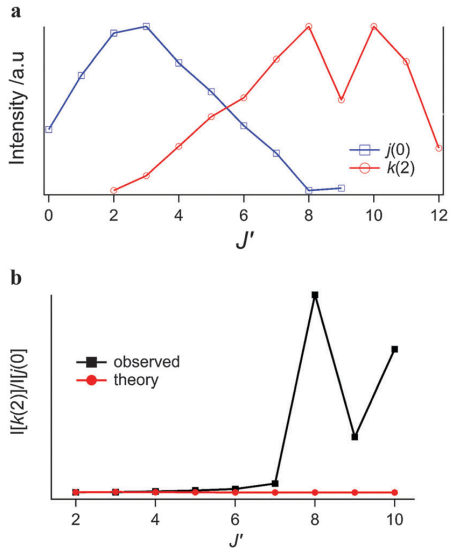

Fig. 4 (a) Total relative rotational line intensities of the $j^3\Sigma^-(0^+;\ v' = 0)$ (blue) and $k^3\Pi_1(v' = 2)$ (red) spectra as a function of J'. (b) Observed total intensity ratios of the Q lines for the $k^3\Pi_1(v' = 2)$ and $j^3\Sigma^-(0^+;\ v' = 0)$ spectra ($I(k(2))/I(j(0))$) (black) as a function of J' and calculated intensity ratios for non-interacting states derived by fitting the data points for $J' = 2$–5 by the expression on the right side of eqn (11b) for μ_0^2, μ_2^2 and $K(k)/K(j)$ as variables.

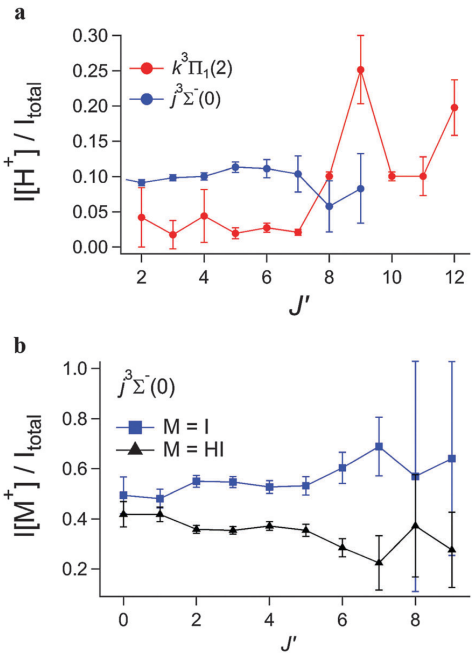

Fig. 5 (a) Relative H^+ ion signal intensities ($I(H^+)/I_{total}$) *vs.* J' derived from the Q rotational lines of the $j^3\Sigma^-(0^+; v' = 0)$ and $k^3\Pi_1(v' = 2)$ spectra. (b) Relative ion signal intensities ($I(M^+)/I_{total}$), $M^+ = I^+$, HI^+ *vs.* J' derived from the Q rotational lines of the $j^3\Sigma^-(0^+; v' = 0)$ spectrum.

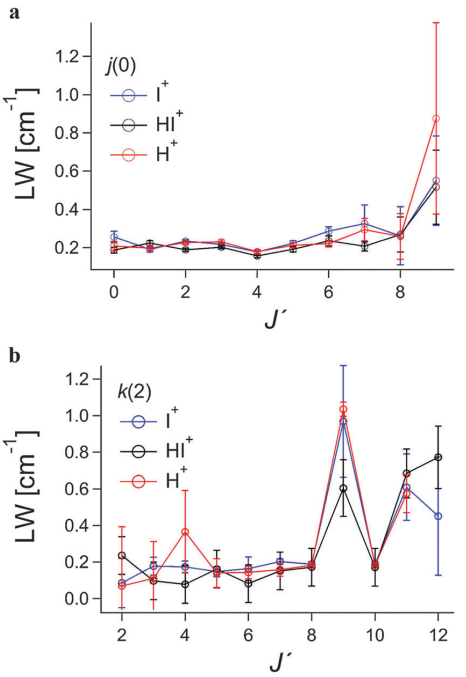

Fig. 6 (a) Rotational linewidths as a function of J' derived from the Q lines of the H^+, I^+, and HI^+ signals for the (a) $j^3\Sigma^-(0^+; v' = 0)$ and (b) $k^3\Pi_1(v' = 2)$ spectra.

A closer look at the H^+ signals for the $k(2)$ and $j(0)$ spectra (Fig. 5a) reveals that the $j(0)$ spectrum shows a distinctly greater propensity for H^+ formation compared to the $k(2)$ spectrum, for low J's. For higher J's ($J' > 7$), on the other hand, the relative H^+ intensity for $j(0)$ decreases slightly, but significantly, whereas, for $k(2)$, it increases. This observation further supports the effect of "intensity borrowing", given that the $j(0)$ state yields a greater amount of H^+ ions (Fig. 1).

The relative contributions of the I^+ and HI^+ ion signals as a function of J' for the $j(0)$ spectrum are shown in Fig. 5b. The curves show clear "mirror image effects"; where relative increase of the I^+ signal is in tandem with a decrease of the HI^+ signal and *vice versa*. No such effect is observed in the $k(2)$ spectrum. As previously stated, a rise in the intensity of a halogen fragment ion signal and a decrease in that of the molecular ion for a Rydberg state is characteristic of increased interactions with an ion-pair state. We believe that this effect can, partly, be attributed to additional non-degenerate interactions with ion-pair vibrational state(s). The sharp change in the relative intensities for $J' = 6$–7, on the other hand, suggests that near-degenerate interactions are also involved.

Line width (LW)-effects

The line-widths of all the ion signals for the $j(0)$ and $k(2)$ spectra as a function of J' are presented in Fig. 6a and b, respectively. For $j(0)$ the line-widths, are small (*ca.* 0.2 cm^{-1}) and close to constant for low J's ($J' = 0$–5), show slight increase for $J' = 6$–7, drop in the value for $J' = 8$ and finally a relatively large increase for $J' = 9$. The line-widths for the $k(2)$ spectral peaks also are low in values and close to constant, within experimental error, for low J's ($J' = 2$–8) as well as for $J' = 10$, whereas a severe line broadening is observed for $J' = 9$ as well as for $J' = 10$ and 11.

Discussion

Additional perturbing or hidden states

The perturbation analyses, mentioned above, revealed several features in the REMPI spectra that could not be explained by near-degenerate interactions between the $j(0)$ and the $k(2)$ states. These are, in all likelihood, a direct result of interactions with other states, close in energy which may be either hidden or not hidden.[55]

$^3\Sigma^-(1)$ state. A number of observations in the $j(0)$ spectrum, mentioned above, suggest that the $j^3\Sigma^-(0^+; v' = 0)$ state is interacting with an unknown (hidden) state. Thus, dips observed in the reduced term value plot for $J' = 7$ (Fig. 3b), increases in relative I^+ signals and corresponding decreases in relative HI^+ signals (Fig. 5b) as well as line-width alterations (Fig. 6a) for $J' = 6$–7 are all indicative of weak, near-degenerate interaction for $J' = 6$–7. A candidate for such a weak perturber, which apparently is not affecting the, close in energy, $k^3\Pi_1(v' = 2)$ state is a state which will satisfy the requirements of being (i) – a triplet state ($\Delta\Sigma = 0$),

(ii) – a Σ state, (iii) – a state of minus parity, "–" and (iv) an $\Omega = 1$ state, *i.e.* a $^3\Sigma^-(1)$ state. Based on the energetics of known or predicted Rydberg states for HI[53] we suggest that this could either be the $g^3\Sigma^-(1)$ ($v' = 2$) state with electron configuration $[\sigma^2\pi^3]6p\pi$ or the $q^3\Sigma^-(1)$ ($v' = 0$) state with electron configuration $[\sigma^2\pi^3]4f\pi$. Therefore, the weak unassigned spectral features, unclear in structure, which are observed between the Q rotational lines for $J' = 6$ and 7 of the $j(0)$ spectrum (see above and Fig. 1), we assign to the Q lines of the corresponding spectrum.

Ion-pair states. The following observations of the $k(2)$ spectrum, all suggest that the $k(2)$ state is interacting with an additional state. Increases in rotational energies (Fig. 3b), relative intensity of the H^+ signals (Fig. 5a) and line broadenings (Fig. 6b), observed for $J' = 11$–12, are all indicative of weak near-degenerate interactions. Whereas, rotational lines for the ion-pair state $V^1\Sigma^+(v' = m + 13)$ for $J' > 8$ have not been observed in REMPI[55] extrapolation of low rotational energy levels to $J' > 8$ reveals that levels $J' = 11$ and 12 are only slightly lower in energy than the corresponding levels of the $k(2)$ state and could be the cause of the observed perturbation effects. Furthermore, absorption spectra[4] suggest that levels higher than $J' = 7$ of $V(m + 13)$ are, indeed, mixed.

Photofragmentations

The two-photon scan region that spans the rotational line spectra of the $k(2)$ and $j(0)$ states of about 73 100–73 260 cm^{-1} (Fig. 1) corresponds to a three-photon excitation region of 109 650–109 890 cm^{-1} (see Fig. 7). This excitation region has been explored in number of studies by various techniques.[35–38,41,45,47] It is above the molecular ion ground states, $X^2\Pi(\Omega = 1/2, 3/2)$, which correlate with $H(n = 1) + I^+(^3P_2)$ and below the first excited bound ionic state, $A^2\Sigma^+$, which correlates with $H(n = 1) + I^{+*}(^1D_2)$. Furthermore, a super-excited state ($HI^{\#}$), which belongs to a Rydberg series that converges to the $A^2\Sigma^+$ state ($[A^2\Sigma^+]5d\pi$), is believed to be found in that region and is likely to play an important role in further ionization processes.[31,35,47]

Velocity map imaging studies coupled with REMPI by Regan *et al.*[45] for four-photon excitation into this region revealed two major H^+ formation mechanisms. The first mechanism (i) involves the formation of $H^*(n = 2) + I(3/2)$, followed by one-photon ionization of $H^*(n = 2)$. The second mechanism (ii) involved the formation of high vibrational levels ($v^+ \geq 15$) of the HI^+ $X^2\Pi$ state followed by one-photon photodissociation *via* the $^2\Pi_{3/2}$ repulsive state to form $H^+ + I(3/2)$. These mechanisms resemble those found to occur in REMPI of HCl[74–77] and HBr.[76,78,79] By analogy with observations for HCl[49,74–76,80,81] and HBr[52,76,78,79] I^+ formation is likely to involve two additional mechanisms, *i.e.*, (iii) autoionization of $HI^{\#}$, above the dissociation limit of the ionic states, to form the molecular ion in an unstable state ($HI^+(\varepsilon)/HI^{+*}(\varepsilon)$) followed by dissociation (see Fig. 7) and (iv) dissociation of $HI^{\#}$ to form iodine in an atomic Rydberg state (I^{**}) followed by photoionization. The significance of the various ion formation mechanisms ((i)–(iv)) depends on the nature of the resonance excited states ($HI^{**}(v', J')$) involved. Formation and ionization of the excited atom fragments (H^* and I^{**}; (i) and (iv)) preferably will occur for long-range excitations as to be expected for ion-pair states or Rydberg states which interact (mix) with ion-pair states. Similarly HI^+/HI^{+*} species are likely to be formed in high v^+ levels, followed by photodissociation to form H^+ in the cases of long range excitations (from ion-pair states or mixed "Rydberg-ion-pair states"), whereas population of low v^+ levels and small or negligible H^+ formation is more likely to follow short-range excitations of pure Rydberg states.

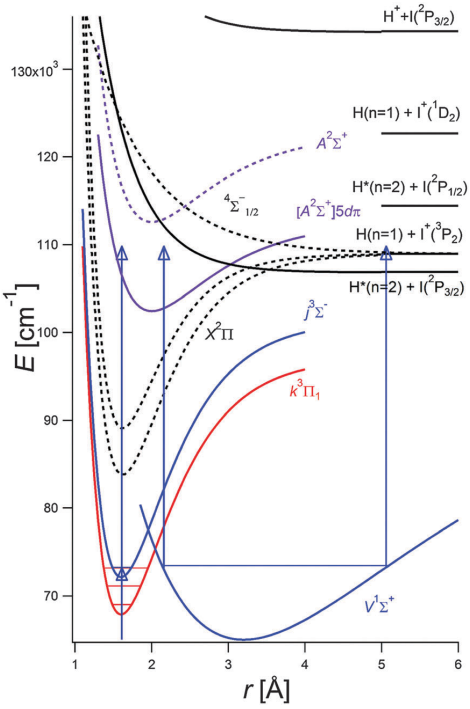

Fig. 7 Potential energy curves, asymptotic energies and photon excitations relevant to state interactions and photofragmentation processes of the $j^3\Sigma^-(0^+; v' = 0)$ and $k^3\Pi_1(v' = 2)$ states as discussed in the paper. The potential curves of the $X^2\Pi$, $A^2\Sigma^+$, $[A^2\Sigma^+]5d\pi$ and the repulsive states are derived from ref. 38, 27, 47 and 21, respectively. For the purpose of this paper, the potential curve of the $V^1\Sigma^+$ ion-pair state was fitted arbitrarily to encompass the lowest observed vibrational state, namely $V(m)$.[4] Arrows, shown correspond to single photon 36 607.6 cm^{-1} excitations.

The photoionization product yields, *via* excitations to the $j(0)$ and $k(2)$ states, are found to be, in descending order as, $I^+ > HI^+ > H^+$ (see Fig. 1 and 5). Whereas the intensity ratios of the I^+ and HI^+ signals is comparable for the two resonance states the relative yield of H^+ is significantly stronger for the $j(0)$ state than for the $k(2)$ state for low J's, but *vice versa* for high J's (see Fig. 1 and 5a).

Photofragmentation of the $j(0)$ state

In accordance with theory,[82] the $j^3\Sigma^-(\Omega' = 0^+, v' = 0)$ state will interact homogeneously with the $V^1\Sigma^+$ ion-pair state through a relatively strong spin–orbit (SO) coupling in the form of non-degenerate level-to-level interactions in addition to the observed near-degenerate interaction with $k(2)$. Therefore, all the ion

formation processes ((i)–(iv)), mentioned in the previous section, whether dominating for short-range (a; Rydberg character) or long-range (b; ion-pair character) excitations are effective to an extent which is determined by the state interaction strength. In the light of our spectral observations and discussion above, we propose the following major photofragmentation processes for HI**, following resonance excitation to the $j(0)$ state,

(a) in the case of a dominating V ion-pair state configuration ($\sigma^1\pi^4\sigma^{*1}$) at long-range:

(i) $HI^{**}(\sigma^1\pi^4\sigma^{*1}) + h\nu \rightarrow HI^{\#}([\sigma^1\pi^3\sigma^{*1}]\text{Ry-}\pi)$;
parallel transition
$HI^{\#}([\sigma^1\pi^4\sigma^{*1}]\text{Ry-}\pi) \rightarrow H^{*}(n = 2) + I$
$H^{*}(n = 2) + h\nu \rightarrow \mathbf{H^+} + e^-$

(ii) $HI^{**}(\sigma^1\pi^4\sigma^{*1}) + h\nu \rightarrow HI^{\#}([\sigma^1\pi^4]5d\pi)$;
perpendicular transition
$HI^{\#}([\sigma^1\pi^4]5d\pi) \rightarrow \mathbf{HI^+(v^+)/HI^{+*}(v^+)} + e^-$;
high v^+; autoionization
$HI^+(v^+)/HI^{+*}(v^+) + h\nu \rightarrow \mathbf{H^+} + I$

(iii) $HI^{**}(\sigma^1\pi^4\sigma^{*1}) + h\nu \rightarrow HI^{\#}([\sigma^1\pi^4]5d\pi)$;
perpendicular transition
$HI^{\#}([\sigma^1\pi^4]5d\pi) \rightarrow HI^+(\varepsilon)/HI^{+*}(\varepsilon) + e^-$
$HI^+(\varepsilon)/HI^{+*}(\varepsilon) \rightarrow H + \mathbf{I^+}$

(iv) $HI^{**}(\sigma^1\pi^4\sigma^{*1}) + h\nu \rightarrow HI^{\#}$
$HI^{\#} \rightarrow H + I^{**}$
$I^{**} + h\nu \rightarrow \mathbf{I^+} + e^-$

(b) in the case of a dominating $j(0)$ Rydberg state configuration ($[\sigma^2\pi^3]5d\pi$) at short-range:

(ii) $HI^{**}([\sigma^2\pi^3]5d\pi) + h\nu \rightarrow HI^{\#}([\sigma^1\pi^4]5d\pi)$;
perpendicular transition
$HI^{\#}([\sigma^1\pi^4]5d\pi) \rightarrow \mathbf{HI^+(v^+)/HI^{+*}(v^+)} + e^-$;
low v^+; autoionization

(iii) $HI^{**}([\sigma^2\pi^3]5d\pi) + h\nu \rightarrow HI^{\#}([\sigma^1\pi^4]5d\pi)$;
perpendicular transition
$HI^{\#}([\sigma^1\pi^4]5d\pi) \rightarrow HI^+(\varepsilon)/HI^{+*}(\varepsilon) + e^-$
$HI^+(\varepsilon)/HI^{+*}(\varepsilon) \rightarrow H + \mathbf{I^+}$

Ions that are formed, are highlighted (bold). According to this scheme, the HI^+ and I^+ ions are both formed *via* long- and short-range excitations, whereas H^+ ions are only formed *via* long-range excitations.

Photofragmentation of the $k(2)$ state

The $k^3\Pi(\Omega' = 1, v' = 2)$ state interacts weakly with the $V^1\Sigma^+(v' = m + 13)$ ion-pair state in the form of heterogeneous, near-degenerate, level-to-level interactions for high J's ($J' = 11$–12) (see above), in addition to the observed near-degenerate interaction with $j(0)$ for $J' \sim 8$–10. Hence, since the $j(0)$ state interacts relatively strongly with the manifold of ion-pair vibrational states (see above), the $k(2)$ state, effectively, experiences interaction with the V ion-pair state for $J' \sim 8$–12, whereas for $J' < 8$ no couplings with the V state are observed. This complies with the observation of a significantly lower H^+ signal seen in the $k(2)$ spectrum for $J' < 8$ compared to that for $J' = 8$–9 suggesting that the H^+ ion formation is strongly associated with a long-range (ion-pair character) excitation as in the case of the $j(0)$ excitation (see above). In light of our spectral observations and discussion above we propose the following major photofragmentation processes for HI**, following resonance excitation to the $k(2)$ state,

(a) in the case of a dominating V ion-pair state configuration ($\sigma^1\pi^4\sigma^{*1}$) for high J's ($J' \sim 8$–12) at long-range: same as for $j(0)$ in the previous section (a(i)–a(iv))

(b) in the case of a dominating $k(2)$ Rydberg state configuration ($[\sigma^2\pi^3]5d\delta$) at short-range ($J' \sim 1$–7):

(ii) $HI^{**}([\sigma^2\pi^3]5d\delta) + h\nu \rightarrow HI^{\#}([\sigma^1\pi^4]5d\delta)$;
perpendicular transition
$HI^{\#}([\sigma^1\pi^4]5d\pi) \rightarrow \mathbf{HI^+(v^+;)/HI^{+};^{*}(v^+;)} + e^-$;
low v^+; autoionization

(iii) $HI^{**}([\sigma^2\pi^3]5d\delta) + h\nu \rightarrow HI^{\#}([\sigma^1\pi^4]5d\delta)$;
perpendicular transition
$HI^{\#}([\sigma^1\pi^4]5d\delta) \rightarrow HI^+(\varepsilon)/HI^{+*}(\varepsilon) + e^-$
$HI^+(\varepsilon)/HI^{+*}(\varepsilon) \rightarrow H + \mathbf{I^+}$

Summary and outlook

Mass-resolved REMPI spectra due to two-photon resonance excitations of HI were recorded in the excitation region of 73 080–73 265 cm^{-1}. The major observed spectral structures were assigned to transitions from the ground molecular state to the $k^3\Pi_1(v' = 2)$ and $j^3\Sigma^-(0^+; v' = 0)$ Rydberg states.[4] Perturbations in the spectral structures, observable as rotational line shifts (LS-effects), line intensity alterations (LI-effects) as well as linewidth alterations (LW-effects), were interpreted and analyzed in terms of near-degenerate level-to-level state interactions. Whereas a number of observations and analyses of localized level-to-level interactions between Rydberg states and ion-pair states have been made for the hydrogen halides, this is the first report of a corresponding work in the case of interactions between two Rydberg states. Perturbation effects in the spectra, which could not be attributed to the $k^3\Pi_1(v' = 2)$–$j^3\Sigma^-(0^+; v' = 0)$ state mixing, were found to be indicative of interactions with – and the presence of – additional states, close in energy. Their appearances (signal intensities) are either very weak or they are hidden from REMPI detection. Thus, based on perturbation effects observed in the $j(v' = 0)$ spectrum, a $^3\Sigma^-(\Omega = 1)$ state, not observed before, with band origin of about 73 200 cm^{-1}, is proposed. Furthermore, effects attributed to interactions between the $k(v' = 2)$ Rydberg state and the $V(v' = m + 13)$ ion-pair states are identified.

The impact of the state interactions on photodissociation and photofragmentation pathways upon additional photoexcitation

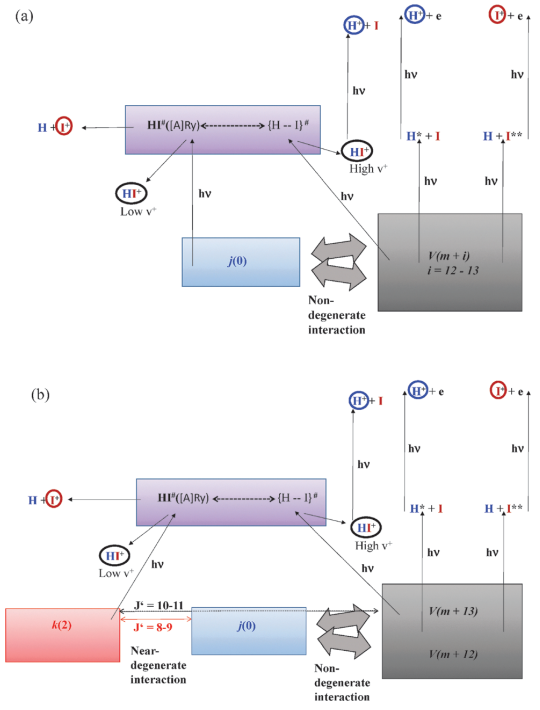

Fig. 8 Schematic figures summarizing state interactions (near- and non-degenerate interactions), photoexcitation and photofragmentation (photodissociation, autoionization, photoionization) processes involved (see main text) with respect to the (a) $j^3\Sigma^-(0^+;\ v' = 0)$ and (b) $k^3\Pi_1(v' = 2)$ Rydberg states. Formed ions are highlighted by circles.

was also explored. Fig. 8a and b summarize the major processes involved following resonance excitations to the $j(v' = 0)$ and $k(v' = 2)$ states, respectively. The $j(v' = 0)$ state, which experiences homogeneous, non-degenerate interactions with the $V(v' = m + 12)$ and $V(v' = m + 13)$ ion-pair vibrational states, for all J' levels, therefore, will form the ions H^+, I^+ and HI^+ *via* one-photon excitations from the interacting V states to super-excited Rydberg states by autoionization (HI^+), photodissociation (H^+) and photoionization (H^+ and I^+) (Fig. 8a). Furthermore, HI^+ and I^+ are formed *via* direct one-photon excitations of the $j(v' = 0)$ Rydberg state to a super-excited Rydberg state by autoionization (HI^+) and photodissociation (H^+). The $k(v' = 2)$ state, which, on the other hand, experiences weak heterogeneous interactions with the $V(v' = m + 13)$ ion-pair state for $J' = 10$–11 and the $j(0)$ state for $J' = 8$–9, therefore, will form the ions H^+, I^+ and HI^+ *via* one-photon excitations from the mixed $V(v' = m + 13)$ state for $J' = 8$–11 only, but I^+ and HI^+ *via* direct excitations of the $k(v' = 2)$ Rydberg state for all J's (Fig. 8b).

Despite the limitations of the standard REMPI technique in terms of detecting photofragments without vector alignments as in *e.g.* velocity map imaging, this study extends the applicability of the REMPI technique to involve the study of photofragmentation pathways which involve Rydberg and ion-par states as intermediates beyond its more common use for spectra recording and analysis. Imaging the individual photofragments of the $j(0)$ *vs.* $k(2)$ system would still bring invaluable insights into the mechanisms that govern photofragmentations in the energy gap of concern.

Acknowledgements

The financial support of the University Research Fund, University of Iceland and the Icelandic Science Foundation (Grant No. 130259-051) is gratefully acknowledged. We would also like to than Huasheng Wang for useful help with the experiments.

References

1 W. C. Price, *Proc. R. Soc. London, Ser. A*, 1938, **167**, 216.
2 S. G. Tilford, M. L. Ginter and A. M. Bass, *J. Mol. Spectrosc.*, 1970, **34**, 327.
3 M. L. Ginter, S. G. Tilford and A. M. Bass, *J. Mol. Spectrosc.*, 1975, **57**, 271.
4 D. S. Ginter, M. L. Ginter and S. G. Tilford, *J. Mol. Spectrosc.*, 1982, **92**, 40.
5 H. T. Wang, W. S. Felps, G. L. Findley, A. R. P. Rau and S. P. McGlynn, *J. Chem. Phys.*, 1999, **67**, 3940–3946.
6 R. S. Mulliken, *Phys. Rev.*, 1937, **51**, 310.
7 J. F. Ogilvie, *Trans. Faraday Soc.*, 1971, **67**, 2205.
8 R. D. Clear, S. J. Riley and K. R. Wilson, *J. Chem. Phys.*, 1975, **63**, 1340–1347.
9 R. Schmiedl, H. Dugan, W. Meier and K. H. Welge, *Z. Phys. A: At. Nucl.*, 1982, **304**, 137–142.
10 P. Brewer, P. Das, G. Ondrey and R. Bersohn, *J. Chem. Phys.*, 1983, **79**, 720–723.
11 G. N. A. van Veen, K. A. Mohamed, T. Baller and A. E. Devries, *Chem. Phys.*, 1983, **80**, 113–120.
12 I. Levy and M. Shapiro, *J. Chem. Phys.*, 1988, **89**, 2900–2908.
13 Z. Xu, B. Koplitz and C. Wittig, *J. Chem. Phys.*, 1989, **90**, 2692–2702.
14 T. N. Kitsopoulos, M. A. Buntine, D. P. Baldwin, R. N. Zare and D. W. Chandler, *SPIE*, 1993, **1858**, 2.
15 V. Kleiman, L. C. Zhu, X. N. Li and R. J. Gordon, *Abstr. Pap. Am. Chem. Soc.*, 1995, **210**, 238-PHYS.
16 L. C. Zhu, V. Kleiman, X. N. Li, S. P. Lu, K. Trentelman and R. J. Gordon, *Science*, 1995, **270**, 77–80.
17 L. Zhu, K. Suto, J. A. Fiss, R. Wada, T. Seideman and R. J. Gordon, *Phys. Rev. Lett.*, 1997, **79**, 4108–4111.
18 J. A. Fiss, L. C. Zhu, K. Suto, G. Z. He and R. J. Gordon, *Chem. Phys.*, 1998, **233**, 335–341.
19 S. R. Langford, P. M. Regan, A. J. Orr-Ewing and M. N. R. Ashfold, *Chem. Phys.*, 1998, **231**, 245–260.
20 P. M. Regan, D. Ascenzi, C. Clementi, M. N. R. Ashfold and A. J. Orr-Ewing, *Chem. Phys. Lett.*, 1999, **315**, 187–193.
21 S. Manzhos, H. P. Loock, B. L. G. Bakker and D. H. Parker, *J. Chem. Phys.*, 2002, **117**, 9347–9352.

22 J. P. Camden, H. A. Bechtel, D. J. A. Brown, A. E. Pomerantz, R. N. Zare and R. J. Le Roy, *J. Phys. Chem. A*, 2004, **108**, 7806–7813.
23 S. R. Ungemach, H. F. Schaefer and B. Liu, *J. Mol. Spectrosc.*, 1977, **66**, 99–105.
24 H. Lefebvre-Brion, A. Giustisuzor and G. Raseev, *J. Chem. Phys.*, 1985, **83**, 1557–1566.
25 A. Mank, M. Drescher, T. Huthfehre, N. Böwering, U. Heinzmann and H. Lefebvre-Brion, *J. Chem. Phys.*, 1991, **95**, 1676–1687.
26 R. J. Le Roy, G. T. Kraemer and S. Manzhos, *J. Chem. Phys.*, 2002, **117**, 9353–9369.
27 A. J. Yencha, P. Baltzer, A. J. Cormack, Y. Li, H. P. Liebermann, A. B. Alekseyev and R. J. Buenker, *J. Chem. Phys.*, 2003, **119**, 5943–5948.
28 A. Brown, *J. Chem. Phys.*, 2005, **122**, 12.
29 D. N. Jodoin and A. Brown, *J. Chem. Phys.*, 2005, **123**, 054301.
30 A. Brown, *Int. J. Quantum Chem.*, 2007, **107**, 2665–2671.
31 J. H. D. Eland and J. Berkowitz, *J. Chem. Phys.*, 1977, **67**, 5034–5039.
32 T. A. Carlson, P. Gerard, M. O. Krause, G. Vonwald, J. W. Taylor and F. A. Grimm, *J. Chem. Phys.*, 1986, **84**, 4755–4759.
33 D. J. Hart and J. W. Hepburn, *Chem. Phys.*, 1989, **129**, 51–64.
34 H. J. Lempka, T. R. Passmore and W. C. Price, *Proc. R. Soc. London, Ser. A*, 1968, **304**, 53.
35 N. Böwering, M. Muller, M. Salzmann and U. Heinzmann, *J. Phys. B: At., Mol. Opt. Phys.*, 1991, **24**, 4793–4801.
36 N. Böwering, H. W. Klausing, M. Muller, M. Salzmann and U. Heinzmann, *Chem. Phys. Lett.*, 1992, **189**, 467–472.
37 N. Böwering, M. Salzmann, M. Muller, H. W. Klausing and U. Heinzmann, *Phys. Rev. A: At., Mol., Opt. Phys.*, 1992, **45**, R11–R14.
38 C. J. Zietkiewicz, Y. Y. Gu, A. M. Farkas and J. G. Eden, *J. Chem. Phys.*, 1994, **101**, 86–94.
39 A. J. Yencha, M. W. Ruf and H. Hotop, *Z. Phys. D: At., Mol. Clusters*, 1994, **29**, 163–177.
40 A. Chanda, W. C. Ho and I. Ozier, *J. Chem. Phys.*, 1995, **102**, 8725–8735.
41 A. J. Cormack, A. J. Yencha, R. J. Donovan, K. P. Lawley, A. Hopkirk and G. C. King, *Chem. Phys.*, 1997, **221**, 175–188.
42 D. J. Gendron and J. W. Hepburn, *J. Chem. Phys.*, 1998, **109**, 7205–7213.
43 S. A. Wright and J. D. McDonald, *J. Chem. Phys.*, 1994, **101**, 238–245.
44 S. T. Pratt and M. L. Ginter, *J. Chem. Phys.*, 1995, **102**, 1882–1888.
45 P. M. Regan, D. Ascenzi, E. Wrede, P. A. Cook, M. N. R. Ashfold and A. J. Orr-Ewing, *Phys. Chem. Chem. Phys.*, 2000, **2**, 5364–5374.
46 H. P. Loock, B. L. G. Bakker and D. H. Parker, *Can. J. Phys.*, 2001, **79**, 211–227.
47 Y. Hikosaka and K. Mitsuke, *J. Chem. Phys.*, 2004, **121**, 792–799.
48 Á. Kvaran, H. S. Wang, K. Matthiasson, A. Bodi and E. Jonsson, *J. Chem. Phys.*, 2008, **129**, 164313.
49 Á. Kvaran, K. Matthiasson and H. S. Wang, *J. Chem. Phys.*, 2009, **131**, 044324.
50 K. Matthiasson, J. M. Long, H. S. Wang and Á. Kvaran, *J. Chem. Phys.*, 2011, **134**, 164302.
51 J. Long, H. Wang and Á. Kvaran, *J. Chem. Phys.*, 2013, **138**, 044308.
52 J. Long, H. R. Hrodmarsson, H. Wang and Á. Kvaran, *J. Chem. Phys.*, 2012, **136**, 214315.
53 H. R. Hrodmarsson, H. S. Wang and A. Kvaran, *J. Mol. Spectrosc.*, 2013, **290**, 5–12.
54 H. R. Hrodmarsson, H. S. Wang and Á. Kvaran, *J. Chem. Phys.*, 2014, **140**, 244304.
55 H. R. Hrodmarsson, H. S. Wang and Á. Kvaran, *J. Chem. Phys.*, 2015, **142**, 244312.
56 J. Long, H. Wang and Á. Kvaran, *J. Mol. Spectrosc.*, 2012, **282**, 20–26.
57 H. R. Hrodmarsson, H. S. Wang and Á. Kvaran, *J. Mol. Spectrosc.*, 2013, **290**, 5–12.
58 H. Lefebvre-Brion and R. W. Field, *The Spectra and Dynamics of Diatomic Molecules*, Elsevier, Amsterdam, 2004.
59 P. A. M. Dirac, *The Principles of Quantum Mechanics*, Oxford University Press, 1930.
60 R. G. Bray and R. M. Hochstrasser, *Mol. Phys.*, 1976, **31**, 1199–1211.
61 R. J. Donovan, in *Gas Kinetics and Energy Transfer*, ed. P. G. Ashmore and R. J. Donovan, The Royal Society of Chemistry, London, 1981, vol. 4, pp. 117–136.
62 Á. Kvaran, H. Wang and Á. Logadóttir, *Recent Research Development in Physical Chemistry*, Transworld Research Network, 1998, vol. 2, pp. 233–244.
63 J. B. Halpern, H. Zacharias and R. Wallenstein, *J. Mol. Spectrosc.*, 1980, **79**, 1–30.
64 R. N. Zare, *Angular Momentum – Understanding Spatial Aspects in Chemistry and Physics*, John Wiley and Sons Inc., USA, 1988.
65 Á. Kvaran, Á. Logadóttir and H. Wang, *J. Chem. Phys.*, 1998, **109**, 5856–5867.
66 D. S. Ginter, M. L. Ginter, S. G. Tilford and A. M. Bass, *J. Mol. Spectrosc.*, 1982, **92**, 55.
67 C. M. Western, *PGOPHER, a Program for Simulating Rotational, Vibrational and Electronic Structure*, University of Bristol, http://pgopher.chm.bris.ac.uk.
68 E. Luc-Koenig, C. V. Morillon and J. Verges, *Phys. Scr.*, 1975, **12**, 199–219.
69 D. S. Green, G. A. Bickel and S. C. Wallace, *J. Mol. Spectrosc.*, 1991, **150**, 303–353.
70 D. S. Green, G. A. Bickel and S. C. Wallace, *J. Mol. Spectrosc.*, 1991, **150**, 354–387.
71 D. S. Green, G. A. Bickel and S. C. Wallace, *J. Mol. Spectrosc.*, 1991, **150**, 388–469.
72 D. S. Green and S. C. Wallace, *J. Chem. Phys.*, 1992, **96**, 5857–5877.
73 Á. Kvaran, H. Wang and B. G. Waage, *Can. J. Phys.*, 2001, **79**, 197–210.
74 A. I. Chichinin, C. Maul and K.-H. Gericke, *J. Chem. Phys.*, 2006, **124**, 224324.

75 A. I. Chichinin, P. S. Shternin, N. Gödecke, S. Kauczok, C. Maul, O. S. Vasyutinskii and K.-H. Gericke, *J. Chem. Phys.*, 2006, **125**, 034310.
76 C. Romanescu and H. P. Loock, *J. Chem. Phys.*, 2007, **127**, 124304.
77 A. I. Chichinin, K.-H. Gericke, S. Kauczok and C. Maul, *Int. Rev. Phys. Chem.*, 2009, **28**, 607–680.
78 C. Romanescu and H. P. Loock, *Phys. Chem. Chem. Phys.*, 2006, **8**, 2940–2949.
79 D. Zaouris, A. Kartakoullis, P. Glodic, P. C. Samartzis, H. R. Hrodmarsson and Á. Kvaran, *Phys. Chem. Chem. Phys.*, 2015, **17**, 10468.
80 C. Romanescu, S. Manzhos, D. Boldovsky, J. Clarke and H. Loock, *J. Chem. Phys.*, 2004, **120**, 767–777.
81 S. Kauczok, C. Maul, A. I. Chichinin and K. H. Gericke, *J. Chem. Phys.*, 2010, **133**, 024301.
82 M. H. Alexander, X. N. Li, R. Liyanage and R. J. Gordon, *Chem. Phys.*, 1998, **231**, 331–343.

Article 7

Two color VMI of HBr: The H(0) and E(1) Rydberg states and the V(m + 7) and V(m + 8) ion-pair states.

Helgi Rafn Hróðmarsson, Huasheng Wang, Ágúst Kvaran, Dimitris Zaouris, Pavle Glodic, Peter C. Samartzis

Manuscript in progress – Unpublished

Helgi Rafn Hróðmarsson performed a significant amount of the data analyses of alignments and some involving the KER spectra. Helgi independently wrote the first draft of the manuscript as presented here.

Rydberg and valence state excitation dynamics: One and Two color VMI study of singlet states in HBr (Manuscript in progress)

Pavle Glodic, Dimitris Zaouris, and Peter C. Samartzis
Institute of Electronic Structure and Laser, Foundation for Research and Technology-Hellas, Vassilika Vouton, 71110 Heraklion, Greece.

Helgi Rafn Hróðmarsson, Huasheng Wang, and Ágúst Kvaran*
Science Institute, University of Iceland, Dunhagi 3, 107 Reykjavík, Iceland.

Total number of pages in manuscript: 19
Tables: 2
Figures: 7 (12 subfigures)
Two color VMI of HBr - draft_160205.docx

Running head title, if needed:

*Correspondence should be addressed to:

Agust Kvaran
Permanent address:
Science Institute,
University of Iceland,
Dunhagi 3, 107 Reykjavík,
Iceland
Phone: +354-525-4672 (A.K. office)
Phone: +354-525-4800 (main office)
Fax: +354-552-8911 (main office)
E-mail: agust@hi.is

Abstract

One and two color velocity map imaging (VMI) techniques, coupled with REMPI, along with mass resolved spectra are complementarily utilized to elucidate the involvement of singlet state interactions in photofragment processes for HBr. The $H^1\Sigma^+(v' = 0)$ and $E^1\Sigma^+(v' = 1)$ Rydberg and the $V^1\Sigma^+(m + 7)$ and $V^1\Sigma^+(m + 8)$ ion-pair resonance states are explored as a function of rotational quantum numbers in the two-photon excitation region of 79 100 – 80 700 cm^{-1}. H^+ and Br^+ images were recorded by one- and two color excitation schemes. Kinetic energy release (KER) spectra and angular distributions were extracted from the data. Mass resolved REMPI spectra as well as angular distributions derived by one color REMPI, revealed the effects of interactions between i) the $E(1)$ and $V(m + 8)$ state and ii) the $H(0)$ state and the $V(m + 7)$ and $V(m + 8)$ states. The two color VMI experiments helped to decipher the role of various repulsive valence states in fragmentation processes and predissociations of the resonance excited states.

I. INTRODUCTION

Ever since the revolutionary work on photofragmentations by Eppink and Parker with the velocity map imaging technique (VMI),[1, 2] the study of fragmentation dynamics has exploded with applications of both 2D[3] and 3D[4] imaging methods. Such experiments yield a wealth of dynamical information regarding the nature of fragmentations and the anisotropy of photoproduct scattering. The VMI techniques have been successfully employed in resolving the complex fragmentation pathways involved in resonance enhanced multiphoton ionization (REMPI) excitations.

Multiphoton excitations of the hydrogen halides have become a benchmark for studies of high energy Rydberg and valence states and the interactions between them. At high energies, the density of states increases, resulting in complicated and perturbed spectra where excitation dynamics involve predissocitation, autoionization, and curve crossings. The information

reservoir derived from REMPI spectra of the hydrogen halides is steadily increasing with extensive work performed on HCl,[5-28] HBr,[15, 20, 28-34] and HI.[15, 35-43] Furthermore, multiphoton excitations coupled with velocity map imaging have been complimentarily utilized to elucidate both photodissociation and photofragmentation pathways in HCl,[44-49] HBr,[45, 47, 49-52] and HI.[39]

For HBr, fragmentation studies feature examinations of the photodissociations via excitations to low energy repulsive states,[45, 50, 53, 54] photodissociations through intermediate Rydberg states[47, 49, 52] and ion-pair states,[49, 52] superexcited state reconstructions,[51] and formation of bromine atoms from clusters.[55] Some of the experimental studies have utilized *ab initio* calculations,[30, 47, 54] which turned out to be useful in resolving various properties, such as potential curves,[56, 57] ion distributions,[30] spin-orbit branching ratios,[58] and anisotropy parameters.[59]

Recently, one color VMI coupled with (2 + *n*) REMPI were used to investigate the interactions between the $E^1\Sigma^+(v' = 0)$ Rydberg state and the $V^1\Sigma^+(v' = m + i)$, $i = 4, 5$, ion-pair states.[52] These had previously been studied by mass resolved REMPI with emphasis on state interactions derived from spectral perturbation effects.[28] From the studies of REMPI spectra,[28] an energetics scheme was proposed to explain the observed perturbation effects. These were found to be helpful in resolving the fragmentation processes examined in the VMI studies.[52] Therein, it was demonstrated that the total kinetic energy releases and angular distributions of the fragmentation processes were largely dependent on quantum level resonance excitations to the *E* state and the *V* ion-pair states and state mixings. The results became an impetus to further study the $E^1\Sigma^+(v' = 1)$ state as well as the $H^1\Sigma^+(v' = 0)$ state, both of which have been shown to experience analogous interactions with the $V^1\Sigma^+(m + 7)$ and $V^1\Sigma^+(m + 8)$ ion-pair states.[34]

In this paper we utilize both one color and two color REMPI coupled with VMI for HBr to investigate photofragmentation pathways. These include interactions between the $E^1\Sigma^+(v' = 1)$ and $H^1\Sigma^+(v' = 0)$ Rydberg states and the $V^1\Sigma^+(m + 7)$ and $V^1\Sigma^+(m + 8)$ ion-pair states.

II. EXPERIMENTAL

The VMI setup used in this work has been described in detail before.[60, 61] Hence, only a brief description will be given here.

The apparatus consists of two differentially pumped chambers. Firstly, a source region which is pumped by a Leybold, DI 3000 diffusion pump. Secondly, a detection region which is pumped by a Leybold, Turbovac 600 turbo-molecular pump. A supersonic molecular beam, typically of a mixture of 15% HBr in He, was formed by expansion through a home-made piezoelectrically actuated nozzle valve before being skimmed prior to entering the detection chamber. A stagnation pressure of $P_0 \leq 1$ bar and a nozzle diameter of 1 mm was used. A skimmer (ø1.5 mm Beam Dynamics) was positioned approximately 5 cm from the nozzle orifice.

A photolysis/photofragment ionization laser beam is focused ($f = 20$ cm) on the geometric focal point of the repeller and extractor plates where it intersects the collimated molecular beam at right angles. In one-color experiments, the laser beam is generated by a pulsed Nd^{3+}:YAG (Spectra Physics Quanta Ray Pro 250) pumping a master oscillator - power oscillator system (Spectra Physics MOPO 730-10) set at the appropriate wavelength. In two-color experiments, a second excimer-pumped (Lambda Physik LPX300, operating with XeCl) pulsed-dye laser (Lambda Physik LDP3000) pulses are also used with an appropriate dye and a BBO crystal to achieve (2 + 1) REMPI of the quantum-state-selected photofragments generated by the MOPO system. In the case of two-color experiments, the two lasers are counter-propagating and focused onto the collimated molecular beam by $f = 30$ cm lenses. The photolysis laser is used to generate neutral fragments and after a suitable time delay, the probe laser is used to ionize one of the quantum-state-selected fragments by REMPI. To detect the Br and Br* fragments

(see below), 260.622 nm and 262.540 nm radiations were used to achieve (2 + 1) REMPI through the $4s^24p^4(^3P_2)5d(^4D°_{3/2})$ and $4s^24p^4(^3P_0)5p(^2P°_{1/2})$ Rydberg states, respectively.

The probe laser pulses were delayed with respect to the photolysis pulse, in order to allow a sufficient density of photofragments to build up prior to REMPI detection. Moreover, the time delay had to be carefully adjusted in order to avoid "fly-out" of the photofragments. Typically, the delay was set at about 10 ns.

III. EXCITATION & FRAGMENTATION MECHANISMS

In one color experiments, the two-photon wavenumber region 79 040 – 80 300 cm^{-1} is inspected in terms of resonance excitations to the $E^1\Sigma^+(v' = 1)$ and $H^1\Sigma^+(v' = 0)$ Rydberg states as well as the $V^1\Sigma^+(v' = m + 7)$ and $V^1\Sigma^+(v' = m + 8)$ ion-pair states. The excitations involve transitions from the molecular ground state ($\sigma^2\pi^4$) via "virtual states" which borrow characters from repulsive valence states ($\sigma\pi^4\sigma^*$). These repulsive states have both been inspected by experiment[45, 50, 53] as well as theory[30, 54, 62] and are as follows: $a^3\Pi_1$, $A^1\Pi_1$, $a^3\Pi_{0+}$,and $t^3\Sigma^+_{0,1}$, respectively. The $a^3\Pi_1$ and $A^1\Pi_1$ repulsive states correlate with H + Br whereas the $a^3\Pi_{0+}$,and $t^3\Sigma^+_{0,1}$ states correlated with H + Br*. The following one-photon photodissociation processes, therefore, occur.

$HBr(X^1\Sigma^+ v', J') + h\nu \rightarrow HBr(a^3\Pi_1 / A^1\Pi_1) \rightarrow H + Br$ (1a)

$HBr(X^1\Sigma^+ v', J') + h\nu \rightarrow HBr(a^3\Pi_{0+} / t^3\Sigma^+_{0,1}) \rightarrow H + Br^*$ (1b)

The resonance excitation involves transitions, via the virtual states to a Rydberg state $(\sigma^2\pi^3)nl\lambda$ or an ion-pair state ($\sigma\pi^4\sigma^*$).

$HBr(a^3\Pi_1 / A^1\Pi_1 / a^3\Pi_{0+} / t^3\Sigma^+_{0,1}) + h\nu \rightarrow HBr^{**}(E^1\Sigma^+ / H^1\Sigma^+ / V^1\Sigma^+)$ (2)

The absorption of the third photon can involve different processes. First is autoionization which produces vibrationally excited HBr^+ ions ($\sigma^2\pi^3$).[63, 64]

$HBr^{**}(E^1\Sigma^+ / H^1\Sigma^+ / V^1\Sigma^+) + h\nu \rightarrow HBr^+(X^2\Pi_\Omega, v^+) + e^-$ (3)

The second involves excitations to superexcited Rydberg states ($HBr^{\#}$), with energies higher than the ionic ground state, that correlate with neutral atomic fragments, H* + Br/Br*.

$HBr^{**}(E^1\Sigma^+ / H^1\Sigma^+ / V^1\Sigma^+) + h\nu \rightarrow HBr^{\#} \rightarrow H^*(n = 2) + Br/Br^*$ (4)

Absorption of the fourth photon produces ionized fragments. Thus, vibrationally excited HBr^+ ions are excited to repulsive states which correlate with H^+ + Br/Br* and the H* fragments, produced in (4) are ionized.

$HBr^+(X^2\Pi_\Omega, v^+) + h\nu \rightarrow H^+ + Br/Br^*$ (5a)

$H^*(n = 2) + Br/Br^* + h\nu \rightarrow H^+ + Br/Br^* + e^-$ (5b)

The Br/Br* fragments can be further ionized by (2 + 1) REMPI.

$Br/Br^* + 2\ h\nu \rightarrow Br^{**} + h\nu \rightarrow Br^+$ (6)

In two color REMPI experiments the first color was used to pump the resonance states and the second color was used to probe Br and Br*.

IV. RESULTS

I. Mass resolved (2 + *n*) REMPI

Mass resolved (2 + *n*) REMPI spectra of HBr have been recorded and analyzed in the two-photon excitation region 79 100 cm^{-1} – 80 700 cm^{-1}.[34] Therein, the REMPI spectra of the Rydberg states $E^1\Sigma^+(1)$ and $H^1\Sigma^+(0)$ and the ion-pair states $V^1\Sigma^+(m + 7)$ and $V^1\Sigma^+(m + 8)$ were presented. An energy diagram of these states is presented in Figure 1.

Perturbations due to energy level shifts (i.e. line shifts) of excited states are named *LS-effects*.[40, 41, 43] These can be observed when the energy difference between neighboring levels ($\Delta E_{J',J'-1} = E(J') - E(J' - 1)$) are plotted as a function of J'. Such plots display linearity with a slope of $2B_{v'}$ in the case of unperturbed states. Deviations from linearity are indicative of level-to-level interactions. Such perturbation effects can also be deduced from reduced term value

plots (RTV plots) which are plots of the difference between observed energies, $E_{J'}$, and unperturbed energies, $E_{J'}^0$, given by

$$E_{J'}^0 = \nu^0 + B'J'(J'+1) - D'J'^2(J'+1)^2 \qquad (1)$$

where the parameters ν^0, B', and D' were derived by deperturbation analysis.

Figure 2 presents energy level spacings vs J', as well as RTV plots of the $V^1\Sigma^+(m+8)$ ion-pair state and the $E^1\Sigma^+(1)$ Rydberg state. The $V^1\Sigma^+(m+8)$ state displays a slight decrease in the $\Delta E_{3,2}$ and $\Delta E_{6,7}$ with respect to linearity (Fig. 2(b)). The corresponding RTV plot, however, displays a slight increase in energy for low J's, but a significant decrease in energy for $J' \geq 2$. This suggests that the $V^1\Sigma^+(m+8)$ state is experiencing increasing non-degenerate interactions with J' from a higher lying state; most likely the $E^1\Sigma^+(1)$ state.

The $E^1\Sigma^+(1)$ state displays a significant increase in the spacing between rotational levels from $J' = 3$ and upwards. This effect is complementarily displayed in the corresponding RTV plots (Fig. 2(b)). This further indicates that the $E^1\Sigma^+(1)$ state is mainly interacting with the $V^1\Sigma^+(m+8)$ state.

Signal intensities of the REMPI spectra have been discussed in detail[34] so a short summary will be presented here. $I(Br^+)/I(HBr^+)$ intensity ratios as a function of J' have been shown to be of value in determining ionization rate coefficients, and to provide measures of Br^+ ion formations via excitation to the Rydberg state. These data also give indications to the extent of state mixing. The $H^1\Sigma^+(0)$ state spectrum exhibits a lowering in the values with J' for $J' = 0 - 4$ and an increase for $J' = 4 - 9$. This indicates that the $H^1\Sigma^+(0)$ state experiences decreasing, followed by increasing state mixings, as a function of J', with the $V^1\Sigma^+(m+7)$ and $V^1\Sigma^+(m+8)$ ion-pair states, respectively (Figure 1).

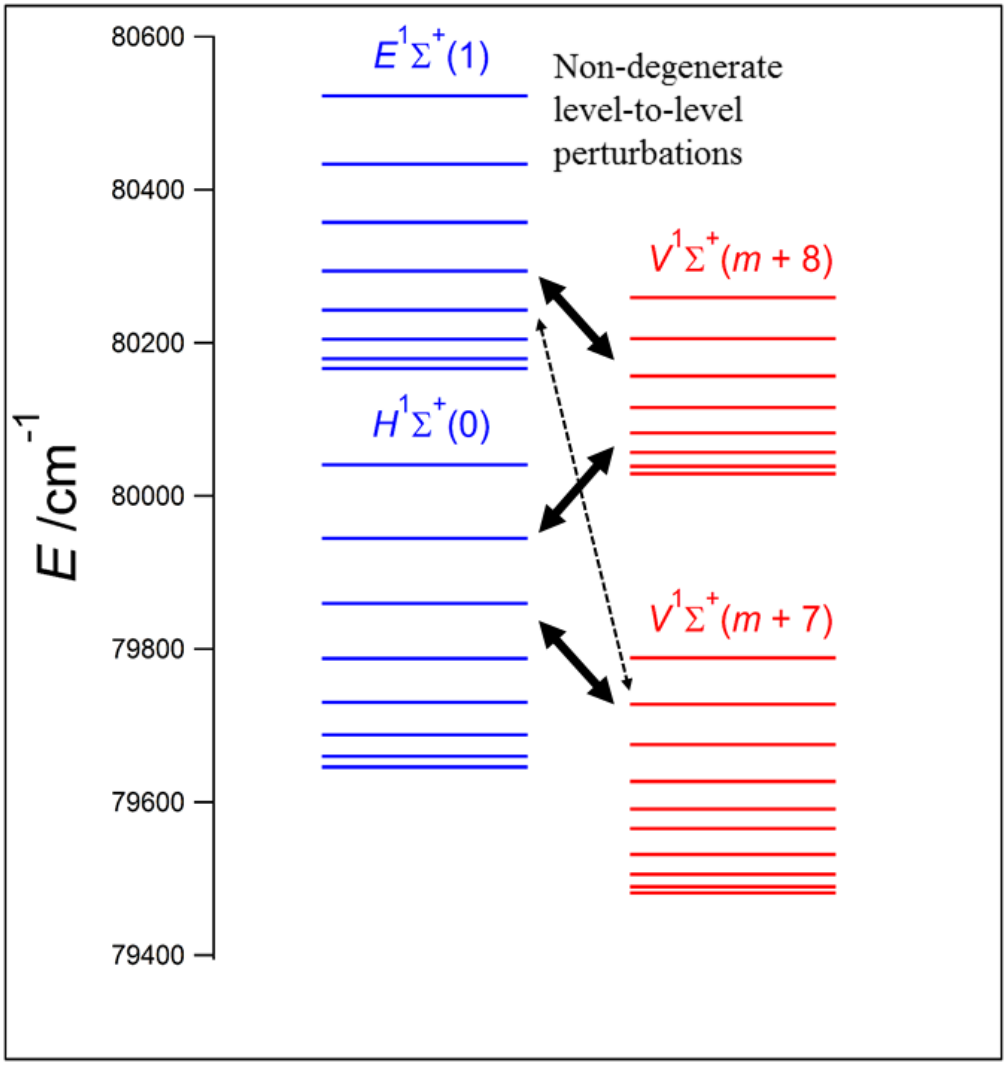

Figure 1. Rotational energy levels derived from observed (2 + n) REMPI spectral lines for the $E^1\Sigma^+(1)$ and $H^1\Sigma^+(0)$ Rydberg states and the $V^1\Sigma^+(m + 7)$ and $V^1\Sigma^+(m + 8)$ ion-pair states. Arrows are indicative of level-to-level state interactions; unbroken arrows indicate strong interactions and broken arrows indicate weak interactions.

The $E^1\Sigma^+(1)$ state spectrum displayed, on average, higher intensity ratio values than the $H^1\Sigma^+(0)$ state spectrum, indicating a greater mixing with the ion-pair state. On the other hand, the $E^1\Sigma^+(1)$ state spectrum displayed a gradual lowering the ratios / mixing with $J´$, for all $J´$s.

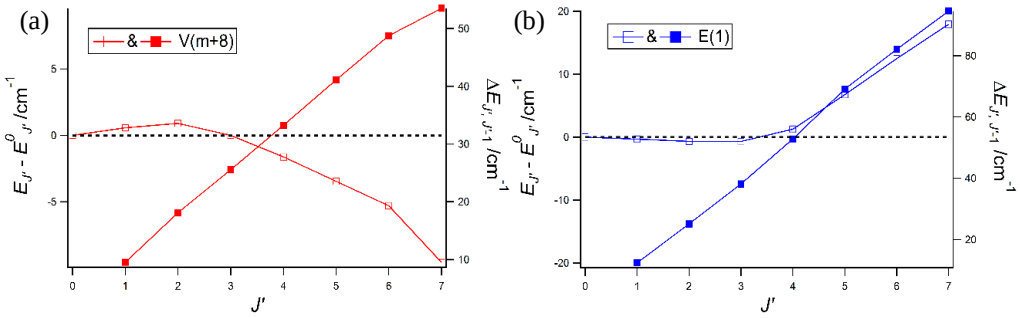

Figure 2. Spacing between rotational levels ($\Delta E_{J',J'-1}$) as a function of J'(filled squares; right vertical axis) and the corresponding reduced term value plot (unfilled squares; left vertical axis) for the $V^1\Sigma^+(m + 8)$ ion-pair state (a) and the $E^1\Sigma^+(1)$ Rydberg state (b).

II. One color VMI

H^+ images were recorded for two-photon resonance excitation from the ground state $X^1\Sigma^+(v' = 0; J'')$ to the $H^1\Sigma^+(v' = 0; J'' = 0 – 9)$ and $E^1\Sigma^+(v' = 1; J'' = 0 – 6)$ Rydberg states, and the $V^1\Sigma^+(v' = m + 7; J'' = 1 – 8)$ and $V^1\Sigma^+(v' = m + 8; J'' = 0 – 7)$ ion-pair states of HBr for Q rotational lines ($J' = J''$). In all of the one color H^+ images, two intense rings are observed for low and medium KERs and a group of weaker ones for high KERs (see Figure 3). These images resemble those obtained for the $E^1\Sigma^+(v' = 0)$ state and $V^1\Sigma^+(v' = m + 4)$ and $V^1\Sigma^+(v' = m + 5)$ ion-pair states.[52] The two intense inner rings correspond to photofragmentations via superexcited states (see mechanism 4 above) and subsequent ionizations of $H^*(n = 2)$. The innermost ring correspondsto the formation of Br* + $H^*(n = 2)$ (the Br* channel) whereas the ring of medium KER corresponds to the formation of Br + $H^*(n = 2)$ (the Br channel). Figure 4 shows the KER spectrum for the $H^1\Sigma^+(v' = 0, J' = 0)$ resonance level. The two KER peaks at ~0.4 and ~0.8 eV correspond to the two intense inner rings in Figure 3, whereas the group of high energy peaks between 1.3 and 2.5 eV correspond to the outermost rings.

The photofragment angular distributions, obtained from the images were fitted by

$$I(\theta) = A(1 + \beta_2 P_2(\cos(\theta)) + \beta_4 P_4(\cos(\theta))) \qquad (2)$$

to derive the parameters β_2 and β_4 ("one-step analysis"[52]). In most cases insignificant variations in the parameter β_2 /angular distributions were observed with J'. However, for the $V^1\Sigma^+(m + 8)$ ion-pair state, significant lowering in β_2, hence increasing perpendicular character of the corresponding transition, was observed for the Br channels and for the $H^1\Sigma^+(0)$ state, a minimum value of the β_2 parameter (hence, largest perpendicular transition character) was obtained for $J' = 4 – 5$. Averaged values of the β_2 parameter for all J's for each H^+ formation channel of all three states are presented in Table 1.

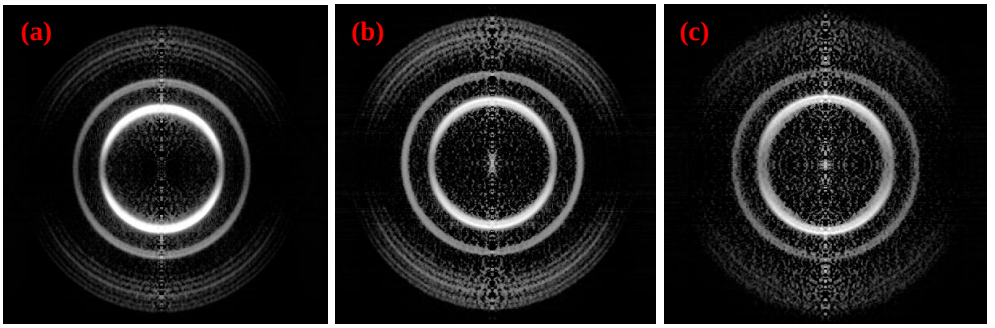

Figure 3. One color H^+ velocity map images for (a) $J' = 0$, (b) $J' = 4$, (c) $J' = 9$ resonance levels of the $H(0)$ Rydberg state.

The mass resolved REMPI spectra of the $H^1\Sigma^+(0)$ state showed clearly resolved *O* and *S* rotational lines. This allowed a "two-step analysis" where the angular distributions were fitted by

$$I(\theta) = AI_f(\theta)I_{ph}(\theta) \quad (3)$$

$$I_f(\theta) = 1 + \beta_{f,2}P_2(\cos(\theta)) + \beta_{f,4}P_4(\cos(\theta)) + \beta_{f,4}P_6(\cos(\theta)) \quad (4)$$

$$I_{ph}(\theta) = 1 + \beta_{ph,2}P_2(\cos(\theta)) + \beta_{ph,4}P_4(\cos(\theta)) + \beta_{ph,6}P_6(\cos(\theta)) \quad (5)$$

where $I_f(\theta)$ and $I_{ph}(\theta)$ represent the distributions of the resonance excitation and photofragmentation steps, respectively. The anisotropy parameter of the resonance step, $\beta_{2,f}$, can be estimated by[52, 64]

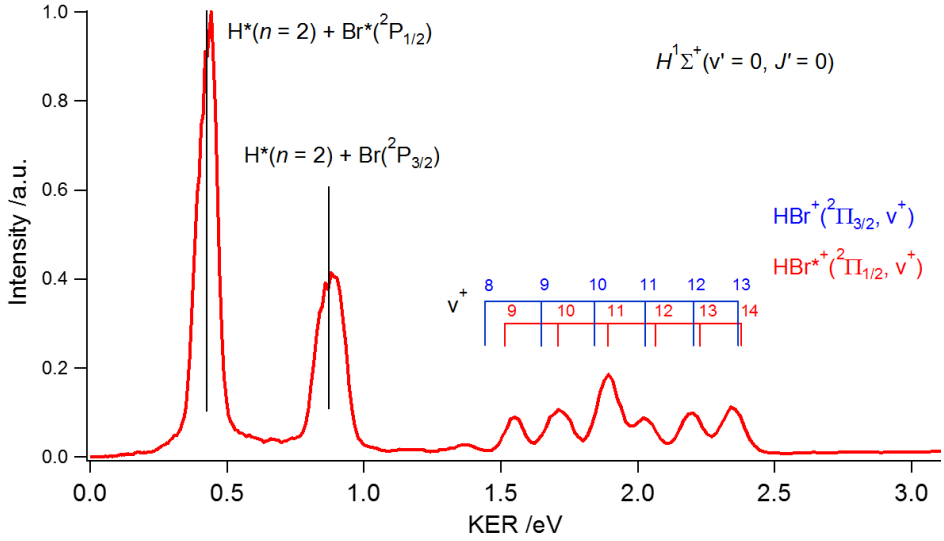

Figure 4. A H^+ kinetic energy release curve for resonance excitation from the ground state, $X(v'' = 0, J'' = 0)$ to the $H(v' = 0, J' = 0)$ state. Peaks corresponding to H^+ formation via the Br^+ (~0.4 eV) and Br^{*+} (~0.8 eV) channels are marked as well as those formed via the HBr^+/HBr^{*+} ionic states (1.3 – 2.5 eV). Predicted KERs are marked by vertical lines.

$$\beta_{f,2} = \frac{2 - 20\,Re[b]}{2 + 25|b|^2} \qquad (6)$$

where the b parameter is extracted from the intensity ratios of the Q, S, and O lines as

$$\frac{I_Q}{I_S} = \frac{10}{3}\frac{(2J''+1)}{(J''+2)}\left[|b|^2\frac{(2J''+3)}{(J'+1)} + \frac{1}{5}\frac{J''}{(2J''-1)}\right] \qquad (7)$$

$$\frac{I_Q}{I_O} = \frac{10}{3}\frac{(2J''+1)}{(J''-1)}\left[|b|^2\frac{(2J''-1)}{J''} + \frac{1}{5}\frac{(J''+1)}{(2J''+3)}\right] \qquad (8)$$

Thus, $\beta_{f,2} = -0.92$ was derived which corresponds to a (virtually) purely perpendicular ($\Sigma \rightarrow \Pi \rightarrow \Sigma$) transition, in close correspondence with our previous two-step analysis for the $E^1\Sigma^+(0)$ state.[52] For a given $\beta_{f,2}$ value of – 0.92, the anisotropy parameters, $\beta_{ph,2}$, $\beta_{ph,4}$, and $\beta_{f,4}$, were derived from the data fitting procedure (Eqs. 3-5). The J' dependent β_2 and β_4 parameters, derived from the "one-step analysis" and the $\beta_{ph,2}$ and $\beta_{ph,4}$ parameters obtained from the "two-

step analysis", for the Br channel, are presented in Figure 5. The $\beta_{f,4}$ parameter was found to be about constant (~0.3±0.1) for all the H^+ formation channels.

Two-step analysis of the other channels (Br*, HBr^+/HBr^+*), gave $\beta_{2,ph}$ values equal to +2 for all J's, corresponding to a purely perpendicular photofragmentation transitions.

Table 1. Averaged β_2 values for the $V^1\Sigma^+(m + 7)$ and $V^1\Sigma^+(m + 8)$ ion-pair states and the $E^1\Sigma^+(1)$ and $H^1\Sigma^+(0)$ Rydberg states for the H^+ formation channels via superexcited repulsive intermediary states yielding i) H*(n = 2) + Br (Br channel) or ii) H*(n = 2) + Br* (Br* channel), and iii) through the HBr^+/HBr^+* ionic states (HBr^+/HBr^+* channels).

	Average values of β_2.		
State	Br channel	Br* channel	HBr^+/HBr^+* channels
$\boldsymbol{V^1\Sigma^+(m + 7)}$	1.6	0.6	1.3
$\boldsymbol{H^1\Sigma^+(0)}$	0.3	1.1	1.7
$\boldsymbol{V^1\Sigma^+(m + 8)}$	0.4	1.2	1.4
$\boldsymbol{E^1\Sigma^+(1)}$	0.6	1.3	1.6

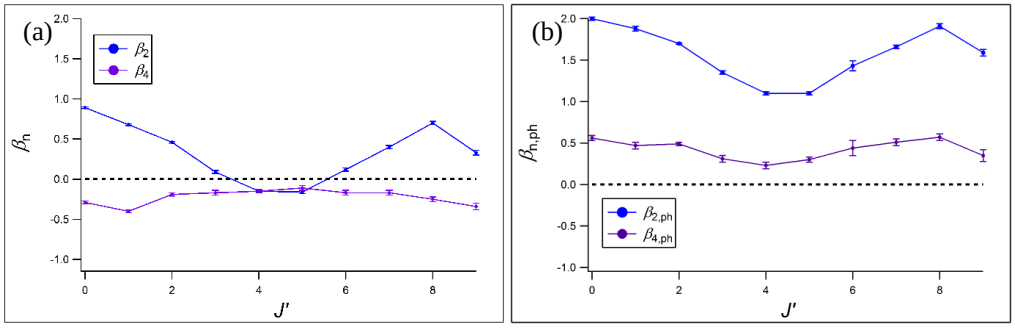

Figure 5. Anisotropy parameters for H^+ formation via the Br channel from the $H^1\Sigma^+(0)$ Rydberg state. (a) Anisotropy parameters, β_2 and β_4, obtained from the "one-step analysis". (b) Anisotropy parameters, $\beta_{2,ph}$ and $\beta_{4,ph}$, obtained from the "two-step analysis".

III. Two color VMI

Images of Br^+ were recorded for two-photon resonance excitation from the ground state to the $H^1\Sigma^+(0)$ and $E^1\Sigma^+(1)$ Rydberg states, and the $V^1\Sigma^+(m + 7)$ and $V^1\Sigma^+(m + 8)$ ion-pair states followed by (2 + 1) REMPI of Br and Br*. Table 2 lists what Br/Br* detections were applied for each of the molecular resonance excitations.

In Figure 6, Br^+ KER curves for the $H^1\Sigma^+(v' = 0)$ Rydberg resonance state are presented. Only one peak is observed for the Br^+ detection (Fig. 6a), whereas two peaks are found for the Br* detection. This general pattern was reproduced in the Br^+ and Br^{*+} KERs for the $E^1\Sigma^+(v' = 1)$, $V^1\Sigma^+(v' = m + 7)$, $V^1\Sigma^+(v' = m + 7)$ states as well. The anisotropy parameters (β_2) of the signal in the Br spectra, were found to be, in general, around –1, indicative of a perpendicular transition. The anisotropy parameters of the signal found at lower KER in the Br* spectrum were about +2, corresponding to a parallel transition, whereas the signal at higher KER was perpendicular in nature.

The peaks present in the Br spectra are at approximately 1.0 eV, which corresponds to one-photon photodissociations to form H + Br. Considering the anisotropy the dissociation must be via the repulsive states $a^3\Pi_1$ and/or $A^1\Pi_1$. The first peaks in the Br* spectra (~0.8 eV) correspond to one-photon photodissociations to form H + Br* via the repulsive states $a^3\Pi_{0+}$ and/or $t^3\Sigma^+_{0,1.}$ The second peaks, however, (at around 5 eV) correspond to two-photon transitions to the molecular resonance states, followed by predissociations via some of the repulsive states to yield H + Br*.

Table 2. Two color images of Br^+ recorded for resonance excitations to the various rotational levels (J') for the $H^1\Sigma^+(0)$ and $E^1\Sigma^+(1)$ Rydberg states, and the $V^1\Sigma^+(m + 7)$ and $V^1\Sigma^+(m + 8)$ ion-pair states followed by (2 + 1) REMPI detections of Br and/or Br* as indicated.

J'	$H^1\Sigma^+(v' = 0)$	$E^1\Sigma^+(v' = 1)$	$V^1\Sigma^+(v' = m + 7)$	$V^1\Sigma^+(v' = m + 8)$
0	Br/Br*	Br	Br/Br*	Br/Br*
1	Br/Br*	Br/Br*	Br/Br*	Br/Br*
2	Br/Br*	Br/Br*	Br/Br*	Br/Br*
3	Br*	Br/Br*	Br/Br*	Br/Br*
4	Br*	Br	Br/Br*	Br
5	Br*		Br/Br*	Br
6	Br*		Br/Br*	Br
7	Br*		Br/Br*	Br
8	Br*		Br/Br*	
9	Br*		Br	

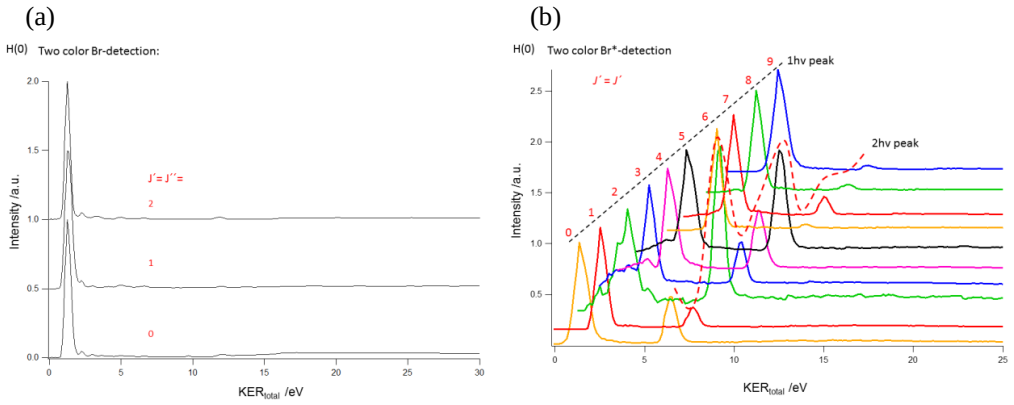

Figure 6. Br^+ (a) and Br^{*+} (b) KER spectra for resonance excitation from the ground state to the $H^1\Sigma^+(0)$ state (Q lines).

DISCUSSION

The β_2 parameters derived for the Br, Br* and HBr^+ channels of the $E(1)$, $H(0)$, and $V(m + 8)$ states are all found to be similar (see Table 1). This implies that the mixing of the $E(1)$ and $H(0)$ Rydberg states with the $V(m + 8)$ ion-pair state, play an important role in the photodissociation processes involved. The parameters for the Br* and HBr^+ channels imply that they are principally parallel in nature, whereas the Br channel exhibits a less parallel character. The corresponding parameters for the $V(m + 7)$ ion-pair state, on the other hand, differ. Greater perpendicular character is observed for the Br* channel but almost purely parallel character for the Br channel. This may be an indication that interactions from other Rydberg states, close in energy, affect the fragmentation process of the $V(m + 7)$ ion-pair state.

The observed trend in the β_2 and $\beta_{2,ph}$ parameters for the $H(0)$ state as a function of J' (Fig. 5) correlates well with observed line intensity effects seen in mass resolved REMPI spectra, suggesting that an increased perpendicular character is associated with less mixing of the $H(0)$ state with the $V(m + 7)$ and $V(m + 8)$ ion-pair states.

The absence of Br^+ signals in the Br detections for the two- color experiments (Fig. 6 (a)), corresponding to energy release of two-photon absorption to the resonance states, indicates that the $a^3\Pi_1$, $A^1\Pi_1$ are of minor importance in predissociation processes of all the states.

The observation of the higher energy peak in the KERs for the Br* detection, for all the states, indicates that in order to achieve two-photon resonances, perpendicular transitions via virtual states ($a^3\Pi_1$ / $A^1\Pi_1$ / $a^3\Pi_{0+}$) is a precondition (see Figure 7). This requires that the repulsive $t^3\Sigma^+_{0,1}$ state/s do not partake as virtual states in the two-photon resonance excitations, as to be expected by the calculated $\beta_{f,2}$ parameter for the $H(0)$ state (–0.92). A likely fragmentation pathway is through interactions between the $H(0)$, $E(1)$, $V(m + 7)$, $V(m + 8)$ states and the $a^3\Pi_{0+}$ state due to relatively strong SO couplings

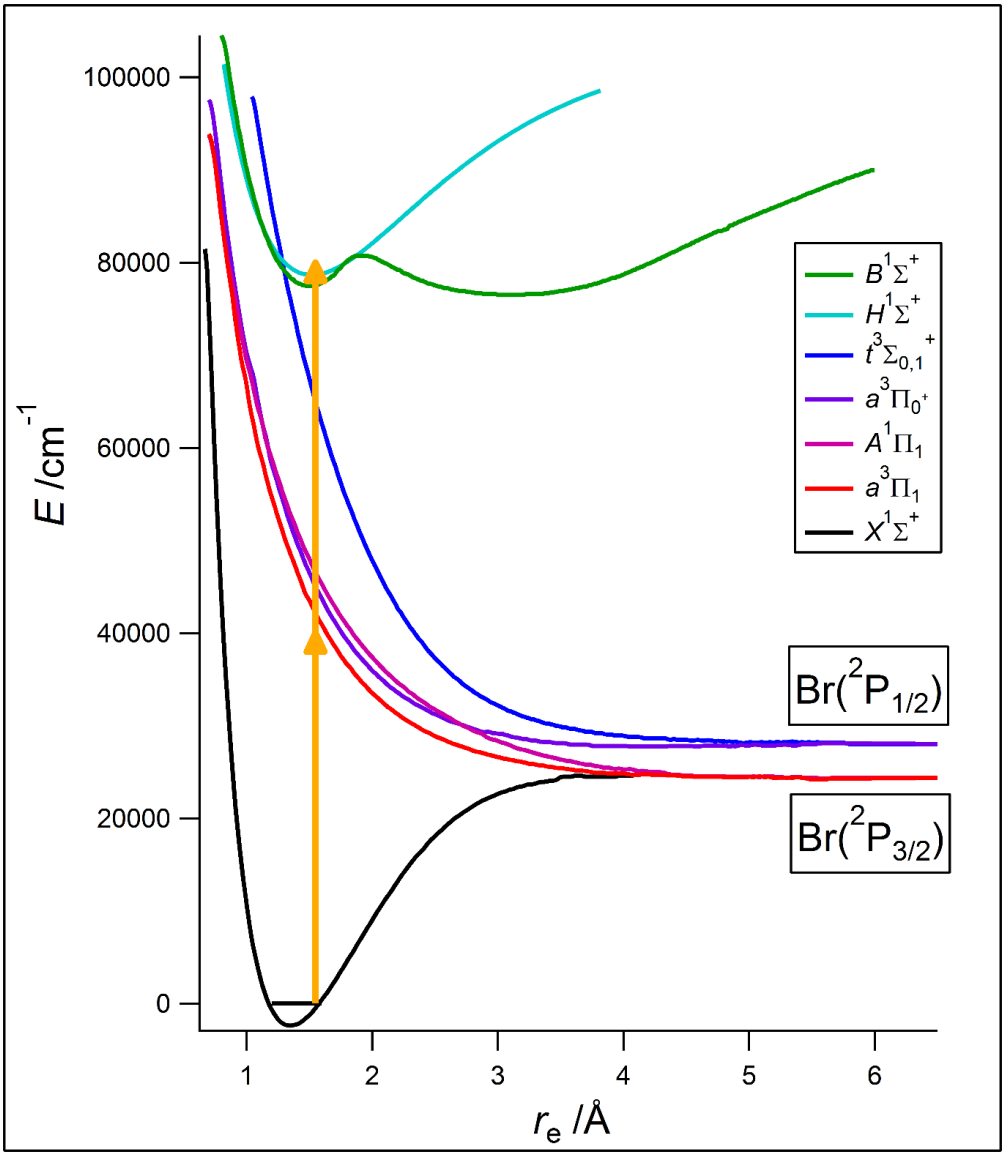

Figure 7. An energy overview diagram of a two-photon excitations to the *H* state and the *E,V* states (presented here as the adiabatic *B* state).

VII. CONCLUSIONS & SUMMARY

Mass resolved REMPI spectra of HBr revealed strong LS-effects for the *E*(1) and *V*(*m* + 8) resonance states. These effects manifest as level-to-level repulsion interactions, but the

repulsion effects are found to be stronger in the $E(1)$ state than in the $V(m + 8)$ state. A likely explanation is that the $V(m + 8)$ also experiences weaker LS-effects from the $H(0)$ state that counteract the stronger LS-effects from the $E(1)$ state. One color imaging of H^+ photoions produced via the three states further corroborate the story of increased aggregate interactions. The angular distribution parameter, β_2, for the $V(m + 8)$ state, gains increased perpendicular character with higher $J´$s. Since fragmentations via ion-pair states are principally parallel in nature, this observation further confirms an increased, aggregate, $J´$ dependent mixing of the $V(m + 8)$ ion-pair state with the $H(0)$ and $E(1)$ Rydberg states.

The effect of a decreasing and increasing mixing of the $H(0)$ state with the $V(m + 7)$ and $V(m + 8)$ states, respectively, as $J´$ increases, is visualized both in data derived from mass resolved REMPI and in velocity map images. This appears as minima in i) –plots of the intensity ratios $I[^iBr^+]/I[H^iBr]$, $i = 79, 81$ and ii) –in plots of the anisotropy parameters (β_2 and $\beta_{ph,2}$) as a function of $J´$ for $J´ = 4 – 5$.

Two color velocity map images of Br^+ reveal that neither the $a^3\Pi_1$ or the $A^1\Pi_1$ repulsive states partake significantly in predissociations of the $H(0)$, $E(1)$, $V(m + 7)$, $V(m + 8)$ states. Furthermore, in order to attain two-photon resonances, perpendicular transitions are of major importance, excluding the $t^3\Sigma^+_{0,1}$ state/s as important intermediates. The $a^3\Pi_{0+}$ state is found to be the likeliest culprit of predissociations to form H + Br* through spin-orbit interactions.

Acknowledgements

The financial support of the University Research Fund, University of Iceland and the Icelandic Science Foundation (Grant No. 130259-051) is gratefully acknowledged.

References

1. A. Eppink and D. H. Parker, *Rev. Sci. Instrum.*, 1997, 68, 3477-3484.
2. D. H. Parker and A. Eppink, *J. Chem. Phys.*, 1997, 107, 2357-2362.
3. M. N. R. Ashfold, N. H. Nahler, A. J. Orr-Ewing, O. P. J. Vieuxmaire, R. L. Toomes, T. N. Kitsopoulos, I. A. Garcia, D. A. Chestakov, S.-M. Wu and D. H. Parker, *Phys. Chem. Chem. Phys.*, 2005, 8, 26-53.
4. A. I. Chichinin, K.-H. Gericke, S. Kauczok and C. Maul, *International Reviews in Physical Chemistry*, 2009, 28, 607-680.
5. T. A. Spiglanin, D. W. Chandler and D. H. Parker, *Chem. Phys. Letters*, 1987, 137, 414-420.
6. E. d. Beer, B. G. Koenders, M. P. Koopmans and C. A. d. Lange, *J. Chem. Soc. Faraday Trans.*, 1990, 86, 2035-2041.
7. D. S. Green, G. A. Bickel and S. C. Wallace, *J. Mol. Spectrosc.*, 1991, 150, 303-353.
8. D. S. Green, G. A. Bickel and S. C. Wallace, *J. Mol. Spectrosc.*, 1991, 150, 354-387.
9. D. S. Green, G. A. Bickel and S. C. Wallace, *J. Mol. Spectrosc.*, 1991, 150, 388-469.
10. K. Wang and V. McKoy, *J. Chem. Phys.*, 1991, 95, 8718-8724.
11. Y. Xie, P. T. A. Reilly, S. Chilukuri and R. J. Gordon, *J. Chem. Phys.*, 1991, 95, 854 - 864.
12. D. S. Green and S. C. Wallace, *J. Chem. Phys.*, 1992, 96, 5857-5877.
13. E. d. Beer, W. J. Buma and C. A. deLange, *J. Chem. Phys.*, 1993, 99, 3252-3261.
14. Á. Kvaran, H. Wang and Á. Logadóttir, in *Recent Res. Devel. in Physical Chem.*, Transworld Research Network, 1998, vol. 2, pp. 233-244.
15. Á. Kvaran, Á. Logadóttir and H. Wang, *J. Chem. Phys.*, 1998, 109, 5856-5867.
16. H. M. Lambert, P. J. Dagdigian and M. H. Alexander, *J. Chem. Phys.*, 1998, 108, 4460.
17. P. M. Regan, S. R. Langford, D. Ascenzi, P. A. Cook, A. J. Orr-Ewing and M. N. R. Ashfold, *Phys. Chem. Chem. Phys.*, 1999, 1, 3247-3251.
18. Á. Kvaran, H. Wang and Á. Logadóttir, *J. Chem. Phys.*, 2000, 112, 10811-10820.
19. P. M. Regan, D. Ascenzi, A. Brown, G. G. Balint-Kurti and A. J. Orr-Ewing, *J. Chem. Phys.*, 2000, 112, 10259-10268.
20. Á. Kvaran, H. Wang and B. G. Waage, *Can. J. Physics*, 2001, 79, 197-210.
21. H. Wang and Á. Kvaran, *J. of Molec. Structure*, 2001, 563, 235-239.
22. Á. Kvaran and H. Wang, *Molecular Physics*, 2002, 100, 3513-3519.
23. Á. Kvaran and H. Wang, *J. Molecular Spectroscopy*, 2004, 228, 143-151.
24. Á. Kvaran, H. S. Wang, K. Matthiasson, A. Bodi and E. Jonsson, *J. Chem. Phys.*, 2008, 129, 164313.
25. K. Matthiasson, H. S. Wang and Á. Kvaran, *J. Mol. Spectros.*, 2009, 255, 1-5.
26. Á. Kvaran, K. Matthiasson and H. S. Wang, *J. Chem. Phys.*, 2009, 131, 044324.
27. K. Matthiasson, J. M. Long, H. S. Wang and Á. Kvaran, *J. Chem. Phys.*, 2011, 134, 164302.
28. J. Long, H. Wang and Á. Kvaran, *J. Chem. Phys.*, 2013, 138, 044308.
29. R. Callaghan and R. J. Gordon, *J. Chem. Phys.*, 1990, 93, 4624-4636.
30. K. Wang and V. McKoy, *J. Chem. Phys.*, 1991, 95, 7872-7879.
31. H. Wang, Á. Logadóttir and Á. Kvaran, Prague, Czech Republic, 1998.
32. D. Ascenzi, S. Langford, M. Ashfold and A. Orr-Ewing, *Phys. Chem. Chem. Phys.*, 2001, 3, 29-43.
33. J. Long, H. Wang and Á. Kvaran, *J. Mol. Spectrosc.*, 2012, 282, 20-26.
34. J. Long, H. R. Hrodmarsson, H.Wang and Á. Kvaran, *J. Chem. Phys.*, 2012, 136, 214315.

35. S. A. Wright and J. D. McDonald, *J. Chem. Phys.*, 1994, 101, 238-245.
36. S. T. Pratt and M. L. Ginter, *J. Chem. Phys.*, 1995, 102, 1882-1888.
37. S. R. Langford, P. M. Regan, A. J. Orr-Ewing and M. N. R. Ashfold, *Chemical Physics*, 1998, 231, 245-260.
38. P. M. Regan, D. Ascenzi, C. Clementi, M. N. R. Ashfold and A. J. Orr-Ewing, *Chem. Phys. Lett.*, 1999, 315, 187-193.
39. P. M. Regan, D. Ascenzi, E. Wrede, P. A. Cook, M. N. R. Ashfold and A. J. Orr-Ewing, *Phys. Chem. Chem. Phys.*, 2000, 2, 5364-5374.
40. H. R. Hrodmarsson, H. S. Wang and Á. Kvaran, *J. Chem. Phys.*, 2015, 142, 244312.
41. H. R. Hrodmarsson, H. S. Wang and Á. Kvaran, *J. Chem. Phys.*, 2014, 140, 10.
42. H. R. Hrodmarsson, H. S. Wang and Á. Kvaran, *J. Mol. Spectros.*, 2013, 290, 5-12.
43. H. R. Hrodmarsson and Á. Kvaran, *(to be published)*, 2015.
44. T. P. Rakitzis, P. C. Samartzis, R. L. Toomes, T. N. Kitsopoulos, A. Brown, G. G. Balint-Kurti, O. S. Vasyutinskii and J. A. Beswick, *Science*, 2003, 300, 1936-1938.
45. T. P. Rakitzis, P. C. Samartzis, R. L. Toomes, L. Tsigaridas, M. Coriou, D. Chestakov, A. Eppink, D. H. Parker and T. N. Kitsopoulos, *Chem. Phys. Lett.*, 2002, 364, 115-120.
46. C. Romanescu, S. Manzhos, D. Boldovsky, J. Clarke and H. Loock, *J. Chem. Phys*, 2004, 120, 767-777.
47. S. Manzhos, C. Romanescu, H. P. Loock and J. G. Underwood, *J. Chem. Phys.*, 2004, 121, 11802-11809.
48. S. Kauczok, C. Maul, A. I. Chichinin and K. H. Gericke, *J. Chem. Phys.*, 2010, 133, 10.
49. C. Romanescu and H. P. Loock, *J. Chem. Phys.*, 2007, 127, 13.
50. T. P. Rakitzis, P. C. Samartzis, R. L. Toomes and T. N. Kitsopoulos, *J. Chem. Phys.*, 2004, 121, 7222-7227.
51. C. Romanescu and H. P. Loock, *Phys. Chem. Chem. Phys.*, 2006, 8, 2940-2949.
52. D. Zaouris, A. Kartakoullis, P. Glodic, P. C. Samartzis, H. R. Hrodmarsson and Á. Kvaran, *Phys. Chem. Chem. Phys.*, 2015, DOI: 10.1039/C5CP00748H.
53. P. M. Regan, S. R. Langford, A. J. Orr-Ewing and M. N. R. Ashfold, *J. Chem. Phys.*, 1999, 110, 281-288.
54. A. G. Smolin, O. S. Vasyutinskii, G. G. Balint-Kurti and A. Brown, *J. Phys. Chem. A*, 2006, 110, 5371-5378.
55. R. Baumfalk, U. Buck, C. Frischkorn, N. H. Nahler and L. Huwel, *J. Chem. Phys.*, 1999, 111, 2595.
56. D. A. Chapman, K. Balasubramanian and S. H. Lin, *Chemical Physics*, 1987, 118, 333-343.
57. A. Banichevich, R. Klotz and S. D. Peyerimhoff, *Molecular Physics*, 1992, 75, 173-188.
58. G. Péoux, M. Monnerville, T. Duhoo and B. Pouilly, *J. Chem. Phys.*, 1997, 107, 70.
59. B. Pouilly and M. Monnerville, *Chemical Physics*, 1998, 238, 437-444.
60. C. R. Gebhardt, T. P. Rakitzis, P. C. Samartzis, V. Ladopoulos and T. N. Kitsopoulos, *Rev. Sci. Instrum.*, 2001, 72, 3848.
61. V. Papadakis and T. N. Kitsopoulos, *Rev. Sci. Instrum.*, 2006, 77, 5.
62. R. S. Mulliken, *Phys. Rev.* , 1937, 51, 310.
63. A. I. Chichinin, C. Maul and K.-H. Gericke, *J. Chem. Phys.*, 2006, 124, 224324.
64. A. I. Chichinin, P. S. Shternin, N. Gödecke, S. Kauczok, C. Maul, O. S. Vasyutinskii and K.-H. Gericke, *J. Chem. Phys.*, 2006, 125, 034310.

7 Erratum for Article 2

Article #2 presents a comprehensive overview of Rydberg and ion-pair states of HI in the two-photon excitation region 69 600 – 72 300 cm^{-1}. There are, however, two errors in the paper that need to be addressed. These are associated with i) the wavelength calibration and ii) the assignment of the $d^3\Pi_0(1)$ Rydberg state.

7.1 Calibration

Table 3 in Article #2 includes Band origins (v^0) and rotational parameters (B_v and D_v) for all the observed states in the energy region of concern. The calibration of the spectrum was based on observed atomic iodine (2 + 1) REMPI peaks. Few atomic peaks are found between 69 600 and 70900 cm^{-1}. Therefore, the band origins of some of the states in that energy range were not clearly determined. Later identification of weak atomic lines in the region of the *Q* lines of the *H*(1) state allowed more precise calibrations as well as reassignment of rotational lines. See Table 12 for corrected values of band origins.

Table 12 HI: Corrections of the band origins (v^0) as presented in Article #2 along with values from Ginter *et al.*[145]

	v^0 (cm^{-1}) corrected	v^0 (cm^{-1}) Ginter et al.[145]	v^0 (cm^{-1}) Article #2
$f^3\Delta_1$ (0)	69 689.0	69 687.9	69 699.9
$V^1\Sigma^+(m + 4)$	69 909.9	69 909.9	69 903.3
$F^1\Delta_2$ (0)	70 229.7	70 228.3	70223.6
$E^1\Sigma^+(1)$	70 242.2	70 242.1	70236.1
$k^3\Pi_0$ (1)	70 322.9	70 320.4	70310.8
$V^1\Sigma^+(m + 5)$	70517.3	70 512.0	70511.0
$m^3\Delta_2(0)$	70 841.6	70 837.6	70841.5
$H^1\Sigma^+(1)$	70 855.5	70 850.5	70866.3

Accordingly, *Q* rotational lines of the $k^3\Pi_0(1)$ state, have also been reassigned. See Table 13.

Table 13 HI: Corrections of *Q* line positions of the $k^3\Pi_0(1)$ state as presented in Article #2.

J´	$k^3\Pi_0(1)$ – *Q lines – corrected*	$k^3\Pi_0(1)$ – *Q lines – Article #2*
0	70322.9	70310.8
1	70320.6	70308.6
2	70315.1	70304.0
3	70307.7	70296.4
4	70296.8	70286.1
5	70284.7	70274.7

7.2 Reassignment of the $d^3\Pi_0(1)$ Rydberg state

A Rydberg state spectrum was observed with band origins of 70 991.6 cm^{-1}. It had not been observed in previous absorption or REMPI experiments. The two most probable reasons why the state had gone unnoticed are i) that its *Q* branch was found right in the midst of a strong iodine atomic line and ii) its other rotational branches are relatively weak.

The original rotational analysis of the spectrum incorrectly suggested a Rydberg state of $\Omega = 0$. This is incorrect since the spectrum exhibits *R* and *P* lines, which excludes $\Omega = 0$ states and implies a Rydberg state of either $\Omega = 1$ or $\Omega = 2$. A revised rotational analysis, revealed that the state is in fact $\Omega = 1$ with a band origin of $\nu^0 = 70989.0$ cm^{-1}.

Additionally, the first *P* line of the state is incorrectly assigned. It is actually the first and only visible *S* line of the $V^1\Sigma^+(m + 6)$ ion-pair state spectrum with band origin of 70952.3 cm^{-1}. A peak at 70967,4 cm^{-1} is therefore reassigned to the first and only visible *P* line.

The intensities of the I^+ lines are generally marginally larger than those of the HI^+ lines. This excludes a $\Lambda = 2$ state. On the other hand, the intensity ratios are very similar to those of other $^3\Pi$ states, e.g. $k^3\Pi_1$ and $m^3\Pi_1$. The new state does, however, not correlate with any vibrational progression of previously observed $^3\Pi_1$ states.[142, 145] Therefore, the likeliest assignment is the previously unobserved $n^3\Pi_1(0)$ Rydberg state with electron configuration $(\sigma^2\pi^3)5d\pi$. No spectra have been previously observed, corresponding to this triplet state assignment; only the $N^1\Pi_1(0)$ state spectrum was observed with the origin of 71780.5 cm^{-1} by D. S. Ginter *et al.*[145]. Rotational assignments are presented in Table 15.

Table 14 Rotational llines due to two-photon resonance transition to the reassigned $n^3\Pi_1(0)$ Rydberg state in HI.

J´	*P*	*Q*	*R*
1		70989.5	70998.5
2	70967.4	70989.3	71009.2
3		70988.0	71024.6
4		70986.8	71039.4
5		70985.7	71051.5
6		70984.6	71059.0
7		70983.0	
8		70981.5	

8 Unpublished work

8.1 When peaks merge – modifying intensity ratios

In Article #3, state interactions between the $H^1\Sigma^+(1)$ and $m^3\Pi_2(0)$ Rydberg states and the $V^1\Sigma^+(m + 6)$ ion-pair state, were evaluated in terms of LS-, LI-, and LW-effects. However, due to severe cases of line shifts, some of the rotational peaks of these excited states merged. I.e. the corresponding energy levels were so radically shifted that some line positions could not be separated from one another. E.g. the peaks corresponding to transitions from $J'' = 5 \rightarrow J' = 5$ and $J'' = 7 \rightarrow J' = 7$ of the $H^1\Sigma^+(1)$ state merged together as did the peaks corresponding to the transitions from $J'' = 8 \rightarrow J' = 8$ of the $H^1\Sigma^+(1)$ state and $J'' = 7 \rightarrow J' = 7$ of the $V^1\Sigma^+(m + 6)$ state.

These peak merges decidedly made the LI-effect analysis a little inaccurate although the intensity ratios of the ion-pair state were presented and correlated well with the observed perturbation effects. With a slight modification, thus allowing the inclusion of the peak corresponding the $J' = 5$ and 7 transition, the intensity ratios of the $H^1\Sigma^+(1)$ state can be used to extract values of α and β for comparison with previous values from the other hydrogen halides.

8.1.1 Intensity ratios of merged peaks

Since the intensities of that single peak correspond to two separate transitions, we set the intensities of I^+ and HI^+ for that peak as

$$I[I^+] = \alpha_2 c^2_{2,J'=5} + \beta_1 c^2_{1,J'=5} + \alpha_2 c^2_{2,J'=7} + \beta_1 c^2_{1,J'=7} \quad (119)$$

$$I[HI^+] = \alpha_1 c^2_{1,J'=5} + \beta_2 c^2_{2,J'=5} + \alpha_1 c^2_{1,J'=7} + \beta_2 c^2_{2,J'=7} \quad (120)$$

Then, the intensity ratio of that peak becomes

$$\frac{I[I^+]}{I[HI^+]} = \alpha \frac{\left(2\gamma + (1-\gamma)\left(c^2_{2,J'=5} + c^2_{2,J'=7}\right)\right)}{\left(2 - \left(c^2_{2,J'=5} + c^2_{2,J'=7}\right)\right)} \quad (121)$$

As the $c^2_{2,J'=5}$ and $c^2_{2,J'=7}$ parameters were both calculated from observed peak positions with eq. (108), the α and β parameters were fitted to the observed intensity ratios obtained from the spectra. The fitted intensity ratios are presented in Figure 19. Compiled results of intensity ratios for HCl, HBr, and HI, are presented in Table 15.

The fitted intensity ratios display some dissimilarities when compared to the experimental values. Firstly, the peak at $J' = 6$ was left out of the fitting procedure because of the uncertainty of the measured intensity ratios. This uncertainty derives from the fact that this

peak coincides with two atomic iodine lines. As a result, the intensity of the I^+ ion is much higher than to be expected, hence, the large uncertainty.

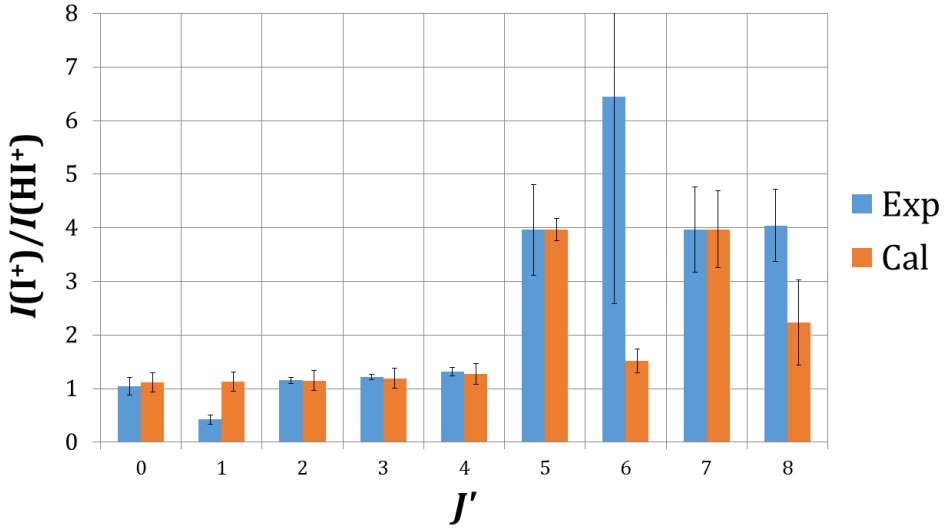

Figure 19 Relative ion-signal intensities ($I[I^+]/I[HI^+]$) vs J' derived from the Q rotational lines resulting from a transition to the $H^1\Sigma^+(1)$ Rydberg state. The blue columns represent the experimental values and the red columns represent the value obtained from fitting the α and β parameters to eq. (122).

Secondly, the peak corresponding to $J' = 8$ does not produce a good fit because it overlaps with the $J' = 7$ line of the $V^1\Sigma^+(m + 6)$ ion-pair state. Therefore, the intensity of the I^+ signal is greater than expected and the intensity ratio is higher than the fitted values.

8.1.2 HCl, HBr, HI comparison

The compiled results of α and β values for HCl, HBr, and HI, are presented in Table 16. Comparison of these results will be discussed here briefly.

Going from HCl towards HI, there is a periodic trend in the values of γ. As the halogen atom increases in size, excitations from Rydberg states yield X^+ to a greater extent. This may in part be due to the periodic decrease in ionization energy of the halogen atoms, i.e. it becomes periodically easier to produce X^+ from Rydberg states. Such periodicities are, however, lacking in the values of α, but they are present in the multiplicative factor $\alpha\beta$. The increasing $\alpha\beta$ factor also supports the previous assumption. I.e. that with increasing periodicity, excitations from mixed Rydberg states yield X^+ to a greater extent.

There is a noteworthy outlier that should be discussed. The α value of the $I^1\Delta_2(0)$ state for HI is 69; approximately 10 times higher than the next values. The $\alpha\beta$ value is, however, close to unity which implies that excitation from the $I^1\Delta_2(0)$ state (which can in good reason be called a pure Rydberg state) yields similar amounts of HI^+ and I^+ ions.

Upon the excitation of a third photon, the HI molecule is excited from the $I^1\Delta_2(0)$ state to approximately 108 000 cm^{-1}. The dissociation continuum of the ionic ground state is approximately 108 900 cm^{-1}. Assuming autoionization, excitation from the $I^1\Delta_2(0)$ state

yield high vibrational progressions of the ionic ground state(s), which can easily dissociate to form H + $I^+(^3P_2)$. It is, therefore, a reasonable assessment that pure Rydberg states display high values of α, when the absorption of a third photon yields highly vibrationally excited HI^+ ions in the ground state.

Table 15 Compiled results of fitted *α*, *γ*, and *αγ* factors for HCl, HBr, and HI.

Rydberg state	*Molecule*	*α*	*γ*	*αγ*	*Ref.*
$f^3\Delta_2(0)$	HCl	4.0	0	0	[227]
$f^3\Delta_1(0)$	HCl	0.5	0.002	0.001	[227]
$g^3\Sigma^+_1(0)$	HCl	0.6	0.004	0.002	[227]
$j^3\Sigma^-_1(0)$	HCl	3.5	0.004	0.01	[229]
$j^3\Sigma^-_{0+}(0)$	HCl	2.1	0.031	0.065	[229]
"State B"	HCl	3.1	0.002	0.006	[229]
$F^1\Delta_2(1)$	HBr	1.3	0.11	0.14	[233]
$E^1\Sigma^+(0)$	HCl	0.9	~0	0	[230]
$E^1\Sigma^+(1)$	HCl	1.1	~0	0	[230]
$E^1\Sigma^+(0)$	HBr	0.2	0.4	0.08	[230]
$O^1\Sigma^+(0)$	HI	0.52	0.93	0.48	[235]
$I^1\Delta_2(0)$	HI	69	0.0040	0.28	[235]
$H^1\Sigma^+(1)$	HI	7.8	0.127	0.99	Unpublished

9 Food for thought – a quantum interpretation

The experiments described in this thesis are firmly based on well-known and studied models derived from quantum mechanics. It is the author's view that it only be appropriate to briefly discuss the experiments in the terms of interpretations of the quantum realm.

When making a measurement upon a quantum system, of any kind, the experimenter is willingly influencing the system by collapsing its wavefunction to give a numerical result in order to extract information about the system. The result is in no way representative of the entire system so in order to obtain a statistically valid interpretation, the experiment must be repeated until the obtained data converge to behavioral patterns that can be fitted with an appropriate model.

REMPI experiments, whether coupled with VMI or not, are simple ion counting techniques. The counted ions are the results of complicated excitation processes where a molecule absorbs a number of photons. This excitation process takes place within the experimental apparatus and is completely hidden from the experimenter. In a way, it is completely analogous to the paradox of Schrödinger's cat. I.e. photons are sent into a box containing a molecule, and the molecule is either ionized, or is fragmented and the fragments are subsequently ionized. Opening the box, containing Schrödinger's cat, is here the equivalent of the micro channel plate (MCP) detector at the end of the time-of-flight tube.

As already discussed in detail, the interactions between a Rydberg state and an ion-pair state are commonly described as the two states being mixed. If we consider a single molecule and excite it with two photons to the mixed Rydberg state, would the configuration be that of the Rydberg state or the ion-pair state? The answer is by no mean straightforward. Intuitively, since the two-photon excitation wavenumber of the laser corresponds with an eigenvalue of the Rydberg state, one might be inclined to make the assumption that the electron configuration of the Rydberg state is simply a Rydberg electron orbiting an ion core. This assumption is based on a human bias that assumes that things are a *certain* way and not the other. Which is wrong.

In the quantum realms of the universe, uncertainty is law. The so-called mixing of the two states is a measure of the probability that future measurements yield a specific result; autoionization vs fragmentation through either state. The mixing is descriptive of the inherent uncertainty of electronic behavior in molecules.

By applying the quantum theory in this way to molecules we are granted a predictive toolkit. A chemical augury, whose divination foresees molecular behavior, all based on probabilities derived from quantum uncertainties.

Measuring the state mixing quantitatively, the molecule must be further excited; until it or its fragments are ionized. In our experiments, the ions are diverted via electric fields into the time-of-flight tube where the ions are counted as a function of flight time, or axiomatically mass. A particular mass signal implies that, for a certain excitation wavelength of the

radiation, the molecule went through a certain excitation scheme to yield a fragment with that mass. The simultaneous appearance of another mass signal that corresponds to a different excitation scheme, implies that for a single eigenvalue of an excited state, various possibilities exist when the molecule absorbs another photon. These different possibilities correspond to an excitation of a different electron configuration. Thus, in a mixed state the molecule simultaneously exhibits the behavior of two (or more) distinctive electron configurations. The molecule is both present in a Rydberg state and ion-pair state. But, the physical properties of this mixed state (or the extent of state mixing) are measureable by repeating the experiments for an enormous amount of molecules. Furthermore, these properties change with different sets of electron configurations and axiomatically, with molecules. Different molecules, different sets of simultaneous electron configurations, different photoproducts of different excitation radiation.

Everything is uncertain. Duality is chiseled into the fabric of our being. Until we open the box…

10 Outlook

10.1.1 HI

Additionally to the published work, two-photon REMPI experiments of HI were performed up to 74 500 cm^{-1}. There, new states are observed but they have not yet been assigned due to their complexity. Preferably, scans to higher wavenumbers are required to obtain a better overview of the excited states in this region. The three-photon REMPI study of HI by P. M. Regan *et al.*[300] reported several Rydberg states in the 82 050 – 83 250 cm^{-1} energy region; just below the ionization potential at approximately 83 780 cm^{-1}. Scanning the region connecting the study by P. M. Regan *et al.* and this work (or the absorption measurements by D. S. Ginter *et al.*[145]) would a challenging, but intriguing task. I.e. recording and documenting all the observable excited states by two-photon selection rules below the ionization limit. To assist in assignments, the use of linearly and circularly polarized radiation as well as synchronous experiments on DI, would prove conducive as with the previously referenced experiments.

Since several new Rydberg and ion-pair states have been observed, and some reassigned, in this work on HI, it might as well be useful to revisit the experiments of the first Rydberg states of HI by M. L. Ginter *et al.*[142] and S. G. Tilford *et al.*[139] to, perhaps, reevaluate some of the spectral assignments with multi-photon REMPI.

Velocity map imaging experiments might also be useful towards understanding some the fragmentation mechanisms reported. E.g. the interaction scheme between the $k^3\Pi_1(2)$ state and the $j^3\Sigma^-(0)$ state would be an interesting subject to study with VMI to inspect the H^+ formation routes.

10.1.2 CH_3I, CH_2I_2, CHI_3

Recently, an in-depth investigation into the formation of CH from CH_xBr_{4-x} photodissociation via two-photon REMPI was reported.[252] Similar experiments on the iodo-methane family of molecules have commenced in order to study their CH formation routes analogously. Likewise, photofragmentation pathways involving Rydberg states will be studied by analyzing the resulting I^+ mass signals.

10.1.3 HCl

Concurrently, two-photon REMPI experiments are being performed at higher energies than previously obtained by the two-photon experiments by Green *et al.*[202-205] The objective of these measurements is to develop a comprehensive catalogue of all the molecule's ion-pair states up to the molecule's ionization limit. The results will be used for analysis of quantum defects relative to the search of heavy Rydberg states. If the previously described two-photon REMPI experiments on HI come to fruition, the search for heavy Rydberg states may be expanded to include HI as well as HCl.

References

1. Lemoine, M.G., *Equilibres Chimiques entre l'Hydrogene et l'Iode Gazeux.* Ann. Chim. Phys., 1877. **12**.
2. Bodenstein, M., *Die Zersetzung des Jodwasserstoffgases im Licht.* Zeitschrift für Physik, 1897. **22**, 23.
3. Burmeister, W., *Untersuchungen über die Ultraroten Absorptionsspektra Einiger Gase*. 1913. 589.
4. Bahr, E.V., *Die Ultrarote Absorption der Gase.* Verhandlungen der deutschen physikalischen Gesellschaft, 1913. **15**, 710.
5. Brinsmade, J.B., and Kemble, E.C., *The Occurrence of Harmonics in the Infra-red Absorption Spectra of Diatomic Gases.* Proceedings of the National Academy of Sciences in the USA, 1917. **3**(6), 420.
6. Imes, E.S., *Measurements on the Near Infra-Red Absorption of Some Diatomic Gases.* The Astrophysical Journal, 1919. **50**, 251.
7. Kratzer, A., *Die Ultraroten Rotationsspektren der Halogenwasserstoffe.* Zeitschrift für Physik, 1920. **3**(5), 289.
8. Schaefer, C., and Thomas, M., *Oberschwingungen in Ultraroten Absorptionsspektren.* Zeitschrift für Physik, 1922. **12**, 330.
9. Czerny, M., *Messungen im Rotationsspektrum des HCl im Langwelligen Ultrarot.* Zeitschrift für Physik, 1925. **34**, 227.
10. Tingey, H.C., and Gerke, R.H., *The Ultraviolet Absorption Spectra and the Photochemical Decomposition of Gaseous Hydrogen Bromide and Iodide.* Journal of the American Chemical Society, 1926. **48**(7), 1838.
11. Czerny, M., *Die Darstellung der Ultraroten Absorptionsspektren der Halogenwasserstoffe nach der Schrödingerschen Theorie.* Zeitschrift für Physik, 1927. **45**(7-8), 476.
12. Czerny, M., *Die Rotationsspektren der Halogenwasserstoffe.* Zeitschrift für Physik, 1927. **44**(4-5), 235.
13. Meyer, C.F., and Levin, A.A., *On the Absorption Spectrum of Hydrogen Chloride.* Physical Review, 1929. **34**(1), 44.
14. Colby, W.F., *Analysis of the HCl Bands.* Physical Review, 1929. **34**(1), 53.
15. Plyler, E.K., and Barker, E.F., *The Infrared Bands and Molecular Constants of HBr.* Physical Review, 1933. **44**, 984.
16. Herzberg, G., and Spinks, J.W.T., *Photographie der Zweiten Oberschwingung des HCl bei 1,19 μm mit Grosser Dispersion.* Zeitschrift für Physik, 1934. **89**, 474.
17. Salant, E.O., and Kirkpatrick, D.E., *Vibration-Rotation Bands of Hydrogen Fluoride.* Physical Review, 1934. **46**, 318.
18. Kirkpatrick, D.E., and Salant, E.O., *Overtone Absorption Bands of Gaseous HF.* Physical Review, 1935. **48**, 945.
19. Brice, B.A., and Jenkins, F.A., *A New Ultra-Violet Band Spectrum of Hydrogen Chloride.* Nature, 1929. **123**(3112), 944.
20. Kulp, M., *Ultraviolette Salzsäure-Emissionsbanden.* Naturwissenschaften, 1930. **18**(32), 719.

21. Kulp, M., *Analyse und Deutung der Ultravioletten Salzsäurebanden.* Zeitschrift für Physik, 1931. **67**(1-2), 7.
22. Mulliken, R.S., *The Halogen Molecules and Their Spectra. J-J-Like Coupling. Molecular Ionization Potentials.* Physical Review, 1934. **46**, 549.
23. Mulliken, R.S., *The Low Electronic States of Simple Heteropolar Diatomic Molecules I. General Survey.* Physical Review, 1936. **50**, 1017.
24. Mulliken, R.S., *Low Electronic States of Simple Heteropolar Diatomic Molecules III. Hydrogen and Univalent Metal Halides.* Physical Review, 1937. **51**, 310.
25. Mulliken, R.S., *Halogen Molecule Spectra II. Interval Relations and Relative Intensities in the Long Wave-Length Spectra.* Physical Review, 1940. **57**, 500.
26. Mulliken, R.S., *Nature of Electronic Levels in Ultraviolet Spectra of Hydrogen and Alkyl Halides.* Physical Review, 1942. **61**, 277.
27. Pauling, L., *The Nature of the Chemical Bond. III. The Transition from One Extreme Bond Type to Another.* Journal of the American Chemical Society, 1932. **54**, 988.
28. Rollefson, G.K., and Booher, J.E., *The Absorption Spectrum and Photochemical Decomposition of Hydriodic Acid.* Journal of the American Chemical Society, 1931. **53**, 1728.
29. Bates, J.R., Halford, J.O., and Anderson, L.C., *A Comparison of Some Physical Properties of Hydrogen and Deuterium Bromides.* J. Chem. Phys., 1935. **3**, 531.
30. Bates, J.R., Halford, J.O., and Anderson, L.C., *A Comparison of Some Physical Properties of Hydrogen and Deuterium Iodides.* J. Chem. Phys., 1935. **3**, 415.
31. Goodeve, C.F., and Taylor, A.W.C., *The Continuous Absorption Spectrum of Hydrogen Bromide.* Proceedings of the Royal Society of London. Series A, Mathematical and Physical Sciences, 1935. **152**(875), 221.
32. Goodeve, C.F., and Taylor, A.W.C., *Continuous Absorption Spectrum of Hydrogen Iodide.* Proceedings of the Royal Society of London. Series A, Mathematical and Physical Sciences, 1936. **154**, 181.
33. Price, W.C., *The Absorption Spectra of the Halogen Acids in the Vacuum Ultra-Violet.* Proceedings of the Royal Society of London. Series A, Mathematical and Physical Sciences, 1938. **167**(929), 216.
34. Price, W.C., *The Far Ultraviolet Absorption Spectra and Ionization Potentials of the Alkyl Halides. Part I.* The Journal of Chemical Physics, 1936. **4**(9), 539.
35. Price, W.C., *The Far Ultraviolet Absorption Spectra and Ionization Potentials of the Alkyl Halides. Part II.* The Journal of Chemical Physics, 1936. **4**(9), 547.
36. Woods, L.H., *Rotational Analysis of the Emission Spectrum of CuF.* The Physical Review, 1943. **64**(9-10), 259.
37. Norling, F., *Über die Bandenspektren der Ionisierten Halogenwasserstoffe. I. Bromwasserstoffbanden.* Zeitschrift für Physik, 1935. **95**(3-4), 179.
38. Norling, F., *Über die Bandenspektren der ionisierten Halogenwasserstoffe. II. Chlorohydrid- und Chlordeutridspektren.* Zeitschrift für Physik, 1937. **104**(9-10), 638.
39. Norling, F., *Über die Bandenspektren der Ionisierten Halogenwasserstoffe. III. Feinstruktur und Isotopieeffekte in den Chlorhydrid- und Chlordeutridspektren. Termschema.* Zeitschrift für Physik, 1937. **106**(106), 177.
40. Cooley, J.P., and Rohrbaugh, J.H., *The Production of Extremely Short Electromagnetic Waves.* Physical Review, 1945. **67**, 296.
41. Romand, J., and Vodar, B., *Spectroscopie-Spectre d'Absorption de Lacide Chlorhydrique Gazeux dans la Region de Schumann.* Comptes Rendus Hebdomadaires des Séances de l'Académie des Sciences, 1948. **226**(3), 238.

42. Romand, J., and Vodar, B., *Spectroscopie-Spectres d'Absorption de Lacide Bromhydrique Gazeux et de Lacide Iodhydrique Gazeux dans la Region...* Comptes Rendus Hebdomadaires des Séances de l'Académie des Sciences, 1948. **226**(11), 890.
43. Romand, J., *Spectroscopie-Determination des Courbes d'Energie Potentielle de l'etat Excite des Molecules IH et BrH - Comparaison.* Comptes Rendus Hebdomadaires des Séances de l'Académie des Sciences, 1948. **227**(2), 117.
44. Romand, J., *Absorption Ultraviolette dans la Region de Schumann Etude de ClH, BrH et IH Gazeux.* Annales de Phisique, 1949. **4**, 539.
45. Hanson, E.E., *A Study of Kinetic Energies of Atomic Ions Formed by Electron Impact in Nitric Oxide and Hydrogen Chloride.* Physical Review, 1937. **51**, 86.
46. Safray, E., Romand, J., and Vodar, J., *Ultraviolet Absorption Spectrum of Gaseous Hydrogen Fluoride.* J. Chem. Phys., 1951. **19**, 379.
47. Barrow, R.F., and Caunt, A.D., *The Ultra-Violet Spectrum of a Diatomic Hydride Excited in Hydrogen-Potassium Fluoride Hollow-Cathode Discharges.* Proceedings of the Physical Society A, 1954. **67**, 68.
48. Johns, J.W.C., and Barrow, R.F., *Ultra-Violet Band Systems of HF^+ and DF^+.* Nature, 1957. **179**, 374.
49. Johns, J.W.C., and Barrow, R.F., *Ionization Potential of Hydrogen Fluoride and the Ground-State of the HF^+ Ion.* Nature, 1957. **179**, 1186.
50. Frost, D.C., and McDowell, C.A., *Excited States of the Molecular Ions of Hydrogen Fluoride, Hydrogen Iodide, Water, Hydrogen Sulphide, and Ammonia.* Canadian Journal of Chemistry, 1958. **30**, 39.
51. Frost, D.C., and McDowell, C.A., *Electron Capture Processes in the Hydrogen Halides.* J. Chem. Phys., 1958. **29**(3), 503.
52. Johns, J.W.C., and Barrow, R.F., *The Ultra-Violet Spectra of HF and DF.* Proceedings of the Royal Society of London. Series A, Mathematical and Physical Sciences, 1959. **251**, 504.
53. Jacques, J.K., and Barrow, R.F., *The Transition $V^1\Sigma^+ - X^1\Sigma^+$ in Hydrogen Chloride.* Proceedings of the Physical Society, 1959. **73**, 538.
54. Barrow, R.F., and Stamper, J.G., *The Absorption Spectrum of Gaseous Hydrogen Bromide in the Schuman Region. II. Electronic States.* Proceedings of the Royal Society of London. Series A, Mathematical and Physical Sciences, 1961. **263**, 277.
55. Barrow, R.F., and Stamper, J.G., *The Absorption Spectrum of Gaseous Hydrogen Bromide in the Schuman Region. I. Rotational Analysis.* Proceedings of the Royal Society of London. Series A, Mathematical and Physical Sciences, 1961. **263**, 259.
56. Stamper, J.G., and Barrow, R.F., *The $V^1\Sigma^+$-$N^1\Sigma^+$ Transition of Hydrogen Bromide.* J. Phys. Chem., 1961. **65**, 250.
57. Cadman, P., and Polanyi, J.C., *Production of Electronically Excited Atoms. II. H + HI --> H^2 + I*($^2P_{1/2}$).* J. Chem. Phys., 1968. **72**(11), 3715.
58. Huebert, B.J., and Martin, R.M., *Gas-Phase Far-Ultraviolet Absorption Spectrum of Hydrogen Bromide and Hydrogen Iodide.* J. Phys. Chem., 1968. **78**(8), 3046.
59. Compton, L.E., and Martin, R.M., *Photodissociation Dynamics. Production of I*($^2P_{1/2}$) Atoms in the Photolysis of Hydrogen Iodide.* J. Phys. Chem., 1969. **73**(10), 3474.
60. Waggoner, M.G., Chow, K.W., and Smith, A.L., *Direct-Recording Absorption Spectrometer in the Windowless Vacuum-Ultraviolet: Absorption Spectra of He_2, HF and N_2.* Chem. Phys. Lett., 1969. **3**(2), 151.

61. Lempka, H.J., Passmore, T.R., and Price, W.C., *The Photoelectron Spectra and Ionized States of the Halogen Acids.* Proceedings of the Royal Society of London. Series A, Mathematical and Physical Sciences, 1968. **304**, 53.
62. Lonardo, G.D., and Douglas, A.E., *The Electronic Spectrum of HF. I. The $B^1\Sigma^+$ - $X^1\Sigma^+$ Band System.* Canadian Journal of Chemistry, 1973. **51**, 434.
63. Douglas, A.E., and Greening, F.R., *Electronic Spectra of HCl and HF.* Can. J. Phys., 1979. **57**(10), 1650.
64. Dibeler, V.H., Walker, J.A., and McCulloh, D.E., *Photoionization Study of the Dissociation Energy of Fluorine and the Heat of Formation of Hydrogen Fluoride.* J. Chem. Phys., 1969. **51**(10), 4230.
65. Barrow, R.F., Long, D.A., and Millen, D.J., *Molecular Spectroscopy*. Specialist Periodical Reports. Vol. 1-6. 1978, London: Royal Society of Chemistry.
66. Kolos, W., and Wolniewicz, L., *Potential Energy Curves for the $X^1\Sigma_g^+$, $b^3\Pi_u^+$, and C^1P_u States of the Hydrogen Molecule.* J. Chem. Phys., 1965. **43**(7), 2429.
67. Clementi, E., *SCFMO Wave Functions for the Hydrogen Fluoride Molecule.* J. Chem. Phys., 1962. **36**(1), 33.
68. McLean, A.D., and Yoshimine, M., *Computed Ground-State Properties of FH and ClH.* J. Chem. Phys., 1967. **47**(1), 3256.
69. Cade, P.E., and Huo, W.M., *Electronic Structure of Diatomic Molecules. VI.A. Hartree-Fock Wavefunctions and Energy Quantities for the Ground States of the First-Row Hydrides, AH.* J. Chem. Phys., 1967. **47**(2), 614.
70. Bender, C.F., and Davidson, E.R., *Correlation Energy and Molecular Properties of Hydrogen Fluoride.* J. Chem. Phys., 1967. **47**(2), 360.
71. Bender, C.F., and Davidson, E.R., *Theoretical Study of Several Electronic States of the Hydrogen Fluoride Molecule.* J. Chem. Phys., 1968. **49**(11), 4989.
72. Lee, T., Dutta, N.C., and Das, T.P., *Many-Body Perturbation Theory for Molecules Based on a United Atom Model.* Physics Review Letters, 1970. **25**(4), 204.
73. Brundle, C.R., *Ionization and Dissociation Energies of HF and DF and Their Bearing on $D°_0$ (F_2).* Chem. Phys. Lett., 1970. **7**(3), 317.
74. Berkowitz, J., *Experimental Potential Energy Curves for $X^2\Pi$ and $^2\Sigma^+$ States of HF^+.* Chem. Phys. Lett., 1971. **11**(1), 21.
75. Julienne, P.S., Krauss, M., and Wahl, A.C., *Hartree-Fock Energy Curves for $X^2\Pi$ and $^2\Sigma^+$ States of HF^+.* Chemistry and Physics of Lipids, 1971. **11**(1), 16.
76. Bondybey, V., Pearson, P.K., and Schaefer, H.F., *Theoretical Potential Energy Curves for OH, HF^+, HF, HF^-, NeH^+, and NeH.* J. Chem. Phys., 1972. **57**(3), 1123.
77. Lonardo, G.D., and Douglas, A.E., *Electronic Spectra of HF and F_2.* J. Chem. Phys., 1972. **56**(10), 5186.
78. Krauss, M., and Neumann, D., *Multi-Configurational Self-Consistent Field Calculation of Dissociation Energy and Electronic Structure of Hydrogen Fluoride.* Mol. Phys., 1974. **27**(4), 917.
79. Lie, G.C., and Clementi, E., *Study of the Electronic Structure of Molecules. XXI. Correlation Energy Corrections as a Functional of the Hartree Fock Density and its Applications to the Hydrides of the Second-Row Atoms.* J. Chem. Phys., 1974. **60**(4), 1275.
80. Banna, M.S., Mills, B.E., Davis, D.W., and Shirley, D.A., *X-ray Photoemission Molecular Orbitals of Hydrogen Fluoride and the Fluorinated Methanes.* J. Chem. Phys., 1974. **61**(11), 4780.

81. Bartlett, R.J., and Silver, D.M., *Many-body Perturbation Theory Applied to Electron Pair Correlation Energies. I. Closed Shell Firstrow Diatomic Hydrides.* J. Chem. Phys., 1975. **62**(8), 3258.
82. Bartlett, R.J., and Silver, D.M., *Many-Body Perturbation Theory Applied to Electron Pair Correlation Energies. I. Closed-Shell First-Row Diatomic Hydrides.* J. Chem. Phys., 1975. **62**(8), 3258.
83. Dunning, T.H., *The Low Lying States of Hydrogen Fluoride: Potential Energy Curves for the $X^1\Sigma^+$, $^3\Sigma^+$, $^3\Pi$, and $^1\Pi$ States.* J. Chem. Phys., 1976. **65**(10), 3854.
84. Sileo, R.N., and Cool, T.A., *Overtone Emission Spectroscopy of HF and DF: Vibrational Matrix Elements and Dipole Moment Function.* J. Chem. Phys., 1976. **65**(1), 117.
85. Wilson, S., *Diagrammatic Perturbation Theory: Potential Curves for the Hydrogen Fluoride Molecule.* Mol. Phys., 1978. **35**(1), 1.
86. Amos, R.D., *MCSCF Calculations of Properties of Hydrogen Fluoride.* Mol. Phys., 1978. **35**(6), 1765.
87. Brion, C.E., Hood, S.T., Suzuki, I.H., Weigold, E., and Williams, G.R.J., *Momentum Distributions and Ionization Potentials for the Valence Orbitals of Hydrogen Fluoride and Hydrogen Chloride.* J. Electron Spectrosc. Relat. Phenom., 1980. **21**(1), 71.
88. Segal, G.A., and Wolf, K., *Theoretical Calculation of the Potential Curves of the States of HF below 14 eV.* Chem. Phys., 1981. **56**(3), 321.
89. Niessen, W.v., Cederbaum, L.S., Domcke, W., and Diercksen, G.H.F., *Green´s Function Calculations on the Complete Valence Ionization Spectra of HF, HCl, HBr and HI.* Chem. Phys., 1981. **56**(1), 43.
90. Bettendorff, M., Buenker, R.J., Peyerimhoff, S.D., and Romelt, J., *Ab Initio CI Calculation of the Effects of Rydberg-Valence Mixing in the Electronic Spectrum of the HF Molecule.* Z. Phys. A.-Hadrons Nuclei, 1982. **304**(2), 125.
91. Hitchcock, A.P., Williams, G.R.J., Brion, C.E., and Langhoff, P.W., *Experimental and Theoretical Studies of the Valence-Shell Dipole Excitation Spectrum and Absolute Photoabsorption Cross Section of Hydrogen Fluoride.* Chem. Phys., 1984. **88**(1), 65.
92. Kumar, A., and Meath, W.J., *Integrated Dipole Oscillator Strengths and Dipole Properties for Ne, Ar, Kr, Xe, HF, HCl, and HBr.* Canadian Journal of Chemistry, 1985. **63**(7), 1616.
93. Chang, T.C., Hsue, C.S., Ruttink, P.A., and Schwarz, W.H.E., *Compromise Orbital Calculations by an Improved MC-GBT Approach - Core Excited States of HF*. Chem. Phys., 1985. **93**(3), 405.
94. Brown, A., and Balint-Kurti, G.G., *Spin-Orbit Branching in the Photodissociation of HF and DF. II A Time-Dependent Wave Packet Study of Vibrationally Mediated Photodissociation.* J. Chem. Phys., 2000. **113**(5), 1879.
95. Balint-Kurti, G.G., Orr-Ewing, A.J., Beswick, J.A., Brown, A., and Vasyutinskii, O.S., *Vector Correlations and Alignment Parameters in the Photodissociation of HF and DF*. J. Chem. Phys., 2002. **116**(24), 10760.
96. Lavin, C., Martín, I., and Velasco, A.M., *Spectral Properties of Hydrogen Fluoride in the Discrete and Continuum Regions (Rydberg Series in Hydrogen Fluoride).* The Astrophysical Journal, 2006. **644**(2), 1334.
97. Pitarch-Ruiz, J., Sanchez-Marin, J., Lavin, C., Velasco, A.M., and Martin, I., *Rydberg, Valence and Mixed States in the Vertical Spectrum of HF*. Chem. Phys. Lett., 2009. **476**(4-6), 151.

98. Cacelli, I., *Calculation of the Photoabsorption of HF in the Vacuum UV.* Chem. Phys. Lett., 1996. **249**(1-2), 149.
99. Nesbet, R.K., *Electronic Structure of HCl.* J. Chem. Phys., 1964. **41**(1), 100.
100. Cade, P.E., and Huo, W.M., *Electronic Structure of Diatomic Molecules. VII. A. Hartree-Fock Wavefunctions and Energy Quantities for the Ground States of the Second-Row Hydrides, AH.* J. Chem. Phys., 1967. **47**(2), 649.
101. Greening, F.R., *A United Atom Treatment of the Rydberg States of Linear Molecules with 2ΠCores.* Chem. Phys. Lett., 1975. **34**(3), 581.
102. Ahlrichs, R., Keil, F., Lischka, H., Kutzelnigg, W., and Staemmler, V., *PNO-CI (Pair Natural Orbital Configuration Interaction) and CEPA-PNO (Coupled electron Pair Approximation with Pair Natural Orbitals) Calculations of Molecular Systems. III. The Molecules MgH_2, AlH_3, SiH_4, PH_3 (Planar and Pyramidal), H_2S, HCl, and the Ar Atom.* J. Chem. Phys., 1975. **63**(1), 455.
103. Meyer, W., and Rosmus, P., *PNO-CI and CEPA Studies of Electron Correlation Effects. III. Spectroscopic Constants and Dipole Moment Functions for the Ground State of the First-Row and Second-Row Diatomic Hydrides.* J. Chem. Phys., 1975. **63**(6), 2356.
104. Bartlett, R.J., and Silver, D.M., *Many- Body Perturbation Theory Applied to Electron Pair Correlation Energies. II. Closed-Shell Second-Row Diatomic Hydrides.* J. Chem. Phys., 1976. **64**(11), 4578.
105. Williams, J.H., and Amos, R.D., *An SCF and CI Study of the Properties of the HCl and Cl_2 Molecules.* Chem. Phys. Lett., 1980. **70**(1), 162.
106. Hirst, D.M., and Guest, M.F., *Excited States of HCl - An Ab Initio Configuration-Interaction Investigation.* Mol. Phys., 1980. **41**(6), 1483.
107. Bettendorff, M., Peyerimhoff, S.D., and Buenker, R.J., *Clarification of the Assignment of the Electronic Spectrum of Hydrogen Chloride Based on Ab Initio CI Calculations.* Chem. Phys., 1982. **66**(3), 261.
108. Van Dishoeck, E.F., Van Hemert, M.C., and Dalgarno, A., *Photodissociation Processes in the HCl Molecule.* J. Chem. Phys., 1982. **77**(7), 3693.
109. Lefebvre-Brion, H., and Keller, F., *Competition between Autoionization and Predissociation in the HCl and DCl Molecules.* J. Chem. Phys., 1989. **90**(12), 7176.
110. Pradhan, A.D., Kirby, K.P., and Dalgarno, A., *Theoretical Study of HCl^+ - Potential Curves, Radiative Lifetimes, and Photodissociation Cross Sections.* J. Chem. Phys., 1991. **95**(12), 9009.
111. Alexander, M.H., Pouilly, B., and Duhoo, T., *Spin-Orbit Branching in the Photofragmentation of HCl.* J. Chem. Phys., 1993. **99**(3), 1752.
112. Yencha, A.J., Kaur, D., Donovan, R.J., Kvaran, A., Hopkirk, A., Lefebvre-Brion, H., and Keller, F., *Ion-Pair Formation in the Photodissociation of HCl and DCl.* J. Chem. Phys., 1993. **99**(7), 4986.
113. Alexander, M.H., Li, X.N., Liyanage, R., and Gordon, R.J., *Spin-orbit Branching in the Predissociation of the $C^1\Pi$ in State of HCl and DCl: A Manifestation of Quantum Interference.* Chem. Phys., 1998. **231**(2-3), 331.
114. Lambert, H.M., Dagdigian, P.J., and Alexander, M.H., *Spin-Orbit Branching in the Photofragmentation of HCl at Long Wavelength.* J. Chem. Phys., 1998. **108**(11), 4460.
115. Liyanage, R., Gordon, R.J., and Field, R.W., *Diabatic Analysis of the Electronic States of Hydrogen Chloride.* J. Chem. Phys., 1998. **109**(19), 8374.

116. Li, Y., Bludsky, O., Hirsch, G., and Buenker, R.J., *Ab Initio Configuration Interaction Study of the Predissociation of the (4s), (4pσ) $^{1,3}\Pi$, and (4pπ) $^{3}\Sigma^{+}$ Rydberg States of HCl and DCl.* J. Chem. Phys., 2000. **112**(1), 260.
117. Regan, P.M., Ascenzi, D., Brown, A., Balint-Kurti, G.G., and Orr-Ewing, A.J., *Ultraviolet Photodissociation of HCl in Selected Rovibrational States: Experiment and Theory.* J. Chem. Phys., 2000. **112**(23), 10259.
118. Pitarch-Ruiz, J., de Meras, A.S., Sanchez-Marin, J., Velasco, A.M., Lavin, C., and Martin, I., *Low-Lying Rydberg States of HCl.* J. Phys. Chem. A, 2008. **112**(14), 3275.
119. Lefebvre-Brion, H., Liebermann, H.P., and Vazquez, G.J., *Adiabatic Versus Diabatic Descriptions of the Lowest Rydberg and Valence $^{1}\Sigma^{+}$ states of HCl.* J. Chem. Phys., 2011. **134**(20), 204104.
120. Chapman, D.A., Balasubramanian, K., and Lin, S.H., *A Theoretical Study of Spectroscopic Properties and Transition Moments of HBr.* Chem. Phys., 1987. **118**(3), 333.
121. Chapman, D.A., Balasubramanian, K., and Lin, S.H., *Theoretical Study of the Negative Ions of HBr and HI.* Phys. Rev. A, 1988. **38**(12), 6098.
122. Wang, K.H., and McKoy, V., *Rotational Branching Ratios and Photoelectron Angular Distributions in Resonance Enhanced Multiphoton Ionization of HBr via the $F^{1}\Delta_{2}$ Rydberg State.* J. Chem. Phys., 1991. **95**(11), 7872.
123. Banichevich, A., Klotz, R., and Peyerimhoff, S.D., *Predissociation of the Ions HBr^{+} and DBr^{+}.* Mol. Phys., 1992. **75**(1), 173.
124. Peoux, G., Monnerville, M., Duhoo, T., and Pouilly, B., *Spin-Orbit Branching in the Photodissociation of HBr: Time-Independent, Time-Dependent, and Semi-Classical Calculations.* J. Chem. Phys., 1997. **107**(1), 70.
125. Smolin, A.G., Vasyutinskii, O.S., Balint-Kurti, G.G., and Brown, A., *Photodissociation of HBr. 1. Electronic Structure, Photodissociation Dynamics, and Vector Correlation Coefficients.* J. Phys. Chem. A, 2006. **110**(16), 5371.
126. Brown, A., *The Photo Dissociation of Hydrogen Iodide: Is it Adiabatic?* Int. J. Quantum Chem., 2007. **107**(14), 2665.
127. Ungemach, S.R., III, H.F.S., and Liu, B., *Theoretical Dipole Moment Function of the $X^{1}\Sigma^{+}$ State of HI.* J. Mol. Spectrosc., 1977. **66**, 99.
128. Chapman, D.A., Balasubramanian, K., and Lin, S.H., *Relativistic Configuration Interaction Calculations on the Low-Lying Electronic States of HI.* Chem. Phys. Lett., 1985. **118**(2), 192.
129. Lefebvre-Brion, H., Giusti-Suzor, A., and Raseev, G., *Theoretical Study of the Spin-Orbit Autoionization in Molecules Application to the HI Photoionization Spectrum.* J. Chem. Phys., 1985. **83**(4), 1557.
130. Chapman, D.A., Balasubramanian, K., and Lin, S.H., *Electronic Dipole Transition Moments from the Relativistic CI Wave Function: Application to HI.* J. Chem. Phys., 1987. **87**(9), 5325.
131. Levy, I., and Shapiro, M., *Theory of Electronic Branching in the Photodissociation of HI and DI.* J. Chem. Phys., 1988. **89**(5), 2900.
132. Alekseyev, A.B., Liebermann, H.-P., Kokh, D.B., and Buenker, R.J., *On the Ultraviolet Photofragmentation of Hydrogen Iodide.* J. Chem. Phys., 2000. **113**(15), 6175.
133. Balakrishnan, N., Alekseyev, A.B., and Buenker, R.J., *Ab Initio Quantum Mechanical Investigation of the Photodissociation of HI and DI.* Chem. Phys. Lett., 2001. **341**(5-6), 594.

134. Le Roy, R.J., Kraemer, G.T., and Manzhos, S., *1 Potential, 2 Potentials, 3 Potentials-4: Untangling the UV Photodissociation Spectra of HI and DI.* J. Chem. Phys., 2002. **117**(20), 9353.
135. Camden, J.P., Bechtel, H.A., Brown, D.J.A., Pomerantz, A.E., Zare, R.N., and Le Roy, R.J., *Probing Excited Electronic States Using Vibrationally Mediated Photolysis: Application to Hydrogen Iodide.* J. Phys. Chem. A, 2004. **108**(39), 7806.
136. Alekseyev, A.B., Kokh, D.B., and Buenker, R.J., *HI Photofragmentation Revisited. Comment on "Probing Excited Electronic States Using Vibrationally Mediated Photolysis: Application to Hydrogen Iodide"*. J. Phys. Chem. A, 2005. **109**(13), 3094.
137. Tilford, S.G., Ginter, M.L., and Vandersl.Jt, *Electronic Spectra and Structure of Hydrogen Halides - $b^3\Pi_i$ an $C^1\Pi_1$ States of HCl and DCl.* J. Mol. Spectrosc., 1970. **33**(3), 505.
138. Ginter, M.L., and Tilford, S.G., *Electronic Spectra and Structure of Hydrogen Halides $b^3\Pi_i$ and $C^1\Pi_1$ States of HBr and DBr.* J. Mol. Spectrosc., 1970. **34**(2), 206.
139. Tilford, S.G., Ginter, M.L., and Bass, A.M., *Electronic Spectra and Structure of Hydrogen Halides $b^3\Pi_i$ and $C^1\Pi_1$ States of HI and DI.* J. Mol. Spectrosc., 1970. **34**(2), 327.
140. Tilford, S.G., and Ginter, M.L., *Electronic Spectra and Structure of Hydrogen Halides - States Associated with $(\sigma^2\pi^3)c\pi$ and $(\sigma^2\pi^3)c\sigma$ Configurations of HCl and DCl.* J. Mol. Spectrosc., 1971. **40**(3), 568.
141. Ginter, M.L., and Tilford, S.G., *Electronic Spectra and Structure of Hydrogen Halides - States Associated with $(\sigma^2\pi^3)c\pi$ and $(\sigma^2\pi^3)c\sigma$ Configurations of HBr and DBr.* J. Mol. Spectrosc., 1971. **37**(1), 159.
142. Ginter, M.L., Tilford, S.G., and Bass, A.M., *Electronic Spectra and Structure of Hydrogen Halides - States Associated with $(\sigma^2\pi^3)c\pi$ and $(\sigma^2\pi^3)c\sigma$ Configurations of HI and DI.* J. Mol. Spectrosc., 1975. **57**(2), 271.
143. Ginter, D.S., and Ginter, M.L., *Electronic Spectra and Structure of the Hydrogen Halides: Characterization of the Electonic Structure of HCl Lying between 82 900 and 93 500 cm^{-1} above $X^1\Sigma^+$*. J. Mol. Spectrosc., 1981. **90**(1), 177.
144. Ginter, D.S., Ginter, M.L., and Tilford, S.G., *Electronic Spectra and Structure of the Hydrogen Halides: Characterization of the Electronic Structure of HBr and DBr Lying between 79 500 and 83 900 cm^{-1} above $X^1\Sigma^+$*. J. Mol. Spectrosc., 1981. **90**(1), 152.
145. Ginter, D.S., and Ginter, M.L., *Electronic Spectra and Structure of the Hydrogen Halides: Characterization of the Electronic Structure of HI Lying between 67 800 and 74 400 cm^{-1} above $X^1\Sigma^+$*. J. Mol. Spectrosc., 1982. **92**(1), 40.
146. Ginter, D.S., Ginter, M.L., Tilford, S.G., and Bass, A.M., *Electronic Spectra and Structure of the Hydrogen Halides: Characterization of the Electronic Structure of DI Lying between 67800 and 74 400 cm^{-1} above $X^1\Sigma^+$*. J. Mol. Spectrosc., 1982. **92**(1), 55.
147. Berkowitz, J., Chupka, W.A., Guyon, P.M., Holloway, J.H., and Spohr, R., *Photoionization Mass Spectrometric Study of F_2, HF, and DF*. J. Chem. Phys., 1971. **54**(12), 5165.
148. Guyon, P.M., Spohr, R., Chupka, W.A., and Berkowtiz, J., *Threshold Photoelectron Spectra of HF, DF, and F_2.* J. Chem. Phys., 1976. **65**(5), 1650.
149. Banna, M.S., and Shirley, D.A., *Molecular Photoelectron Spectroscopy at 132.3 eV. Methane, the Fluorinated Methanes and Hydrogen Fluoride.* Chem. Phys. Lett., 1975. **33**(3), 441.

150. Jr., R.W.S., and Thomas, T.D., *Auger Electron Spectrum and Ionization Potentials of the HF Molecule.* Phys. Rev. A, 1975. **11**(5), 1491.
151. Spence, D., and Noguchi, T., *Feshback Resonances Associated with Rydberg States of the Hydrogen Halides.* J. Chem. Phys., 1975. **63**(1), 505.
152. Mathur, D., and Hasted, J.B., *Electronic Spectroscopy of Hydrogen Fluoride Resonanced.* Chem. Phys., 1978. **34**(1), 29.
153. Brion, C.E., McCarthy, I.E., Suzuki, I.H., and Weigold, E., *Momentum Distributions for the Valence Orbitals of Hydrogen Fluoride.* Chem. Phys. Lett., 1979. **67**(1), 115.
154. Carnovale, F., and Brion, C.E., *Absolute Dipole Oscillator Strengths for Molecular and Dissociative Photoionization of Hydrogen Fluoride.* Chem. Phys., 1983. **74**(2), 253.
155. Carnovale, F., Tseng, R., and Brion, C.E., *Absolute Oscillator Strengths for the Photoabsorption and Partial Photoionization of Hydrogen Fluoride.* J. Phys. B-At. Mol. Opt. Phys., 1981. **14**(24), 4771.
156. Hitchcock, A.P., and Brion, C.E., *K-Shell Excitation of HF and F_2 Studied by Electron Energy-Loss Spectroscopy.* J. Phys. B-At. Mol. Opt. Phys., 1981. **14**(22), 4399.
157. Salama, A., and Hasted, J.B., *Electron Energy Loss Spectrum of Hydrogen Fluoride.* J. Phys. B-At. Mol. Opt. Phys., 1976. **9**(11), L333.
158. Nee, J.B., Suto, M., and Lee, L.C., *Photoabsorption Cross Section of HF at 107-145 nm.* J. Phys. B-At. Mol. Opt. Phys., 1985. **18**(10), L293.
159. Myer, J.A., and Samson, J.A.R., *Vacuum Ultraviolet Absorption Cross Sections of CO, HCl, and ICN between 1050 and 2100 Å.* J. Chem. Phys., 1970. **52**(1), 266.
160. Sheasley, W.D., and Mathews, C.W., *The Emission Spectra of $H^{35}Cl^+$, $H^{37}Cl^+$, $D^{35}Cl^+$, and $D^{37}Cl^+$ in the Region 2700-4100 Å.* J. Mol. Spectrosc., 1973. **47**, 420.
161. Inn, E.C.Y., *Absorption Coefficient of HCl in the Region 1400 to 2200 Å.* Journal of Atmospheric Sciences, 1975. **32**(12), 2375.
162. Wang, R.G., Dillon, M.A., and Spence, D., *Electron Spectroscopy of Hydrogen Chloride from 5 to 19 eV.* J. Chem. Phys., 1984. **80**(1), 63.
163. York, T.A., and Comer, J., *Electron Energy-Loss Studies Using a Position-Sensitive Multidetector Electron Spectrometer: The Spectrum of Hydrogen Chloride.* J. Phys. B-At. Mol. Opt. Phys., 1984. **17**(12), 2563.
164. Nee, J.B., Suto, M., and Lee, L.C., *Quantitative Photoabsorption and Fluorescence Study of HCl in Vacuum Ultraviolet.* J. Chem. Phys., 1986. **85**(2), 719.
165. Baig, M.A., Hormes, J., Connerade, J.P., and Garton, W.R.S., *Rotational Analysis of a New Electronic Transition of HBr and DBr.* J. Phys. B-At. Mol. Opt. Phys., 1981. **14**(4), L147.
166. Chanda, A., Ho, W.C., Dalby, F.W., and Ozier, I., *Fine and Hyperfine Structure in the Vibrational Spectrum of the $X^2\Pi$ State of HBr^+.* J. Mol. Spectrosc., 1995. **169**(1), 108.
167. Nee, J.B., Suto, M., and Lee, L.C., *Quantitative Spectroscopy of HBr in the 105-235 nm Region.* J. Chem. Phys., 1986. **85**(9), 4919.
168. Yencha, A.J., Cormack, A.J., Donovan, R.J., Lawley, K.P., Hopkirk, A., and King, G.C., *Threshold Photoelectron Spectroscopy of HBr and DBr.* Chem. Phys., 1998. **238**(1), 133.
169. Brion, C.E., Dyck, A., and Cooper, G., *Absolute Photoabsorption Cross-Sections (Oscillator Strengths) for Valence and Inner Shell Excitations in Hydrogen Chloride, Hydrogen Bromide and Hydrogen Iodide.* J. Electron Spectrosc. Relat. Phenom., 2005. **144**, 127.

170. Ogilvie, J.F., *Semi-Experimental Determination of a Repulsive Potential Curve for Hydrogen Iodide.* Transactions of the Faraday Society, 1971. **67**(584), 2205.
171. Clear, R.D., Riley, S.J., and Wilson, K.R., *Energy Partitioning and Assignment of Excited States in the Ultraviolet Photolysis of HI and DI.* J. Chem. Phys., 1975. **63**(4), 1340.
172. Eland, J.H.D., and Berkowitz, J., *Photoionization Mass Spectroscopy of HI and DI at High Resolution.* J. Chem. Phys., 1977. **67**(11), 5034.
173. Carlson, T.A., Fahlman, A., Krause, M.O., Keller, P.R., Taylor, J.W., Whitley, T., and Grimm, F.A., *Angle Resolved Photoelectron Spectroscopy of the Valence Shells in HI and CH_3I as a Function of Photon Energy from 13 to 90 eV.* J. Chem. Phys., 1984. **80**(8), 3521.
174. Schmiedl, R., Dugan, H., Meier, W., and Welge, K.H., *Laser Doppler Spectroscopy of Atomic Hydrogen in the Photodissociation of HI.* Z. Phys. A.-Hadrons Nuclei, 1982. **303**(2), 137.
175. Xu, Z., Koplitz, B., and Wittig, C., *Determination Reaction Pathways and Spin-Orbit Populations in the Photodissociation of HBr and HI Using Velocity-Aligned Doppler Spectroscopy.* J. Phys. Chem., 1988. **92**(19), 5518.
176. Xu, Z., Koplitz, B., and Wittig, C., *Velocity Aligned Doppler Spectroscopy.* J. Chem. Phys., 1989. **90**(5), 2692.
177. Brewer, P., Das, P., Ondrey, G.S., and Bersohn, R., *Measurement of the Relative Populations of $I(^2P_{1/2})$ and $I(^2P_{3/2})$ by Laser Induced Vacuum Ultraviolet Fluorescence.* J. Chem. Phys., 1983. **79**(2), 720.
178. Carlson, T.A., Gerard, P., Krause, M.O., Wald, G.V., Taylor, J.W., and Grimm, F.A., *Autoionization Between the Ionization Thresholds for the $^2\Pi_{3/2}$ and $^2\Pi_{1/2}$ States of HI^+.* J. Chem. Phys., 1986. **84**(9), 4755.
179. Hart, D.J., and Hepburn, J.W., *Vacuum Ultraviolet Laser Photoionization Spectroscopy: A High-Resolution Study of Spin-orbit Autoionization in HI.* Chem. Phys., 1989. **129**(1), 51.
180. Huth-Fehre, T., Mank, A., Drescher, M., Böwering, N., and Heinzmann, U., *Rotationally Resolved Fano Effect of HI Molecules: An Experimental Study Using Coherent Vacuum-Ultraviolet Radiation.* Physical Review Letters, 1990. **64**(4), 396.
181. Böwering, N., Muller, M., Salzmann, M., and Heinzmann, U., *Angle-Resolved Measurements of the Photoelectron Spin Polarization in the Photoionization of HI Molecules.* J. Phys. B-At. Mol. Opt. Phys., 1991. **24**(22), 4793.
182. Mank, A., Drescher, M., Huth-Fehre, T., Böwering, N., Heinzmann, U., and Lefebvre-Brion, H., *Photoionization of Jet-Cooled HI with Coherent Vacuum Radiation: Evidence for Hund's Case (e).* J. Chem. Phys., 1991. **95**(3), 1676.
183. Böwering, N., Salzmann, M., Müller, M., Klausing, H.W., and Heinzmann, U., *Vibrationally Resolved Photoelectron-Spin-Polarization Spectroscopy of HI Molecules.* Phys. Rev. A, 1992. **45**(1), R11.
184. Böwering, N., Klausing, H.W., Müller, M., Salzmann, M., and Heinzmann, U., *Observation of Vibrational Excitation in Photoelectron Spectroscopy of HI^+ $^2\Pi_i$.* Chem. Phys. Lett., 1992. **189**(4-5), 467.
185. Zietkiewicz, C.J., Gu, Y.Y., Farkas, A.M., and Eden, J.G., *Photoelectron Spectroscopy of the Multiphoton Ionization and above Threshold Ionization of HI at 532 nm annd 355 nm.* J. Chem. Phys., 1994. **101**(1), 86.
186. Yencha, A.J., Ruf, M.W., and Hotop, H., *Penning Ionization Electron Spectrometry of Hydrogen Iodide.* Zeitschrift für Physik D, 1994. **29**(3), 163.

187. Chanda, A., Ho, W.C., Dalby, F.W., and Ozier, I., *Hyperfine Resolved Rovibrational Spectrum of the $X^2\Pi$ State of HI^+.* J. Chem. Phys., 1995. **102**(22), 8725.
188. Lugez, C.L., Jacox, M.E., and Thompson, W.E., *The Vibrational Spectra of Molecular Ions Isolated in Solid Neon. XIII. Ions Derived from HBr and HI.* J. Chem. Phys., 1996. **105**(10), 3901.
189. Cormack, A.J., Yencha, A.J., Donovan, R.J., Lawley, K.P., Hopkirk, A., and King, G.C., *High-Resolution Threshold Photoelectron Spectroscopy of Hydrogen Iodide.* Chem. Phys., 1997. **221**(1-2), 175.
190. Yencha, A.J., Baltzer, P., Cormack, A.J., Li, Y., Liebermann, H.P., Alekseyev, A.B., and Buenker, R.J., *High-Resolution Photoelectron Spectroscopy of HI and DI: Experimental and Theoretical Analysis of the $A^2\Sigma^+$ Ion System.* J. Chem. Phys., 2003. **119**(12), 5943.
191. Ravaine, B., Porsev, S.G., and Derevianko, A., *Marked Influence of the Nature of the Chemical Bond on CP-Violating Signature in Molecular Ions HBr^+ and HI^+.* Physical Review Letters, 2005. **94**(1), 013001.
192. Isaev, T.A., Petrov, A.N., Mosyagin, N.S., and Titov, A.V., *In Search of the Electron Electric Dipole Moment: Relativistic Correlation Calculations of the P,T-Violating Effect in the Ground State of HI^+.* Physical Review Letters, 2005. **95**(16), 163004.
193. Wight, C.A., and Leone, S.R., *Excimer Laser Photolysis Studies of Translational-to-Vibrational Energy Transfer in Collisions of H and D Atoms with CO.* J. Chem. Phys., 1983. **78**(8), 4875.
194. Johnson, P.M., Berman, M.R., and Zakheim, D., *Non-Resonant Multiphoton Ionization Spectroscopy: The Four Photon Ionization Spectrum of Nitric Oxide.* J. Chem. Phys., 1975. **62**(6), 2500.
195. Johnson, P.M., *Multiphoton Ionization Spectroscopy: A New State of Benzene.* J. Chem. Phys., 1975. **62**(11), 4562.
196. Johnson, P.M., and Otis, C.E., *Molecular Multiphoton Spectroscopy with Ionization Detection.* Annual Reviews in Physical Chemistry, 1981. **32**, 139.
197. Ashfold, M.N.R., and Howe, J.D., *Multiphoton Spectroscopy of Molecular Species.* Annual Reviews in Physical Chemistry, 1994. **45**, 57.
198. Arepalli, S., Presser, N., Robie, D., and Gordon, R.J., *Detection of Cl Atoms and HCl Molecules by Resonantly Enhanced Multiphoton Ionization.* Chem. Phys. Lett., 1985. **118**(1), 88.
199. Arepalli, S., Presser, N., Robie, D., and Gordon, R.J., *The Detection of Bromine Atoms by Resonant Enhanced Multiphoton Ionization.* Chem. Phys. Lett., 1985. **117**(1), 64.
200. Spiglanin, T.A., Chandler, D.W., and Parker, D.H., *Mass Resolved Laser Ionization Spectroscopy of HCl.* Chem. Phys. Lett., 1987. **137**(5), 414.
201. Tashiro, L.M., Ubachs, W., and Zare, R.N., *The HF and DF $B^1\Sigma^+$-$X^1\Sigma^+$ and $C^1\Pi$-$X^1\Sigma^+$ Band Systems Studied by 1 XUV + 1 UV Resonance Enhanced Multiphoton Ionization.* J. Mol. Spectrosc., 1989. **138**(1), 89.
202. Green, D.S., Bickel, G.A., and Wallace, S.C., *(2+1) Resonance Enhanced Multiphoton Ionization of Hydrogen Chloride in a Pulsed Supersonic Jet - Spectroscopic Survey. 1.* J. Mol. Spectrosc., 1991. **150**(2), 303.
203. Green, D.S., Bickel, G.A., and Wallace, S.C., *(2+1) Resonance Enhanced Multiphoton Ionization of Hydrogen Chloride in a Pulsed Supersonic Jet - Spectroscopy and Rydberg Approximately Valence Interactions of the $^1\Sigma^+(0^+)$ and $^3\Sigma^-(1, 0^+)$ States. 2.* J. Mol. Spectrosc., 1991. **150**(2), 354.

204. Green, D.S., Bickel, G.A., and Wallace, S.C., *(2+1) Resonance Enhanced Multiphoton Ionization of Hydrogen Chloride in a Pulsed Supersonic Jet - Vacuum Wavenumbers of Rotational Lines with Detailed Band Analysis for Excited Electronic States of HCl-35. 3.* J. Mol. Spectrosc., 1991. **150**(2), 388.
205. Green, D.S., and Wallace, S.C., *2-Photon Spectroscopy, Rydberg Similar to Valence Interactions and Superexcited State Dissociation of HCl Probed by Resonance Enhanced Multiphoton Ionization.* J. Chem. Phys., 1992. **96**(8), 5857.
206. Callaghan, R., and Gordon, R.J., *The Multiphoton Ionization Spectrum of HBr. I. 74000 to 85000 cm^{-1}.* J. Chem. Phys., 1990. **93**(7), 4624.
207. de Beer, E., Koenders, B.G., Koopmans, M.P., and Delange, C.A., *Multiphoton Ionization Processes in HCl Studied by Photoelectron Spectroscopy.* J. Chem. Soc.-Faraday Trans., 1990. **86**(11), 2035.
208. Wang, K.H., and McKoy, V., *Rotationally Resolved Photoelectron Spectra in Resonance Enhanced Multiphoton Ionization of HCl via the $F^1\Delta_2$ Rydberg State.* J. Chem. Phys., 1991. **95**(12), 8718.
209. Xie, Y.J., Reilly, P.T.A., Chilukuri, S., and Gordon, R.J., *Perturbations in the Multiphoton Ionization Spectrum of the $F^1\Delta$ State of HCl.* J. Chem. Phys., 1991. **95**(2), 854.
210. de Beer, E., Buma, W.J., and Delange, C.A., *Resonance Enhanced Multiphoton Ionization Photoelectron Spectroscopy and Pulsed-Field Ionization via the $F^1\Delta_2(v'=0)$ and $f^3\Delta_2(v'=0)$ Rydberg States of HCl.* J. Chem. Phys., 1993. **99**(5), 3252.
211. Zhu, Y.F., Grant, E.R., Wang, K., McKoy, V., and Lefebvre-Brion, H., *Spin-Orbit Autoionization and Intensities in the Double-Resonant Delayed Pulsed Field Threshold Photoionization of HCl.* J. Chem. Phys., 1994. **100**(12), 8633.
212. Liyanage, R., Yang, Y.A., Hashimoto, S., Gordon, R.J., and Field, R.W., *Electronic Control of the Spin-Orbit Branching Ratio in the Photodissociation and Predissociation of HCl.* J. Chem. Phys., 1995. **103**(15), 6811.
213. Xie, J.C., and Zare, R.N., *Determination of Absolute Thermal Rate Constants for the Charge Transfer Reaction DBr^+ ($^2\Pi_i$,v^+)+HBr--> HBr^+($^2\Pi_i$, v'^+)+DBr.* J. Chem. Phys., 1992. **96**(6), 4293.
214. Philippson, J.N., Shiell, R.C., Reinhold, E., and Ubachs, W., *Observation of Molecular Hyperfine Structure in the Extreme Ultraviolet: The HF C-X spectrum.* J. Chem. Phys., 2008. **129**(17), 174310.
215. Wright, S.A., and McDonald, J.D., *Multiphoton Ionization Spectroscopy of Hydrogen Iodide.* J. Chem. Phys., 1994. **101**(1), 238.
216. Pratt, S.T., and Ginter, M.L., *2-Photon Spectroscopy of HI in the 69600-73600 cm^{-1} Region.* J. Chem. Phys., 1995. **102**(5), 1882.
217. Ascenzi, D., Langford, S.R., Ashfold, M.N.R., and Orr-Ewing, A.J., *3+1 Resonance Enhanced Multiphoton Ionization Spectroscopy of HBr.* Phys. Chem. Chem. Phys., 2001. **3**(1), 29.
218. Kvaran, A., Logadottir, A., and Wang, H., *(2+1) REMPI Spectra of Ω=0 States of the Hydrogen Halides: Spectroscopy, Perturbations and Excitation Mechanisms.* J. Chem. Phys., 1998. **109**(14), 5856.
219. Kvaran, Á., Wang, H., and Logadóttir, Á., *Rotational REMPI Spectroscopy; Halogen Containing Compounds.* Recent Research Developments in Physical Chemistry, 1998. **2**, 233.
220. Kvaran, A., Sigurbjornsson, O.F., and Wang, H.S., *REMPI-TOF Studies of the HF Dimer.* J. Mol. Struct., 2006. **790**(1-3), 27.

221. Kvaran, A., Wang, H., and Logadottir, A., *Resonance Enhanced Multiphoton Ionization of the Hydrogen Halides: Rotational Structure and Anomalies in Rydberg and Ion-Pair States of HCl and HBr.* J. Chem. Phys., 2000. **112**(24), 10811.
222. Kvaran, A., Wang, H.S., and Waage, B.G., *Three- and Two-Photon Absorption Spectroscopy: REMPI of HCl and HBr.* Can. J. Phys., 2001. **79**(2-3), 197.
223. Wang, H., and Kvaran, A., *Three-Photon Absorption Spectroscopy: (3+1)REMPI of HCl ($I^1\Delta_2$-$X^1\Sigma^+$).* J. Mol. Struct., 2001. **563**, 235.
224. Kvaran, A., and Wang, H.S., *Three-Photon Absorption Spectroscopy: The L($^1\Phi_3$) and m($^3\Pi_1$) States of HCl and DCl.* Mol. Phys., 2002. **100**(22), 3513.
225. Kvaran, A., and Wang, H.S., *Three- and Two-Photon Absorption of Ω=3 states and State in HCl and DCl: Identification Interaction Analysis.* J. Mol. Spectrosc., 2004. **228**(1), 143.
226. Kvaran, A., Wang, H.S., Matthiasson, K., Bodi, A., and Jonsson, E., *Two-dimensional (2+n) resonance enhanced multiphoton ionization of HCl: Photorupture channels via the $F^1\Delta_2$ Rydberg state and ab initio spectra.* J. Chem. Phys., 2008. **129**(16), 164313.
227. Kvaran, A., Matthiasson, K., and Wang, H.S., *Two-Dimensional (2+n) Resonance Enhanced Multiphoton Ionization of HCl: State Interactions and Photorupture Channels via Low-Energy Triplet Rydberg States.* J. Chem. Phys., 2009. **131**(4), 044324.
228. Matthiasson, K., Wang, H.S., and Kvaran, A., *Two-Dimensional (2+n) REMPI of HCl: Observation and Characterisation of a New Rydberg State.* J. Mol. Spectrosc., 2009. **255**(1), 1.
229. Matthiasson, K., Long, J.M., Wang, H.S., and Kvaran, A., *Two-Dimensional Resonance Enhanced Multiphoton Ionization of (H^iCl); i=35, 37: State Interactions, Photofragmentations and Energetics of High Energy Rydberg States.* J. Chem. Phys., 2011. **134**(16), 164302.
230. Long, J.M., Wang, H.S., and Kvaran, A., *Photofragmentations, State Interactions, and Energetics of Rydberg and Ion-Pair States: Resonance Enhanced Multiphoton Ionization via E and V (B) States of HCl and HBr.* J. Chem. Phys., 2013. **138**(4), 044308.
231. Kvaran, A., Waage, B.G., and Wang, H., *What to See and What Not to See in Three-Photon Absorption: (3+1) REMPI of HBr.* J. Chem. Phys., 2000. **113**(5), 1755.
232. Long, J.M., Wang, H.S., and Kvaran, A., *Rydberg and Ion-Pair States of HBr: New REMPI Observations and Analysis.* J. Mol. Spectrosc., 2012. **282**, 20.
233. Long, J.M., Hrodmarsson, H.R., Wang, H.S., and Kvaran, A., *Photofragmentations, State Interactions, and Energetics of Rydberg and Ion-Pair States: Two-Dimensional Resonance Enhanced Multiphoton Ionization of HBr via Singlet-, Triplet-, Ω=0 and 2 states.* J. Chem. Phys., 2012. **136**(21), 214315.
234. Hrodmarsson, H.R., Wang, H.S., and Kvaran, A., *New REMPI Observations and Analyses for Rydberg and Ion-Pair States of HI.* J. Mol. Spectrosc., 2013. **290**, 5.
235. Hrodmarsson, H.R., Wang, H.S., and Kvaran, A., *Photofragmentation, State Interaction, and Energetics of Rydberg and Ion-Pair States: Resonance Enhanced Multiphoton Ionization of HI.* J. Chem. Phys., 2014. **140**(24), 244304.
236. Hrodmarsson, H.R., Wang, H., and Kvaran, A., *State Interactions and Illumination of Hidden States through Perturbations and Observations of New States: High Energy Resonance Enhanced Multiphoton Ionization of HI.* The Journal of Chemical Physics, 2015. **142**(24), 244312.

237. Hrodmarsson, H.R., and Kvaran, Á., *Revealing Photofragmentation Dynamics through Interactions between Rydberg States: REMPI of HI as a Case Study.* PCCP, 2015. **17**(48), 32517.
238. Yencha, A.J., Kela, D.K., Donovan, R.J., Hopkirk, A., and Kvaran, A., *Ion-Pair (Br^+Br^-) Formation from Photodissociation of Br_2 near the 1st Ionization Limit.* Chem. Phys. Lett., 1990. **165**(4), 283.
239. Kvaran, A., Yencha, A.J., Kela, D.K., Donovan, R.J., and Hopkirk, A., *Vibrationally Resolved Excitation Functions for Direct Ion-Pair (I^++I^-) Formation from Photodissociation of I_2.* Chem. Phys. Lett., 1991. **179**(3), 263.
240. Kvaran, A., Jonsdottir, S.O., and Þorgeirsson, T.E., *Mechanism of Vibrational-Relaxation and Intersystem Crossing within Excited Ion-Pair States of I_2.* Proc. Indian Acad. Sci.-Chem. Sci., 1991. **103**(3), 417.
241. Huasheng, W., Asgeirsson, J., Kvaran, A., Donovan, R.J., Flood, R.V., Lawley, K.P., Ridley, T., and Yencha, A.J., *Rotationally Resolved (2+1) REMPI Spectra of Gerade Rydberg States of Molecular Iodine - The (v'=0, v'=1) Band of the Dalby System.* J. Mol. Struct., 1993. **293**, 217.
242. Kvaran, A., Wang, H.S., and Asgeirsson, J., *The Dalby System of Iodine Revisited - Rotationally Resolved (2+1) REMPI Spectra of the Rydberg State $[^2\Pi_{1/2}]_C$6S,1g of I_2.* J. Mol. Spectrosc., 1994. **163**(2), 541.
243. Kvaran, A., Wang, H.S., Johannesson, G.H., and Yencha, A.J., *REMPI Spectra of I_2 - The $[^2\Pi_{3/2}]_C$ 5d,1g Rydberg State and Interactions with Ion-Pair States.* Chem. Phys. Lett., 1994. **222**(5), 436.
244. Yencha, A.J., Hopkirk, A., Hiraya, A., Donovan, R.J., Goode, J.G., Maier, R.R.J., King, G.C., and Kvaran, A., *Threshold Photoelectron-Spectroscopy of Cl_2 and Br_2 up to 35 eV.* J. Phys. Chem., 1995. **99**(19), 7231.
245. Johannesson, G.H., Wang, H.S., and Kvaran, A., *REMPI Spectra of Cl_2: Vibrational and Rotational Analysis of the $2^1\Pi_g$ Rydberg States of $^{35}Cl_2$, $^{35}Cl^{37}Cl$, and $^{37}Cl_2$.* J. Mol. Spectrosc., 1996. **179**(2), 334.
246. Kvaran, A., Johannesson, G.H., and Wang, H.S., *Rotational Perturbations in the (2+1) REMPI Spectrum of the Rydberg State $[^2\Pi_{3/2}]_c$ 5d;1g of I_2.* Chem. Phys., 1996. **204**(1), 65.
247. Kvaran, A., Yencha, A.J., Lawley, K.P., and Donovan, R.J., *Analyses of the 290-400 nm Oscillatory Continua due to Transitions from the E(0^+) Ion-Pair State of BrCl.* Mol. Phys., 1992. **75**(1), 197.
248. Kaur, D., Yencha, A.J., Donovan, R.J., Kvaran, A., and Hopkirk, A., *Ion-Pair (X^++Y^-) Formation from Photodissociation of the Interhalogen Molecules BrCl, ICl, and IBr.* Org. Mass Spectrom., 1993. **28**(4), 327.
249. Kvaran, A., Wang, H.S., and Johannesson, G.H., *REMPI Spectra of IBr - Vibrational and Rotational Analysis of the $[B^2\Pi_{1/2}]_C$ 6s, 1 Rydberg States of $I^{79}Br$ and $I^{81}Br$.* J. Phys. Chem., 1995. **99**(13), 4451.
250. Kvaran, A., Wang, H.S., Matthiasson, K., and Bodi, A., *Two-Dimensional (2+n) REMPI of CH_3Br: Photodissociation Channels via Rydberg States.* J. Phys. Chem. A, 2010. **114**(37), 9991.
251. Long, J.M., Wang, H.S., and Kvaran, A., *Resonance-Enhanced Multiphoton Ionization of CH_2Br_2: Rydberg States, Photofragmentation, and CH Spectra.* J. Phys. Chem. A, 2014. **118**(10), 1826.
252. Hafliðason, A., Wang, H., and Kvaran, Á., *Long Term Puzzles of the CH and CD Energetics and Related Phenomena Revisited: Solutions Sought through REMPI*

Photofragmentations of Bromomethanes. Phys. Chem. Chem. Phys., 2016. **18**(3), 1797.

253. Kvaran, A., Sveinbjornsson, K., Long, J.M., and Wang, H.S., *Two-dimensional REMPI of CF_3Br: Rydberg states and photofragmentation channels.* Chem. Phys. Lett., 2011. **516**(1-3), 12.
254. Bodi, A., Kvaran, A., and Sztaray, B., *Thermochemistry of Halomethanes CF_nBr_{4-n} (n=0-3) Based on iPEPICO Experiments and Quantum Chemical Computations.* J. Phys. Chem. A, 2011. **115**(46), 13443.
255. Matthiasson, K., Wang, H.S., and Kvaran, A., *(2+n) REMPI of Acetylene: Gerade Rydberg States and Photorupture Channels.* Chem. Phys. Lett., 2008. **458**(1-3), 58.
256. Zhang, J., Riehn, C.W., Dulligan, M., and Wittig, C., *An Experimental Study of HF Photodissociation: Spin-Orbit Branching Ratio and Infrared Alignment.* J. Chem. Phys., 1996. **104**(18), 7027.
257. Tonokura, K., Matsumi, Y., Kawasaki, M., Tasaki, S., and Bersohn, R., *Photodissociation of Hydrogen Chloride at 157 and 193 nm: Angular Distributions of Hydrogen Atoms and Fine Structure Branching Ratios of Chlorine Atoms in the ^2P_j Levels.* J. Chem. Phys., 1992. **97**(11), 8210.
258. Zhang, J., Dulligan, M., and Wittig, C., *Photodissociation of HCl at 193.3 nm: Spin-orbit Branching Ratio.* J. Chem. Phys., 1997. **107**(5), 1403.
259. Strizhev, A., Li, X.N., Liyanage, R., and Gordon, R.J., *A Unified Model of the Dynamics and Spectroscopy of the $g^3\Sigma_{0^-}$ and $E^1\Sigma^+$ States of Hydrogen Chloride.* J. Chem. Phys., 1998. **108**(3), 984.
260. Regan, P.M., Langford, S.R., Ascenzi, D., Cook, P.A., Orr-Ewing, A.J., and Ashfold, M.N.R., *Spin-Orbit Branching in Cl(^2P) Atoms Produced by Ultraviolet Photodissociation of HCl.* Phys. Chem. Chem. Phys., 1999. **1**(14), 3247.
261. Regan, P.M., Langford, S.R., Orr-Ewing, A.J., and Ashfold, M.N.R., *The Ultraviolet Photodissociation Dynamics of Hydrogen Bromide.* J. Chem. Phys., 1999. **110**(1), 281.
262. Rakitzis, T.P., Samartzis, P.C., Toomes, R.L., Tsigaridas, L., Coriou, M., Chestakov, D., Eppink, A.T.J.B., Parker, D.H., and Kitsopoulos, T.N., *Photofragment Alignment from the Photodissociation of HCl and HBr.* Chem. Phys. Lett., 2002. **364**(1-2), 115.
263. Veen, G.N.A.v., Mohamed, K.A., Baller, T., and Vries, A.E.d., *Photofragmentation of HI in the First Continuum.* Chem. Phys., 1983. **80**, 113.
264. Kalyanamaran, C., and Sathyamurthy, N., *Channel Control in a Chemical Reaction. Vibrational Enhancement of I*/I Branching Ratio in HI Photodissociation.* Chem. Phys. Lett., 1993. **209**(1,2), 52.
265. Langford, S.R., Regan, R.M., Orr-Ewing, A.J., and Ashfold, M.N.R., *On the UV Photodissociation Dynamics of Hydrogen Iodide.* Chem. Phys., 1998. **231**(2-3), 245.
266. Gendron, D.J., and Hepburn, J.W., *Dynamics of HI Photodissociation in the A Band Absorption via H-atom Doppler Spectroscopy.* J. Chem. Phys., 1998. **109**(17), 7205.
267. Regan, P.M., Ascenzi, D., Clementi, C., Ashfold, M.N.R., and Orr-Ewing, A.J., *The UV Photodissociation of HI Revisited: REMPI Measurements of I(^2P) Atom Spin-Orbit Branching Fractions.* Chem. Phys. Lett., 1999. **315**(3-4), 187.
268. Chandler, D.W., and Houston, P.L., *Two Dimensional Imaging of State-Selected Photodissociation Products Detected by Multiphoton Ionization.* J. Chem. Phys., 1987. **87**(2), 1445.
269. Parker, D.H., and Eppink, A.T.J.B., *Photoelectron and Photofragment Velocity Map Imaging of State-Selected Molecular Oxygen Dissociation/Ionization Dynamics.* J. Chem. Phys., 1997. **107**(7), 2357.

270. Eppink, A.T.J.B., and Parker, D.H., *Velocity Map Imaging of Ions and Electrons Using Electrostatic Lenses: Application in Photoelectron and Photofragment Ion Imaging of Molecular Oxygen.* Rev. Sci. Instrum., 1997. **68**(9), 3477.
271. Ashfold, M.N.R., Nahler, N.H., Orr-Ewing, A.J., Vieuxmaire, O.P.J., Toomes, R.L., Kitsopoulos, T.N., Garcia, I.A., Chestakov, D.A., Wu, S.M., and Parker, D.H., *Imaging the Dynamics of Gas Phase Reactions.* Phys. Chem. Chem. Phys., 2006. **8**(1), 26.
272. Chichinin, A.I., Gericke, K.H., Kauczok, S., and Maul, C., *Imaging Chemical Reactions-3D Velocity Mapping.* Int. Rev. Phys. Chem., 2009. **28**(4), 607.
273. Heck, A.J.R., and Chandler, D.W., *Imaging Techniques for the Study of Chemical Reaction Dynamics.* Annual Reviews in Physical Chemistry, 1995. **46**, 335.
274. Levine, R.D., and Bernstein, R.B., *Molecular Reaction Dynamics and Chemical Reactivity*. 1987, New York: Oxford University Press.
275. Baumfalk, R., Buck, U., Frischkorn, C., Nahler, N.H., and Huwel, L., *Photodissociation of HBr Molecules and Clusters: Anisotropy Parameters, Branching Ratios, and Kinetic Energy Distributions.* J. Chem. Phys., 1999. **111**(6), 2595.
276. Rakitzis, T.P., Samartzis, P.C., Toomes, R.L., Kitsopoulos, T.N., Brown, A., Balint-Kurti, G.G., Vasyutinskii, O.S., and Beswick, J.A., *Spin-Polarized Hydrogen Atoms from Molecular Photodissociation.* Science, 2003. **300**(5627), 1936.
277. Rakitzis, T.P., Samartzis, P.C., Toomes, R.L., and Kitsopoulos, T.N., *Measurement of Br Photofragment Orientation and Alignment from HBr Photodissociation: Production of Highly Spin-Polarized Hydrogen Atoms.* J. Chem. Phys., 2004. **121**(15), 7222.
278. Manzhos, S., Romanescu, C., Loock, H.P., and Underwood, J.G., *Two-Photon State Selection and Angular Momentum Polarization Probed by Velocity Map Imaging: Application to H Atom Photofragment Angular Distributions from the Photodissociation of Two-Photon State Selected HCl and HBr.* J. Chem. Phys., 2004. **121**(23), 11802.
279. Romanescu, C., Manzhos, S., Boldovsky, D., Clarke, J., and Loock, H.P., *Superexcited State Reconstruction of HCl Using Photoelectron and Photoion Imaging.* J. Chem. Phys., 2004. **120**(2), 767.
280. Romanescu, C., and Loock, H.P., *Photoelectron Imaging Following 2+1 Multiphoton Excitation of HBr.* Phys. Chem. Chem. Phys., 2006. **8**(25), 2940.
281. Chichinin, A.I., Maul, C., and Gericke, K.H., *Photoionization and Photodissociation of HCl($B^1\Sigma^+$, J=0) Near 236 and 239 nm Using Three-Dimensional Ion Imaging.* J. Chem. Phys., 2006. **124**(22), 224324.
282. Chichinin, A.I., Shternin, P.S., Godecke, N., Kauczok, S., Maul, C., Vasyutinskii, O.S., and Gericke, K.H., *Intermediate State Polarization in Multiphoton Ionization of HCl.* J. Chem. Phys., 2006. **125**(3), 034310.
283. Romanescu, C., and Loock, H.P., *Proton Formation in 2+1 Resonance Enhanced Multiphoton Excitation of HCl and HBr via (Ω=0) Rydberg and Ion-Pair States.* J. Chem. Phys., 2007. **127**(12), 124304.
284. Kauczok, S., Maul, C., Chichinin, A.I., and Gericke, K.H., *Proton Formation Dynamics in the REMPI 2+n Process via the $F^1\Delta_2$ and $f^3\Delta_2$ Rydberg States of HCl Investigated by Three-Dimensional Velocity Mapping.* J. Chem. Phys., 2010. **133**(2), 024301.

285. Maul, C., Chichinin, A.I., and Gericke, K.-H., *Multiphoton Ionization and Fragmentation of Hydrogen Chloride: A Diatomic Still Good for a Surprise.* Journal of Atomic, Molecular, and Optical Physics, 2011. **2011**, 410108.
286. Poretskiy, M., Chichinin, A.I., Maul, C., and Gericke, K.H., *Simultaneous Imaging of Both Product Ions: Exploring Gateway States for HCl as a Benchmark Molecule.* Phys. Chem. Chem. Phys., 2014. **16**(36), 19741.
287. Broderick, B.M., Chernyak, V.Y., Smolin, A.G., Vasyutinskii, O.S., and Suits, A.G., *Imaging Detection of Spin-Polarized Hydrogen Atoms.* Chem. Phys. Lett., 2015. **635**, 350.
288. Manzhos, S., Loock, H.P., Bakker, B.L.G., and Parker, D.H., *Photodissociation of Hydrogen Iodide in the A-band Region 273-288 nm.* J. Chem. Phys., 2002. **117**(20), 9347.
289. Brown, A., *Photodissociation of HI and DI: Polarization of Atomic Photofragments.* J. Chem. Phys., 2005. **122**(8), 084301.
290. Jodoin, D.N., and Brown, A., *Photodissociation of HI and DI: Testing Models for Electronic Structure via Polarization of Atomic Photofragments.* J. Chem. Phys., 2005. **123**(5), 054301a.
291. Wang, F.Y., Lu, I.C., Yuan, K.J., Cheng, Y., Wu, M., Parker, D.H., and Yang, X.M., *Photodissociation Dynamics of HI and DI at 157 nm.* Chem. Phys. Lett., 2007. **449**(1-3), 18.
292. Zhang, D.F., Abdel-Hafiez, A., and Zhang, B., *Studies on the Photodissociation Dynamics of HI Molecule within the A Band Range.* Chem. Phys., 2007. **342**(1-3), 119.
293. Zhang, D.F., *Exploration for Electronic Transitions and Photodissociation Mechanism of Hydrogen Iodide.* J. Math. Chem., 2009. **46**(2), 576.
294. Zhu, L.C., Kleiman, V., Li, X.N., Lu, S.P., Trentelman, K., and Gordon, R.J., *Coherent Laser Control of the Product Distribution Obtained in the Photoexcitation of HI.* Science, 1995. **270**(5233), 77.
295. Kleiman, V., Zhu, L.C., Li, X.N., and Gordon, R.J., *Coherent Phase-Control of the Product Distribution Obtained by the Photoexcitation of HI.* Abstracts of the Papers of the American Chemical Society, 1995. **210**, 238.
296. Zhu, L.C., Kleiman, V., and Gordon, R.J., *Coherent Phase-Control of the Photoexcitation of HI.* Abstracts of the Papers of the American Chemical Society, 1995. **209**, 49.
297. Zhu, L.C., Suto, K., Fiss, J.A., Wada, R., Seideman, T., and Gordon, R.J., *The Effect of Resonances on the Coherent Control of the Ionization and Dissociation of HI and DI.* Physical Review Letters, 1997. **79**(21-24), 4108.
298. Fiss, J.A., Zhu, L.C., Suto, K., He, G.Z., and Gordon, R.J., *Mechanism of the Coherent Control of the Photoionization and Photodissociation of HI and DI.* Chem. Phys., 1998. **233**(2-3), 335.
299. Wang, S.M., Yuan, K.J., Niu, Y.Y., Han, Y.C., and Cong, S.L., *Phase Control of the Photofragment Branching Ratio of the HI Molecule in Two Intense Few-Cycle Laser Pulses.* Phys. Rev. A, 2006. **74**(4), 043406.
300. Regan, P.M., Ascenzi, D., Wrede, E., Cook, P.A., Ashfold, M.N.R., and Orr-Ewing, A.J., *Photodissociation and Photoionization of Highly Excited HI Molecules.* Phys. Chem. Chem. Phys., 2000. **2**(23), 5364.
301. Loock, H.P., Bakker, B.L.G., and Parker, D.H., *Photodissociation of Superexcited States of Hydrogen Iodide: A Photofragment Imaging Study Using Resonant Multiphoton Excitation at 13.39 and 15.59 eV.* Can. J. Phys., 2001. **79**(2-3), 211.

302. Hikosaka, Y., and Mitsuke, K., *Autoionization and Neutral Dissociation of Superexcited HI Studied by Two-Dimensional Photoelectron Spectroscopy.* J. Chem. Phys., 2004. **121**(2), 792.
303. Neufeld, D.A., Zmuidzinas, J., Schilke, P., and Phillips, T.G., *Discovery of Interstellar Hydrogen Fluoride.* The Astrophysical Journal, 1997. **488**(2), L141.
304. Peng, R., Yoshida, H., Chamberlin, R.A., Phillips, T.G., Lis, D.C., and Gerin, M., *A Comprehensive Survey of Hydrogen Chloride in the Galaxy.* The Astrophysical Journal, 2010. **723**(1), 218.
305. Jura, M., *Chlorine Bearing Molecules in Interstellar Clouds.* Astrophysical Journal, 1974. **190**(1), L33.
306. Smith, P.L., Yoshino, K., Black, J.H., and Parkinson, W.H., *Oscillator Strengths for Lines of the (0, 0) and (1, 0) Bands of the $C^1\Pi$-$X^1\Sigma^+$ System of HCl and the Abundance of HCl in Diffuse Interstellar Clouds.* The Astrophysical Journal, 1980. **238**(1), 874.
307. Jr., B.F., and Lodders, K., *Atmospheric Chemistry of the Brown Dwarf Gliese 229B: Thermochemical Equilibrium Predictions.* The Astrophysical Journal, 1996. **472**(1), L37.
308. Zhu, C., Krems, R., Dalgarno, A., and Balakrishnan, N., *Chemistry of Hydrogen Fluoride in the Interstellar Medium.* The Astrophysical Journal, 2002. **577**(1), 795.
309. Neufeld, D.A., Wolfire, M.G., and Schilke, P., *The Chemistry of Fluorine-Bearing Molecules in Diffuse and Dense Interstellar Gas Clouds.* The Astrophysical Journal, 2005. **628**(1), 260.
310. Neufeld, D.A., and Wolfire, M.G., *The Chemistry of Interstellar Molecules Containing the Halogen Elements.* The Astrophysical Journal, 2009. **706**(2), 1594.
311. Chayer, P., Vennes, S., Dupuis, J., and Kruk, J.W., *Abundance of Elements beyond the Iron Group in Cool DO White Dwarfs.* Astrophysical Journal, 2005. **630**(2), L169.
312. Kitchin, C.R., *Exoplanets: Finding, Exploring and Understanding Alien Worlds*. 2012, New York, Dordrecht, Heidelberg, London: Springer.
313. Marcy, G.W., and Butler, R.P., *Precision Radial-Velocities with an Iodine Absorption Cell.* Publications of the Astronomical Society of the Pacific, 1992. **104**(674), 270.
314. Butler, R.P., Marcy, G.W., Williams, E., McCarthy, C., Dosanjh, P., and Vogt, S.S., *Attaining Doppler Precision of 3 m/s.* Publications of the Astronomical Society of the Pacific, 1996. **108**(724), 500.
315. Wright, J.T., Fakhouri, O., Marcy, G.W., Han, E., Feng, Y., Johnson, J.A., Howard, A.W., Fischer, D.A., Valenti, J.A., Anderson, J., and Piskunov, N., *The Exoplanet Orbit Database.* Publications of the Astronomical Society of the Pacific, 2011. **123**(902), 412.
316. Hudson, R.D., and Reed, E.I., *The Stratosphere - Present and Future*. 1979: NASA Reference Publication 1049.
317. Jenkin, M.E., Cox, R.A., and Candeland, D.E., *Photochemical Aspects of Tropospheric Iodine Behaviour.* J. Atmos. Chem., 1985. **2**(4), 359.
318. Chameides, W.L., and Davis, D.D., *Iodine - It's Possible Role in Tropospheric Photochemistry.* Journal of Geophysical Research - Oceans and Atmospheres, 1980. **85**(NC12), 7383.
319. Stutz, J., Hebestreit, K., Alicke, B., and Platt, U., *Chemistry of Halogen Oxides in the Troposhere: Comparison of Model Calculations with Recent Field Data.* J. Atmos. Chem., 1999. **34**(1), 65.

320. Vogt, R., Crutzen, P.J., and Sander, R., *A Mechanism for Halogen Release from Sea-Salt Aerosol in the Remote Marine Boundary Layer.* Nature, 1996. **383**(6598), 327.
321. Vogt, R., Sander, R., Glasow, R.V., and Crutzen, P.J., *Iodine Chemistry and its Role in Halogen Activation and Ozone Loss in the Marine Boundary Layer: A Model Study.* J. Atmos. Chem., 1999. **32**(3), 375.
322. Bale, C.S.E., Ingham, T., Commane, R., Heard, D.E., and Bloss, W.J., *Novel Measurements of Atmospheric Iodine Species by Resonance Fluorescence.* J. Atmos. Chem., 2008. **60**(1), 51.
323. Pasteka, L.F., Borschevsky, A., Flambaum, V.V., and Schwerdtfeger, P., *Search for Variation of Fundamental Constants: Strong Enhancements in $X^2\Pi$ Cations of Dihalogen and Hydrogen Halides.* Phys. Rev. A, 2015. **92**(1), 012103.
324. Reinhold, E., and Ubachs, W., *Heavy Rydberg States.* Mol. Phys., 2005. **103**(10), 1329.
325. Wang, C.H., Kelley, M., Buathong, S., and Dunning, F.B., *Dynamics of Heavy-Rydberg Ion-Pair Formation in K(14p,20p)-SF_6, CCl_4 Collisions.* J. Chem. Phys., 2014. **140**(23), 234306.
326. Buathong, S., Kelley, M., Wang, C.H., and Dunning, F.B., *Probing Dissociative Electron Attachment through Formation of Heavy-Rydberg Ion-Pair States in Rydberg Atom Collisions.* Chem. Phys. Lett., 2015. **618**, 153.
327. Donovan, R.J., Lawley, K.P., and Ridley, T., *Heavy Rydberg Behaviour in High Vibrational Levels of Some Ion-Pair States of the Halogens and Inter-Halogens.* J. Chem. Phys., 2015. **142**(20), 204306.
328. Donovan, R.J., Lawley, K.P., and Ridley, T., *A Heavy Rydberg Quantum Defect Analysis of the Perturbed $D(0_u^+)$ Ion-Pair State of Br_2.* Chem. Phys., 2015. **463**, 145.
329. Mollet, S., and Merkt, F., *Dissociation Dynamics of Ion-Pair States of Cl_2 at Principal Quantum Numbers beyond 1500.* Phys. Rev. A, 2010. **82**, 032510.
330. Hoffmann, N., *Photochemical Reactions as Key Steps in Organic Synthesis.* Chem. Rev., 2008. **108**(3), 1052.
331. Ciamician, G., *The Photochemistry of the Future.* Science, 1912. **36**, 385.
332. Gardiner, S.H., Lipciuc, M.L., and Vallance, C., *Gas-Phase Retro-Diels-Alder Reactions of Cyclohexene, 1-Methylcyclohexene, and 4-Methylcyclohexene following Photoexcitation at 193 nm: A Velocity Map Imaging Study.* J. Phys. Chem. A, 2015. **119**(50), 12218.
333. Zaouris, D., Kartakoullis, A., Glodic, P., Samartzis, P.C., Hrodmarsson, H.R., and Kvaran, A., *Rydberg and Valence State Excitation Dynamics: A Velocity Map Imaging Study Involving the E-V State Interaction in HBr.* Phys. Chem. Chem. Phys., 2015. **17**(16), 10468.
334. Schrödinger, E., *An Undulatory Theory of the Mechanics of Atoms and Molecules.* The Physical Review, 1926. **28**(6), 1049.
335. Heisenberg, W., *Über Quantentheoretishe Umdeutung Kinematisher und Mechanischer Beziehungen.* Zeitschrift für Physik, 1925. **33**, 879.
336. Dirac, P.A.M., *The Principles of Quantum Mechanics*. 1930, Oxford: Oxford University Press.
337. Griffiths, D.J., *Introduction to Quantum Mechanics*. 2005, New Jersey: Pearson Education International.
338. Landau, L.D., and Lifshitz, L.M., *Quantum Mechanics, Third Edition: Non-Relativistic Theory*. Vol. 3. 1977, Oxford: Pergamon.
339. Wheeler, N., *Higher-Order Spectral Perturbation.* (unpublished) Reed Cellege report, 2000.

340. Dunham, J.L., *The Wentzel-Brillouin-Kramers Method of Solving the Wave Equation.* Physical Review, 1932. **41**, 713.
341. Dunham, J.L., *The Energy Levels of a Rotating Vibrator.* Physical Review, 1932. **41**, 721.
342. Huber, K.P., and Herzberg, G., *Molecular Spectra and Molecular Structure IV. Constants of Diatomic Molecules*. 1979, New York: Van Nostrand.
343. Born, M., and Oppenheimer, J.R., *Zur Quantentheorie der Molekeln.* Ann. Phys., 1927. **84**, 457.
344. Hagedorn, G.A., and Joye, A., *Mathematical Analysis of Born-Oppenheimer Approximations.* Spectral theory and mathematical physics: a Festschrift in honor of Barry Simon's 60th birthday, In:Proc Sympos Pure Math 76, Part 1, Amer Math Soc. Providence, RI, 2007, 203.
345. Lefebvre-Brion, H., and Field, R.W., *The Spectra and Dynamics of Diatomic Molecules*. 2004: Elsevier Academic Press.
346. Zare, R.N., *Angular Momentum - Understanding Spatial Aspects in Chemistry and Physics*. 1988, New York: John Wiley & Sons.
347. Brits, L., *Euler angles, vector of*, Euler.png, Editor. 2008: Wikipedia.org.
348. Bray, R.G., and Hochstrasser, R.M., *Two-Photon Absorption by Rotating Diatomic Molecules.* Mol. Phys., 1976. **31**(4), 1199.
349. Halpern, J.B., Zacharias, H., and Wallenstein, R., *Rotational Line Strengths in Two- and Three-Photon Transitions in Diatomic Molecules.* J. Mol. Spectrosc., 1980. **79**(1), 1.
350. Kramida, A., Ralchenko, Y., Reader, J., and Team, N.A., *NIST Atomic Spectra Database (ver. 5.3) [Online]*. 2015: National Institute of Standards and Technology, Gaithersburg, MD.
351. Rakitzis, T.P., *Direct Measurement of Photofragment Alignment from Unnormalized Abel-Invertible Images.* Chem. Phys. Lett., 2001. **342**(1-2), 121.
352. Rives, P., Teyssier, J.L., Galy, J., Birot, A., Brunet, H., and Asselman, H., *Kinetic Study of the 308 and 345 nm Emissions of the Molecule XeCl.* J. Chem. Phys., 1995. **102**(3), 1217.
353. WaveMetrics, *IGOR Pro*. 2013.
354. Western, C.M., *PGOPHER*. 2014, University of Bristol.
355. Samartzis, P.C., Sakellariou, I., Gougousi, T., and Kitsopoulos, T.N., *Photofragmentation Study of Cl_2 Using Ion Imaging.* J. Chem. Phys., 1997. **107**(1), 43.
356. Gebhardt, C.R., Rakitzis, T.P., Samartzis, P.C., Ladopoulos, V., and Kitsopoulos, T.N., *Slice Imaging: A New Approach to Ion Imaging and Velocity Mapping.* Rev. Sci. Instrum., 2001. **72**(10), 3848.
357. Papadakis, V., and Kitsopoulos, T.N., *Slice Imaging and Velocity Mapping Using a Single Field.* Rev. Sci. Instrum., 2006. **77**(8), 083101.
358. Proch, D., and Trickl, T., *A High-Intensity Multi-Purpose Piezoelectric Pulsed Molecular Beam Source.* Rev. Sci. Instrum., 1989. **60**(4), 713.
359. Dong, F., Lee, S.-H., and Liu, K., *Reactive Excitation Functions for F + p-H_2 / n-H_2/D_2 and the vibrational branching for F + HD.* J. Chem. Phys., 2000. **113**(9), 3633.
360. Ran, Q., Matsiev, D., Auerbach, D.J., and Wodtke, A.M., *An Advanced Molecule-Surface Scattering Instrument for Study of Vibrational Energy Transfer in Gas-Solid Collisions.* Rev. Sci. Instrum., 2007. **78**(10), 104104.

Appendix: Conference presentations

Posters

New Observations and Perturbations in the (2+n) REMPI spectra of HI. RSC Spectroscopy and Dynamics Group Meeting. St. Catherine‘s College. 5.-7. January 2014. Oxford (England).

Photofragmentations and energetics of Rydberg and ion-pair states in the (2+n) REMPI spectra of HI. The 23rd International Conference on High Resolution Molecular Spectroscopy, 2.-6.September 2014. Bologna (Italy).

Exploring E-V State Interactions in HBr via REMPI & VMI Experiments. RSC Spectroscopy and Dynamics Group Meeting. University of Nottingham 6.-8. January 2015. Nottingham (England).

Illuminating Hidden States through Perturbations: New Observations in High Energy REMPI of HI. The biennial meeting of the Icelandic chemical society. „Ráðstefna Efnís“ 17. October 2015. Reykjavík (Iceland).

Revealing Photofragmentation Dynamics through Interactions between Rydberg States: REMPI of HI as a Case Study. The biennial meeting of the Icelandic chemical society. „Ráðstefna Efnís“ 17. October 2015. Reykjavík (Iceland).

Talks

New Observations and Perturbations in the (2+n) REMPI spectra of HI. RSC Spectroscopy and Dynamics Group Meeting. St. Catherine‘s College. 5.-7. January 2014. Oxford (England).

Utilization of Spectroscopy in the Determination of the Origins of Life. Seminar at The Science Institute of the University of Iceland. 4.April 2014. Reykjavík (Iceland).

Exploring E-V State Interactions Related Dynamics in HBr via coupled REMPI and VMI experiments. RSC Spectroscopy and Dynamics Group Meeting. University of Nottingham 6.-8. January 2015. Nottingham (England).

Exploring State Interactions and Related Dynamics in the Hydrogen Halides with REMPI and VMI Experiments. Seminar at The Science Institute of the University of Iceland. 20. March 2015. Reykjavík (Iceland).

REMPI and VMI of HBr and HI. Visit to the Sackler Laboratory for Astrophysics (SLA), 9. June 2015, Leiden (The Netherlands).

Efnafræði og alheimurinn: Að búa til líf á 15 mínútum (e. Chemistry and the universe: Constructing life in 15 minutes), Annual Science Day of the University of Iceland, 31. October 2015, Reykjavík (Iceland).